پژوهش های خشکسالی و تغییراقلیم

دوره دوم، شماره چهارم، پیاپی ۸، زمستان ۱۴۰۳

Scientific Journal

Journal of Drought and Climate change Research

Volume 2, Issue 4, Serial Number 8, March 2025, 1-184.

Print ISSN: 2980-9819 **Online ISSN:**3092-6076

license number of the Ministry of Culture and Islamic Guidance: 92041

Address: Iran-South Khorasan - Birjand - 5th km of Kerman road - Agricultural Science and Natural Resources Campus, University of Birjand, Birjand, Iran

Tel: +98 56 31027609

Email: jdcr@birjand.ac.ir

Web: https://jdcr.birjand.ac.ir/

Original Article

Journal of Drought and Climate change Research (JDCR)

Winter 2025, Vol. 2, No. 8, pp 1-30

10.22077/jdcr.2024.7369.1063

Assessment of Groundwater Dynamics in the Kabul Basin: Implications for Sustainable Management

Nematullah Hasani[1], Farhad Hajian[2], Abbas Ali Ghezelsofloo[3], Ali Haji Elyasi[4], Mobin Eftekhari[5*]

1- Department of Civil Engineering, Water and Hydraulic Structures, Mashhad Branch, Islamic Azad University, Mashhad, Iran.
2- Department of Civil Engineering, Neyshabur Branch, Islamic Azad University, Neyshabur, Iran.
3- Department of Civil Engineering, Mashhad Branch, Islamic Azad University, Mashhad, Iran.
4- Department of Civil Engineering, College of Engineering, University of Tehran, Tehran, Iran.
5- Department of Water Engineering, University of Birjand, Birjand, Iran.

*** corresponding author: mobineftekhari@yahoo.com**

Keywords:
Water resource management, Population growth, Qualitative changes, Droughts, Water scarcity.

Received:
13 March 2024

Revised:
12 Aug 2024

Accepted:
18 Aug 2024

Abstract

Groundwater, particularly from aquifers in Afghanistan's arid and semi-arid eastern basin, has long served as a primary water source for industry, agriculture, and domestic use. However, population growth and recurrent droughts, along with insufficient planning, have led to a troubling trend of over-extraction in recent decades. Effective groundwater management focusing on controlled extraction that aligns with aquifer capacity, is essential for long-term sustainability. This study employs ArcGIS software to assess quantitative and qualitative shifts in groundwater dynamics within the Kabul Basin. Data from 54 wells, monitored at various intervals from 2005 to 2020, were meticulously analyzed, incorporating geological, climatic, and hydrological parameters. The findings reveal significant fluctuations in groundwater levels, with an average decline of 16.5 meters over the 13-year study period. The groundwater level decreased by 12 meters in some parts of the Kabul aquifers, at a rate of 80 centimeters per year. Particularly in the Paghman-Darulaman and central Kabul aquifers, we observed alterations in flow distribution patterns. Water quality parameters also changed, with 82% of samples collected in November 2020 showing electrical conductivity values greater than 1,000 µS/cm, compared to 73% in 2004, indicating increasing salinity. The total groundwater storage loss in the Kabul aquifer during the study period was estimated at 358 million cubic meters. Groundwater consumption in 2020 was approximately 277 million cubic meters, twice the natural recharge rate. Future projections indicate an accelerated depletion of groundwater reserves, especially in densely populated urban regions like Kabul, necessitating immediate intervention to avert impending water scarcity crises.

How to cite this article:
Hasani, N., Hajian, F., Ghezelsofloo, A.A., Haji Elyasi, A. & Eftekhari, M. (2024). Assessment of Groundwater Dynamics in the Kabul Basin: Implications for Sustainable Management. *Journal of Drought and Climate change Research* (JDCR), 2(8), 1-30. 10.22077/jdcr.2024.7369.1063

Introduction

Groundwater is a crucial component of the world's dynamic and renewable water resources, playing a vital role in the water cycle and serving as a reliable reserve during critical periods, making it an essential strategic resource (Pereira et al., 2009). Given the constant and renewable nature of groundwater, its preservation is of utmost importance. However, human activities are increasing environmental pollution, exposing groundwater to various contaminants. Understanding the potential impacts of human activities on groundwater quality has become increasingly important for its sustainable use and extraction (Mouser & Rizzo, 2004; Eftekhari et al., 2024). Water scarcity is an escalating global challenge, particularly acute in arid and semi-arid regions where groundwater often serves as the primary water source for urban, agricultural, and industrial needs. The Kabul Basin in Afghanistan exemplifies this critical issue, where rapid urbanization and population growth have placed unprecedented pressure on groundwater resources (Zaryab et al., 2022). As the capital city's population surged from approximately 1 million in 2001 to 5.3 million in 2021, the demand for water has intensified, leading to overexploitation of aquifers and subsequent environmental concerns (Manawi et al., 2020).

The sustainability of groundwater resources is intricately linked to the delicate balance between extraction rates and natural recharge. However, in many urban areas worldwide, this balance has been disrupted by human activities. Kabul, like other rapidly expanding cities in water-stressed regions, faces the dual challenge of meeting increasing water demands while preserving its groundwater resources for future generations. This situation is further complicated by climate change, which alters precipitation patterns and potentially impacts groundwater recharge rates (Hussaini et al., 2021; Khodabandeh Baygi et al., 2023).

Understanding the quantity and quality of groundwater resources is crucial for maintaining and optimally managing water supplies, especially during droughts and periods of water scarcity. Groundwater pollution is of greater concern than surface water pollution because the time between the onset of contamination and the manifestation of its effects can span several years. As a result, identifying and addressing the source of contamination is often costly and time-consuming (Ibrahim et al., 2010; Dehkordi & Pourmoghaddas, 2006). While some pollutants, such as agricultural waste, are biodegradable and can be reduced relatively easily, others, like heavy metals (e.g., cadmium, lead, and arsenic), are non-biodegradable and highly toxic. A critical issue with heavy metals is their inability to be metabolized

by the body (Hadizadeh et al., 2009). Once heavy metals enter the body, they are not excreted but accumulate in tissues such as fat, muscles, bones, and joints, leading to various diseases and adverse health effects. Neurological disorders, various cancers, and, in severe cases, death are among the potential outcomes of heavy metal exposure. Moreover, the accumulation of heavy metals in plants and their entry into the food chain exacerbate the associated risks (Karbasi and Bayati, 2001).

The reduction of groundwater levels and the deterioration of water quality due to over-extraction beyond the capacity of aquifers not only have negative environmental impacts but also diminish livelihood opportunities in the region. Additionally, uncontrolled withdrawals can lead to land subsidence, which has garnered the attention of regional officials (Ranjbar & Jafari, 2009). Given that protecting water resources and ensuring their sustainable performance is cost-effective, water resource management and planning should be prioritized in each region (Valayati, 2002). Groundwater recharge and levels are influenced by various factors, including cropping patterns and their intensity, irrigation methods, climatic parameters (such as precipitation frequency and intensity, temperature, evaporation, and transpiration), and soil hydraulic properties, such as hydraulic conductivity (Hajian, 2021). In recent years, several studies have highlighted the growing concerns regarding groundwater depletion and contamination in urban areas. For instance, Manawi et al. (2020) investigated urban flooding in Kabul, emphasizing the interconnection between surface water management and groundwater recharge. Hussaini et al. (2021) focused on site selection for managed aquifer recharge in Kabul, addressing the need for artificial recharge to combat groundwater depletion. (Tani & Tayfur, 2021) evaluated the groundwater potential zones in the Kabul River Basin, Afghanistan, using GIS and AHP. The results show that the very good potential zones are mainly located in the downstream and central parts of the basin, while only 18% of the annual precipitation recharges the groundwater. (Hilal et al., 2024) employed GIS, AHP, and remote sensing to assess groundwater potential in the Moulouya Basin, using seven parameters including drainage density, lithology, and precipitation. The area was classified into five zones of groundwater potential, with 26% very high and 51% high potential. The model's accuracy was validated using 96 well/borehole data points, achieving a high correlation coefficient, with 89.5% of boreholes located in high and very high potential zones.

These studies underscore the urgency of comprehensive groundwater management in rapidly urbanizing regions. However,

there remains a significant knowledge gap in understanding the long-term quantitative and qualitative changes in groundwater resources in the Kabul Basin, particularly in relation to rapid urbanization and climate variability. Previous studies have not fully integrated spatial and temporal analyses of groundwater level fluctuations with water quality parameters over an extended period, nor have they comprehensively assessed the impact of land-use changes on groundwater dynamics in this region.

Our study aims to bridge this gap by employing an innovative approach that combines GIS-based spatial analysis with long-term temporal data to provide a holistic assessment of groundwater resources based on quantity and quality of water in the Kabul Basin. Specifically, this research:

- Analyzes groundwater level fluctuations and flow distribution patterns from 2005 to 2020 using data from 54 wells.
- Assesses changes in water quality parameters, focusing on electrical conductivity, nitrates, and other key indicators.
- Quantifies the impact of land-use changes, particularly urbanization, on groundwater recharge and quality.
- Estimates the current groundwater balance and projects future trends under various scenarios.

By integrating these multiple facets, our study provides a more comprehensive understanding of the groundwater system in the Kabul Basin than previous research. This approach allows for a nuanced analysis of the interplay between urbanization, climate variability, and groundwater dynamics, offering valuable insights for sustainable water resource management in rapidly developing urban areas.

The findings of this study have significant implications for water resource management policies in Kabul and similar urban areas in arid and semi-arid regions. By identifying critical areas of groundwater depletion and quality degradation, this research can inform targeted interventions and sustainable management strategies, contributing to long-term water security in the region.

Materials and Methods

As previously mentioned, this research aims to monitor the spatial quantitative and qualitative changes in groundwater within the Kabul basin, investigating the impact of excessive exploitation and groundwater level decline on its quality, particularly focusing on salinization, nitrate levels, and heavy metal contamination. To gather the necessary data for assessing groundwater level decline and its effects on quality, information on the average groundwater depth is first collected. Groundwater depth measurements are then taken from selected observation wells within the aquifer zone

to create a long-term variation graph of the groundwater table and absolute groundwater levels. Additionally, the electrical conductivity of the groundwater is measured over a specific period to prepare a hydrograph.

Sampling is conducted using standard methods, and laboratory analysis is performed to evaluate the data. The data collected includes various groundwater quality parameters, such as calcium, electrical conductivity, salinity, pH, magnesium, dissolved salt concentrations, water hardness, sodium, nitrate, potassium, sulfate, fluoride, chloride, total dissolved solids, iron, manganese, copper, aluminum, cyanide, alumina, and dissolved oxygen levels in the wells. Finally, the aquifer is simulated in both quantitative and qualitative aspects, with the input and output balances of surface and groundwater in the Kabul basin plotted. Management solutions are then proposed to address and control critical conditions.

Study Area

Kabul, the capital of Afghanistan, is situated in the central part of the Kabul River basin, which forms a smooth alluvial plain dating from the Neogene to the Quaternary periods. This area is commonly referred to as the "Kabul Basin." Located in eastern Afghanistan, the Kabul River basin lies between approximately 34°31' north latitude and 69°12' east longitude, with a total drainage area of 375 square kilometers (Hussaini et al., 2021). The basin's average elevation is about 1,800 meters above sea level, with prominent mountain ranges including Paghman, Qurugh, Shir Darwaza, Wais-e-Qarni, and Safi. The Kabul River and its tributaries flow through this region. Kabul is characterized by a continental climate. Although recent weather data are scarce, historical data recorded by the World Meteorological Organization from 1956 to 1983 indicate that the average temperature in January was as low as -7.1°C, while the average temperature in July exceeded 32.1°C, with an annual rainfall of less than 500 millimeters (Zaryab et al., 2022). Geological structures in this region include anticlines, synclines, hills, and faults. As the most populous city in Afghanistan, Kabul's population growth may necessitate increased water resources for drinking and food production.

The Kabul basin consists of three interconnected aquifers with thicknesses ranging from 20 to 70 meters. The study area extends from a Neogene alluvial basin to the Quaternary period. Groundwater in the basin is replenished by three main rivers. The aquifer's raw materials have high permeability and infiltration capacity. In the deeper parts of the aquifer, semi-diagenetic conglomerate rocks have formed due to the high density of space, reducing the voids and internal connections, which

in turn decreases well water production. The primary groundwater recharge occurs after snowmelt, primarily through direct absorption from the rivers (Hussaini et al., 2021). The geological map and geographical location of the study area are shown in Fig 1.

The northern margin of the Kabul basin consists of Paleoproterozoic metamorphic rocks such as gneiss and schist. The mountains on the southern edges are mainly composed of Neoproterozoic and Mesozoic metamorphic rocks, along with sedimentary rocks like limestone and dolomite. The basin is surrounded by mountain ranges, with its lower part consisting of various metamorphic rocks such as amphibolite, quartzite, slate, and marble (Zaryab et al., 2022). A digital elevation model (DEM) map showing the elevation of the study area is provided in Figure 1. The DEM map, with a resolution of 30 meters, was downloaded from the USGS public geospatial data portal and clipped using ArcGIS.

Two important rivers enter the study area, playing a critical role in the water balance. The Kabul River flows from west to east, joining various tributaries before eventually reaching the Indus River in Pakistan. One of its main tributaries, the Logar River, drains the Logar Valley watershed in the south, covering about 10,000 square kilometers. The confluence of these two rivers occurs in the center of the Kabul Basin, within the city of Kabul.

Study Procedure

In general, this study is divided into three parts, in each part steps have been taken to reach the main goal. These three steps include the following:

a) Preparation of Base Maps:

Initially, base maps of the Kabul basin were created, covering aspects such as geology, topography, slope, surface runoff, thickness of the unsaturated zone, permeability, soil type, land use, waterways, residential areas, contour lines, and quality parameters. These maps were developed using geographic information systems (ArcGIS) by inputting the necessary data into the software.

b) Collection of Well Data:

At this stage, data from piezometer wells and water observations in the Kabul basin, provided by the Ministry of Energy and Water, were collected. To assess changes in groundwater levels and elevations in the study area, 54 selected piezometer wells from the groundwater monitoring network were used. Recorded values and groundwater elevations were collected for each well.

c) Data Analysis for Plotting Relevant Graphs and Maps

Quantitative geophysical maps, including contour lines of the groundwater table in the basin, were prepared and compared with well depths and aquifer capacity, which are represented as points with

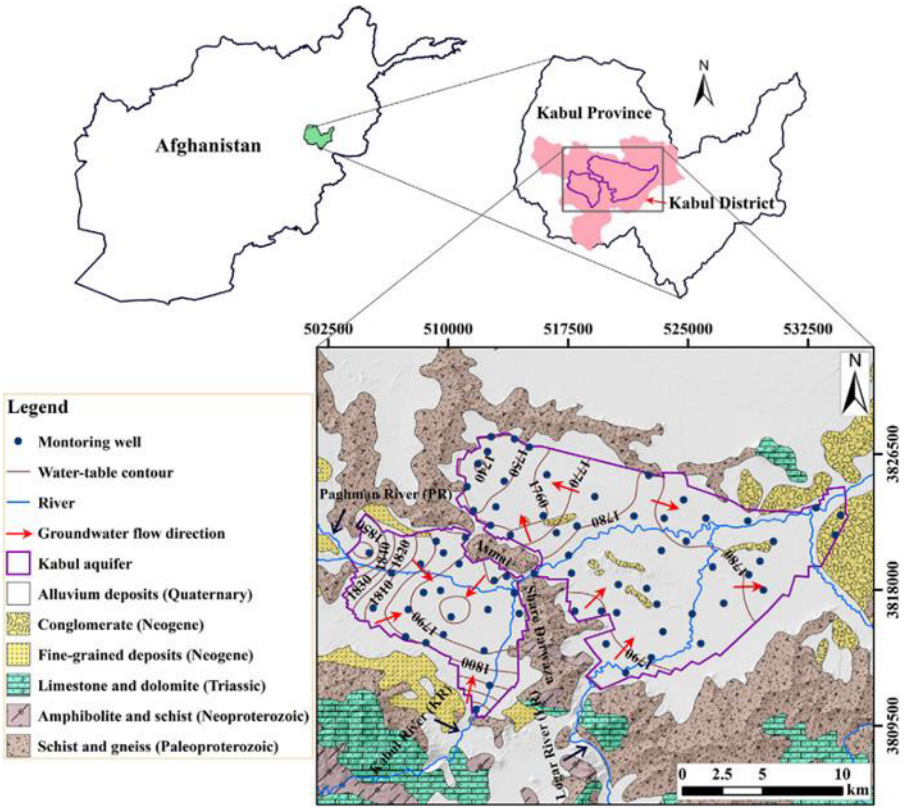

Fig 1. Geological map and location of the study area (Zaryab et al., 2022)

the same groundwater level. Qualitative isochemical maps were generated based on 2020 statistics for water quality parameters in the Kabul basin's groundwater table, provided by the Ministry of Energy and Water. These were compared with research results obtained in 2004. The framework for conducting the research is illustrated in the following figure (Fig 2).

Effective Criteria in Groundwater Recharge

In this study, four criteria were considered that these effect on groundwater recharge. These criteria are the data used in this study. Each of them is described below. It should be noted that these data are obtained from reports or through GIS software. The spatial distribution of these criteria is illustrated in Figure 3, which includes maps of slope, surface infiltration rate, drainage density, and the thickness of the unsaturated zone. These maps provide a comprehensive overview of the study area's suitability for groundwater recharge.

Slope

Slope is a critical factor in classifying potential groundwater recharge areas. Higher slopes lead to faster water flow and increased erosion, reducing the potential for groundwater recharge (Hussaini et al.,

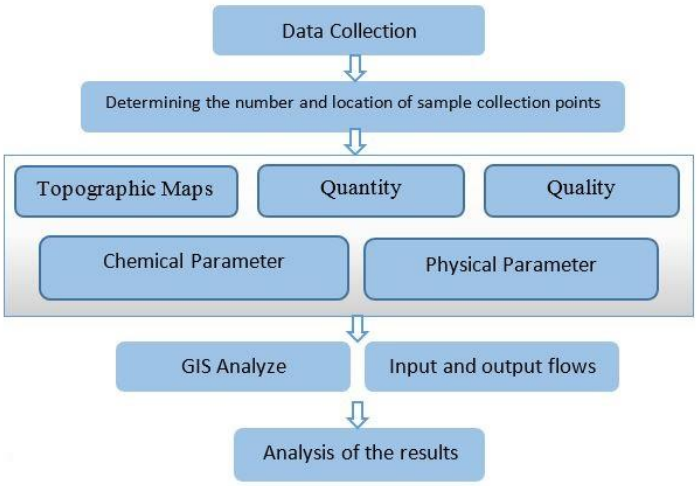

Fig 2. Proposed flow diagram of the modeling procedure and steps in the current steps

2021). In contrast, sedimentary basins, floodplains, and low-lying flat areas are more conducive to groundwater recharge due to the longer travel time of water to downstream locations, allowing sufficient time for infiltration into the soil.

A slope map for the study area was generated using spatial analysis tools in ArcMap software, utilizing DEM data with a cell size of 30 meters and a pixel depth of 16 bits. Based on previous studies, areas with slopes greater than 10% are considered unsuitable for groundwater recharge. Consequently, the slope map was categorized into two main classes: 0-10% (suitable area) and greater than 10% (unsuitable area). The suitable range (0-10%) was further divided into three subcategories. In the study area, the slope ranges from 0% to 31%, and the complete slope map was classified into four classes: 0-2%, 2-5%, 5-10%, and greater than 10%. The majority of the study area falls within the 0-2% and 2-5% subcategories, with some areas of higher slopes around the hills within the study area.

Surface Infiltration Rate

The surface infiltration rate is crucial for groundwater recharge, as it determines the extent to which rainfall and surface water contribute to replenishing groundwater. Areas with high surface infiltration rates are considered suitable for groundwater recharge. In this study, no field measurements were available for this criterion. Consequently, the surface infiltration rate for the study area was derived using the relationship between soil texture and water infiltration rate as proposed by the Food and Agriculture Organization (FAO, 1979; Ghayomian et al., 2007). A soil surface infiltration rate map was produced and classified using ArcGIS software. The map was divided into four classes to assess the suitability of

areas for groundwater recharge: unsuitable (less than 15 mm/hr), moderate (15-25 mm/hr), suitable (25-45 mm/hr), and very suitable (greater than 45 mm/hr).

Drainage Density

Drainage density is a measure of the total length of stream channels per unit area within a watershed (Shroder & Ahmadzai, 2016). It is typically calculated by dividing the total length of the channels by the area of the watershed, yielding a value for drainage density. Drainage density is inversely proportional to permeability (Carlston, 1963). High drainage density suggests favorable conditions for surface water flow, but it also indicates a lower potential for groundwater recharge. The drainage density (in kilometers per square kilometer) was calculated using the following equation:

$$DD = (\sum Li)/A \quad (1)$$

Where (Li) represents the total length of all stream channels in kilometers, and (A) is the area of the study region in square kilometers (Hussaini et al., 2021)

A drainage density map for the area was created using spatial analysis tools in ArcGIS, based on the digital elevation model (DEM) of the region. This map was classified into four categories for groundwater recharge assessment: 0-0.5 (very suitable), 0.5-1.5 (suitable), 1.5-2 (moderate), and greater than 2 (unsuitable). The drainage density in the area ranges from 0 to 4.6 kilometers per square kilometer.

It's important to note that while drainage density was considered in the analysis, its impact on selecting suitable groundwater recharge sites is limited. This is because the study area is urbanized, and urbanization has altered the natural drainage network, reducing the relevance of this criterion. Therefore, it was assigned a low level of importance.

Urban flooding is a significant challenge in the northern part of Kabul city. In recent years, heavy rainfall has led to frequent urban flooding, primarily due to excessive rainfall combined with inadequate drainage systems. This problem is further exacerbated by unsustainable urban expansion, changes in the catchment area, and an increase in impermeable surfaces. Over the decades, Kabul's drainage infrastructure has not kept pace with population growth, leading to a higher frequency of urban flooding (Manawi et al., 2020).

Thickness Of Unsaturated Zone

In areas where the water table is near the surface and groundwater is not being extracted, recharge can cause the water table to rise, potentially resulting in marshland formation. In other words, if the natural underground reservoir has limited storage capacity, successful recharge is less certain (Mahdavi et al.,

2010). Therefore, the thickness of the unsaturated zone—the distance from the ground surface to the water table—is a critical factor in identifying suitable sites for groundwater recharge.

In this study, water-table depth measurements were collected from 100 observation wells. An interpolated map of the unsaturated zone thickness was then created using the inverse distance weighting (IDW) method. This map illustrates the variation in unsaturated zone thickness across the study area. According to previous research, groundwater recharge is unlikely to be successful if the thickness of the unsaturated zone is less than 10 meters. However, sites with an unsaturated zone thickness greater than 10 meters are considered suitable for recharge. The map was classified into four categories based on suitability for groundwater recharge: very suitable (>30 m), suitable (20–30 m), moderate (10–20 m), and unsuitable (0–10 m).

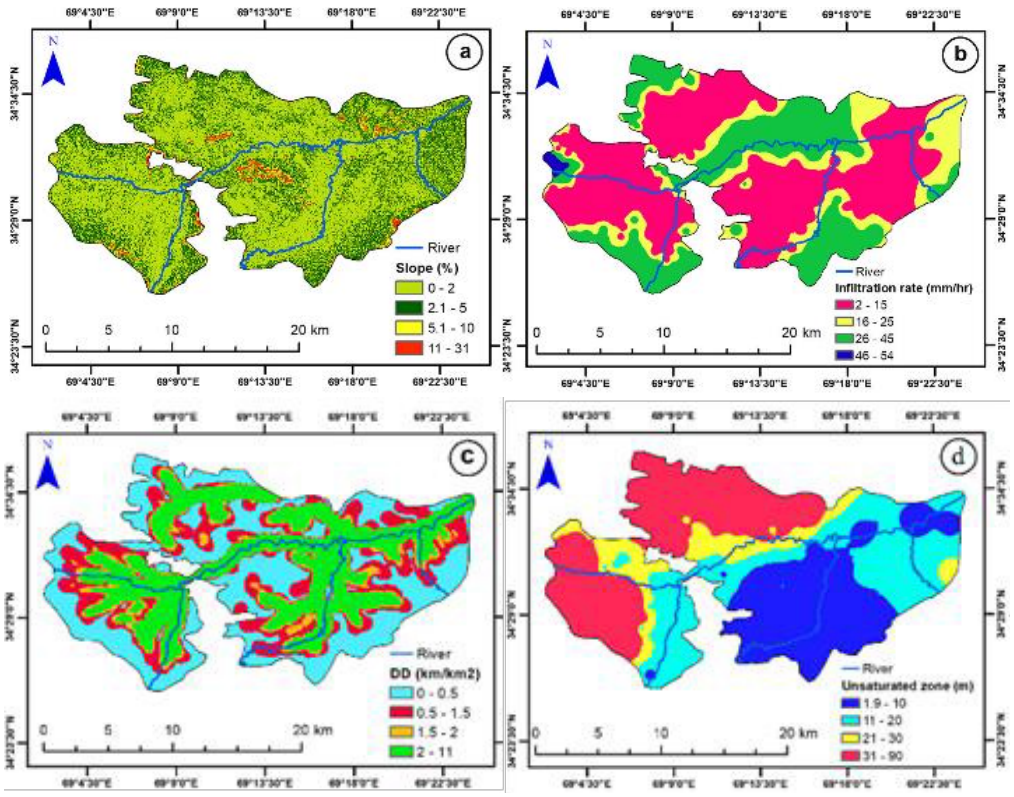

Fig 3. Maps of effective groundwater criteria: a) Slope, b) Surface infiltration rate, c) Drainage density, d) Unsaturated zone.

Results and Discussion

This section presents the results of our comprehensive analysis of groundwater dynamics in the Kabul Basin from 2005 to 2020. The analysis includes quantitative changes in groundwater levels, alterations in flow patterns, shifts in water quality parameters, and the impacts of land use

changes on the basin's hydrology. We utilized data from 54 wells, monitored at various intervals, and integrated geological, climatic, and hydrological parameters to provide a comprehensive overview of the groundwater system's evolution over the study period. The findings are detailed through statistical analyses, spatial mapping, and temporal trend assessments, offering insights into the complex interactions between natural processes and anthropogenic influences on the basin's groundwater resources.

Changes in Groundwater Level

The hydrograph indicates a continuous decline in groundwater levels within the basin (Figure 4). This decline can be divided into two distinct periods: 2005-2011 and 2011-2020. During 2005-2011, the groundwater level decreased slowly, but this decline accelerated significantly from 2011 to 2020. Figure 4 illustrates that the groundwater level has notably dropped across most of the basin, particularly in the northwestern part of the Central Kabul aquifer and in the Paghman-Darulaman aquifer in the southeast.

The hydrograph reveals that, in some areas of the Kabul aquifers, the groundwater level has decreased by up to 12 meters (at a rate of 80 centimeters per year) over the past 15 years (2005-2020). The rate of decline has markedly increased since 2011, likely due to factors such as population growth, changes in precipitation patterns, and urban expansion. Since late 2001, Kabul city has experienced rapid population growth, with the population rising from approximately 1 million in 2001 to 5.3 million in 2021 (Afghanistan Public Policy Research Organization, 2012; National Statistics and Information Authority, 2021). Currently, more than 70% of the population resides in unplanned settlements (Barbe, 2013). During the study period, the Heshmat Khan wetland—the last remaining marsh in the Kabul basin—and a significant number of shallow wells have dried up due to overexploitation.

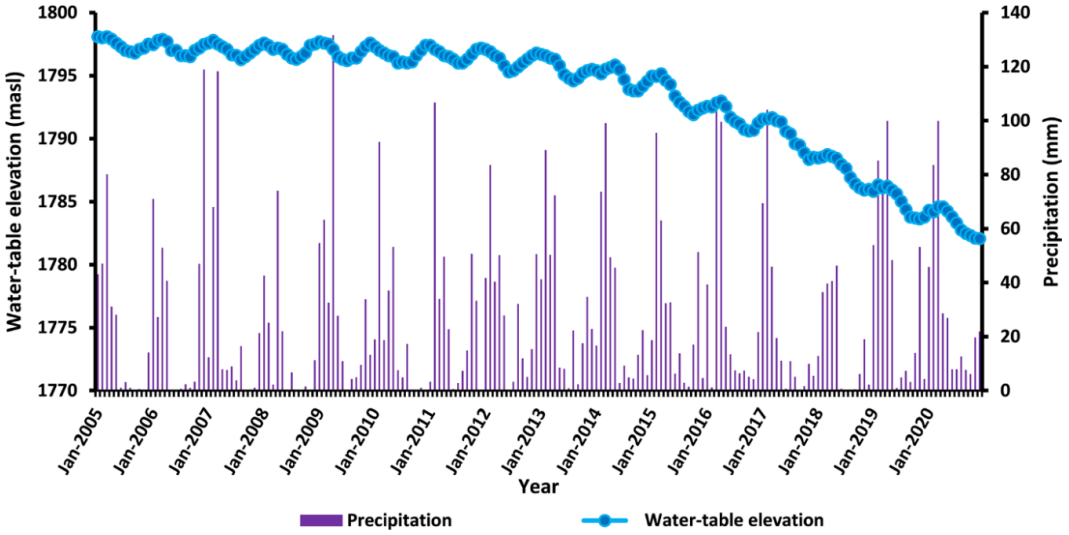

Fig 4. Changes in Groundwater Level in the Kabul Basin (2005-2020)

In areas of the aquifers where the water table is shallow, groundwater levels are sensitive to seasonal changes. During the rainy season, the water table rises after a few weeks of precipitation. Generally, groundwater levels decrease during the dry period (May to December) and increase during the rainy season (January to April) each year.

Impact of land use/land Cover on Groundwater

In the study area, four types of land use have been identified (Figure 5). The land use map illustrates how different land use and land cover (LULC) classes have shifted over time across various regions. Notably, agricultural land has significantly decreased, from 106.5 square kilometers in 2000 to 72.5 square kilometers in 2020. Conversely, urban areas have expanded substantially, increasing from 160.9 square kilometers in 2000 to 410.2 square kilometers in 2020. Additionally, barren lands have reduced from approximately 762.6 square kilometers in 2000 to 546.3 square kilometers in 2020. The LULC analysis indicates a significant increase in built-up areas in Kabul city between 2000 and 2020, with a notable expansion of new urban areas towards the city's outskirts.

Groundwater Flow Directions

Natural groundwater recharge in the Kabul Basin has been impacted by rapid urbanization, leading to a decrease in recharge in urban areas due to the construction of buildings and roads. Figure 6 depicts groundwater level contours and flow directions for the aquifer system in December 2004 and December 2020. The contour lines for groundwater levels in 2004 and 2020 are shown in blue and purple/dark purple, respectively.

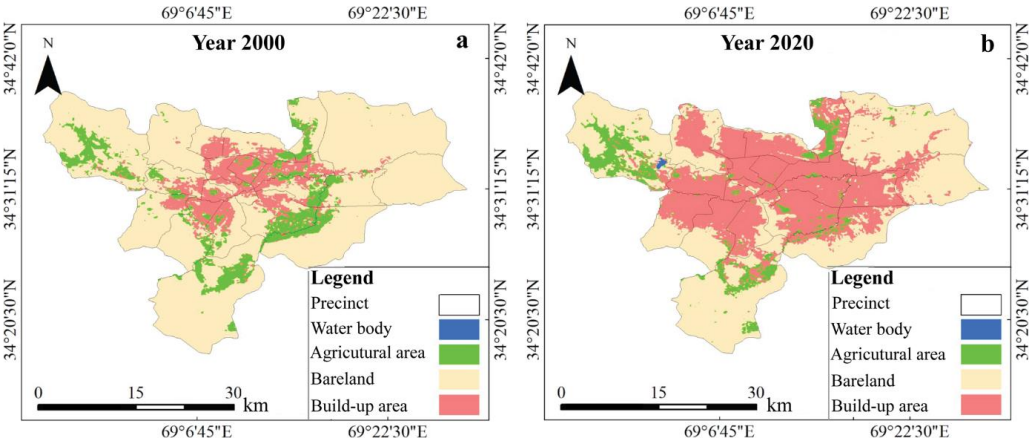

Fig 5. Groundwater Contour Lines and Flow Directions in December 2004 and December 2020 for the Aquifer System

Figure 7 illustrates significant changes in groundwater flow direction over the study period. In 2004, groundwater flow moved from the west and southwest towards the east along the rivers in the western basin and from the south and southwest towards the basin's center, subsequently flowing north and east in the eastern basin. According to Figure 6, groundwater from the Paghman-Darulaman aquifer was discharged into the central Kabul aquifer through the narrow Shir Darwaza pass. By 2020, the flow direction in the western basin had shifted, with groundwater now flowing towards the central part of the basin. While the groundwater flow direction in the eastern basin remained similar to 2004, changes are evident in the central and northwestern parts of the basin, where flow has become concentrated towards the northwest. These changes in groundwater flow direction are primarily attributed to excessive pumping and rapid, irregular urbanization.

Additionally, Figure 7 illustrates a decline in groundwater levels in the Kabul aquifer from 2007 to 2020. The most significant reductions have occurred in the southwestern region of the Paghman-Darulaman aquifer and the northwestern part of the central Kabul aquifer. This decline is primarily due to reduced aquifer reserves, increased population, and heightened groundwater use for urban and agricultural purposes. Conversely, the areas with the smallest decline are in the eastern and northeastern parts of the central Kabul aquifer, where groundwater levels have remained relatively stable throughout the study period.

To address the groundwater depletion in the Kabul Basin, it is essential to implement effective management strategies. These should focus on reducing groundwater exploitation, enhancing natural recharge, and ensuring the sustainability of groundwater resources. Key measures

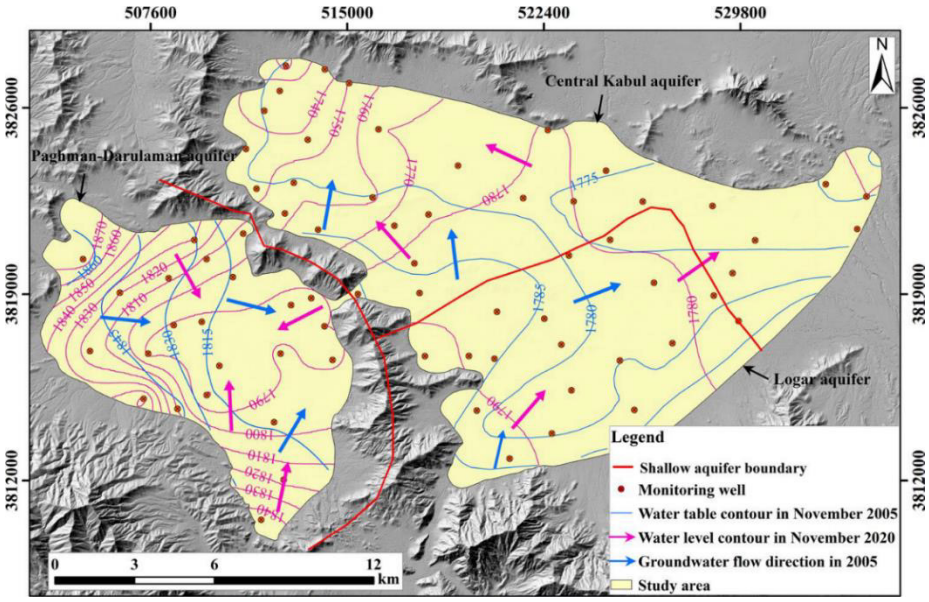

Fig 6. Horizontal distribution of hydraulic head (meters) and groundwater flow directions in December 2004 and December 2020.

include promoting water conservation, adopting artificial recharge techniques, and developing alternative water sources. Additionally, efficient monitoring and regulation of groundwater extraction are crucial to prevent overexploitation.

Figure 8 shows that, over the 13-year study period, groundwater levels throughout the Kabul Basin have generally decreased, with the exception of a small area in the Begrami section, where water levels have increased by approximately 2 meters (MeldebeKova et al., 2020). This increase in the Begrami section is likely due to river recharge and the return of irrigation water (Saffi, 2019). The decline in groundwater levels has led to the drying up of most shallow wells in the northwestern and southwestern parts of the study area (Saffi, 2019; Zaryab et al., 2022).

Given the current trends, groundwater resources in the Paghman-Darulaman and central Kabul aquifers are expected to continue declining. As illustrated in Figure 7, the Afshar and Alauddin water lands in the Paghman-Darulaman aquifer (Mills, 2020) are significant sources of groundwater, with substantial annual discharge through public water supply wells. Additionally, rapid and unplanned urbanization in the western basin has led to a proliferation of private and public wells in the Paghman-Darulaman aquifer (Noori & Singh, 2023; Pereira et al., 2009). Notably, almost all deep wells (>150 meters) drilled in the past decade have been located in the Paghman-Darulaman and central Kabul aquifers. The surge in water demand due to rapid urbanization has exacerbated groundwater overexploitation,

particularly in the southwestern Paghman-Darulaman and northwestern central Kabul aquifers. To mitigate this, it is crucial to reduce water extraction from the Afshar and Alauddin water lands while increasing extraction from the Logar water lands.

A more precise approach to estimating the volume of declining groundwater resources involves combining groundwater level change maps with maps of aquifer thickness and properties. Several studies have assessed the rate of groundwater decline in the Kabul aquifer using various methods, including water level measurements, groundwater modeling, and remote sensing data.

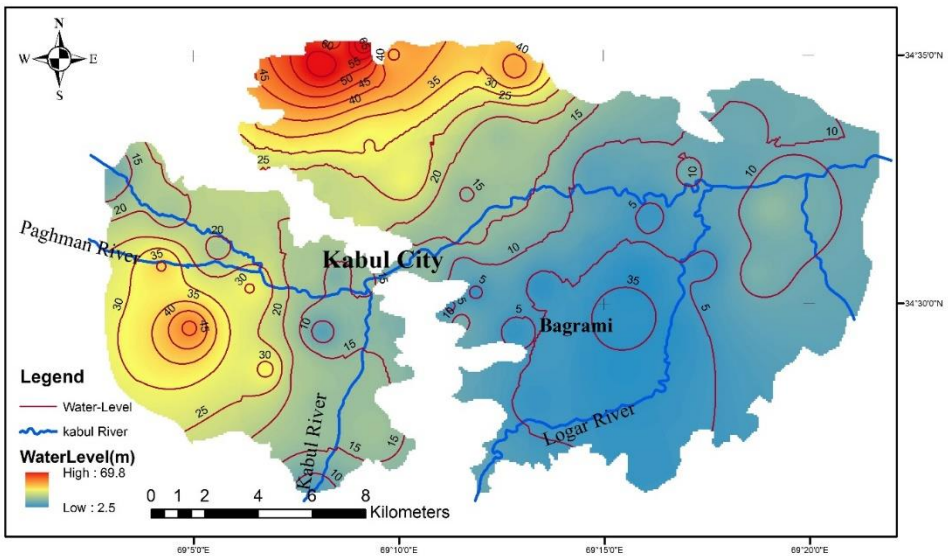

Fig 7. Changes in groundwater level from November 2007 to November 2020

Fluctuations Of Groundwater Level

According to Figure 8, the average groundwater level in the Kabul Basin decreased by approximately 16.5 meters from 2007 to 2020. The aquifer spans a total area of 271 square kilometers, with a specific yield estimated at 0.08. This results in an estimated loss of 358 million cubic meters of water from the Kabul aquifer over the study period. The decline in groundwater resources is closely linked to rapid urbanization within the Kabul Basin.

The hydrograph for the city, along with maps showing changes in the groundwater level of the Paghman-Darulaman aquifer, indicates that the average static water level at a depth of 20 meters decreased by about 0.55 meters from 2007 to 2020 (Figure 8). Research suggests that high population densities have led to localized reductions in groundwater levels, attributed to increased net recharge from domestic sewage wells, industrial and agricultural activities, and intensified water extraction compared to the overall groundwater level in the Kabul Basin.

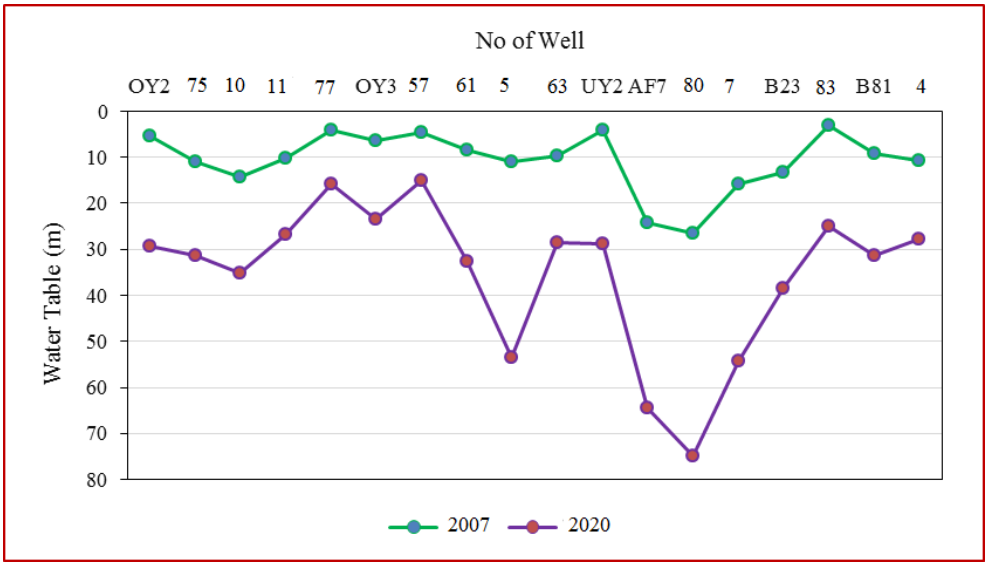

Fig 8. Changes in groundwater level of upper Kabul (Paghman-Darulaman)

The water levels in wells observed in Kabul city have been analyzed (Figure 8). Recent groundwater extraction has caused a gradual decline in groundwater levels. Changes in water levels for wells 148 (OY2), 152 (OY3), and 140 (TW3) are illustrated in Figure 9.

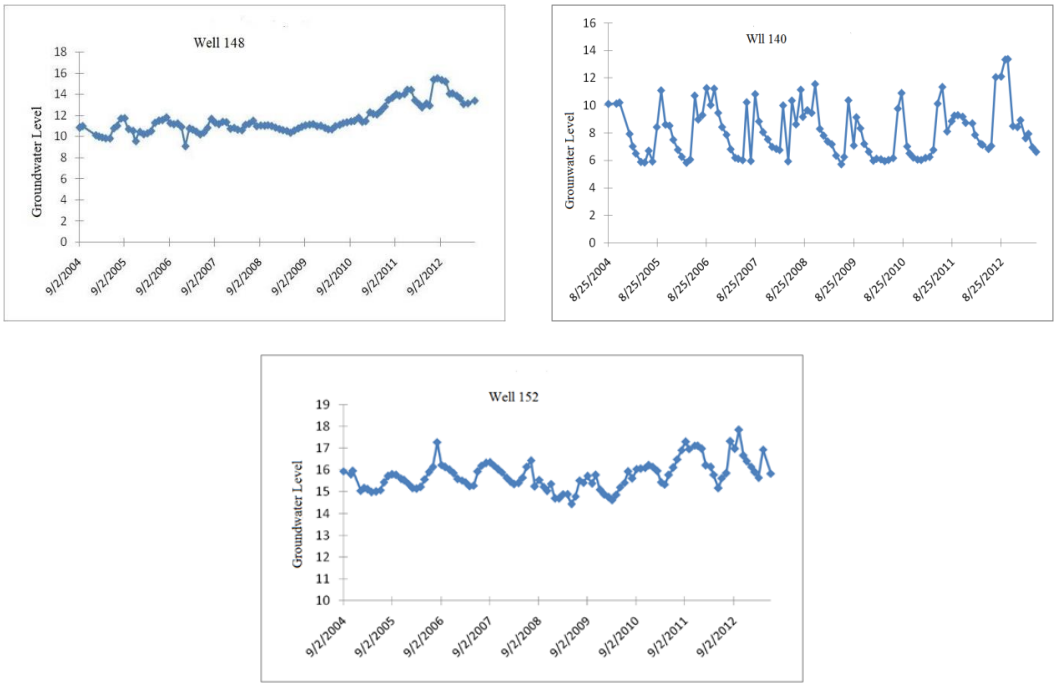

Fig 9. Fluctuations of underground water depth in observation wells 140, 148 and 152

Rapid urbanization and the overexploitation of groundwater resources in the Kabul Basin have adversely affected both dryland and aquatic ecosystems. Extensive groundwater extraction has led to the complete desiccation of the Heshmat Khan wetland (Saffi, 2019). According to a study by MeldebeKova et al. (2020), vertical subsidence of up to 5.3 centimeters per year was observed in the southwestern part of the Paghman-Darulaman Basin, where groundwater levels have significantly declined due to overuse. Additionally, rapid urbanization has significantly altered groundwater flow patterns in both the Paghman-Darulaman and Central Kabul aquifers.

Water Balance Of Kabul Basin

According to research conducted by the Japan International Cooperation Agency in 2011, the total and average water balance of the Kabul Basin over a 10-year period is presented. The data show that the surface water balance has been slightly negative on average over the past decade, with a deficit of 746 million cubic meters per year, which is approximately 0.5% of total precipitation. The total water balance for the Kabul Basin can be expressed by Equation 2:

$$\Delta S = P + Q_{in} - E - ET - Q_{out} - A \quad (2)$$

Where:

ΔS = Change in storage

P = Precipitation

Qin = Surface water inflow

E = Evaporation

ET = Evapotranspiration

Q_{out} = Surface water outflow

A = Abstraction (groundwater withdrawal)

This equation encompasses all major components of the water balance in the basin, including inputs (precipitation and surface water inflow), outputs (evaporation, evapotranspiration, surface water outflow, and groundwater abstraction), and the resultant change in storage.

The primary source of surface water inflow, derived from river flow, amounted to 351.8 million cubic meters per year (70.2%), followed by precipitation, which contributed 146.6 million cubic meters per year (29.2%). Major runoff losses were 325.2 million cubic meters per year (64.8%), with evaporation and transpiration accounting for 115.4 million cubic meters per year (23.0%). Recharge from the surface system was 25.2 million cubic meters per year, representing approximately 5% of total surface losses and 17.2% of precipitation (Japan International Cooperation Agency, 2011).

Total water balance of surface and groundwater in the Kabul Basin (2000–2009). This table summarizes key hydrological components, including precipitation, surface water inflow, recharge, and groundwater abstraction. Data show a slightly negative water

Table. 1 -The total water balance of surface and groundwater in the Kabul Basin for the years 2000-2009 (JICA).

Surface Water Balance Unit; TCM/year

Basin	Rain	Run-in	Inlet	Inundate	Recharge	Evap	Run Off	Dam Out	Sur Bal
Darulaman	30722.0	293919.7	123788.6	182.1	7578.3	22161.8	418839.8	0.0	33.0
Central Kabul	28706.2	681391.8	0.0	13699.7	6953.0	22056.9	661958.1	20668.0	-138.8
Logar	39180.2	469239.4	228025.0	1509.1	10698.1	31065.9	681494.1	15761.2	-1066.8
Total	98608.5	1444550.8	351813.6	3091.0	25229.3	75284.5	1762292.0	36429.2	-1172.6
Basin Total	146611.0	0.0	351813.6	3091.0	25229.3	115387.0	325216.0	36429.2	-734.0

Unit; TCM/year

Groundwater balance

Basin	Recharge	Inflow	Inundate	PmpUp	Outflow	SubBal	Volume
Darulaman	7578.3	6242.1	182.1	12759.6	2333.8	-1455.1	5509653.9
Central Kabul	6953.0	6276.1	1399.1	4138.4	8800.0	-1109.1	3830789.4
Logar	10698.1	5406.4	1509.1	8129.8	6632.2	-166.7	4846915.9
Total	25229.3	17924.6	3091.0	25027.7	17766.2	-2730.9	14187359.2
Basin Total	25229.3	4369.0	3091.0	25027.7	3210.0	-2730.9	13028448.0

balance in the basin, highlighting an average annual deficit of 746 million cubic meters. Surface water runoff accounts for a significant loss, while groundwater abstraction contributes to the declining storage trend. These findings emphasize the urgent need for water conservation measures and improved management practices in the Kabul Basin and Summary of physical and chemical results of groundwater samples from the Kabul aquifers (2004 and 2020). This table compares critical water quality parameters, including pH, electrical conductivity (EC), and dissolved oxygen (DO), across two sampling periods. The data reveal a marked increase in EC values, indicating rising groundwater salinity. These changes suggest worsening water quality, likely due to over-abstraction and contamination from urban and agricultural activities. The findings underscore the need for improved water quality monitoring and targeted interventions to mitigate salinity risks in the Kabul aquifers (Table 1).

In the groundwater system, the primary source of recharge was 25.2 million cubic meters per year (85.2%) from surface water, followed by subsurface inflow at 4.4 million cubic meters per year (14.7%). The main groundwater loss was due to pumping, which accounted for 25 million

cubic meters per year (79.8%), with groundwater outflow contributing 3.2 million cubic meters per year (10.2%). The total groundwater storage was 7,860 million cubic meters. Over a 10-year period, the average annual decline in groundwater storage was 2.7 million cubic meters, with approximately 9.2% attributed to groundwater abstraction and 1.9% to precipitation.

Figure 10 illustrates that the volume of surface water in the Kabul Basin significantly exceeds that of groundwater. The negative balance in groundwater storage is reflected in the overall decline in groundwater levels.

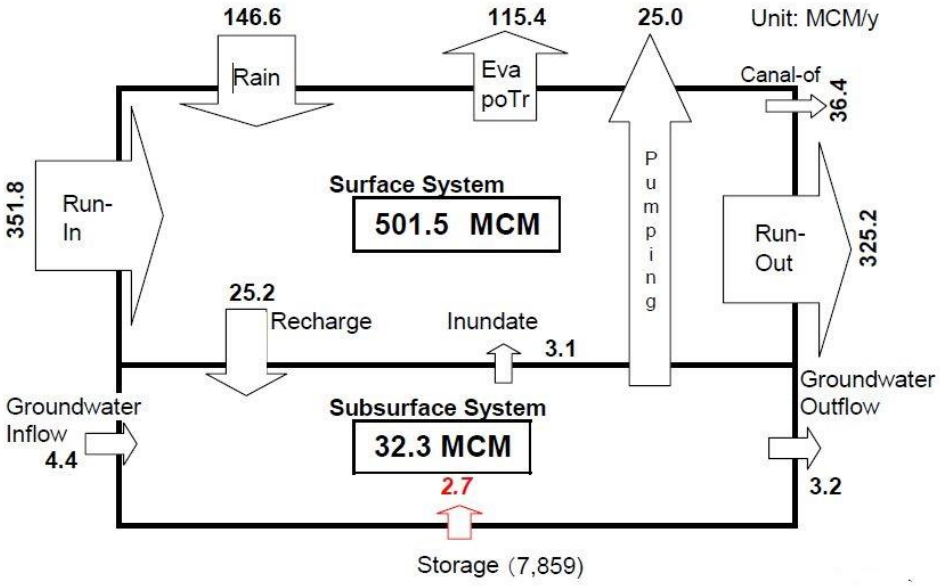

Fig 10. The total water balance of the Kabul basin (average of 2009-2000)

Figure 11 illustrates the factors influencing natural groundwater recharge in the Kabul aquifers. Data from river flow measurements indicate that in 2020, approximately 587 million cubic meters of water entered the Kabul Basin from the Paghman, Kabul, and Logar rivers. Of this, river infiltration into the subsurface accounted for about 9% of the total volume of water entering the basin in 2020.

Natural recharge data from river flows indicate that in 2020, approximately 587 million cubic meters of water entered the Kabul Basin from the Paghman, Kabul, and Logar rivers. Additionally, river infiltration into the subsurface constituted about 9% of the total water volume entering the basin that year.

Groundwater Recharge Rate

Rapid urbanization and the overexploitation of groundwater resources in the Kabul Basin have adversely impacted both dryland and aquatic ecosystems. The extensive overuse of groundwater has led to the complete desiccation of the Heshmat

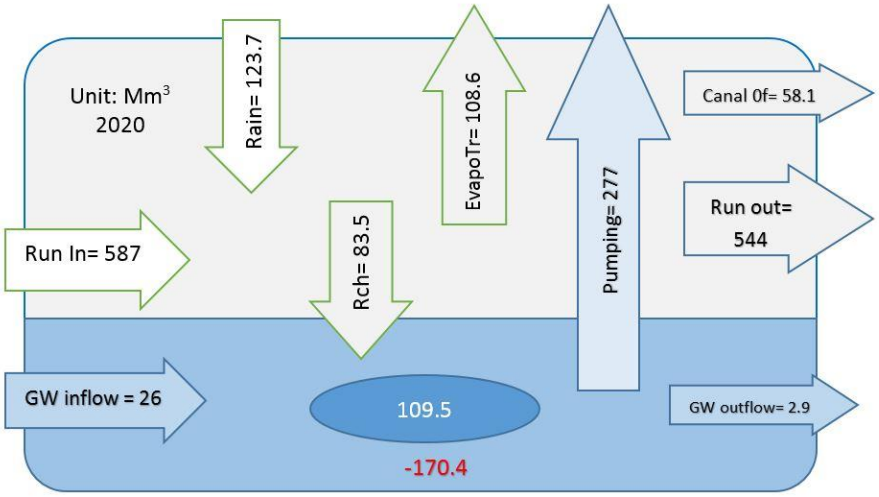

Fig 11. Total water balance of the Kabul basin (2020)

Khan wetland (Saffi, 2019). Research by MeldebeKova et al. (2020) indicates that the maximum vertical subsidence in the southwestern part of the Paghman-Darulaman Basin reached 5.3 centimeters per year, attributed to rapid groundwater level declines caused by overexploitation. Additionally, urbanization has significantly altered groundwater flow in the Paghman-Darulaman and Central Kabul aquifers.

To address these issues, urgent measures are needed to mitigate groundwater depletion and enhance recharge. Strategies should include promoting water conservation practices, implementing artificial recharge methods, and developing alternative water sources. Groundwater extraction must be regulated to match recharge rates, and a comprehensive water allocation policy for Kabul should be established. Those exceeding the prescribed water limits should face penalties three times the standard rate.

Moreover, adjustments in industrial practices are necessary to resolve conflicts between water supply and demand. Potential water resources in the Kabul Basin, such as the Maidan, Panjshir, and Salang rivers, should be utilized to ease the pressure on Kabul's aquifers. Managed Aquifer Recharge (MAR) projects, like the pilot project conducted by DACAAR in Kabul from 2017 to 2020, which demonstrated local increases in groundwater levels, should be expanded to reduce aquifer stress.

Additionally, rainwater and surface water collection through recharge wells, pits, and channels can bolster groundwater levels during the rainy season. Prioritizing collected rainwater for household use before recharging groundwater and raising awareness about rainwater collection's importance are critical steps.

The key factors contributing to the decline in groundwater resources in the Kabul

Basin include:

Conversion of Irrigated Lands: Formerly irrigated lands and orchards around Kabul have been converted to residential areas, reducing natural water infiltration and groundwater replenishment.

Loss of Water Bodies and Grasslands: Historical wetlands and grasslands, such as the Ab-e-Chakan wetland and various grasslands around Kabul, which once played a significant role in groundwater regulation and purification, have been destroyed or degraded.

Increase in Impermeable Surfaces: The proliferation of concrete dams, roads, and other impermeable structures in Kabul has decreased groundwater recharge. Additionally, insufficient attention to engineering standards in construction and a lack of proper water and sewage infrastructure contribute to the problem.

Neglect of Conservation Buffers: Encroachment on conservation buffer zones around water stations exacerbates the issue.

Population Growth and Poor Management: The rapid increase in population, now exceeding 5.3 million, combined with inadequate management practices, has led to unsustainable groundwater extraction. Unauthorized well drilling further exacerbates the depletion.

Drought and Climate Change: Despite Afghanistan not being classified as a drought-prone country, persistent droughts and climate change have reduced snowfall, leading to decreased water availability and altered recharge patterns.

Decline in Vegetation Cover: The loss of vegetation in the Asmai Mountains and surrounding hills has increased rainwater runoff and decreased infiltration rates.

Inefficient Water Use: Inefficient and unregulated use of available water resources, coupled with a lack of conservation efforts, highlights the need for improved water management and conservation practices across various sectors.

Addressing these factors through targeted interventions and comprehensive management strategies is essential to reversing the trends of groundwater depletion and ensuring sustainable water resources for the Kabul Basin.

The Quality Status Of Groundwater Resources

The statistical parameters of groundwater samples collected from the Kabul aquifer in July to November 2004 and November 2020 are summarized in Table 2. The pH of the groundwater was neutral during both sampling periods. The average temperature of the groundwater samples remained consistent across both periods. Dissolved oxygen (DO) measurements indicated that the groundwater was aerobic in both sampling periods. Electrical conductivity (EC) values ranged from 497 to 8,290

µS/cm in 2004 and from 618 to 9,600 µS/cm in 2020. The highest EC values were recorded at sampling points 166.2 in 2004 and W15 in 2020, with values of 8,290 and 9,600 µS/cm, respectively. In 2004, approximately 73% of the groundwater samples had EC values exceeding 1,000 µS/cm, while in November 2020, 82% of the samples had EC values above this threshold. This increase may suggest a gradual rise in groundwater salinity, potentially driven by population growth and over-abstraction.

The majority of groundwater samples from the Kabul central and Logar aquifers exhibited moderately saline to saline characteristics, whereas nearly all samples from the Paghman-Darulaman aquifer were classified as fresh water. The broad range of EC values might be attributed to the presence of brackish lake deposits in the Kabul central aquifer, which could influence the variability in EC readings. Pollution maps based on various parameters are illustrated in Figure 12.

Shallow groundwater depths and sewage infiltration into the aquifer have led to various types of groundwater pollution.

Table 2. Summary of the physical and chemical results of sampling points in the Kabul aquifers.

parameter	Unit	Measured in July to November 2004				Measured in November 2020			
		Minimum	Mean	Maximum	SD	Minimum	Mean	Maximum	SD
PH		6.94	7.50	8.37	0.3	7.00	7.60	8.10	0.23
T	C^o	10.90	15.50	21.60	1.90	6.00	15.40	17.80	2.10
DO	mg/L	0.40	7.10	14.90	3.40	2.10	5.25	9.60	1.88
EC	µS/cm	497.00	1760.0	8290	837.0	618.0	1640.00	9600	3149.1
Ca^{2+}	mg/L	35.00	81.50	334.00	51.80	20.50	76.65	362.70	63.70
Mg^{2+}	mg/L	6.60	92.00	590.00	104.80	12.30	82.40	684.0	139.4
Na^{+}	mg/L	14.60	145.40	1630.00	244.30	20.50	94.15	3014.00	567.8
K^{+}	mg/L	2.00	8.30	31.60	5.50	2.16	7.05	74.00	14.00
HCO_3^{-}	mg/L	102.50	402.20	651.10	141.60	183.00	429.90	840.00	173.40
Cl^{-}	mg/L	8.20	208.90	2750.00	3030.00	7.30	135.00	3997.00	838.60
SO_4^{2+}	mg/L	16.10	233.80	3030.00	492.00	19.80	114.00	4573.00	988.40
NO_3	mg/L	1.00	31.00	182.00	33.20	3.98	13.72	120.41	21.00

This contamination is a significant factor contributing to the high infant mortality rates in these areas. The following sections will assess the quality of pollutants in the water wells of Kabul city. A critical issue in this watershed is the inadequate water supply and sewage collection infrastructure in residential areas. In many residential areas, particularly in villages, drinking water is sourced from shallow

hand-dug wells that are situated near sewage absorption wells, exacerbating the risk of contamination.

It should be noted that the results of this study are consistent with the previous studies that conducted research in this field, such as (Tani & Tayfur, 2021; Manawi et al. 2020).

The comprehensive analysis of groundwater dynamics in the Kabul Basin from 2005 to 2020 reveals several critical issues that warrant in-depth discussion:

The observed average decline of 16.5 meters in groundwater levels over the

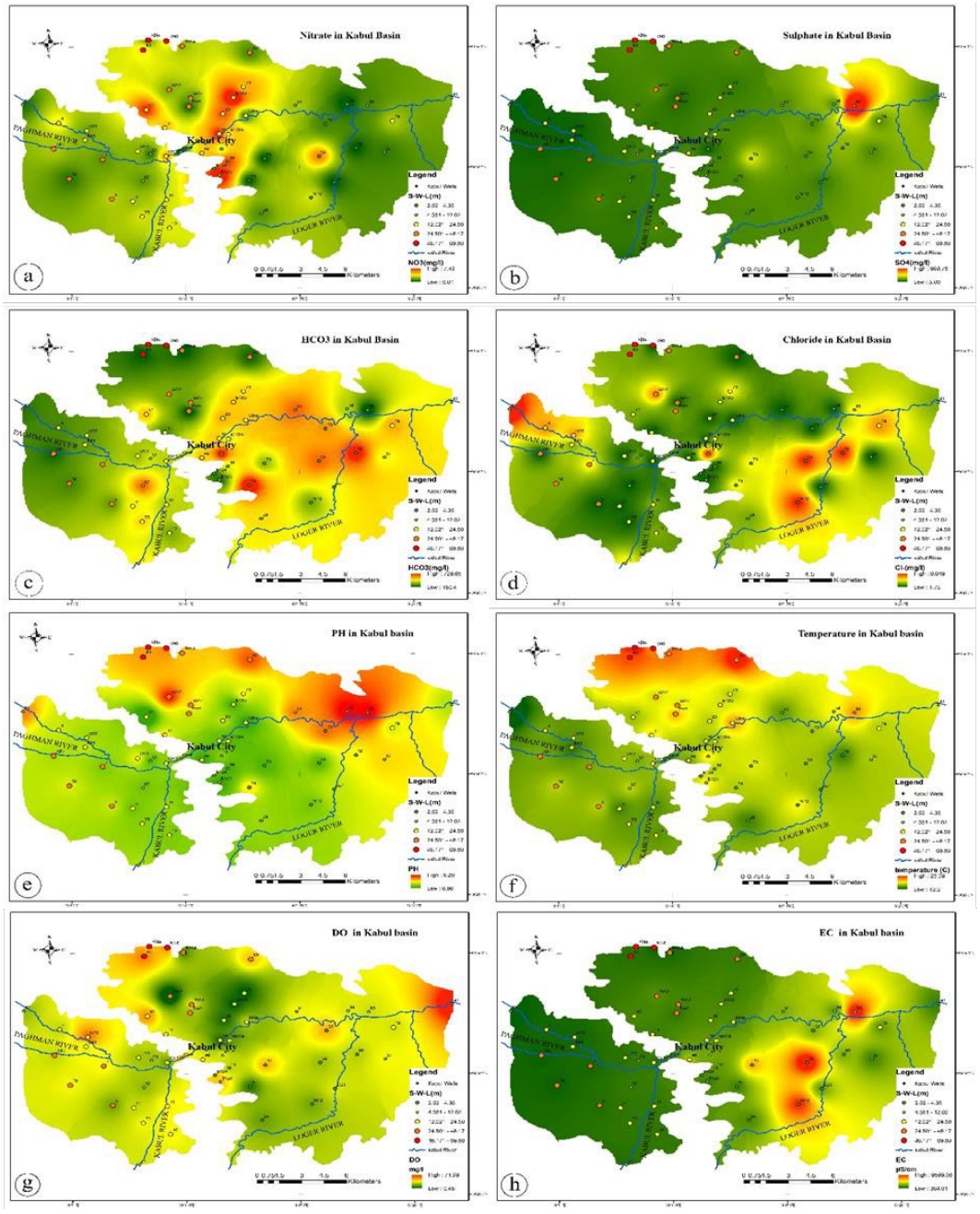

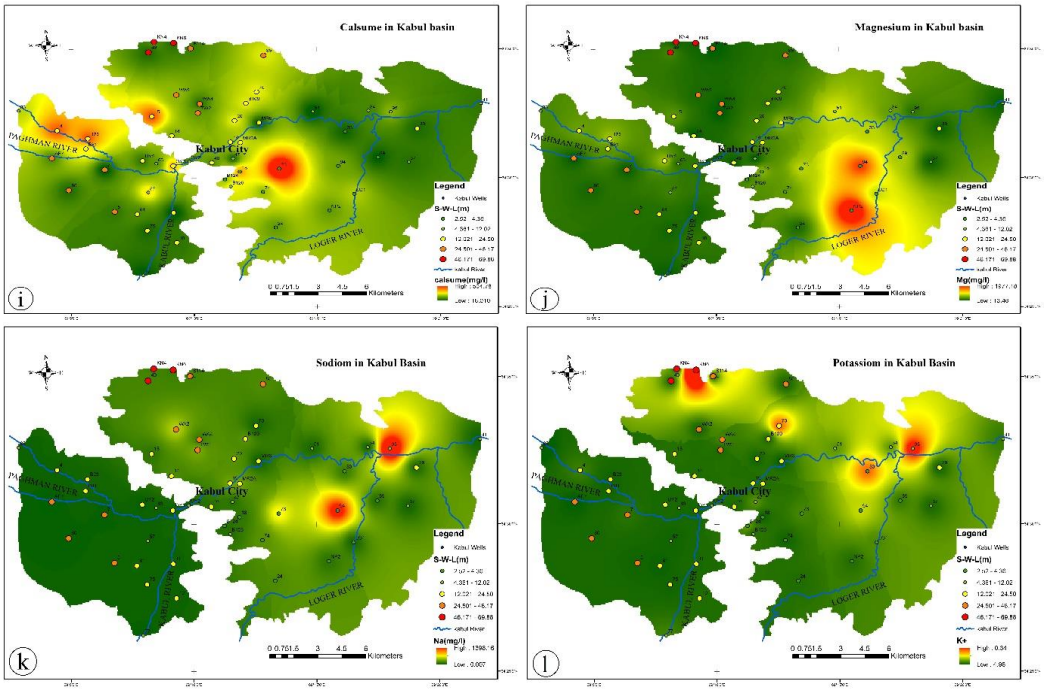

Fig 12. Map of result: a) Nitrate, b) Sulphate, c) HCO3, d) Chloride, e) PH, f) Temperature, g) DO, h) EC, i) Calcium j) Magnesium, k) Sodium, l) Potassium

13-year study period, with localized declines of up to 12 meters, is a significant concern. This depletion rate, averaging 80 cm per year in some areas, exceeds natural recharge rates by a factor of two to six. The alteration in groundwater flow directions, particularly in the Paghman-Darulaman and Central Kabul aquifers, suggests a fundamental shift in the basin's hydrogeological dynamics. These changes are likely driven by intensive pumping and unregulated urban expansion, which have disrupted the natural groundwater flow patterns.

The dramatic land use changes observed, with urban areas expanding from 160.9 km² to 410.2 km² between 2000 and 2020, have significantly altered the basin's hydrological balance. The reduction in agricultural areas and increase in impervious surfaces has likely decreased natural recharge rates and accelerated surface runoff. This urbanization-induced hydrological alteration presents a challenge for sustainable groundwater management, as it reduces the system's natural resilience to over-extraction.

The increase in groundwater samples with electrical conductivity (EC) values exceeding 1,000 µS/cm from 73% in 2004 to 82% in 2020 indicates a concerning trend of increasing salinity. This trend may be attributed to several factors, including over-extraction leading to the mobilization of deeper, more saline water, and potential contamination from urban

and agricultural sources. The spatial variability in EC values, particularly in the Central Kabul aquifer, suggests complex hydrogeochemical processes that warrant further investigation.

The water balance analysis revealing groundwater extraction (277 million m^3 in 2020) significantly exceeding natural recharge rates highlights the unsustainable nature of current water use practices. The identification of river infiltration as the main recharge component (9% of total inflow) underscores the importance of surface-groundwater interactions in the basin's hydrology. This imbalance raises questions about the long-term viability of current extraction rates and the need for integrated surface and groundwater management strategies.

The desiccation of the Heshmat Khan wetland and observed land subsidence (up to 5.3 cm/year in some areas) are tangible manifestations of the ecological impacts of groundwater depletion. These environmental changes may have cascading effects on local ecosystems and potentially on the structural integrity of urban infrastructure. The loss of wetlands also reduces the natural water purification and flood mitigation services these ecosystems provide.

While not explicitly quantified in the study, the mention of recurrent droughts and climate variability suggests an additional stressor on the groundwater system. The interplay between climate-induced recharge variability and increased extraction demands during dry periods likely exacerbates the observed groundwater depletion trends.

The rapid population growth in Kabul, from approximately 1 million in 2001 to 5.3 million in 2021, with over 70% residing in unplanned settlements, presents significant challenges for water resource management. The socio-economic implications of groundwater depletion, including potential water scarcity and quality issues, may disproportionately affect vulnerable populations and could lead to social and economic instability if not addressed.

The study's findings highlight the urgent need for robust groundwater management policies and practices. The current imbalance between extraction and recharge, coupled with the complexities of rapid urbanization and climate variability, necessitates a multi-faceted approach to water resource management. This may include demand management strategies, artificial recharge initiatives, and the development of alternative water sources.

Conclusion

Since 2001, Kabul city has experienced rapid urbanization, with groundwater serving as the primary source for residential, agricultural, and industrial use. The results indicate that groundwater

resources in Kabul have been depleting faster than they are being replenished. Analysis reveals significant changes in land use and vegetation cover within the Kabul basin. Notably, agricultural areas have substantially decreased, while urban areas have expanded significantly.From 2005 to 2011, the decline in groundwater levels was gradual. However, between 2011 and 2020, this decline accelerated markedly. Groundwater levels have decreased considerably across most parts of the basin, particularly in the northwestern section of the central Kabul aquifer and the southeastern Paghman-Darulaman aquifer. The hydrograph illustrates that groundwater levels in some areas have fallen by 12 meters from 2005 to 2020, at an average rate of 80 centimeters per year, significantly altering local groundwater flow patterns during the study period. Additionally, changes in groundwater flow, especially in the Paghman-Darulaman and central Kabul aquifers, reflect substantial disruptions to the natural hydrogeological system. These changes are more pronounced than those observed in other rapidly urbanizing basins, suggesting a higher vulnerability of the Kabul aquifer system to anthropogenic influences. These findings collectively indicate that the Kabul Basin is approaching a critical threshold of water resource sustainability. The situation demands immediate and comprehensive action to avert an impending water crisis.

Key recommendations include:

- Implementing stringent groundwater extraction regulations
- Investing in artificial recharge projects and water-efficient technologies
- Developing alternative water sources such as rainwater harvesting and wastewater reuse
- Improving urban planning to enhance natural recharge

While the study provides valuable insights, it also reveals knowledge gaps that require further investigation. These include a more detailed understanding of the spatial and temporal variability in recharge processes, the impact of climate change on long-term groundwater dynamics, and the potential for managed aquifer recharge in mitigating depletion trends. The results clearly indicate that the extensive decline in groundwater in the Kabul basin is significantly attributed to anthropogenic factors. If appropriate measures are not taken at this stage, the decline in groundwater is likely to continue rapidly, especially in densely populated urban areas. Ultimately, the residents of Kabul will face severe water scarcity in the near future.This emphasizes the urgent need for implementing effective management strategies to ensure sustainable use of groundwater resources in the region. The results highlight the importance of sustainable groundwater management in the face of rapid urbanization, increasing

water demand in the Kabul basin, and the necessity of joint efforts to address this issue. Moreover, Future research should focus on developing predictive models to forecast long-term groundwater trends under various management scenarios, enabling proactive and sustainable water resource management in this rapidly evolving urban environment.

References

Afghanistan Public Policy Research Organization. (2012). Classification or accommodation: Newcomers and host communities in Districts 5, 7, and 13 in Kabul. Migration and Urban Development, Kabul.

Barbe, D. (2013). Population displacement and urban transition in Kabul city: Current spatial structure, Sciences Po-Fall, social issues, and recommendations for a new development plan.

Carlston, C. W. (1963). Drainage density and stream flow, U.S. *Geological Survey Professional Paper*. https://doi.org/10.3133/pp422C

Dehkordi, P., and Pourmoghaddas, H. (2006). Investigating the impact of industrial wastewater on the chemical quality of groundwater: A case study, Proceedings of the First Specialized Conference on Environmental Engineering. [In Persian]

Eftekhari, M., Khozeymehnezhad, H., & Elyasi, A. H. (2024). Prediction and assessment of groundwater quality in a geographic information system environment using machine learning methods (semi-arid regions). *Journal of Chinese Soil and Water Conservation*, 55(2), 84-93. https://doi.org/10.29417/JCSWC.202406_55(2).0004

Ghayomian, J., Mohseni, M., Feiznia, S., Nouri, B., and Malekian, A. (2007). Application of GIS techniques to determine areas most suitable for artificial groundwater recharge in a coastal aquifer in southern Iran, *Journal of Asian Earth Sciences*, 29(2–3), 364–374. https://doi.org/10.1016/j.jseaes.2006.11.002

Hadizadeh, H., Bakhshi, A., Besharati, J., and Jafarzadeh, F. (2009). Hydrogeochemistry and geochemistry of Quaternary sediments in western Mashhad (from Golestan Dam to Kahou Village) for assessing toxic elements in soil and water, Research Committee of Khorasan Razavi Regional Water Company. [In Persian]

Hajian, F. (2021). Analysis of climate variables and groundwater levels in the Nishapur watershed. In Proceedings of the 10th National Conference on Energy and Sustainable Environmental Resources. Islamic Azad University, Nishapur Branch, Nishapur. [In Persian]

Hussaini, M., Farahmand, A., Sherstha, S., Neupane, S., & Abrunhosa, A. (2021). Site selection for managed aquifer recharge in the city of Kabul, Afghanistan, using a multi-criteria decision analysis and geographic information system. *Environmental Earth Sciences*, 80(12). https://doi.org/10.1007/s10040-021-02408-x.

Ibrahim, A., Ehrampoush, M., Ghaneian, M., Davoudi, M., Hashemi, H., & Behzadi, S. (2010). Investigation of the chemical quality of groundwater in the vicinity of the municipal landfill, in 2009. *Journal of Health System Research*, 6(2), 24-30. [In Persian].

Japan International Cooperation Agency (JICA). (2011). The study on groundwater resources potential in Kabul basin in the

Islamic Republic of Afghanistan: Final report, Part 2 (pp. 18-19).

Karbasi, A., & Bayati, A. (2001). Biogeochemistry (p. 256). Tehran: Kavoshghalam Publishing. [In Persian]

Khodabandeh Baygi, R., Ghezelsofloo, A. A., Eftekhari, M., and Rastgoo, M. (2023). Impacts of climate change on the statistical trends of monthly and annual flood discharges in the Kashafrood River Basin, Iran, *Journal of Drought and Climate Change Research*, 1(2), 27–40. https://doi.org/10.22077/jdcr.2022.5797.1000

Mack, T. J., Chornack, M. P., Coplen, T. B., Plummer, L. N., Rezai, M. T., & Verstraeten, I. M. (2013). Availability of water in the Kabul Basin, Afghanistan. U.S. *Geological Survey Fact Sheet* 2010-3037 (4 p.). https://pubs.usgs.gov/fs/2010/3037/

Mahdavi, A., Tabatabaei, S. H., Nouri, M., & Mahdavi, R. (2010). Identification of groundwater artificial recharge sites using fuzzy logic: A case study of Shahrekord Plain, Iran. *Iranian Journal of Irrigation and Drainage*, 6(2), 1013–1027. [In Persian]

Manawi, S. M. A., Nasir, K. A. M., Shitu, M. S., & Sediqi, M. N. (2020). Urban flooding in the northern part of Kabul City: Causes and mitigation. *Earth Systems and Environment*. https://doi.org/10.1007/s41748-020-00165-7.

Meldebekova, G., Yu, C., Li, Z., & Song, C. (2020). Quantifying ground subsidence associated with aquifer overexploitation using space-borne radar interferometry in Kabul, Afghanistan. *Remote Sensing*, 12(15), 2461. https://doi.org/10.3390/rs12152461.

Mills, L. (2020). Regional groundwater model.

Mouser, P., & Rizzo, D. (2004). Evaluation of geostatistics for combined hydrochemistry and microbial community fingerprinting at a waste disposal site. In Proceedings of the 2004 World Water and Environmental Resources Congress (pp. 1-11). Environmental and Water Resources Institute of the American Society of Civil Engineers, Salt Lake City.

National Statistic and Information Authority (NSIA). (2021). Estimated population of Afghanistan 2020–21. Kabul: National Statistic and Information Authority.

Noori, A. R., & Singh, S. K. (2023). Assessment of seasonal groundwater quality variation employing GIS and statistical approaches in Kabul basin, Afghanistan. *Environmental Development and Sustainability*. https://doi.org/10.1007/s10668-022-02876-5.

Pereira, L. S., Cordery, I., & Lacovides, I. (2009). Groundwater use and recharge. In Coping with Water Scarcity (Chapter 7, pp. 133-174). Springer Science. https://doi.org/10.1007/978-1-4020-9579-5_7

Ranjbar, M., & Jafari, N. (2009). Investigation of the factors influencing land subsidence in Eshtehard Plain. *Iranian Geographical Society Journal*. 6(19), 155-166. [In Persian]

Saffi, M. H. (2019). National alarming on groundwater natural storage depletion and water quality deterioration of Kabul City and immediate response to the drinking water crises. Kabul: DACAAR.

Shroder, J., & Ahmadzai, S. J. (2016). Trans boundary water resources in Afghanistan: Climate change and land-use implications.

Tani, H., & Tayfur, G. (2021). Identification of groundwater potential zones in Kabul River Basin, Afghanistan. *Groundwater for Sustainable Development*, 15, 100666. https://doi.org/10.1016/j.gsd.2021.100666

Valayati, S. (2002). The impact of excessive

groundwater extraction from wells on salinization of the Jangal Plain aquifer (Torbat Heydarieh). *Geographical Research Quarterly*, 67, 91-106. [In Persian]

Zaryab, A., Naseery, H. R., & Alijani, F. (2022). The effects of urbanization on the groundwater system of the Kabul shallow aquifers, Afghanistan. *Hydrogeology Journal*. 30,429-443. https://doi.org/10.1007/s10040-021-02445-6.

Original Article

Journal of Drought and Climate change Research (JDCR)

Winter 2025, Vol. 2, No. 8, pp 31-54

10.22077/jdcr.2024.7510.1067

Removal Efficiency of Sugarcane Bagasse Biochar for Uptake of Sodium Ion from Aqueous Solution: Nonlinear Isotherm and Kinetics Modelling

Jalil Kermannezhad[1], Hassan TorabiPoodeh[2*], Elham Ghanbari-Adivi[3,4], Babak ShahiNejad[5]

1- Ph.D student, Department of Water Engineering, Faculty of Agriculture, Lorestan University, KhoramAbad, Iran.
2- Professor, Department of Water Engineering, Faculty of Agriculture, Lorestan University, KhoramAbad, Iran.
3- Associate Professor, Department of Water Engineering, Faculty of Agriculture, Shahrekord University, Shahrekord, Iran.
4- Nanotechnology Research Center, Shahrekord University, Shahrekord, Iran.
5- Assistant Professor, Department of Water Engineering, Faculty of Agriculture, Lorestan University, KhoramAbad, Iran.
*** corresponding author: ghanbariadivi@sku.ac.ir**

Keywords:
Activation, KOH (Potassium hydroxide), Microwave, Magnetization.

Received:
13 April 2024

Revised:
16 Aug 2024

Accepted:
18 Aug 2024

Abstract

This research examines sodium removability from agricultural wastewater using sugarcane bagasse sorbents, which helps ease the pressure on water resources during droughts. The biochar was produced in an electric furnace, activated with KOH, microwave-heated, and magnetized using a 2:1 ratio of Iron (III) chloride hexahydrate to Iron (II) sulfate heptahydrate. Three KOH-to-biochar ratios, microwave powers, and activation times were used, while sodium concentrations in wastewater samples were adjusted to 2, 4, and 8 g/l with sodium nitrate. Results indicated that higher initial sodium concentrations improved removability. Activated nano biochar achieved 74.4% more sodium removal than non-nano biochar on average. Magnetization reduced sodium removal by an average of 18.8%, with reductions ranging from 10.9% to 31.6%. The activated nano biochar's removability was 1.6 times greater than that of the non-activated version, and magnetization decreased efficiency by 20%. The highest sodium removal occurred at a 3:1 activator-to-biochar ratio during the 200 and 400 W treatments, achieving maximum removability of 61.4% for activated nano biochar and 58.3% for the magnetized version.

How to cite this article:
Kermannezhad, J., TorabiPoodeh, H., Ghanbari-Adivi, E. & ShahiNejad, B. (2024). Removal Efficiency of Sugarcane Bagasse Biochar for Uptake of Sodium Ion from Aqueous Solution: Nonlinear Isotherm and Kinetics Modelling. *Journal of Drought and Climate change Research* (JDCR), 2(8), 31-54. 10.22077/jdcr.2024.7510.1067

Introduction

Irrigation water salinity is a very serious problem in different parts of the world, especially in arid and semi-arid regions. The increasing prevalence of sodium ions in freshwater systems has raised concerns regarding its environmental impact and subsequent implications for water quality. Adsorption has emerged as a promising method for sodium removal from aqueous solutions, particularly with the application of biochar derived from agricultural byproducts such as sugarcane bagasse. This literature review delves into nonlinear kinetic and isotherm models that describe the adsorption processes of sodium ions onto modified sugarcane bagasse biochar. The use of saline water in agriculture can have significant environmental, economic, and social consequences. Irrigating with saline water increases the concentration of salts in the soil, which can lead to soil salinity. This reduces the ability of plants to absorb water and nutrients. Excess salts in the soil can hinder plant growth and performance. Plants experience stress in saline conditions, which may cause them to weaken or dry out. Salinity can decrease the yield of both agricultural and horticultural products. Additionally, the quality of produced goods is also affected. Also it can affect the physical and chemical properties of the soil, leading to changes in water behavior, such as permeability and water-holding capacity (Ehtaiwesh, 2022). Additionally, the rising demand for fresh water driven by population growth will intensify pressure on water resources in the future. This will make the reliance on saline and unconventional water sources a significant concern, particularly in regions already experiencing water scarcity. Meanwhile, agriculture, the largest consumer of water globally, suffers from the use of saline water, which not only diminishes crop yields but also degrades soil structure and harms the environment. Although such measures as leaching, local irrigation, cultivating saline-water-resistant crops and saline-fresh-water mixing can enable the use of saline water in irrigation, they have short-term effects and cannot fully solve the salinity problem (Ayers & Westcot, 1985; Siyal et al., 2002; Dudley et al., 2008; Naik & Panda, 2008). The wastewater desalination and its reuse is a relatively new approach in the water industry that solves saline-water problems through various methods, but it is uneconomical due to high equipment costs and energy consumption especially in agriculture where water consumption and costs are much higher. Adsorption is a process in which one substance becomes incorporated into another, typically involving a liquid adsorbing a gas or a solid absorbing a liquid or gas. It is distinct from adsorption, where molecules adhere to a surface. In environmental science and engineering, absorption is often

utilized to remove contaminants from air or water through various materials known as adsorbents (Pourhakkak et al., 2021). Common adsorbents used in these processes include activated carbon, zeolites, and resins. Each of these materials has its own strengths and weaknesses when it comes to capacity, selectivity, and environmental impact (Crini et al,. 2019). Activated carbon, zeolites, and resins are traditional adsorbents used for various applications such as water purification. Activated carbon is effective for adsorbing organic compounds but is costly to produce and maintain. Zeolites are useful for ion exchange, yet they may not remove organic contaminants, and high-quality varieties can be expensive and scarce. Resins are synthetic polymers that remove ions but are sensitive to pH and temperature, which can hinder their effectiveness, and their production poses environmental concerns. Overall, while these materials are valuable, they have significant limitations that may affect their practical applications (Yılmazoğlu, 2021).

Kinetic studies are essential for understanding the adsorption rates and mechanisms. Commonly used models include pseudo-first-order and pseudo-second-order kinetics. According to Ho and McKay (2000), pseudo-second-order kinetics often provides a better fit for adsorption data, indicating that chemisorption may be the rate-controlling step. Nonlinear regression techniques allow for more accurate parameter estimation in the context of adsorption kinetics. Nonlinear forms of the pseudo-second-order model have been utilized, leading to improved fit and understanding of the dynamics involved in adsorption (Revellame et al., 2020; López-Luna et al., 2019).

The understanding of how sodium ions interact with biochar under equilibrium conditions is crucial. Langmuir and Freundlich models are often employed. The Langmuir model assumes monolayer adsorption on a surface with a finite number of identical sites, while the Freundlich model is an empirical equation indicating multilayer adsorption. Recent work by Kasraee et al. (2022) highlights the applicability of nonlinear forms of these models in assessing adsorption behavior.

Nonlinear isotherm modeling allows for the fitting of adsorption data without linearization, which can introduce bias. By employing nonlinear regression analysis, researchers have observed better predictive capabilities in characterizing sodium uptake in MPPMC (the modified Pinus massoniana pollen microcarriers) systems (Li et al., 2024).

Factors such as pH, temperature, and modification techniques significantly impact the efficiency of sodium ion adsorption. Modifying sugarcane bagasse

through chemical alteration enhances the surface area and functional groups available for ion exchange (Mubarak et al., 2024).

The use of modified sugarcane bagasse biochar proves to be a viable option for sodium removal, supported by rigorous nonlinear kinetic and isotherm modeling. The effectiveness of adsorption depends on various factors, and continuous research into these mechanisms clarifies the pathways that lead to improved environmental remediation techniques.

As activated carbon is made from such inexpensive materials as wood, coal, oil, coke, sawdust and plant waste, it is quite economical and highly capable of removing a wide range of organic and inorganic pollutants from aquatic and gaseous environments (Wu et al., 2008; Jamil et al., 2010; Mehrabinia and Ghanbari-Adivi, 2022; Mehrabinia et al., 2021).

Natural materials and agricultural/ industrial wastes are effective and low-cost adsorbents due to their functional groups like hydroxyl and carboxyl. However, accurately predicting their adsorption processes is challenging because of their complex chemistry, requiring a deep understanding of the interactions involved (Kietlinska & Renman, 2005; Oliveira et al., 2005). Agricultural by-products primarily consist of cellulose, which, when submerged in water, acquires a negative charge and interacts with cations, leading to significant adsorption capacity for various cations (Shang et al., 2003). Rahal et al. (2023) investigated the removal of sodium ions from water by using date pits activated with sulfuric acid. They investigated the effect of activation time, initial sodium concentration, contact time and pH on sodium removal. The specific surface areas of natural and activated date pits were measured as 645.46 and 825.03 m^2/g, respectively. According to their results, the maximum sodium absorption capacity was observed at a contact time of 90 min, the initial concentration was 600 mg/l, the pH was 9.0 and the adsorbent dose was 0.1 g/l. Their findings showed that the Freundlich isotherm model and the pseudo-second order model had the best agreement with the measured values. Hettiarachchi et al. (2016) studied the efficiency of the phosphoric acid-activated coconut straw biochar in removing sodium and magnesium ions from saline water and showed that the removal rate of these ions from NaCl and $MgCl_2$ (0.2 mol/dm^3 standard solutions) was about 50%, which increased to 80 and 72%, respectively, under repeated filtrations. Musie et al. (2023) investigated the removal of sodium ions from water by using raw bean husk and raw bean husk activated with sulfuric acid. They investigated the ability to remove sodium ions by treated raw bean husk with different activation time and

concentrations of sulfuric acid. The initial concentration of sodium ions in their study was 1643 mg/l and the absorbent ratio of the adsorbent was 12.5 g/l. According to their results, the maximum removal was 27.8% for the activator concentration of 4 mol/l and the contact time of 6 hours. Also, the BET results for bean husk and activated bean husk were measured as 0.67 and 0.44 m^2/g, respectively. According to their results, the optimal removal results for bean husk and activated bean husk for a contact time of 3 hours, a pH equal to 10, an initial concentration of sodium of 3486 mg/l and an adsorbent dosage of 0.5 g/L were measured as 20.7% and 17.23%, respectively. They also reported that the Langmuir model and the pseudo-second-order model had the best agreement with the measured values.

Kharel et al. (2016) investigated the effectiveness of wheat and rice husk ashes in reducing water hardness, with hardness levels ranging from 236 to 580 mg/l and ash concentrations from 2.5 to 25 g/l. They found that wheat husk ash achieved the highest reduction of 81% (67 mg/g) at 17.5 g/l, while rice husk ash reduced hardness by 58% (44 mg/g) at 22.5 g/l. Increasing the ash concentration beyond these levels did not further reduce hardness. Wheat husk ash was more effective due to its higher content of alkali metal oxides. Although both ashes reduced water hardness, they did not render the water drinkable because of increased alkalinity. Singh et al. (2017) studied the sodium adsorption ratio (SAR) reduction rate in saline water and showed that it was 27.83, 25.52, 22.21 and 15.46% for paddy husk ash, paddy straw biochar, activated biochar and coco peat, respectively; the equilibrium contact time for all absorbents was 15 min. Doing columnar tests on combined rice paddy husk-laterite soil filters, Chowdhury et al. (2022) used columnar tests on combined rice paddy husk-laterite soil filters to see how they affected lowering the salinity of the water. They found that the average rate was 26.61 and the highest rate was 42.86%. Bindhu et al. (2021) studied the water-hardness-reducing effects and found that the highest rates, after 3 hours of contact time, were 84.38, 62.5 and 31.25% for 2, 20 and 1 gr of potato powder, coconut activated carbon and wheat husk ash, respectively.

Studies conducted so far on removing sodium from effluents by such low-cost adsorbents as agricultural/industrial wastes are limited. This study investigates the sodium removability of agricultural wastewater using sugarcane bagasse adsorbents. Also, it investigates the effectiveness of activated nano biochar, non-nano activated biochar and magnetic nano biochar in sodium removal. Assess the impact of different activation methods and conditions, including ratios of KOH to biochar, microwave powers, and activation

times, on the sodium removal efficiency investigated. The main objective of this study is to investigate the linear and nonlinear isotherms and kinetic behavior of sodium ion adsorption using chemically treated magnetic activated carbon synthesized from sugarcane bagasse waste. Further research suggested approaches include experimenting with different treatment methods, such as acids or heating, and combining bagasse with other natural adsorbents. Additionally, the impact of environmental factors like temperature, pH, and contact time on salt removal efficiency should be investigated. Finally, testing various forms of sugarcane bagasse, such as powder or pellets, can help identify the most effective form for adsorption.

Materials and methods

1.Materials

Sugarcane bagasse (SB) was provided by Hakim Farabi Agro-Industry Co., a sugar mill in Khouzestan Province (48_360E, 30_590N), southwest of Iran. NaOH (99.0 wt%), potassium hydroxide (KOH, 85.0 wt%) and hydrochloric acid (HCl, 38 wt%) were purchased from MERCK Co. Nitrogen (99.999%) was supplied by Wuhan Zagrosgas Air & Gas Co.

To prepare the biochar, this research used the sugarcane bagasse as a primary biomass by: 1) washing it several times with ordinary and distilled water and drying it in the open air to remove its remaining salts; 2) crushing it with an industrial mill and placing it in an oven at 60 °C for 24 hours to remove its excess moisture; 3) grinding the crushed bagasse with a small mill for further milling; 4) passing it through 60 and 100 mesh sieves in two stages for more uniformity and 5) placing it in closed containers (Nie et al., 2018).

1.1.Biochar

Biomass was converted to biochar (BC) using a heat-programmable electric furnace, where the temperature rise was set at 5 ° C/min for a uniform heat distribution. Bagasse was placed inside a steel reactor, into which nitrogen gas was injected at a fixed flow rate and prevented it from oxidation. Biomass was kept at 600 ° C for 2 hours thereafter, the furnace was turned off while nitrogen gas was injected, and the temperature was slowly lowered to that of the lab (Iwuozor et al., 2022). Considering the sizes of the furnace and reactor, each time 20 gr of biomass was placed in the reactor and about 5 gr of biochar was produced after the carbonization process, the biochar production efficiency under these conditions was about 25%.

1.2.Nano biochar

Nano biochar (N-BC) was produced by a planetary ball mill with ceramic cup and bullets (Figure 1), where the bullet-to-biochar weight ratio was 15:1 and the rotation speed was 300 rpm (Kathiresan

& Sivaraj, 2016; Mehrabinia et al., 2022). The useful mill-activity time was 2, 4 and 6 hours and it worked for 3 minutes and rested for 1 minute to prevent the temperature to rising and cohesive masses to forming in the samples; As size and uniformity of particles were important, use of a gradation device was made.

1.3.Activated nano biochar

1.3.1.Chemical reaction with activator

Chemically activated nano biochar was produced using KOH with weight ratios of 2:1, 3:1, and 4:1. For different ratios, KOH was dissolved in deionized water in separate containers and then biochar was added to the solution. The suspension was stirred on a hotplate for 2 hours at 80 ° C, kept at room temperature for 24 hours and then dried in the oven for another 24 hours at 105 ° C.

1.3.2.Activation in microwave

To activate the KOH-nano biochar mix, a domestic microwave oven with adjustable time and power settings was used (Nasri et al., 2017). The microwave chamber was isolated, with only two openings for nitrogen gas to enter and exit, creating an inert atmosphere. The samples were microwaved under nitrogen for varying durations (5, 10, and 15 minutes) and power levels (200, 400, and 700 watts). Afterward, they were washed multiple times with hot deionized water to achieve a neutral pH post-pyrolysis. Finally, the activated nano biochar (AN-BC) samples were dried at 105° C for 24 hours.

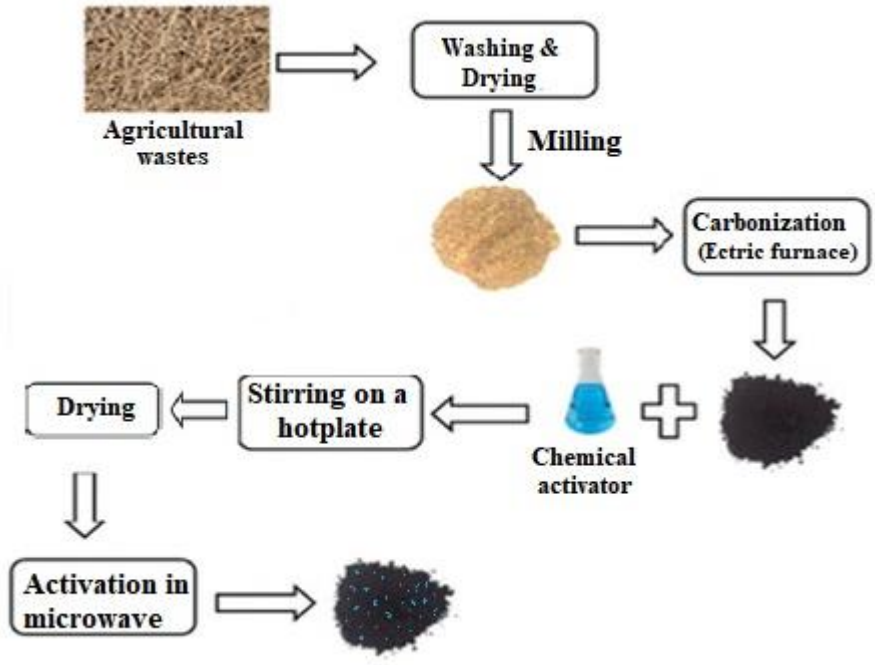

Fig 1. Schematic of production stages of active biochar

1.4.Magnetic biochar

To magnetize adsorbents using Nasri et al. (2017) and Wu et al. (2018) methods, magnetic activated nano biochar (MKN-BC) was produced using iron (III) chloride hexahydrate and a 0.05 mol/l magnetic suspension of iron (II) sulfate heptahydrate (1:2 ratio). The KN-BC was mixed with the magnetic suspension and stirred at 6 rpm for 2 hours at 80 ° C, and the samples were dried for 24 hours at 105 ° C.

1.4.1.Activation in microwave

The initial biochar was subjected to microwave treatment at power levels of 200, 400, and 700 watts for durations of 5, 10, and 15 minutes, with nitrogen gas introduced during the activation process. To enhance the specific surface area of the biochar, following the methods of Wu et al. (2015) and Cheng et al. (2017), deionized hot water was immediately added to the sample container post-activation. The adsorbents were then repeatedly washed with this water to achieve a neutral pH. The MKN-BC samples were subsequently dried in an oven at 105°C for 24 hours.

In this study, the abbreviations BC, Ka-BC, KaN-BC, and MKaN-BC refer to biochar, activated non-nano biochar, activated nano biochar, and magnetic activated nano biochar, respectively. The index ‘a’ indicates the KOH/BC ratio. The microwave power and activation duration are denoted by two numbers following the adsorbent name; for example, MK3N-BC-400-10 signifies magnetic activated nano biochar with a KOH/BC ratio of 3, microwave power of 400 watts, and an activation period of 10 minutes.

1.5.Drainage samples

Saline samples were taken from sugarcane drains where the sodium content was about 4 g/l and the amount of sodium in the samples was set to be 2, 4 and 8 g/l using sodium nitrate and deionized water.

Bach tests

To assess the sodium removal capability of the produced adsorbents from drainage, the batch (discrete) method was employed. In this method, 0.75 g of the adsorbent was added to 50 ml of water. The mixture was stirred on a shaker at 150 rpm for 12 hours, then filtered through paper to measure the sodium content. A total of 729 samples (with three iterations) were used to evaluate the sodium removal efficiency of the adsorbents. Additionally, 138 samples were utilized to study the kinetics and isotherms related to the removal process using MK_3N-BC-400-10.

Physical and chemical parameters

A flame photometer was used to measure the residual sodium ions in the samples and the EC and pH values were measured using the related devices (portable Jenway meters). The samples were weighed with a 3 decimal-accuracy digital scale and the DLS method (HORIBA model) was used to determine the particle size and gradation

of biochar particles.

Kinetics of sodium adsorption

Adsorption kinetics is an important factor in the design of adsorption tests and its models are either reaction-based (pseudo-first-order, pseudo-second-order and Elovich) or diffusion-based (intraparticle, internal-pore and external-film) (Sarici-Ozdemir, 2012). To study the biochar sodium adsorption kinetics, 0.75 gr of adsorbent was added to a 50 ml solution containing 10 g/l sodium in 10 separate containers and stirred with a 150 rpm-shaker at room temperature. Each container was then removed from the shaker in a 0-720 minute time-range and its sodium content was measured after passing the suspension through filter paper. The optimum contact time was measured by the adsorption kinetics test with MK_3N-BC-400-10 and the biochar-adsorbed sodium ions were found by Equation 1 from the difference between the initial and equilibrium ion concentrations in the remaining solution (Zhan et al., 2016):

$$q_e = \frac{(C_0 - C_e) \times V}{m} \quad (1)$$

Where C_0 and C_e are, respectively, the initial and equilibrium concentrations of the desired elements in the solution (mg/l), V is the suspension volume (l) and m is the adsorbent mass (g). The kinetics of the adsorption process have been studied using the pseudo-first-order, pseudo-second-order and diffusion kinetic models (Equations. 2, 3 and 4, respectively).

Pseudo-first-order kinetic model

The linear and non-linear pseudo-first-order kinetic equations are as follows:

$$\log(q_e - q_t) = log\ q_e - log\left(\frac{k_1 t}{2.303}\right) \quad (2)$$

$$q_t = q_e(1 - e^{-k_1 t}) \quad (3)$$

Where q_t is the ion adsorbed in time t (mg/g), q_e is the ion adsorbed in equilibrium time (mg/g), k_1 is the speed constant of the model (l/min) and t is time (min). Plotting log (q_e-q_t) versus t will yield a linear relation wherein k_1 and q_e are, respectively, the slope and y-intercept of the drawn line.

Pseudo-second-order kinetic model

The linear pseudo-second-order kinetic equation is as follows:

$$\frac{t}{q_t} = \frac{1}{k_2 q_e^2}\frac{t}{q_e} \quad (4)$$

$$q_t = \frac{k_2 q_e^2 t}{1 + k_2 q_e t} \quad (5)$$

Where q_e, q_t and t are those defined in Equation 1 and K_2 is the kinetic constant of the model (g/mg.min). Plotting t/q_t versus t will yield a linear relation wherein k_2 and q_e are, respectively, the slope and y-intercept of the drawn line (Deniz & Karaman, 2011).

Intraparticle diffusion kinetic model

The following equation, a diffusion-based model, describes competitive and multi-

stage adsorptions (first on the surface, then on the adsorbent):

$$q_t = k_p t^{0.5} + c \quad (6)$$

Where K_p is the model speed constant (mg/g.min$^{0.5}$) and C (mg/g) is the boundary layer thickness (the parameter that affects the increase or decrease of the diffusion rate). The slope of the q_t regression line versus $t^{0.5}$ will determine the K_{dif} parameter and its y-intercept will yield C (Ramachandran et al., 2011).

Isotherm adsorption models

Adsorption in a solid-liquid system involves extracting the solute from the solution and accumulating it on the adsorbent's surface, leading to a dynamic equilibrium between the solute concentration in the solution and on the adsorbent surface (Nikkhah et al., 2016). The adsorption isotherm is crucial for optimizing adsorbent usage as it illustrates how the pollutant interacts with the adsorbent (Crini et al., 2008). To investigate sodium adsorption, 0.75 g of adsorbent was added to containers with 50 ml of solutions at varying sodium concentrations (3, 5, 10, 15, 20, and 25 g/l). The mixture was stirred for 24 hours at 150 rpm, filtered, and the sodium concentration was measured; experiments were conducted on MK3N-BC-400-10. The Langmuir and Freundlich isotherm models were used to describe the biochar sodium-adsorption data.

Langmuir isotherm model

The Langmuir adsorption isotherm is found on several key assumptions: 1) Adsorption occurs at specific, homogeneous sites on the adsorbent, 2) each dye molecule occupies only one site at a time, 3) the adsorbent has a finite capacity, and 4) all sites are identical and possess similar energy. This isotherm serves as an experimental equation, indicating that as the adsorption sites on an adsorbent become occupied, the adsorption energy decreases exponentially (Khaled et al., 2009). The linear and nonlinear models of this isotherm are as follows:

$$\frac{c_e}{q_e} = \frac{1}{k_a Q_m} + \frac{1}{Q_m} \times c_e \quad (7)$$

$$q_e = \frac{Q_m K_a C_e}{1 + K_a C_e} \quad (8)$$

Where C_e is the equilibrium concentration of the liquid phase (mg/l), q_e is the adsorbent's absorption capacity (mg/g), Q_m is the maximum absorption capacity of the adsorbent (mg/g) and K_a is the absorption equilibrium constant (l/mg) which is related to the apparent energy of the absorption. Plotting C_e/q_e versus C_e should show a straight line with a slope of $1/Q_m$.

Freundlich isotherm model

Freundlich isotherm presents a relationship as follows for non-ideal and reversible adsorption. This experimental model can be used for multilayer adsorption with heterogeneous heat distribution and

adsorption on heterogeneous surfaces (Foo & Hameed., 2010). The linear and nonlinear models of this isotherm are as follows:

$$\ln q_e = \ln k_f + \frac{1}{n_f} \ln c_e \quad (9)$$

$$q_e = K_f C_e^{1/n_f} \quad (10)$$

where q_e is the adsorbent's absorption capacity at equilibrium time (mg/g), C_e is the adsorbent equilibrium concentration in solution (mg/l), K_f is the Friendlich constant (l/g) related to the bond energy and shows the amount of ions adsorbed on the adsorbent per unit equilibrium concentration, $1/n_f$ is the heterogeneity parameter and n_f is the deviation from the absorption line; adsorption is linear, chemical or physical if $n_f = 1$, $n_f < 1$ or $n_f > 1$, respectively.

To compare and evaluate the accuracy of the isothermal models and adsorption kinetics applied in this study, use was made of the correlation coefficient and standard estimation error (SSE) (Eq. 7, below):

$$SEE = \sqrt{\frac{\sum(Y_o - Y_p)^2}{N-1}} \quad (11)$$

Where Y_o and Y_p, are the observed and predicted values, respectively, and N is the number of samples.

Results and discussion

1.Activated nano biochar and Magnetic activated nano biochar

First, activated biochar (K-BC), activated nano biochar (KN-BC), and magnetic activated nano biochar (MKN) were used to remove sodium ions in different treatments. The percentage of sodium removal by these adsorbents is summarized in Table 1.

Table 1. The percentage of sodium removability by activated biochar, activated nano biochar & Magnetic activated nano biochar

		K-BC			KN-BC			MKN		
Initial concentration of sodium (g/l)		2	4	8	2	4	8	2	4	8
		Sodium removal (%)								
Microwave power	T(200W)	9.2	16.2	30.6	25.6	33.5	46.0	17.5	23.4	38.2
	T(400W)	13.3	22.8	39.1	26.9	40.6	53.3	21.5	34.8	47.5
	T(700W)	10.0	21.6	31.9	26.5	37.7	49.4	19.6	29.6	43.7

The study demonstrates that increasing the initial sodium concentration enhances sodium removability, with activated nano biochar being more effective than non-nano adsorbents. The largest effectiveness difference observed was 179.5% at 200 W microwave power and 2 g/l sodium concentration. As sodium concentration

increases, the difference in removability between nano and non-nano adsorbents decreases, with removability being 74.5% greater for nano adsorbents overall. Yang et al. (2018) tested the copper, lead, and zinc removability of corn stalk magnetic nano biochar and found it to be, respectively, 24.04, 54.04 and 16.74% with activated biochar and 80.96, 97.51 and 54.84% with activated nano biochar.. Nano biochar is more effective than non-nano biochar for removing contaminants because it has a much larger surface area and smaller, more numerous pores that improve adsorption. Its high reactivity enhances interactions with contaminants, and its nano-sized particles provide better access to solution. Furthermore, the surface charge of nano biochar strengthens electrostatic attraction with oppositely charged contaminants, thereby boosting its pollutant removal capabilities (Rajabi et al., 2023).

Magnetization reduces sodium removability by 18.8% compared to activated biochar, and the specific surface area of the adsorbent decreases from 745 to 459 m^2/g due to magnetization. In order to check the ability of the magnetic adsorbent, a strong magnet was used to separate the magnetized biochar particles from the solution (Xin et al., 2017). . When sodium concentrations increase, more sodium ions are available for biochar to interact with, making it easier to remove them. Higher sodium concentrations can help saturate the binding sites on biochar. This means that the biochar can effectively release other substances it might be holding onto, allowing for better removal of sodium (Medyńska-Juraszek et al., 2021).

An inverse relationship is noted between initial sodium concentration and removability reduction, with the highest removability reduction at 200 W and 2 g/l sodium concentration.

The optimal activator-to-adsorbent ratio for sodium removability is found to be 3 (K3) at 200 and 400 W. Increasing the ratio from 2 to 3 enhances removability, while further increases to 4 decrease it. Reducing the activator ratio from 3 to 2 decreases sodium removability by 4-8%, while increasing it to 4 reduces removability by 12-16% across different adsorbents.

2.Adsorption kinetics

To determine the sodium-adsorption kinetic model of the magnetic activated nano adsorbent, three kinetic models were used: 1) pseudo-first-order, 2) pseudo-second-order and 3) diffusion to study how sodium was adsorbed. The key differences between the pseudo-first-order and pseudo-second-order models in adsorption kinetics are mainly in how they describe the speed of adsorption. The pseudo-first-order model suggests that the rate of adsorption is proportional to the difference between the maximum adsorption capacity and the amount already adsorbed. In contrast, the

pseudo-second-order model indicates that the rate depends on the square of the amount adsorbed. The diffusion model focuses on how the movement of particles affects the adsorption process (Simonin, 2016). In model (1), the pollutant adsorption rate at any given time is directly proportional to the instantaneous pollutant concentration and the amount adsorbed to the adsorbent. Model (2) is based on the solid-phase adsorption capacity and assumes the adsorption rate is dependent on chemical adsorption. Model (3) examines the pollutant transfer into adsorbent based on the transfer rate of particles inside its pores (Li et al., 2022). Effects of contact-time on sodium removability were investigated for MK_3N-BC-200-10, MK_3N-BC-400-10 and MK_3N-BC-700-10.

Treatments at 200 and 700 W reached equilibrium after 480 minutes, while the 400 W treatment took 540 minutes. The adsorption rate decreases over time, approaching zero at equilibrium. The slope of the adsorption graph declines after 200 minutes for all adsorbents, indicating that sodium ions are initially adsorbed on the surface for up to 200 minutes. Once the surface is saturated, sodium ions penetrate the adsorbent cavities. As contact time increases, absorption improves due to more opportunities for interaction with functional groups. At equilibrium, sodium removal was 239 mg/g for 200 W, 260 mg/g for 400 W, and 201 mg/g for 700 W treatments.

Linear and nonlinear quasi-first-order kinetic models were drawn to the measured data for three absorbers; which Figure 2 presents the non-linear mode. The correlation coefficients for, respectively, MK_3N-BC-200-10, MK_3N-BC-400-10 and MK_3N-BC-700-10 are 0.97, 0.99 and 0.96, concluding that the pseudo-first-order kinetic model fits well with the real data, and the maximum and minimum constant adsorption rates relate to MK_3N-BC-700-10 and MK_3N-BC-400-10, respectively. The slope of the fitted line is negative in all three absorbers because, over time, more sodium is absorbed on the adsorbent surface. According to Figure 2, the nonlinear pseudo-first-order model has a satisfactory match with the real values.

Fitting the linear pseudo-second-order model to the measured data showed that the correlation coefficients were highly less than the pseudo-first-order model because during the first 60 min, the adsorption rate was high and more sodium was absorbed on the adsorbent surface, causing the t/q_t ratio to decrease, but after that, the t/q_t increased with a decrease in the adsorption rate.

As shown, for times less than 60 min, this kinetic model does not fit well to the measured data, but after 60 min, the correlation is better. Since adherence of the kinetic data to this model is an indication of chemical adsorption in the

adsorption process (Nikkhah et al., 2016), it can be concluded that, before 60 min, the dominant adsorption mechanism is not chemical.

In Figure 3, the non-linear second-order pseudo- model is presented. As shown in the Table 2, the non-linear pseudo-second-order model has provided far better results compared to the linear model.

The fitting of adsorption data using the intraparticle diffusion kinetic model reveals a strong correlation between the fitted line and measured values, indicating that sodium ion diffusion in the adsorbents occurs at a nearly uniform rate. This suggests that intraparticle diffusion is a significant factor in sodium adsorption from the start of the process. The MK3N-BC-400-10 treatment shows a longer time to reach equilibrium and a higher amount of adsorbed sodium (qt), indicating that its pore structure is more effective for sodium removal compared to the other two adsorbents (Fig. 4).

Table (2) lists the sodium-adsorption results of linear and non-linear kinetics models by magnetic activated nano biochar adsorbents. Comparing the sum of squared errors shows that, compared to the pseudo-second-order model, the pseudo-first-order model has estimated the maximum sodium adsorption closer to the real values. Considering the correlation coefficients and the sum of squared errors, the pseudo-first-order kinetic model and the intraparticle diffusion model conformed most to the measured data. According to Table 2, linear and nonlinear pseudo-first-order models have almost similar coloration values, although the linear model has a much lower SEE value and has more accurately estimated qe values. Compared to the linear model, the nonlinear pseudo-second-order model has a more accurate estimate of qe.

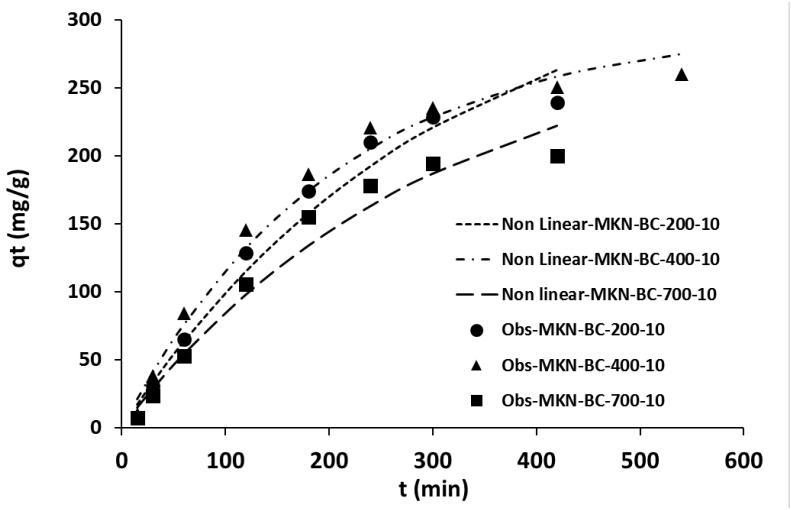

Fig 2. Fitting of the non-linear pseudo-first-order kinetic model to the measured values

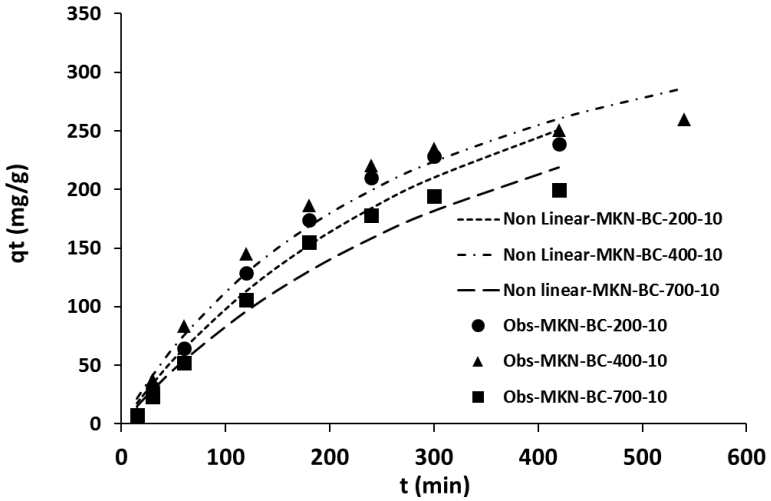

Fig 3. Fitting of the non-linear pseudo-second-order kinetic model to the measured values

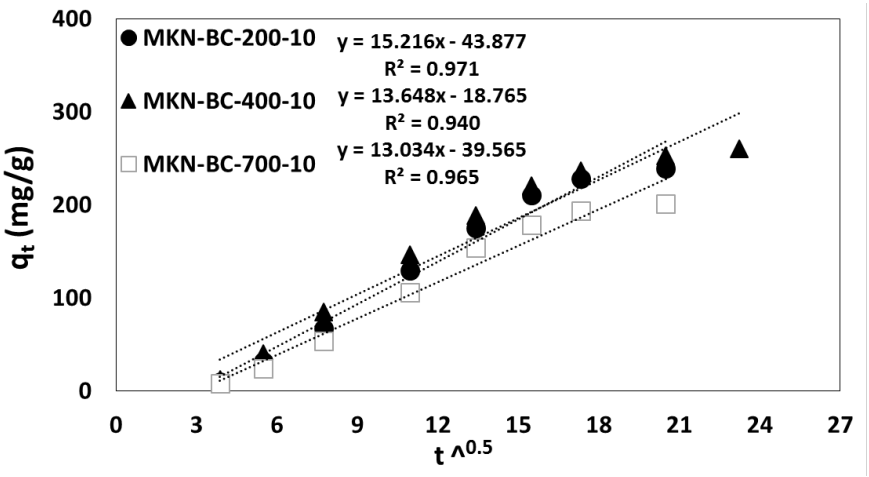

Fig 4. Fitting the intraparticle diffusion kinetic model to the measured values

3.Adsorption isotherm

According to isothermal curves that are used to describe the adsorption process at different concentrations, this process is strongly influenced by adsorption kinetics (Limousin et al., 2007). Although experimental isothermal models with 2, 3 or even 4 parameters can be used to understand the absorption mechanism, the 2-parameter ones are preferred due to their simplicity because if the data are well consistent with them, there is no need to use more complex models (Nadavala et al., 2009). Among isothermal models, since Langmuir and Friendlich are two common, widely used 2-parameter models (Mousavi et al., 2010), they have been used to study the adsorbents' behavior and capacity. The Langmuir and Freundlich isotherm models help explain how adsorbents like magnetically activated nano biochar behave and how much they can hold. The Langmuir model assumes that there's a maximum capacity for adsorption,

Table 2. Results of the fitting of kinetic linear and non-linear models to the measured values

	Linear				Non-linear			
pseudo-first-order	SSE	R2	K1	qe	SSE	R2	K1	qe
MK_3N-BC-200-10	0.091	0.9718	0.01036	313.1	14.665	0.975	0.003	349.408
MK_3N-BC-400-10	0.032	0.9969	0.00852	299.2	11.663	0.986	0.005	295.088
MK_3N-BC-700-10	0.111	0.9643	0.01105	278.6	13.997	0.969	0.003	291.948
pseudo-second-order	SSE	R2	k2	qe	SSE	R2	k2	qe
MK_3N-BC-200-10	0.289	0.3248	1.73E-06	769.2	16.72	0.96	5.1E-6	487.7
MK_3N-BC-400-10	0.292	0.7828	2.04E-06	833.3	16.56	0.97	7.8E-06	439.8
MK_3N-BC-700-10	0.319	0.2367	2.9E-07	1666.6	15.5	0.96	5.0E-06	448.8
pseudo-second-order (separated)	SSE	R2	k2	qe				
MK_3N-BC-200-10	0.038	0.9504	4.37E-06	555.5				
MK_3N-BC-400-10	0.041	0.9866	1.45E-05	370.3				
MK_3N-BC-700-10	0.070	0.8496	3.42E-06	555.5				
intraparticle diffusion	SSE	R2	Kp	c				
MK_3N-BC-200-10	0.011	0.9714	15.216	-43.877				
MK_3N-BC-400-10	0.019	0.9404	13.648	-18.765				
MK_3N-BC-700-10	0.011	0.9652	13.034	-39.565				

while the Freundlich model suggests that adsorption occurs on a heterogeneous surface with no limit. Key findings show that as sodium concentration increases, the adsorbent capacity and percentage sodium removal vary, providing insight into how effective the adsorbent is under different conditions and improving our understanding of the overall adsorption process (Khayyun, and Mseer, 2019).

Increasing the initial sodium concentration in the solution enhances sodium adsorption by the studied adsorbents. Specifically, raising the concentration from 3 to 25 g/l results in increased sodium absorption by 3, 3.5, and 2.6 times for the 200, 400, and 700 W treatments, respectively. The slope of the sodium removal curve shows a decreasing trend with higher initial concentrations. For the 400 W treatment, the slope remains unchanged below 10 g/l, while it decreases for the 200 and 700 W treatments, indicating that the 400 W treatment has a higher absorption capacity and is less affected by increased sodium concentration.

As sodium concentration rises, the slope reduces across all adsorbents, with the graphs becoming nearly horizontal for concentrations above 20 g/l. In terms of percent removal, increasing the initial concentration from 3 to 10 g/l shows little change, but raising it from 10 to 25 g/l leads to a reduction in percent removal by 52%, 46%, and 57% for the 200, 400, and 700 W treatments, respectively.

Among Langmuir model assumptions, one considers a monolayer adsorption process, another assumes a uniform adsorbent surface and a third omits interactions among adsorbed molecules (Senturk et al., 2009). The maximum sodium adsorption

capacities based on the Langmuir isothermal model are 344.8 mg/g for 200 W, 416.6 mg/g for 400 W, and 294.1 mg/g for 700 W.

Since the Langmuir isotherm model is highly consistent with the measured values and the correlation coefficient is above 99% for all three adsorbents, the sodium adsorption on their surfaces is done as a monolayer.

According to Figure 5, the nonlinear Langmuir model for the 400 W treatment did not have a good estimate of the real values. The Freundlich model assumes that particles are placed on the adsorbent surface in several layers. Figure (6) shows how the Freundlich model fits the data.

As shown in Figure 6, the correlation coefficients between the measured data and the Freundlich model are about 90%, which is lower than that of the Langmuir model. Table 3 presents the parameters of the Langmuir and Freundlich isothermal models. The nonlinear Freundlich model has a relatively accurate estimate of the real values for all treatments.

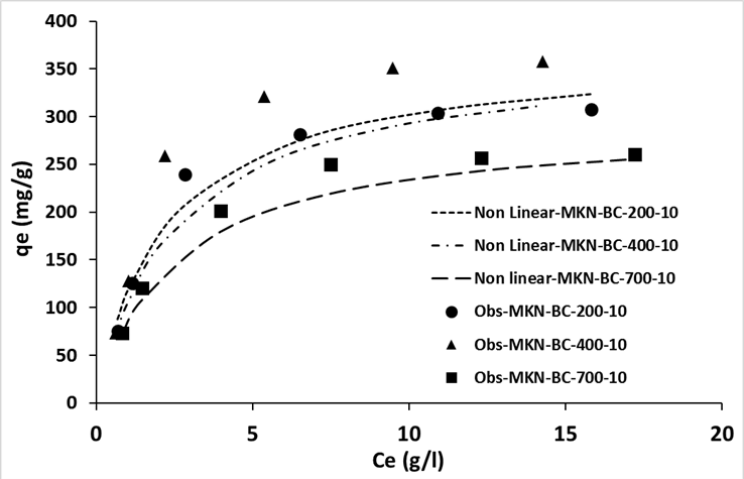

Fig 5. Fitting of the non-linear Langmuir isotherm model to the measured values

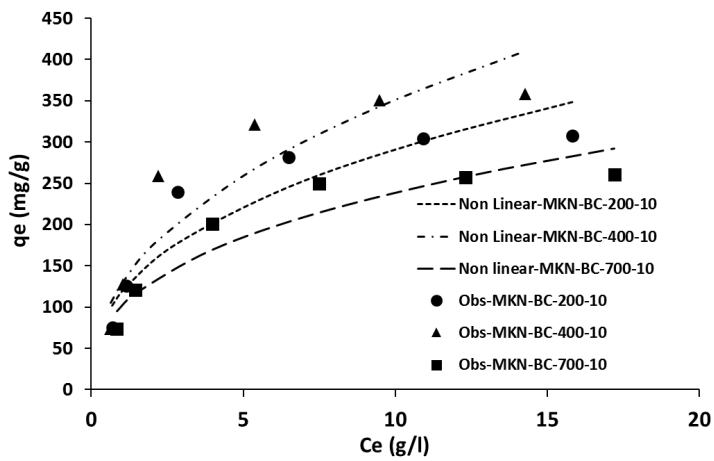

Fig 6. Fitting the non-linear Freundlich isotherm model to the measured values

Table 3. Fitting the adsorption isotherm models to the measured values

	Linear				Non-linear			
Langmuir	SSE	R^2	Ka	qe	SSE	R^2	Ka	qe
MK_3N-BC-200-10	1.28	0.9948	0.00055	344.82	17.42	0.96	0.00045	368.7
MK_3N-BC-400-10	1.23	0.9911	0.0005	416.66	61.88	0.81	0.00039	366.7
MK_3N-BC-700-10	1.55	0.9955	0.00047	294.11	18.77	0.94	0.00039	292.8
Freundlich	SSE	R^2	k_f	$1/n_f$	SSE	R^2	k_f	$1/n_f$
MK_3N-BC-200-10	0.2	0.8787	6.02	0.4258	38.86	0.86	7.74	0.39
MK_3N-BC-400-10	0.3	0.8698	5.06	0.4669	50.30	0.85	6.27	0.43
MK_3N-BC-700-10	0.16	0.9097	5.10	0.4206	27.33	0.89	7.76	0.37

As shown, since the average correlation coefficients are 0.9938 and 0.886 for the Langmuir and Freundlich models, respectively, the former is more consistent with the measured data. The n_f parameter is more than 1 for all three adsorbents; hence, the sodium adsorption process is mostly physical. According to table 3, Langmuir and Freundlich linear models have a better match with the real values. Also, the Langmuir model has estimated more accurate values than the Freundlich model.

The analysis of sugarcane bagasse biochar's efficiency in removing sodium ions from aqueous solutions highlights the importance of using nonlinear isotherm and kinetics models over linear ones for accurate representation. While linear models simplify the adsorption process and may lead to misinterpretations, nonlinear models better account for variations in adsorption capacity and dynamics, particularly at higher concentrations. Nonlinear modeling provides a superior fit to experimental data, enhances understanding of adsorption mechanisms, and is more adaptable to varying conditions. Overall, these models significantly improve insights into the effectiveness of biochar in environmental remediation, suggesting that future research should focus on nonlinear approaches for reliable data interpretation.

Conclusions

This study highlights the effectiveness of various biochar adsorbents, particularly activated nano biochar (KN-BC), in removing sodium ions from solutions. The results indicate that sodium removal efficiency increases with higher initial sodium concentrations, and nano biochar outperforms non-nano variants due to its larger surface area and enhanced adsorption properties. Although the magnetization of biochar slightly reduces sodium removability, the magnetically activated nano biochar (MKN) still demonstrates significant adsorption capabilities.

Kinetic studies reveal that the pseudo-first-order model best fits the adsorption data, suggesting that the initial adsorption mechanism is predominantly physical rather than chemical. The intraparticle diffusion model further supports the notion that sodium ion diffusion plays a critical role throughout the adsorption process.

Isothermal models, specifically Langmuir and Freundlich, were employed to analyze adsorption behavior. The Langmuir model showed a superior fit, indicating a monolayer adsorption process, while the Freundlich model suggested a heterogeneous surface with physical adsorption characteristics. The maximum sodium adsorption capacities were determined, with notable differences across treatments, emphasizing the influence of operational parameters such as microwave power.

Overall, the findings underscore the potential of using activated and nano biochar as effective adsorbents for sodium ion removal in wastewater treatment applications. Future research could explore optimizing conditions further and investigating the removal of other contaminants using similar methodologies. This work contributes valuable insights into the design and application of biochar-based materials for environmental remediation.

Abbreviation

BC: Biochar
N-BC: Nano biochar
Ka-BC: Activated non-nano biochar
KaN-BC: Activated nano biochar
MKaN-BC: Magnetic activated nano biochar
MKN-BC: Magnetic activated nano biochar
AN-BC: Activated nano biochar
KOH: Potassium hydroxide
W: Watts

Declarations

Ethical Approval

Not applicable.

Competing interests

On behalf of all authors, the corresponding author states that there is no conflict of interest.

Authors' contributions

Funding

Availability of data and materials

The datasets generated during and/or analyzed during the current study are available from the corresponding author on reasonable request.

Acknowledgments

This study was funded by the University of Lorestan, Lorestan, Iran. The support of this organization is appreciated. Also authors grateful of the Khuzestan Sugar Cane Research and Training Institute,

Khuzestan, Iran for its financial support.

References

Ayers, R. S., & Westcot, D. W. (1985). *Water quality for agriculture* (Vol. 29, p. 174). Rome: Food and agriculture organization of the United Nations. https://www.academia.edu/download/94774091/book_rs_ayers_and_wetscot.pdf

Bindhu, B. K., Shaji, H., Kuruvila, K. J., Nazerine, M., & Shaji, S. (2021, March). Removal of total hardness using low cost adsorbents. In *IOP Conference Series: Materials Science and Engineering* (Vol. 1114, No. 1, p. 012089). IOP Publishing. https://doi.org/10.1088/1757-899X/1114/1/012089

Cheng, S., Zhang, S., Zhang, L., Xia, H., Peng, J., & Wang, S. (2017). Microwave-Assisted Preparation of Activated Carbon from Eupatorium Adenophorum: Effects of Preparation Parameters. *High Temperature Materials and Processes*, *36*(8), 805-814. https://doi.org/ 10.1515/htmp-2015-0285

Chowdhury, T., Miah, J., & Banik, B. K. (2022). Low-Cost Salinity Treatment for Drinking Purpose Using Indigenous Materials. In *Advances in Civil Engineering: Select Proceedings of ICACE 2020* (pp. 37-44). Springer Singapore. https://doi.org/10.1007/978-981-16-5547-0_4

Crini, G., & Badot, P. M. (2008). Application of chitosan, a natural aminopolysaccharide, for dye removal from aqueous solutions by adsorption processes using batch studies: A review of recent literature. *Progress in polymer science*, *33*(4), 399-447. https://doi.org/10.1016/j.progpolymsci.2007.11.001

Crini, G., Lichtfouse, E., Wilson, L. D., & Morin-Crini, N. (2019). Conventional and non-conventional adsorbents for wastewater treatment. *Environmental Chemistry Letters*, *17*, 195-213. https://doi.org/10.1007/s10311-018-0786-8

Deniz, F., & Karaman, S. (2011). Removal of an azo-metal complex textile dye from colored aqueous solutions using an agro-residue. *Microchemical Journal*, *99*(2), 296-302. https://doi.org/10.1016/j.microc.2011.05.021

Dudley, L., Ben-Gal, A., & Shani, U. (2006, November). Influence of plant, soil and water properties on the leaching fraction. In *Agronomy Abstracts P* (Vol. 25711). https://scisoc.confex.com/crops/ 2006am/techprogram/P25711.HTM

Ehtaiwesh, A. F. (2022). The effect of salinity on nutrient availability and uptake in crop plants. *Scientific Journal of Applied Sciences of Sabratha University*, 55-73. https:// doi.org/10.47891/sabujas.v0i0.55-73.

Foo, K.Y., & Hameed, B.H. (2010). Insights into the modeling of adsorption isotherm systems. *Chemical Engineering Journal*, *156*(1), 2-10. DOI:10.1016/j.cej.2009.09.013

Hettiarachchi, E., Perera, R., Chandani Perera, A.D. L., & Kottegoda, N. (2016). Activated coconut coir for removal of sodium and magnesium ions from saline water. *Desalination and Water Treatment*, *57*(47), 22341-22352. DOI:10.1080/19443994.2015.1129649

Iwuozor, K. O., Emenike, E. C., Ighalo, J. O., Omoarukhe, F. O., Omuku, P. E., & Adeniyi, A. G. (2022). A review on the thermochemical conversion of sugarcane bagasse into biochar. *Cleaner Materials*, *6*, 100162. https://doi.org/10.1016/j.clema.2022.100162

Jamil, T.S., Ibrahim, H.S., Abd El-Maksoud,

I.H., & El-Wakeel, S.T. (2010). Application of zeolite prepared from Egyptian kaolin for removal of heavy metals: I. Optimum conditions. *Desalination*, *258*(1-3), 34-40. doi:10.1016/j.desal.2010.03.05

Kasraee, M., Dehghani, M. H., Mahvi, A. H., Nabizadeh, R., Arjmand, M. M., Salari, M., ... & Tyagi, I. (2022). Adsorptive removal of humic substances using cationic surfactant-modified nano pumice from water environment: Optimization, isotherm, kinetic and thermodynamic studies. *Chemosphere*, *307*, 135983. https://doi.org/10.1016/j.chemosphere.2022.135983

Kathiresan, M., & Sivaraj, P. (2016). Preparation and characterization of biodegradable sugarcane bagasse nano reinforcement for polymer composites using ball milling operation. *International Journal of Polymer Analysis and Characterization*, *21*(5), 428-435. doi:10.1080/1023666X.2016.1168061

Khaled, A., El Nemr, A., El-Sikaily, A., & Abdelwahab, O. (2009). Removal of Direct N Blue-106 from artificial textile dye effluent using activated carbon from orange peel: adsorption isotherm and kinetic studies. *Journal of hazardous materials*, *165*(1-3), 100-110. https://doi.org/10.1016/j.jhazmat.2008.09.122

Kharel, H. L., Sharma, R. K., & Kandel, T. P. (2016). Water hardness removal using wheat straw and rice husk ash properties. *Nepal Journal of Science and Technology*, *17*(1), 11-16. https://doi.org/10.3126/NJST.V17I1.25057

Khayyun, T. S., & Mseer, A. H. (2019). Comparison of the experimental results with the Langmuir and Freundlich models for copper removal on limestone adsorbent. *Applied Water Science*, *9*(8), 170. https://doi.org/10.1007/s13201-019-1061-2

Kietlińska, A., & Renman, G. (2005). An evaluation of reactive filter media for treating landfill leachate. *Chemosphere*, *61*(7), 933-940. https://doi.org/10.1016/j.chemosphere.2005.03.036

Li, D., Sun, L., Yang, L., Liu, J., Shi, L., Zhuo, L., Ye, T. and Wang, S., (2024). Adsorption behavior and mechanism of modified Pinus massoniana pollen microcarriers for extremely efficient and rapid adsorption of cationic methylene blue dye. *Journal of Hazardous Materials*, 465, p.133308. https://doi.org/10.1016/j.jhazmat.2023.133308

Li, Y., Gong, D., Zhou, Y., Zhang, C., Zhang, C., Sheng, Y., & Peng, S. (2022). Respiratory Adsorption of Organic Pollutants in Wastewater by Superhydrophobic Phenolic Xerogels. *Polymers*, *14*(8), 1596. https://doi.org/10.3390/polym14081596

Limousin, G., Gaudet, J. P., Charlet, L., Szenknect, S., Barthes, V., & Krimissa, M. (2007). Sorption isotherms: A review on physical bases, modeling and measurement. *Applied geochemistry*, *22*(2), 249-275. https://doi.org/10.1016/j.apgeochem.2006.09.010

López-Luna, J., Ramírez-Montes, L. E., Martinez-Vargas, S., Martínez, A. I., Mijangos-Ricardez, O. F., González-Chávez, M. D. C. A., ... & Vázquez-Hipólito, V. (2019). Linear and nonlinear kinetic and isotherm adsorption models for arsenic removal by manganese ferrite nanoparticles. *SN Applied Sciences*, *1*, 1-19. https://doi.org/10.1007/s42452-019-0977-3

Medyńska-Juraszek, A., Álvarez, M. L., Białowiec, A., & Jerzykiewicz, M. (2021). Characterization and sodium cations sorption capacity of chemically modified biochars produced from agricultural and forestry

wastes. *Materials*, *14*(16), 4714. https://doi.org/10.3390/ma14164714

Mehrabinia, P., & Ghanbari-Adivi, E. (2022). Examining nitrate surface absorption method from polluted water using activated carbon of agricultural wastes. *Modeling Earth Systems and Environment*, *8*(2), 1553-1561. DOI:10.1007/s40808-021-01221-5

Mehrabinia, P., Ghanbari-Adivi, E., Fattahi, R., Samimi, H. A., & Kermanezhad, J. (2021). Nitrate removal from agricultural effluent using sugarcane bagasse active nanosorbent. *Journal of Applied Water Engineering and Research*, *10*(3), 238-249. doi:10.1080/23249676.2021.1982030

Mehrabinia, P., Ghanbari-Adivi, E., Samimi, H. A., & Fattahi, R. (2022). Phosphate removal from agricultural drainage using biochar. *Water Conservation Science and Engineering*, *7*(4), 405-417. DOI: 10.1007/s41101-022-00150-3

Mousavi, A., Asadi, H., Esfandbod, M. (2010). Ion Exchange efficiency of nitrate removal from water 1- equilibrium sorption isotherms for nitrate on resin purolite a-400. *Water and Soil Science, 20*(4), 185. https://watersoil.tabrizu.ac.ir/article_1387.html. [In Persian]

Mubarak, A.A., Ilyas, R.A., Nordin, A.H., Ngadi, N. and Alkbir, M.F.M., (2024). Recent developments in sugarcane bagasse fibre-based adsorbent and their potential industrial applications: A review. International *Journal of Biological Macromolecules*, p.134165. https://doi.org/10.1016/j.ijbiomac.2024.134165

Musie, W., Gonfa, G., & Prabhu, S. V. (2023). Adsorption studies of sodium ions from aqueous solution with natural and sulfuric acid-treated bean seed husk. *Water, Air, & Soil Pollution*, *234*(3), 170. https://doi.org/10.1016/j.agwat.2008.04.010

Nadavala, S. K., Swayampakula, K., Boddu, V. M., & Abburi, K. (2009). Biosorption of phenol and o-chlorophenol from aqueous solutions on to chitosan–calcium alginate blended beads. *Journal of Hazardous Materials*, *162*(1), 482-489. https://doi.org/10.1016/j.jhazmat.2008.05.070

Naik, B. S., Panda, R. K., Nayak, S. C., & Sharma, S. D. (2008). Hydraulics and salinity profile of pitcher irrigation in saline water condition. *Agricultural water management*, *95*(10), 1129-1134. https://doi.org/10.1016/j.agwat.2008.04.010

Nasri, N.S., Zain, H.M., Sidik, H.U., Abdulrahman, A., & Rashid, N.M. (2017). Adsorption Isotherm breakthrough time of acidic and alkaline gases on treated porous synthesized KOH-FeCl 3. 6H 2 O sustainable agro-based material. *Chemical Engineering Transactions*, *61*, 1243-1248. Doi:10.3303/CET1761205

Nie, C., Yang, X., Niazi, N. K., Xu, X., Wen, Y., Rinklebe, J., ... & Wang, H. (2018). Impact of sugarcane bagasse-derived biochar on heavy metal availability and microbial activity: a field study. *Chemosphere*, *200*, 274-282. https://doi.org/10.1016/j.chemosphere.2018.02.134

Nikkhah, A. A., Zilouei, H., & Keshavarz, A. R. (2016). Effect of Structural Modification of Polyurethane Foam by Activated Carbon on the Adsorption of Oil Contaminants from Water. *Journal of Water and Wastewater; Ab va Fazilab (in persian)*, *27*(2), 84-93. [IN Persian]

Oliveira, E.A., Montanher, S.F., Andrade, A.D., Nobrega, J.A., & Rollemberg, M.C. (2005). Equilibrium studies for the sorption of chromium and nickel from aqueous solutions using raw rice bran. *Process Biochemistry*, *40*(11), 3485-3490. DOI:10.1016/j.

procbio.2005.02.026

Pearce, G. K. (2008). UF/MF pre-treatment to RO in seawater and wastewater reuse applications: a comparison of energy costs. *Desalination*, *222*(1-3), 66-73. https://doi.org/10.1016/j.desal.2007.05.029

Pourhakkak, P., Taghizadeh, A., Taghizadeh, M., Ghaedi, M., & Haghdoust, S. (2021). Fundamentals of adsorption technology. In *Interface science and technology* (Vol. 33, pp. 1-70). Elsevier. https://doi.org/10.1016/B978-0-12-818805-7.00001-1

Rahal, Z., Khechekhouche, A., Barkat, A., Sergeevna, S. A., & Hamza, C. (2023). Adsorption of Sodium in an Aqueous Solution in Activated Date Pits. Indonesian Journal of Science and Technology, 8(3), 387-412. DOI: 10.17509/ijost.v8i3.60066

Rajabi, M., Keihankhadiv, S., Suhas, Tyagi, I., Karri, R. R., Chaudhary, M., ... & Singh, P. (2023). Comparison and interpretation of isotherm models for the adsorption of dyes, proteins, antibiotics, pesticides and heavy metal ions on different nanomaterials and non-nano materials—a comprehensive review. Journal of Nanostructure in Chemistry, 13(1), 43-65. https://doi.org/10.1007/s40097-022-00509-x

Ramachandran, P., Vairamuthu, R., & Ponnusamy, S. (2011). Adsorption isotherms, kinetics, thermodynamics and desorption studies of reactive Orange 16 on activated carbon derived from Ananas comosus (L.) *carbon. Journal* of *Engineering and Applied Sciences*, *6*(11), 15-26.

Revellame, E.D., Fortela, D.L., Sharp, W., Hernandez, R. and Zappi, M.E.(2020). Adsorption kinetic modeling using pseudo-first order and pseudo-second order rate laws: A review. *Cleaner Engineering and Technology*, 1, p.100032. https://doi.org/10.1016/j.clet.2020.100032

Sarici-Ozdemir, C. (2012). Adsorption and desorption kinetics behaviour of methylene blue onto activated carbon. *Physicochemical problems of mineral processing*, *48*(2), 441-454.

Senturk, H. B., Ozdes, D., Gundogdu, A., Duran, C., & Soylak, M. (2009). Removal of phenol from aqueous solutions by adsorption onto organ modified Tirebolu bentonite: Equilibrium, kinetic and thermodynamic study. *Journal of hazardous materials*, *172*(1), 353-362. https://doi.org/10.1016/j.jhazmat.2009.07.019

Shang, H., Ouyang, T., Yang, F., & Kou, Y. (2003). A biomass-supported Na2CO3 sorbent for flue gas desulfurization. *Environmental Science &* Technology, *37*(11), 2596-2599. DOI: 10.1021/ es021026o

Simonin, J. P. (2016). On the comparison of pseudo-first order and pseudo-second order rate laws in the modeling of adsorption kinetics. *Chemical Engineering Journal*, *300*, 254-263. https://doi.org/10.1016/j.cej.2016.04.079

Singh, P., Garg, S., Satpute, S., & Singh, A. (2017). Use of rice husk ash to lower the sodium adsorption ratio of saline water. *International Journal of Current Microbiology and Applied Sciences*, *6*(6), 448-458. https://doi.org/10.20546/ijcmas.2017.606.052

Siyal, A. A., Siyal, A. G., & Abro, Z. A. (2002). Salt affected soils their identification and reclamation. https://www.cabidigitallibrary.org/doi/full/10.5555/20023095851

Wu, D., Sui, Y., He, S., Wang, X., Li, C., & Kong, H. (2008). Removal of trivalent chromium from aqueous solution by zeolite

synthesized from coal fly ash. *Journal of Hazardous Materials*, *155*(3), 415-423. https://doi.org/10.1016/j.jhazmat.2007.11.082

Wu, J., Huang, D., Liu, X., Meng, J., Tang, C., & Xu, J. (2018). Remediation of As (III) and Cd (II) co-contamination and its mechanism in aqueous systems by a novel calcium-based magnetic biochar. *Journal of hazardous materials*, *348*, 10-19. https://doi.org/10.1016/j.jhazmat.2018.01.011

Wu, J., Zhang, L., Xia, Y., Peng, J., Wang, S., Zheng, Z., & Zhang, S. (2015). Effect of microwave heating conditions on the preparation of high surface area activated carbon from waste bamboo. *High Temperature Materials and Processes*, *34*(7), 667-674. https://doi.org/10.1515/htmp-2014-0096

Xin, O., Yitong, H., Xi, C., & Jiawei, C. (2017). Magnetic biochar combining adsorption and separation recycle for removal of chromium in aqueous solution. *Water Science and Technology*, *75*(5), 1177-1184. https://doi.org/10.2166/wst.2016.610

Yang, F., Zhang, S., Sun, Y., Cheng, K., Li, J., & Tsang, D.C. (2018). Fabrication and characterization of hydropHilic corn stalk biochar-supported nanoscale zero-valent iron composites for efficient metal removal. *Bioresource Technology, 265*, 490-497. doi:10.1016/j.biortech.2018.06.029

Yılmazoğlu, M., 2021. Organic-Inorganic Ion Exchange Materials for Heavy Metal Removal from Water. Remediation of Heavy Metals, 179-198. https://doi.org/10.1007/978-3-030-80334-6_7

Zhan, T., Zhang, Y., Yang, Q., Deng, H., Xu, J., & Hou, W. (2016). Ultrathin layered double hydroxide nanosheets prepared from a waterin-ionic liquid surfactant-free microemulsion for pHospHate removal from aquatic systems. *Chemical Engineering Journal, 302*, 459-465. doi:10.1016/j.cej.2016.05.073

Original Article

Journal of Drought and Climate change Research (JDCR)

Winter 2025, Vol. 2, No. 8, pp 55-84

10.22077/jdcr.2024.8055.1075

A Hybrid Fuzzy SWARA-VIKOR Model for Sustainable Wastewater Treatment Technology Selection in the Steel Industry

Akram Bemani [1*], Mohammad Hossein Sayadi [2], Mohsen Tayebi[1], Tahere Ardakani [1]

1 Department of Environmental Sciences & Engineering, Faculty of Agriculture & Natural Resources, Ardakan University, Ardakan, Iran.

2 Department of Agriculture, Faculty of Natural Resources and Environment, Shahid Bahonar University of Kerman, Kerman, Iran.

*** corresponding author: A.bemani@ardakan.ac.ir**

Keywords:
Sustainability prioritization, Water scarcity, Resource management Climate resilience, Water conservation.

Received:
19 Aug 2024

Revised:
15 Dec 2024

Accepted:
20 Dec 2024

Abstract

This study proposed an integrated decision-making framework that systematically incorporated specific industrial characteristics with fundamental sustainability considerations. The framework introduced a structured, analytical approach based on a dual methodology, combining SWARA (Step-wise Weight Assessment Ratio Analysis) and VIKOR (Višekriterijumsko kompromisno rangiranje) within a fuzzy logic framework. This integrated approach leveraged the strengths of each technique, offering a robust, multi-dimensional model to support precise and reliable decision-making in complex, sustainability-oriented contexts. The fuzzy SWARA method was used to determine the criteria and sub-criteria weights, followed by fuzzy VIKOR to rank decision alternatives. Five wastewater treatment technologies for the steel industry were identified and prioritized based on sustainability principles. These included CASPF (Conventional Activated Sludge with Mold Flow), MBR (Membrane Bio-Reactor), SBR (Sequencing Batch Reactors), AS (Activated Sludge), and UASB (Up-flow Anaerobic Sludge Blanket). The study demonstrated that this integrated approach yields more reliable and informed decisions in complex evaluations. Findings revealed that experts largely favor SBR technology as the most sustainable option.

How to cite this article:
Bemani, A., Sayadi, M.H., Tayebi, M. & Ardakani, T. (2024). A Hybrid Fuzzy SWARA-VIKOR Model for Sustainable Wastewater Treatment Technology Selection in the Steel Industry. *Journal of Drought and Climate change Research* (JDCR), 2(8), 55-84. 10.22077/jdcr.2024.8055.1075

Introduction

Effective water pollution control is essential for sustainable water management, especially in countries with water scarcity like Iran, where low rainfall and growing population, agriculture, and industry intensify water stress. Iran faces an increasing threat to its aquatic systems due to high effluent levels. (Fetanat et al., 2021a; Mahjouri et al., 2017). The steel industry, a key sector globally and in Iran, contributes significantly to this challenge due to its extensive use across various industries. Steel demand is expected to increase by 1.5 times by 2050 to meet the needs of a growing global population (Zhou et al., 2023). Currently, Iran ranks 14th in global steel production and leads in the Middle East. The steel industry, however, is a major water consumer, using significant volumes for cooling, waste transport, and dust control. This leads to large volumes of wastewater containing a mix of dissolved and chemical pollutants, necessitating varied treatment approaches for pollutant removal. Effective treatments must address solids, oils, greases, organic compounds, and toxic substances (Ali et al., 2022; Zhou et al., 2023). Selecting appropriate wastewater treatment technology (WTT) is essential for sustainability, which entails balancing economic, technical, environmental, and social factors (Singh et al., 2023; Wang et al., 2022). Key criteria for technology selection include acceptability, manageability, and affordability. Since the 1990s, sustainability indicators (SIs) have become vital in evaluating progress toward sustainable development (Chowdhury and Viraraghavan, 2021). This study introduced a structured, mathematical approach to assess SIs and identify sustainable WTTs for the steel industry in Iranian Ghadir, Ardakan.

Wastewater treatment plants were essential for sustainable water management, particularly in evaluating suitable treatment technologies (WTTs) using sustainability indicators (SIs) (Garrido-Baserba et al., 2014; Balkema et al., 2002). SIs address local and regional priorities and help assess if a technology fits specific decision-making contexts (Kalbar et al., 2012a). Environmental, social-cultural, and economic criteria evaluate a solution's effectiveness, while practical criteria assess feasibility (Balkema et al., 2002). Selecting sustainable WTTs using SIs is challenging for policymakers due to trade-offs between social, economic, environmental, and technical impacts and differing stakeholder perspectives (Kalbar et al., 2012b; Huang et al., 2011). MCDM methods support this process by balancing these aspects and integrating diverse criteria and stakeholder input, which is vital in complex decision-making (Figueira et al., 2004; Bottero et al., 2011). In the Conventional Activated Sludge

with Mold Flow (CASPF) technology, sludge is introduced into wastewater, optimizing conditions for the growth of aerobic microorganisms. This method involves directing a significant portion of settled sludge back into a designated pond, enhancing the aeration process and treatment efficiency (Bertanza et al., 2017).

MBR technology also relies on activated sludge but separates sludge using specialized filters. Unlike traditional filtration methods, MBR technology eliminates the need for sedimentation ponds by utilizing membranes capable of filtering particles as small as 0.1 to 0.4 micrometers. However, the system tends to be costlier due to the high expense of these membranes (Pardey et al., 2017). In SBR technology, sedimentation and aeration are used together and in combination. SBR technology has several periods and lasts several days. It takes 3 hours to fill the source and 2 hours to aerate the diffusers and jet aerators. Finally, half an hour should be allowed for the sludge to settle and half an hour for the discharged wastewater to be discharged (Aziz et al., 2020). Activated Sludge technology is the most common process of aerobic purification in which solid and liquid are separated and in the solid phase the least moisture and in the liquid phase the least possible particles remain (Nowrouzi et al., 2021). In UASB technology granular sludge layers are used for wastewater treatment. In this way, wastewater passes through these layers and a reaction is created between the organic matter in the wastewater and the microorganisms in the sludge layer. During this reaction, biogas is produced. These gases are removed from the upper part of the tank and with them, the pollutants are removed (Fetanat et al., 2021a).

Selecting criteria in many studies often stems from literature reviews, but local factors make it critical to include input from regional experts. By gathering both comprehensive literature insights and expert perspectives, decision-making accuracy in MCDM procedures improves. MCDM methods like SWARA and VIKOR, under fuzzy set theory, are effective for assessing multi-criteria decisions, accommodating both measurable and intangible factors simultaneously, and clarifying decision-maker preferences and rankings (Ghenai et al., 2020; Opricovic and Tzeng, 2007).

However, selecting WTTs in sustainable contexts often faces obstacles, including ambiguous data and reliance on local conditions (Mahjouri et al., 2017). Fuzzy set theory, created to handle vagueness (Zadeh, 1965), offers a way to model uncertainty similar to human reasoning, helping manage real-world inaccuracies in decision-making (Ren and Ren, 2018). By providing a flexible structure, fuzzy set theory helps address issues of precision and

supports decisions in complex situations (Cheng and Lin, 2002).

Recent studies have continued to highlight the importance of fuzzy MCDM (multi-criteria decision-making) techniques in selecting optimal wastewater treatment technologies (WWTT) based on criteria like economic, environmental, and technical factors. For example, research by Attri et al. (2022) used a combined fuzzy approach for WWTT selection, considering sustainability aspects, where the Sequencing Batch Reactor (SBR) emerged as a top choice. Additionally, fuzzy AHP combined with TOPSIS has been employed for technology comparison in various settings, emphasizing the role of scenario-based assessments and sustainability in decision-making (Zhang and Ju, 2021; Nuhu et al., 2020). These studies support the broader application of fuzzy methods like SWARA-VIKOR in refining WWTT selections across different industrial contexts

This research aimed to develop a hybrid model using two MCDM methods, SWARA and VIKOR, within a fuzzy framework (Fuzzy SWARA-VIKOR) to address a complex decision-making scenario involving a comprehensive set of sustainability indicators (SIs). The proposed MCDM approach assisted in selecting a sustainable wastewater treatment technology (WTT) from several alternatives, including Conventional Activated Sludge with Mold Flow (CASPF), Membrane Bio-Reactor (MBR), Sequencing Batch Reactors (SBR), Activated Sludge (AS), and Up-flow Anaerobic Sludge Blanket (UASB), tailored for wastewater management in the steel industry of Ghadir, Ardakan, Iran. Evaluation criteria are based on sustainability principles, and three experts were engaged in selecting the most suitable technology. The findings intended to support sustainable wastewater management and promote green growth in the sector.

Material and Methods

Methodology

This research aimed to identify a sustainable wastewater treatment technology for the steel industry in Ardakan, Iran, using Multi-Criteria Decision-Making (MCDM) methods. The fuzzy-based SWARA and VIKOR models were employed to help decision-makers select the most suitable technology, promoting sustainability and green goals in wastewater management. The methodology consists of ten stages, which were outlined in the research, with an overview provided in Figure 1.

The flowchart stages for selecting the appropriate sustainable wastewater treatment technology are as follows:

1. Stage 1: An expert team was invited to discuss the issue.

The expert team in this study likely

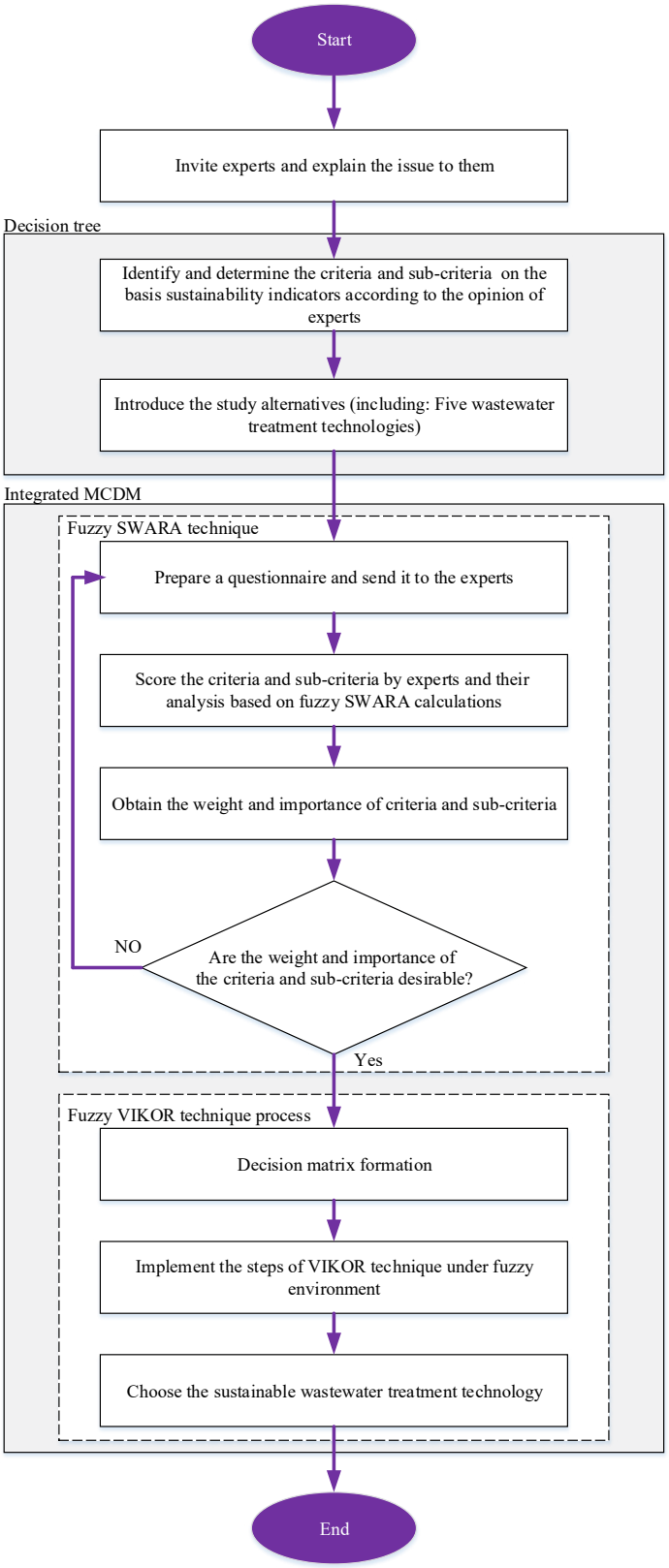

Fig.1. The flowchart of the study approach.

consists of professionals with knowledge and experience in wastewater treatment, environmental management, and sustainability, particularly as they relate to the steel industry. These experts may include environmental engineers, sustainability analysts, and industry consultants who were familiar with the economic, technical, and environmental aspects of wastewater treatment technologies (WTT). The team would contribute insights on criteria for WTT selection, assess the relevance of sustainability indicators, and help guide the application of the fuzzy SWARA-VIKOR model in evaluating the WTT options.

2. Stage 2: A framework of assessment criteria and sub-criteria based on sustainability pillars was identified, using expert opinions and relevant literature.
3. Stage 3: Five wastewater treatment technologies (CASPF, MBR, SBR, Activated Sludge Process, and UASB) were defined as alternatives.
4. Stage 4: A questionnaire was prepared and distributed to experts.
5. Stage 5: Experts evaluate and score the criteria and sub-criteria using fuzzy SWARA calculations.
6. Stage 6: The weights of the criteria and sub-criteria were determined.
7. Stage 7: If the weights were satisfactory, the process continues; if not, the process returns to Stage 2.
8. Stage 8: A decision matrix was formed for the fuzzy VIKOR method, evaluating alternatives based on sub-criteria.
9. Stage 9: The VIKOR method was applied under a fuzzy environment.
10. Stage 10: The most appropriate and sustainable wastewater treatment technology was selected.

Designed decision tree of the research

The designed decision tree for solving the problem of the research consists of four levels, these levels were defined as follows:

Level 1) Objective: Select the appropriate and sustainable WTT;

Level 2) Criteria: Technical (C1), environmental (C2), economic (C3), and social (C4);

Level 3) Sub-criteria: Reliability (SC1), complexity (SC2), efficiency (SC3), odor generation (SC4), sound impact (SC5), insects and other parasites generation (SC6), amount of sludge generation (SC7), Occupational health and safety (SC8), land requirements (SC9), construction costs (SC10), operating and maintenance costs (SC11), waste disposal costs (SC12), social acceptability (SC13) and employment (SC14).

Level 4) Alternatives: CASPF technology (A1), MBR technology (A2), SBR technology (A3), Activated Sludge technology (A4), and UASB technology (A5).

The indicators of sustainability as the framework for assessment criteria

Criteria for assessing the considered alternatives were given in Table 1. Sustainability typically encompasses achieving economic prosperity, social responsibility, and environmental stewardship (Fetanat et al., 2021a). Consequently, sustainability assessment criteria generally align with three core pillars: environmental, social, and economic factors. However, in evaluating sustainability for wastewater treatment and energy production from wastewater, a fourth technical pillar was also considered (Mahjouri et al., 2017). This study aimed to determine a sustainable wastewater treatment technology (WTT) by developing a framework of criteria and sub-criteria across these four pillars, informed by expert insights and prior research. The criteria framework used for evaluating the technologies is outlined in Table 1.

Table 1. The framework of defined criteria and sub-criteria for evaluation

Criteria	Sub-Criteria
C_1: Technical	SC_1: Reliability SC_2: Complexity SC_3: Efficiency
C_2: Environmental	SC_4: Odor generation SC_5: Noise impact SC_6: Insects and other parasites generation SC_7: Amount of sludge generation SC_8: Occupational health and safety
C_3: Economic	SC_9: Land requirements SC_{10}: Construction costs SC_{11}: Operation and maintenance costs SC_{12}: Waste disposal costs
C_4: Social	SC_{13}: Social acceptability SC_{14}: Employment

Alternatives

Based on literature references and expert team input, five wastewater treatment technologies have been identified as potential alternatives for addressing the issue. These technologies were as follows:

- **CASPF technology (A1):** The primary features of CASPF technology include the following (Aziz et al., 2020; Bertanza et al., 2017): Its use is very common in the treatment of various types of waste water;
- The base process of many types of activated sludge processes;
- Capable of converting into many kinds of activated sludge processes including step feeding, selector design, and anoxic/aerobic processes.

Despite its advantages, CASPF technology is generally not recommended for use in many industries due to several limitations:

1. The design requirements for mold flow

aeration in CASPF are more complex and challenging than those of other processes.

2. Balancing the injected oxygen levels with the oxygen demand is difficult to achieve consistently.
3. The management and operational aspects of this process are more complicated compared to alternative technologies.

Figure 2 is demonstrated the schematic of the CASPF process.

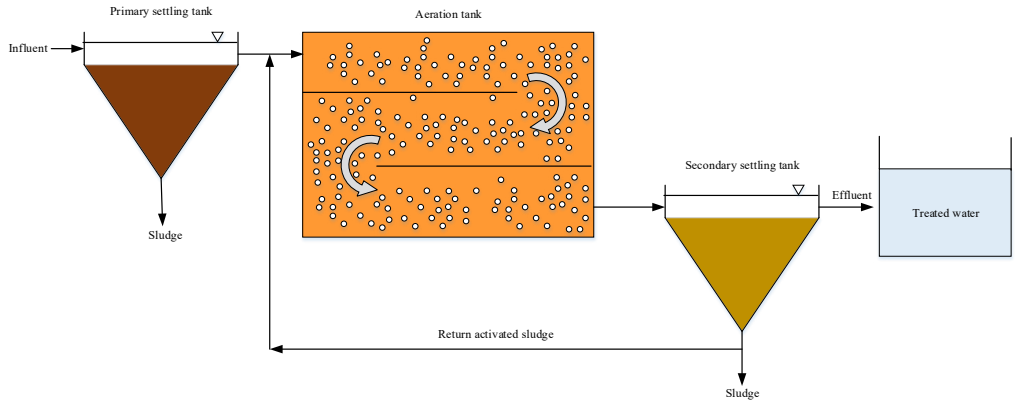

Fig. 2. The CASPF process (Aziz et al., 2020; Bertanza et al., 2017).

MBR technology (A2):

The main properties of MBR technology were as follows (Bertanza et al., 2017):

- Ability to remove all suspended solids;
- The ratio of food to microorganisms;
- Apply high loading rates;
- Production of low excess sludge;
- Relatively little space is required;
- Possibility of automation and less labor force;
- No need for an initial pool;
- High-quality outlet water.

Despite all the advantages of MBR technology in wastewater treatment, its use and implementation were faced with problems and limitations, which can include issues such (Pardey et al., 2017; Santos et al., 2020)directions and trends in academic research as well as commercial developments require further analysis. This paper aims to critically characterize and review worldwide academic research efforts in the area of MBRs as well as focus attention to commercial MBR applications. Various research papers published in peer-reviewed international journals were used as the database for the analysis provided in this paper. After a surge of MBR publications, research appears to have reached a plateau in the last 7 years using both submerged and external MBR units. Although much of the pioneering research occurred in Japan, France and the UK, countries such as South Korea, China and Germany have significantly contributed to the research pool in the last 5 years. The

primary research focus has been on water filtration MBRs with limited growth in extractive and gas diffusion MBRs which still hold un-tapped potential. Fundamental aspects studied in academic research predominantly involve issues related to fouling, microbial characterization and optimizing operational performance. Zenon occupies the majority of the MBR market in America, whereas Kubota and Mitsubishi-Rayon has a larger number of installations in other parts of the world. Due to more stringent regulations and water reuse strategies, it is expected that a significant increase in MBR plant capacity and widening of application areas will occur in the future. Potential application areas include nitrate removal in drinking water treatment, removal of endocrine disrupting compounds from water and wastewater streams; enhancing bio-fuels production via membrane assisted fermentation and gas extraction and purification MBRs. Treatment technology for water recycling encompasses a vast number of options. Membrane processes are regarded as key elements of advanced wastewater reclamation and reuse schemes and are included in a number of prominent schemes world-wide, e.g. for artificial groundwater recharge, indirect potable reuse as well as for industrial process water production. Membrane bioreactors (MBRs:

1. The need for high initial investment,
2. High cost of membrane replacement,
3. Higher energy consumption than common activated sludge methods,
4. Membrane clogging, and
5. Flow reduction.

The MBR technology schematic is indicated in Figure 3.

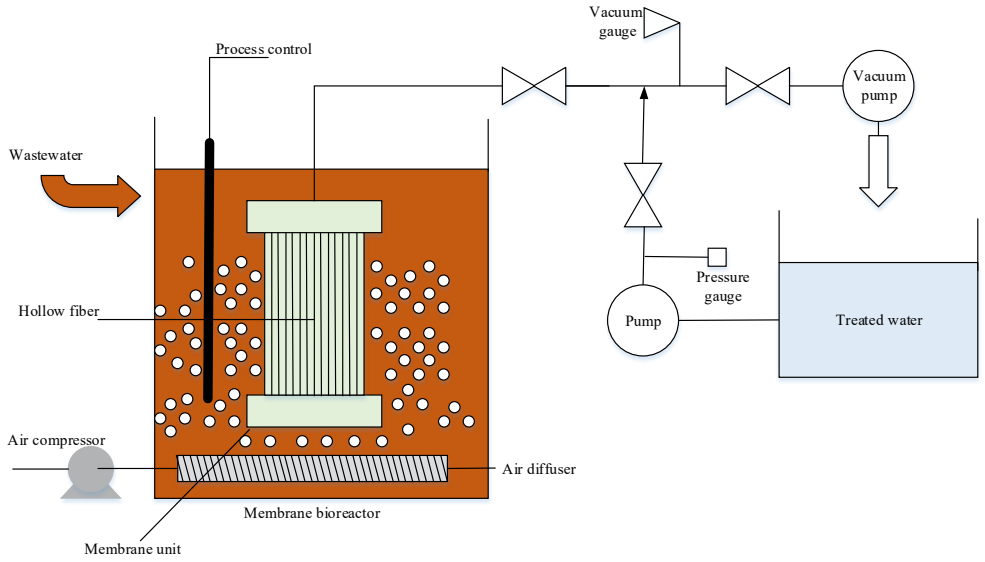

Fig. 3. The MBR technology (Pardey et al., 2017)

directions and trends in academic research as well as commercial developments require further analysis. This paper aims to critically characterize and review worldwide academic research efforts in the area of MBRs as well as focus attention to commercial MBR applications. Various research papers published in peer-reviewed international journals were used as the database for the analysis provided in this paper. After a surge of MBR publications, research appears to have reached a plateau in the last 7 years using both submerged and external MBR units. Although much of the pioneering research occurred in Japan, France and the UK, countries such as South Korea, China and Germany have significantly contributed to the research pool in the last 5 years. The primary research focus has been on water filtration MBRs with limited growth in extractive and gas diffusion MBRs which still hold un-tapped potential. Fundamental aspects studied in academic research predominantly involve issues related to fouling, microbial characterization and optimizing operational performance. Zenon occupies the majority of the MBR market in America, whereas Kubota and Mitsubishi-Rayon has a larger number of installations in other parts of the world. Due to more stringent regulations and water reuse strategies, it is expected that a significant increase in MBR plant capacity and widening of application areas will occur in the future. Potential application areas include nitrate removal in drinking water treatment, removal of endocrine disrupting compounds from water and wastewater streams; enhancing bio-fuels production via membrane assisted fermentation and gas extraction and purification MBRs. Treatment technology for water recycling encompasses a vast number of options. Membrane processes are regarded as key elements of advanced wastewater reclamation and reuse schemes and are included in a number of prominent schemes world-wide, e.g. for artificial groundwater recharge, indirect potable reuse as well as for industrial process water production. Membrane bioreactors (MBRs.

- **SBR technology (A3):** The main features of SBR technology include the following items (Aziz et al., 2020; Kim et al., 2019):

➢ Decrease in initial investment;
➢ Reduction of excreted sludge volume;
➢ Do not wash activated sludge during peak flow times;
➢ Reduced energy consumption compared to activated sludge systems;
➢ High resistance to hydraulic and organic shocks;
➢ Achieve very high efficiency;
➢ Perform all purification operations in one reactor;
➢ No need to return the sludge;

- Easy to develop and increase its capacity;
- No need a final clarifier and return sludge pumping.

This technology can have very good efficiency in industries, especially steel, and it can be used as a suitable and sustainable option in wastewater treatment and the reuse of its effluent.

Figure 4 shows the schematic scheme of the SBR technology.

primary treatment, secondary treatment, and tertiary treatment or polishing. In secondary treatment, dissolved oil and other organic pollutants may be consumed biologically by microorganisms. Biological treatment of complex chemicals in the petroleum industry wastewaters is specially challenging due to the inhibition and/or toxicity of these compounds when they serve as microbial substrates. Processes such as sequencing batch reactor (SBR.

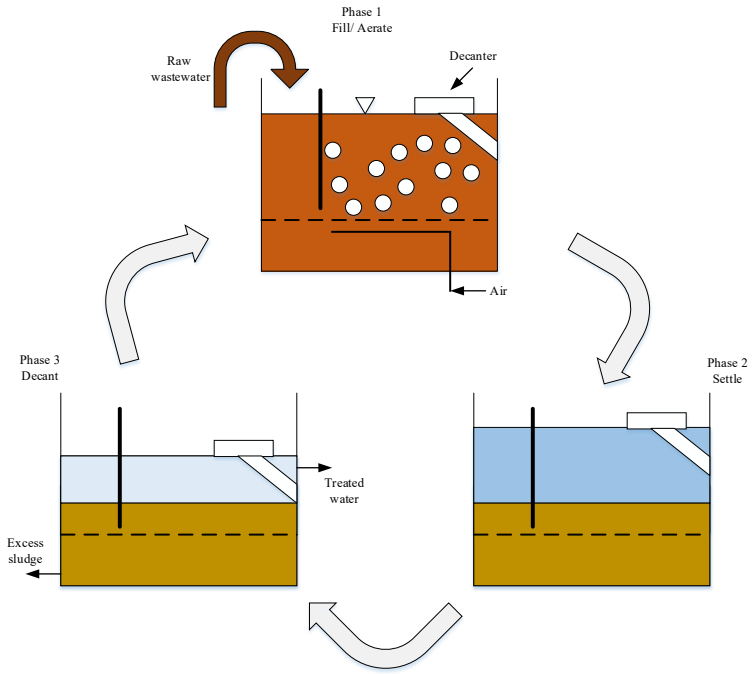

Fig. 4. The SBR technology (Jafarinejad, 2017)

- **Activated Sludge technology (A4):** The advantages of this technology were as follows (Nowrouzi et al., 2021; Pranoto et al., 2019)coal mining operations generally involve a huge number of workers. This\ u00a0condition causes its own challenges in managing environmental impacts that\u00a0potentially generated from human activities. One of them is domestic wastewater.\ u00a0Domestic waste water is waste water that comes from activities of daily living of\u00a0humans related to water usage. In mining operations, domestic wastewater is\u00a0generated

from office and residential areas. Because of the potential impact on the\u00a0environment, domestic wastewater must be treated before flowing to natural water\u00a0bodies. Since the beginning of mining operations in 1990s, PT Kaltim Prima Coal has\u00a0been building and operating Domestic Wastewater Treatment Plant (IPALD:

- High efficiency and efficiency in the removal of organic matter;
- Affordability in terms of economic costs;
- The use in different situations with different temperatures and PH.

Disadvantages that limit the use of this technology in the industry were as follows:

1. The need for relatively high electrical and mechanical equipment,
2. Increased imports and valuation compared to other types of wastewater treatment processes,
3. More need for specialized personnel and skilled personnel for maintenance than most purification systems, and
4. High costs of wastewater treatment plants owing to higher energy use during the years of operation.

The activated sludge system schematic is indicated in Figure 5.

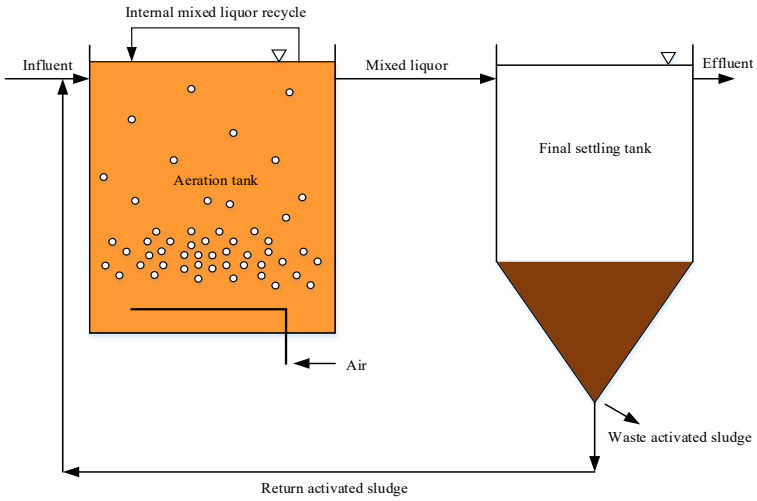

Fig. 5 The activated sludge system.

- **UASB technology (A5):** Important features of this technology are as follows (Adhikari and Lohani, 2019):
  - The space required to create UASB technology is not large. Since the load on the UASB system is 10 times higher than the aerobic system, the space required for the UASB system is one-tenth of the space that the aerobic system needs for the treatment of the same volume of wastewater.
  - In the UASB system, usable energy is produced in the form of biogas, 75% of which is methane gas. This gas is

applied in industrial heating systems or as a source for wastewater heating.

- The UASB system can be used to treat wastewater with very high pollution intensity and concentration between 1500 and 50 thousand mg of COD per liter.
- About 95% of the COD produced in this system is converted to biogas and the remaining 5% is converted to new cells or sludge. The amount of sludge produced in this system is about 10% of sludge that is produced by the same volume of wastewater but aerobically. Reducing sludge production also reduces its disposal cost significantly.

Due to its valuable features, this technology is an appropriate option for the production of wastewater into energy, and the energy produced by it can be used for other parts. Implementing this technology for wastewater treatment helps to navigate the wastewater management sector toward the aims of green growth and sustainability (Adhikari and Lohani, 2019; Cruz-Salomón et al., 2017; Fetanat et al., 2021a).

Figure 6 illustrates the schematic scheme of the UASB technology.

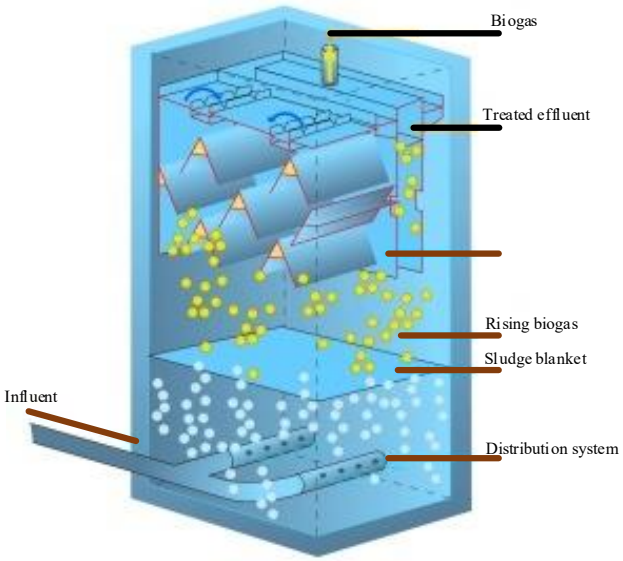

Fig. 6. The UASB technology (Fetanat et al., 2021a).

Integrated decision-making methodology

In the current work, an integrated decision-making model based on MCDM methods was applied. The model was the fuzzy-based SWARA and VIKOR for applying and implementing WTT in the steel industry of Iranian Ghadir in Ardakan city. The SWARA technique was utilized for weighting the criteria and the VIKOR technique was employed for prioritizing alternatives. Figure 7 shows a hybrid algorithm schematic related to the proposed model based on hierarchy.

the role of waste management sector shifts from being a regulator to being a facilitator. Instead of just regulating waste flows, the sector tries to encourage businesses to address all aspects of circular economy sustainability in a more efficient manner. The sustainability assessment in the sector lacks a hybrid method to aggregate the sustainability dimensions of circular economy strategies into a single summary indicator. This process is a multiple-criteria decision-making problem that requires the integration of circular economy strategies to form the sustainability indices. In order to make the right choices here, this study proposes a fuzzy three-phase group multiple-criteria decision-making approach. This approach integrates fuzzy analytic network process (fuzzy ANP.

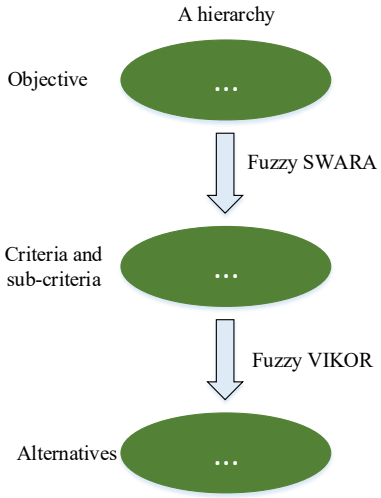

Fig. 7. Hybrid algorithm of decision-making (Fetanat et al., 2021b)

Fuzzy approach

The fuzzy approach, first introduced in 1965 (Zadeh, 1965), offers a mathematical and systematic method for decision-making in complex systems requiring sophisticated modeling. By using linguistic terms and expert knowledge, it facilitates decision-making when precise data were unavailable or hard to quantify. Ambiguous terms were converted into mathematical scales through fuzzy logic, enabling clearer assessments despite incomplete or

inaccessible data. This approach is especially beneficial in real-world scenarios where direct, measurable data were limited. Consequently, fuzzy logic has gained prominence for addressing uncertainty in decision-making processes (Chou and Chang, 2008; Lin and Wu, 2008).The TFN (triangular fuzzy number) $\tilde{N}$ was as three numbers (l, m, u), and the function of membership $\mu^{\tilde{N}}(x)$ was expressed by the formula (1): (1)

$$\mu^{\tilde{N}}(x)=\begin{cases}0 & x<l\\ (x-l)/(m-l) & l\le x\le m\\ (u-x)/(u-m) & m\le x\le u\\ 0 & x>u\end{cases}$$

where l, m, and u were real numbers in the range $l\le m\le u$. Figure 8 shows a TFN diagram.

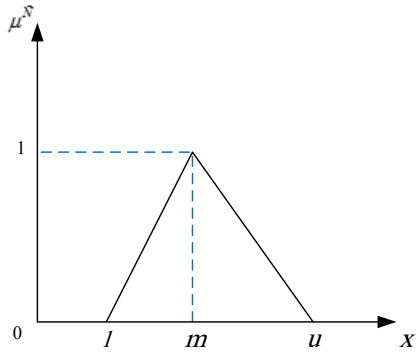

Fig. 8. A TFN (Fetanat et al., 2019).

Linguistic scales can be shown using fuzzy scales. Table 2 presents the scales based on a fuzzy approach equivalent to linguistic scales.

Table 2. The Linguistic and fuzzy scales of the study.

Linguistic scales	Abbreviation	TFN
None	N	(0, 0, 0.1)
Very low	VL	(0, 0.1, 0.2)
Low	L	(0.1, 0.2, 0.3)
Fairly low	FL	(0.2, 0.3, 0.4)
More or less low	MLL	(0.3, 0.4, 0.5)
Medium	M	(0.4, 0.5, 0.6)
More or less good	MLG	(0.5, 0.6, 0.7)
Fairly good	FG	(0.6, 0.7, 0.8)
Good	G	(0.7, 0.8, 0.9)
Very good	VG	(0.8, 0.9, 1)
Excellent	E	(0.9, 1, 1)

Fuzzy SWARA technique

The SWARA technique, a time-efficient MCDM method, exceled in capturing expert insights regarding the relative importance of criteria to determine their weights. It is particularly useful in complex or unconventional environments where it manages vague and imprecise data through fuzzy logic. The fuzzy approach stands out for its ability to assess criteria on a

relative, flexible scale, accommodating both numerical and linguistic variables. Consequently, fuzzy-based SWARA was employed here to calculate weights for defined criteria and sub-criteria. The steps to implement this technique were outlined by Agarwal et al. (2020) and Prajapati et al. (2019).

1. The selected criteria or sub-criteria for the decision-making process were classified in a descending order, based on the team of experts. Because the making decisions on the real subject were riddled with uncertainties, the linguistic scales used for proposing expects more independence. The linguistic scales given through a TFN were employed. The fuzzy assessment scales showed in Table 2.
2. This step started with the second criteria or sub-criteria, where the experts determined a linguistic scale for each criterion or sub-criteria j on the basis of the relative significance of the former (j-1) criteria or sub-criteria, for each criterion or sub-criteria based upon Table 2. This proportion was termed the comparative importance of average value, $\hat{b}_j$ (Keršulienė et al., 2010).
3. The coefficient $\hat{p}_j$ was computed as follows:

$$\hat{p}_j = \begin{cases} 1 & j = 1, \\ \hat{b}_j + 1 & j > 1, \end{cases} \quad (5)$$

The recalculated fuzzy weight $\hat{z}_j$ was calculated by the following formula:

$$\hat{z}_j = \begin{cases} 1 & j = 1, \\ \dfrac{\hat{z}_{(j-1)}}{\hat{p}_j} & j > 1, \end{cases} \quad (2)$$

4. The relative criteria and sub-criteria weights were computed by the following formula.

$$\hat{k}_j = \frac{\hat{z}_j}{\sum_{p=1}^{n} \hat{z}_p} \quad (3)$$

where, $\hat{k}_j$ denoted the relative fuzzy weight of the j^{th} criteria or sub-criteria, and n shows the number of criteria or sub-criteria.

5. Defuzzification of the obtained weight of the j^{th} criteria or sub-criteria was ulfilled by the center-of-area method which was the most employed (Turskis et al., 2019).

$$k_j = \frac{1}{3}\hat{k}_j = \frac{1}{3}(\hat{k}_{j\alpha} + \hat{k}_{j\beta} + \hat{k}_{j\gamma}) \quad (4)$$

where, the k_j showed defuzzified relative fuzzy weight of the j^{th} criteria or sub-criteria.

Fuzzy VIKOR technique

The VIKOR technique, specifically developed for multi-criteria optimization within complex systems, demonstrated superior decision-making capabilities due to its use of the v index and emphasis on achieving collective agreement. This has positioned VIKOR as a preferred choice in

recent research for addressing challenges involving conflicting criteria and sub-criteria (Chang, 2010; Opricovic and Tzeng, 2007). The method was structured to rank and select options based on their closeness to an ideal solution, which was particularly valuable in complex decision-making contexts. The relative significance of each alternative, with respect to the weighted sub-criteria, was determined by applying fuzzy scales, as outlined in Table 2.

Decision-making matrix formation

In this matrix, scoring alternatives based on sub-criteria completed according to the fuzzy scales. Figure 9 shows the schematic of the decision-making matrix of the study under the fuzzy scales.

$$\tilde{f} = \begin{array}{c} \\ A_1 \\ A_2 \\ \vdots \\ A_{m_{alt}} \end{array} \begin{array}{c} \begin{array}{cccc} SC_1 & SC_2 & & SC_{n_{sub}} \end{array} \\ \begin{bmatrix} \tilde{r}_{11} & \tilde{r}_{12} & \cdots & \tilde{r}_{1n_{sub}} \\ \tilde{r}_{12} & \tilde{r}_{22} & \cdots & \tilde{r}_{2n_{sub}} \\ \vdots & \vdots & \ddots & \vdots \\ \tilde{r}_{m_{alt}1} & \tilde{r}_{m_{alt}2} & \cdots & \tilde{r}_{m_{alt}n_{sub}} \end{bmatrix} \end{array} \quad (6)$$

Fig. 9. The decision-making matrix under the fuzzy scales.

here, the alternatives included $A_i,\ i=1,\ 2,\ \ldots, m_{alt}$, the sub-criteria define as $SC_j,\ j=1,\ 2,\ \ldots,\ n_{sub}$.

The arithmetic means approach was used to collect the responses of the expert team and to calculate triangular fuzzy numbers (TFNs). Using the method of Yager, fuzzy scales were taken out of the fuzzy mode and fuzzy numbers that were the result of the opinions of the expert team were summed up. The formula of the Yager method is as follows:

$$\tilde{N}_{i,j} = \int_0^1 \frac{1}{2}\left(\left(\tilde{N}_{i,j}\right)_\alpha^1 + \left(\tilde{N}_{i,j}\right)_\alpha^u\right) \quad (8)$$

$$d\alpha = \frac{l_{i,j} + 2m_{i,j} + u_{i,j}}{4} \quad (9)$$

In the following, implementing the computational process of the fuzzy VIKOR technique was introduced.

Computational steps of fuzzy VIKOR technique

The calculation steps of this technique were under Figure 10(Chang, 2010).

The following were the steps for calculating the fuzzy VIKOR technique for prioritizing the considered alternatives and choosing the most appropriate alternative according to the m_{alt} alternatives and n_{sub} sub-criteria (Chang, 2010; Sayadi et al., 2009).

Step 1. Decision-making matrix normalization:

Normalizing the decision matrix of the research was calculated by employing the formula (7).

$$f_{ij} = \frac{r_{ij}}{\sqrt{\sum_{i=1}^{m_{alt}} r_{ij}^2}} \quad (7)$$

Step 2. The ideal (positive) and anti-ideal

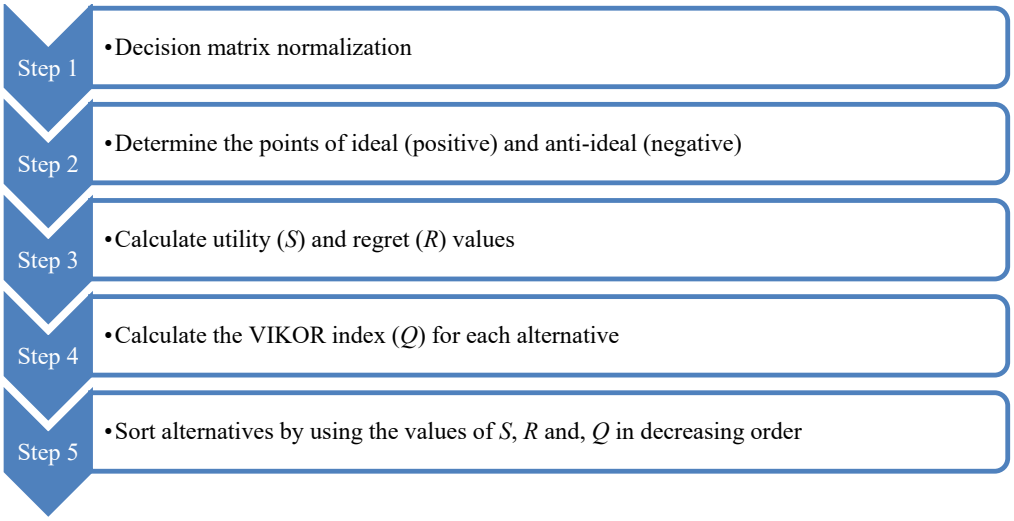

Fig 10. Steps of fuzzy VIKOR method.

(negative) points determination:

here, the values related to the best f_j^* and the worst f_j^- of each column belonging to the decision-making matrix were determined. The formulas of these two were presented as follows:

$$f_j^* = Max\left\{f_{ij}\right\} \qquad f_j^- = Min\left\{f_{ij}\right\} \qquad (12)$$
$$\forall i = 1,\ldots,m_{alt} \qquad \forall j = 1,\ldots,n_{sub}$$

Step 3. The values calculation of utility (S) and regret (R) for each alternative:

In this step, the desired value (utility) and the undesirable value (regret) were calculated. The S and R formulas were given as follows:

$$S_i = \sum_{j=1}^{n} w_j \frac{(f_j^* - f_{ij})}{(f_j^* - f_i^-)} \qquad (13)$$

$$R_i = Max\left[w_j \frac{(f_j^* - f_{ij})}{(f_j^* - f_j^-)}\right] \qquad (14)$$

Step 4. The calculation of the VIKOR index (Q) for each alternative.

This index was calculated by using the formula (10):

$$Q_i = v\left[\frac{S_i - S^*}{S^- - S^*}\right] + (1-v)\left[\frac{R_i - R^*}{R^- - R^*}\right] \qquad (10)$$

In the above formula:

$$S^- = MaxS_i \qquad R^- = MaxR_i$$
$$S^* = Min\ S_i \qquad R^* = Min\ R_i$$

v: The maximum weight was the group utility, which was considered equal to 0.5.

Step 5. The alternatives sort by using the S, R, and, Q values in decreasing order.

The obtained values of S, R, and Q were arranged in three prioritization lists in decreasing order. Therefore, the alternative with having the smallest value of Q was chosen as the optimal alternative, if the two following conditions were satisfied.

Condition 1. If alternatives A1 and A2 had the first and second rank among m_{alt} alternatives, formula (11) must be established:

$$Q(A_2) - Q(A_1) > \frac{1}{(m_{alt} - 1)} \qquad (11)$$

Condition 2. Alternative A1 must be the best alternative in at least one of the lists of *R* and *S* (Chang, 2010; Opricovic and Tzeng, 2007; Yücenur and Senol, 2021)it has some problems when solving MCDM problems .This study discussed existing problems in the traditional VIKOR method. The objective of this study was to develop a modified VIKOR method to avoid numerical difficulties in solving problems by the traditional VIKOR method .Several synthetic experiments were designed and assessed to verify the improvement of solution efficiency of the modified VIKOR method in MCA\ .u00a9 2009 Springer Science+Business Media B.V» ,«.author« » }] :dropping-particle» ,«» : «family: « »Chang» ,«given» : «Chia Ling» ,«non-dropping-particle» ,«» : «parse-names« :false» ,suffix» ,[{ «» : «container-title» : «Environmental Monitoring and Assessment» ,«id» : «ITEM» ,«1-issue« » ,«1-4» :issued» } : «date-parts] : « » ,{ [[«2010»]page,«339-344» : « »title» : «A modified VIKOR method for multiple criteria analysis» ,«type: « »article-journal» ,«volume,{ «168» : « »uris»] : «http//:www.mendeley.com/documents?/uuid7=f7eb11c2-dcc474-c-b649-3c9ad30d0f61» } ,{ [«id» : «ITEM-» ,«2itemData» } : «DOI/10.1016» : «j.ejor» ,«2006.01.020.ISSN,«03772217» : « »abstract» : «The VIKOR method was developed to solve MCDM problems with conflicting and noncommensurable) different units.

Results and Discussion

The results from the SWARA and VIKOR techniques, conducted within a fuzzy framework, were presented here. This hybrid fuzzy-based SWARA-VIKOR model had been applied to address the selection of a sustainable wastewater treatment technology (WTT) for the steel industry in Iranian Ghadir, located in Ardakan, Iran. By employing this model, five WTT alternatives were evaluated based on 14 defined sustainability indicators (SIs).

The calculations result of the proposed hybrid model

The numerical values of the proposed integrated model were given as follows:

Computing the criteria weights and sub-criteria employing the technique of fuzzy SWARA

The present part showed the findings of the SWARA method under the fuzzy environment to weigh the determined criteria. After a brainstorming meeting, the expert team ordered all the criteria or sub-criteria in decreasing arrangement regarding their importance. The relative importance of the average value, , of each criterion or sub-criteria was assessed by the experts 'group utilizing fuzzy scales presented in Table 2. The formula (2) was employed for the computation of the fuzzy coefficient,

$\hat{p}_j$. Next, formulas (3) and (4) calculate the recalculated fuzzy weight, $\hat{z}_j$, and the relative fuzzy weight, $\hat{k}_j$, of criterion or sub-criteria, respectively (see Tables 3 and 4). Defuzzification of the relative fuzzy weight, k_j, of each criteria or sub-criteria was performed utilizing the center-of-area method by using the formula (5).

The findings of this technique were given as follows:

Table 3. Findings of fuzzy SWARA to weight criteria.

Criteria	$\hat{b}_j$			$\hat{p}_j$			$\hat{z}_j$			$\hat{k}_j$			k_j
C_3	-	-	-	1	1	1	1	1	1	0.9487	0.9751	1.0080	0.6043
C_1	0.80	0.83	0.87	1.80	1.83	1.87	0.5556	0.5464	0.5348	0.3707	0.3695	0.3669	0.2282
C_2	0.77	0.80	0.83	1.77	1.80	1.83	0.3139	0.3036	0.2922	0.1804	0.1763	0.1719	0.1090
C_4	0.70	0.73	0.77	1.70	1.73	1.77	0.1846	0.1755	0.1651	0.0988	0.0949	0.0904	0.0585

Table 4. Findings of fuzzy SWARA to weight sub-criteria.

Sub-criteria	$\hat{b}_j$			$\hat{p}_j$			$\hat{z}_j$			$\hat{k}_j$			k_j
SC_{10}				1	1	1	1	1	1	0.6881	0.7323	0.7809	0.5208
SC_{11}	0.80	0.83	0.87	1.80	1.83	1.87	0.5556	0.5464	0.5348	0.2928	0.3004	0.3063	0.2128
SC_{12}	0.77	0.8	0.83	1.77	1.80	1.83	0.3139	0.3036	0.2922	0.1467	0.1472	0.1470	0.1043
SC_9	0.70	0.73	0.77	1.70	1.73	1.77	0.1846	0.1755	0.1651	0.0814	0.0801	0.0780	0.0567
SC_3	0.53	0.57	0.63	1.53	1.57	1.63	0.1207	0.1118	0.1013	0.0517	0.0496	0.0465	0.0350
SC_8	0.50	0.53	0.57	1.50	1.53	1.57	0.0804	0.0731	0.0645	0.0339	0.0319	0.0291	0.0224
SC_1	0.43	0.5	0.53	1.43	1.50	1.53	0.0563	0.0487	0.0422	0.0235	0.0210	0.0188	0.0150
SC_7	0.37	0.43	0.50	1.37	1.43	1.50	0.0411	0.0341	0.0281	0.0170	0.0146	0.0125	0.0104
SC_{14}	0.43	0.5	0.53	1.43	1.50	1.53	0.0287	0.0227	0.0184	0.0118	0.0097	0.0081	0.0070
SC_4	0.33	0.37	0.43	1.33	1.37	1.43	0.0216	0.0166	0.0128	0.0089	0.0071	0.0057	0.0051
SC_2	0.33	0.37	0.53	1.33	1.37	1.53	0.0162	0.0121	0.0084	0.0067	0.0051	0.0037	0.0037
SC_{13}	0.20	0.33	0.43	1.20	1.33	1.43	0.0135	0.0091	0.0059	0.0055	0.0039	0.0026	0.0028
SC_6	0.20	0.33	0.47	1.20	1.33	1.47	0.0113	0.0068	0.0040	0.0046	0.0029	0.0018	0.0022
SC_5	0.20	0.33	0.37	1.20	1.33	1.37	0.0094	0.0051	0.0029	0.0038	0.0022	0.0013	0.0017

Tables 3 and 4 displayed the calculated weights for the study's criteria and sub-criteria. In these tables, criteria (in Table 3) and sub-criteria (in Table 4) were first organized in descending order, based on expert opinions. The criteria and sub-criteria were then scored using linguistic variables from Table 2, which were converted into triangular fuzzy numbers (TFNs). Applying the Yager method, these TFNs were then reduced to single values. As a result, each criterion and sub-criterion had three scores, except for the last column, which listed the normalized weights calculated for assessment. The value in column $\hat{k}_j$ and k_j were derived using the center-to-area method, and results were normalized in the last column.

Determining the most critical criteria for selecting a sustainable WTT could be complex, but the proposed integration of the fuzzy SWARA-VIKOR methods with sustainability indicators (SIs) offered a systematic and thorough framework. Through the fuzzy SWARA approach, criteria weights were precisely obtained to guide the selection of a sustainable WTT for the Iranian Ghadir steel industry in Ardakan, Iran.

In Table 3, among four criteria, economic criterion (C_3), with a value of 0.2661 had the highest rank among other criteria, followed by the technical criterion (C_1), with a weight of 0.2538. Then the environmental criteria (C2), and social criteria (C4), with weights of 0.2446 and 0.2355, respectively, were in the next ranks.

Table 4 illustrated the weights of the sub-criteria defined for all four technical, environmental, economic, and social criteria. Among these, economic sub-criteria including construction costs (SC_{10}), with a value (0.5208), operation and maintenance costs (SC_{11}), with weight (0.2128), and sludge disposal costs (SC_{12}), with a value (0.1043) were the foremost sub-criteria that overshadows the choice of appropriate and sustainable WTT. Because the factors of cost management systems or financial planning had an effective effect on industrial actions and the establishment of technologies in the industry. It is required to assign adequate financial resources to implement suitable and sustainable technologies like WTT for upgrading sustainable wastewater management in diverse industries like the steel industry. Among technical sub-criteria, efficiency (SC_3) and reliability (SC_1) were the two most significant sub-criteria of technical, having weights with the values of 0.0350 and 0.0150, respectively. Because these sub-criteria were related to the important sectors of the avoidance of wasting materials, energy, capital, and time doing work and robustness to the failure in the wastewater treatment equipment of industries. Occupational health and safety (SC_8), amount of sludge generation (SC_7), and odor generation (SC_4) were the highest importance among environmental sub-criteria, having weights with values of (0.0224), (0.0104), and (0.0051), respectively. Owing to they affect the health of individuals. Social acceptability (SC_{14}), was the most significant sub-criteria among social sub-criteria, having a weight value of 0.0070. It was taken into consideration as a very important criterion in the use of wastewater treatment systems. Therefore, these were the topmost of the importance in implementing an appropriate and sustainable WTT for the steel industry of Iranian Ghadir in Ardakan city, Iran.

Finally, this prioritization of criteria and sub-criteria corresponds to the real situation in the steel industry chain in Iran that most economic and technical criteria were effective in selecting, transferring, and implementing technology, especially in sustainable wastewater management of these industries.

The prioritization of candidate alternatives employing the method of fuzzy VIKOR

In the present part, after obtaining the criteria and sub-criteria weights, the

prioritization of the candidate alternatives and selection of the most sustainable alternative was obtained by using the VIKOR method under the fuzzy environment. Five alternatives were evaluated (A_1, A_2, A_3, A_4, and A_5). The experts or decision-makers (DMs) assess each alternative utilizing a fuzzy assessment scale and construct the decision-making matrix (DMM) of fuzzy VIKOR (see Tables 5 and 6). Next, formula (7) was employed to calculate the normalized values of the DMM (see Table 7). Then, the best f_j^* and the worst f_j^- values of each column of the decision-making matrix were determined by the formula (8) (see Table 8). Formulas (9), (10), and (11) were used for obtaining the values of *S*, *R*, and *Q*, respectively. The alternatives were sorted by using the values of *S*, *R,* and, *Q* indices in decreasing order and alternatives were ranked according to these indices (see Tables 9, 10, and 11). Therefore, the option with having the smallest value of *Q* was determined as the most sustainable alternative, if the two conditions of the VIKOR technique were satisfied.

The findings of this technique were shown as follows:

Table 5. Linguistic importance of the five candidate alternatives concerning the sub-criteria by the three DMs.

DMs	Alter	SC1	SC2	SC3	SC4	SC5	SC6	SC7	SC8	SC9	SC10	SC11	SC12	SC13	SC14
DM_1	A_1	L	M	VL	L	L	G	M	L	L	VL	VL	VL	L	L
	A_2	G	G	FG	VL	VL	L	MLL	G	L	MLL	M	MLL	L	L
	A_3	VG	VG	MLG	L	VL	M	VG	MLL	G	L	MLG	FG	M	MLL
	A_4	VL	VL	MLL	L	M	VL	M	VG	MLL	VL	L	VL	VL	M
	A_5	MLG	MLL	G	FG	L	VL	G	MLG	MLL	M	MLL	VL	MLL	VL
DM_2	A_1	MLL	MLL	M	MLL	MLG	MLG	MLL	MLG	MLL	M	M	L	MLL	MLG
	A_2	MLG	MLG	G	M	L	MLL	MLG	MLG	MLG	M	MLL	M	MLG	MLL
	A_3	VG	G	G	MLG	M	MLL	G	MLG	G	MLL	G	G	MLL	MLG
	A_4	L	M	MLG	MLL	M	MLL	M	MLL	MLG	L	MLL	M	M	MLL
	A_5	G	MLG	MLG	G	MLG	L	MLG	G	M	MLL	M	L	M	M
DM_3	A_1	M	MLG	MLL	M	M	M	MLG	M	M	MLL	MLL	FL	M	M
	A_2	M	M	VG	MLL	FL	M	FG	M	M	FG	MLG	FG	M	M
	A_3	G	G	VG	M	MLL	MLG	G	FG	M	M	VG	VG	MLG	FG
	A_4	FL	FG	M	MLG	MLL	MLG	FG	MLG	FG	FL	M	MLL	MLL	MLG
	A_5	VG	FG	M	VG	M	FL	M	VG	FG	MLG	FG	FL	FG	MLL

The linguistic values of this table were converted to triangular fuzzy and then, using the Yager method, they were taken out of the TFNs and converted into single values as given the following table.

Table 6. Single values of the five alternatives relative to the defined sub-criteria of the research.

	SC1	SC2	SC3	SC4	SC5	SC6	SC7	SC8	SC9	SC10	SC11	SC12	SC13	SC14
A_1	0.43	0.5	0.33	0.37	0.43	0.63	0.5	0.43	0.37	0.33	0.33	0.2	0.37	0.43
A_2	0.63	0.63	0.8	0.33	0.2	0.37	0.57	0.63	0.43	0.53	0.5	0.53	0.43	0.37
A_3	0.87	0.83	0.77	0.43	0.33	0.5	0.83	0.57	0.7	0.37	0.77	0.8	0.5	0.57
A_4	0.2	0.53	0.43	0.5	0.33	0.5	0.53	0.5	0.57	0.2	0.37	0.33	0.33	0.5
A_5	0.77	0.57	0.63	0.8	0.43	0.2	0.63	0.57	0.53	0.5	0.43	0.2	0.53	0.33

Then, the normalized values of the Table 6 were given in Table 7. It is shown as follows:

Table 7. Normalized values of the alternatives relative to the defined sub-criteria of the research.

	SC1	SC2	SC3	SC4	SC5	SC6	SC7	SC8	SC9	SC10	SC11	SC12	SC13	SC14
A1	0.1483	0.1634	0.1115	0.1523	0.2500	0.2864	0.1634	0.1593	0.1423	0.1710	0.1375	0.0971	0.1713	0.1955
A2	0.2172	0.2059	0.2703	0.1358	0.1163	0.1682	0.1863	0.2333	0.1654	0.2746	0.2083	0.2573	0.1991	0.1682
A3	0.3000	0.2712	0.2601	0.1770	0.1919	0.2273	0.2712	0.2111	0.2692	0.1917	0.3208	0.3883	0.2315	0.2591
A4	0.0690	0.1732	0.1453	0.2058	0.1919	0.2273	0.1732	0.1852	0.2192	0.1036	0.1542	0.1602	0.1528	0.2273
A5	0.2655	0.1863	0.2128	0.3292	0.2500	0.0909	0.2059	0.2111	0.2038	0.2591	0.1792	0.0971	0.2454	0.1500

The obtained results for f_j^* and f_j^- is shown as follows:

Table 8. The obtained results for f_j^* and f_j^-.

	SC1	SC2	SC3	SC4	SC5	SC6	SC7	SC8	SC9	SC10	SC11	SC12	SC13	SC14
Sub-criteria weight	0.5208	0.2128	0.1043	0.0567	0.0350	0.0224	0.0150	0.0104	0.0070	0.0051	0.0037	0.0028	0.0022	0.0017
A1	0.1483	0.1634	0.1115	0.1523	0.2500	0.2864	0.1634	0.1593	0.1423	0.1710	0.1375	0.0971	0.1713	0.1955
A2	0.2172	0.2059	0.2703	0.1358	0.1163	0.1682	0.1863	0.2333	0.1654	0.2746	0.2083	0.2573	0.1991	0.1682
A3	0.3000	0.2712	0.2601	0.1770	0.1919	0.2273	0.2712	0.2111	0.2692	0.1917	0.3208	0.3883	0.2315	0.2591
A4	0.0690	0.1732	0.1453	0.2058	0.1919	0.2273	0.1732	0.1852	0.2192	0.1036	0.1542	0.1602	0.1528	0.2273
A5	0.2655	0.1863	0.2128	0.3292	0.2500	0.0909	0.2059	0.2111	0.2038	0.2591	0.1792	0.0971	0.2454	0.1500
f_j^*	0.5208	0.2712	0.2703	0.3292	0.2500	0.2864	0.2712	0.2333	0.2692	0.2746	0.3208	0.3883	0.2454	0.2591
f_j^-	0.0690	0.1634	0.1115	0.1358	0.1163	0.0909	0.1634	0.1593	0.1423	0.1036	0.1375	0.0971	0.1528	0.1500

The values obtained for the indices of *S*, *R*, and *Q* were shown as follows:

Table 9. Obtained results of S, R and Q for the five alternatives.

Alternatives	*S*	*R*	*Q*
A1	0.8432	0.4294	0.7854
A2	0.6077	0.3499	0.4249
A3	0.3337	0.2545	0.0000
A4	0.8911	0.0975	1.0000
A5	0.5458	0.0986	0.2649

The alternatives were sorted by using the values of *S*, *R,* and, *Q* indices in decreasing order as illustrated the following table:

Table 10. Sorted values of S, R, and Q.

Alternatives	Sorted values of *S*	Alternatives	Sorted values of *R*	Alternatives	Sorted values of *Q*
A4	0.8911	A1	0.4294	A4	1.0000
A1	0.8432	A2	0.3499	A1	0.7854
A2	0.6077	A3	0.2545	A2	0.4249
A5	0.5458	A5	0.0986	A5	0.2649
A3	0.3337	A4	0.0975	A3	0.0000

The alternatives were ranked according to these indices as given in the following table:

Table 11. Alternatives ranking by S, R, and Q.

	Alternatives ranking		
	S	*R*	*Q*
1	A_3	A_1	A_3
2	A_5	A_2	A_5
3	A_2	A_3	A_2
4	A_1	A_5	A_1
5	A_4	A_4	A_4

Two conditions of the VIKOR technique were as follows:

Condition 1:

$$Q(A_5)-Q(A_3)>\frac{1}{(5-1)} \quad \rightarrow \quad 0.2649-0>\frac{1}{4}$$

Condition 2:

The third alternative (A_3) in *S* and *R* was also the best.

Therefore, the alternative with having the smallest value of *Q* was determined as the most sustainable alternative, if the two conditions of the VIKOR technique were satisfied. To this, since the lowest value based on the *Q* index was assigned to the third alternative (A_3) and the two conditions were also met, thus this alternative was selected as the most appropriate alternative. It was SBR technology. This technology had its characteristics and was a cheap system to treat low and high volumes of wastewater. In addition, a valuable advantage of SBR technology was that do not require a clarifier. Hence, it saves money and was affordability for the steel industry of Iranian Ghadir in Ardakan city, Iran. Based on the results, the fifth alternative (A_5) ranks second. It was UASB technology. The unique capabilities of this technology have attracted much attentions in recent years to generate energy from the wastewater treatment process. For industry, such as steel was the most suitable alternative if it seeks to produce energy with wastewater treatment. The study (Fetanat et al., 2021a) assessed several technologies for energy production from wastewater treatment, and the results showed that UASB technology was among the technologies evaluated as the most appropriate and sustainable alternative.

This study aligns with previous research in sustainable wastewater treatment technology (WTT) selection, particularly studies that emphasize a balance between economic, technical, and environmental criteria. For example:

1. **Economic Priorities:** Research by Fetanat et al. (2021) and Aziz et al. (2020) has similarly highlighted economic factors—specifically Construction costs and Operation and maintenance costs—as crucial considerations in WTT choice, especially in developing regions where budget constraints were significant.

2. **Technical Aspects:** The importance of technical criteria like Efficiency and Reliability was echoed in studies by Mahjouri et al. (2017) and Chang (2010), where these indicators were emphasized as central to achieving optimal treatment performance and ensuring system resilience. These studies also prioritize technologies with stable, reliable outputs for wastewater treatment.
3. **Environmental Considerations:** Environmental factors, particularly those concerning occupational health, sludge management, and odor control, were stressed in prior research, such as by Bertanza et al. (2017) and Pardey et al. (2017), which underscore the need for safer, more environmentally sound WTT systems. In these studies, MBR technology sometimes ranks higher due to its filtration capabilities, although its costs were a limiting factor.
4. **Methodological Approach:** While past studies, including those by Opricovic and Tzeng (2007) and Chou and Chang (2008), often apply VIKOR alone or use fuzzy MCDM methods like AHP or TOPSIS, this study's hybrid fuzzy SWARA-VIKOR approach was unique. The combined model offers refined weighting and prioritization, allowing for nuanced decision-making that considers economic, technical, and environmental criteria simultaneously.
5. **Technology Rankings:** Similar to this study, other research often ranks SBR as a top choice for industrial WTT due to its adaptability and effectiveness, particularly in studies with industrial application contexts (Ren and Ren, 2018). However, in studies prioritizing environmental sustainability, MBR was sometimes rated higher, despite its higher costs, for its advanced particle filtration capability (Lin and Wu, 2008).

Recent research emphasizes a strong need for sustainable wastewater treatment in the steel industry. Studies like Purkait et al. (2023) focus on various advanced techniques such as ozonation and electrocoagulation for steel industry wastewater remediation, underscoring the importance of both economic and environmental considerations. This approach complements the findings of this study, which used hybrid MCDM models to prioritize technologies based on criteria such as cost, efficiency, and environmental impact. Additionally, both studies highlight the complexity of wastewater treatment in steel plants and the critical role of sustainable solutions in the industry's wastewater management strategies. In summary, this research builds on a foundation established by similar studies, adding value with a novel hybrid MCDM model that balances conflicting

criteria more effectively for WTT selection in complex industrial settings. This structured framework provides a practical tool for policymakers aiming for sustainable development in the industrial wastewater sector, particularly within regions with resource constraints.

Conclusion

This study seeks to identify key sustainability indicators and select the most suitable wastewater treatment technology (WTT) for the Iranian Ghadir steel industry in Ardakan, using a comprehensive model to address complex decision-making conditions. Given the technical challenges and rising costs of WTT, a systematic approach was crucial. The research proposes a hybrid model combining SWARA and VIKOR techniques with fuzzy logic to effectively compare multiple conflicting criteria. Results indicate that Construction costs and Operation and maintenance costs were the most influential economic indicators, while Efficiency and Reliability were central to technical performance. In terms of environmental impact, Occupational health and safety, Amount of sludge generation, and Odor generation rank highly, with Noise impact being least influential.

The Sequencing Batch Reactor (SBR) emerged as the most sustainable WTT option, followed by UASB, highlighting the value of fuzzy SWARA in defining criteria based on sustainability principles and fuzzy VIKOR in ranking alternatives. This was the first application of the model in Iran's steel industry, offering policymakers a structured framework for sustainable decision-making in wastewater management. The authors anticipate that this model will guide the industry toward sustainability goals and facilitate future technological advancements for sustainable industrial systems.

References

Ali, I., Gupta, V. K., & Saleh, T. A. (2022). Emerging treatment technologies for industrial wastewater: A critical review. *Journal of Environmental Management*, *302*, 114004. https://doi.org/10.1016/j.jenvman.2022.114004

Adhikari, J. R., & Lohani, S. P. (2019). Design, installation, operation and experimentation of septic tank – UASB wastewater treatment system. *Renewable Energy*, *143*, 1406–1415. https://doi.org/10.1016/j.renene.2019.04.059

Agarwal, S., Kant, R., & Shankar, R. (2020). Evaluating solutions to overcome humanitarian supply chain management barriers: A hybrid fuzzy SWARA – Fuzzy WASPAS approach. *International Journal of Disaster Risk Reduction*, *51*, 101838. https://doi.org/10.1016/j.ijdrr.2020.101838

Attri, R., Sharma, L., & Singh, K. (2022). A combined fuzzy approach for wastewater treatment technology selection considering sustainability aspects. *Journal of Environmental Management*, *300*(1), 123-135. https://doi.

org/10.1016/j.jenvman.2022.112233

Aziz, S. Q., Omar, I. A., Bashir, M. J. K., & Mojiri, A. (2020). Stage by stage design for primary, conventional activated sludge, SBR and MBBR units for residential wastewater treatment and reusing. *Advances in Environmental Research*, *9*, 233–249.

Balkema, A. J., Preisig, H. A., Otterpohl, R., & Lambert, F. J. D. (2002). Indicators for the sustainability assessment of wastewater treatment systems. *Urban Water*, *4*, 153–161. https://doi.org/10.1016/S1462-0758(02)00014-6

Bertanza, G., Canato, M., Laera, G., Vaccari, M., Svanström, M., & Heimersson, S. (2017). A comparison between two full-scale MBR and CAS municipal wastewater treatment plants: Techno-economic-environmental assessment. *Environmental Science and Pollution Research*, *24*, 17383–17393. https://doi.org/10.1007/s11356-017-9409-3

Bottero, M., Comino, E., & Riggio, V. (2011). Application of the analytic hierarchy process and the analytic network process for the assessment of different wastewater treatment systems. *Environmental Modelling & Software*, *26*, 1211–1224. https://doi.org/10.1016/j.envsoft.2011.04.002

Chang, C. L. (2010). A modified VIKOR method for multiple criteria analysis. *Environmental Monitoring and Assessment*, *168*, 339–344. https://doi.org/10.1007/s10661-009-1117-0

Cheng, C. H., & Lin, Y. (2002). Evaluating the best main battle tank using fuzzy decision theory with linguistic criteria evaluation. *European Journal of Operational Research*, *142*, 174–186. https://doi.org/10.1016/S0377-2217(01)00280-6

Chou, S. Y., & Chang, Y. H. (2008). A decision support system for supplier selection based on a strategy-aligned fuzzy SMART approach. *Expert Systems with Applications*, *34*, 2241–2253. https://doi.org/10.1016/j.eswa.2007.03.001

Chowdhury, P., & Viraraghavan, T. (2021). An assessment of eco-friendly treatment technologies for industrial wastewater. *Water Environment Research*, *93*(5), 619–632. https:// doi.org// 10.57519/crret.2021.10089

Cruz-Salomón, A., Meza-Gordillo, R., Rosales-Quintero, A., Ventura-Canseco, C., Lagunas-Rivera, S., & Carrasco-Cervantes, J. (2017). Biogas production from a native beverage vinasse using a modified UASB bioreactor. *Fuel*, *198*, 170–174. https://doi.org/10.1016/j.fuel.2016.11.046

Fetanat, A., Mofid, H., Mehrannia, M., & Shafipour, G. (2019). Informing energy justice-based decision-making framework for waste-to-energy technologies selection in sustainable waste management: A case of Iran. *Journal of Cleaner Production*, *228*, 1377–1390. https://doi.org/10.1016/j.jclepro.2019.04.215

Fetanat, A., Tayebi, M., & Mofid, H. (2021a). Water-energy-food security nexus based selection of energy recovery from wastewater treatment technologies: An extended decision-making framework under intuitionistic fuzzy environment. *Sustainable Energy Technologies and Assessments*, *43*, 100937. https://doi.org/10.1016/j.seta.2020.100937

Fetanat, A., Tayebi, M., & Shafipour, G. (2021b). Management of waste electrical and electronic equipment based on circular economy strategies: Navigating a sustainability transition toward waste management

sector. *Clean Technologies and Environmental Policy*, *23*, 343–369. https://doi.org/10.1007/s10098-020-02006-7

Figueira, J., Greco, S., & Ehrgott, M. (2005). Multiple criteria decision analysis: State of the art surveys. *Operations Research & Management Science*, Springer-Verlag New York, 2005. https://doi.org/10.1007/b100605

Garrido-Baserba, M., Hospido, A., Reif, R., Molinos-Senante, M., Comas, J., & Poch, M. (2014). Including the environmental criteria when selecting a wastewater treatment plant. *Environmental Modelling & Software*, *56*, 74–82. https://doi.org/10.1016/j.envsoft.2013.11.008

Ghenai, C., Albawab, M., & Bettayeb, M. (2020). Sustainability indicators for renewable energy systems using a multi-criteria decision-making model and extended SWARA/ARAS hybrid method. *Renewable Energy*, *146*, 580–597. https://doi.org/10.1016/j.renene.2019.06.157

Huang, I. B., Keisler, J., & Linkov, I. (2011). Multi-criteria decision analysis in environmental sciences: Ten years of applications and trends. *Science of the Total Environment*, *409*(19), 3676–3684. https://doi.org/10.1016/j.scitotenv.2011.06.022

Jafarinejad, S. (2017). Recent developments in the application of sequencing batch reactor (SBR) technology for the petroleum industry wastewater treatment. *Chemistry International*, *3*, 342–350. https://doi.org/10.5281/zenodo.1473343

Kalbar, P. P., Karmakar, S., & Asolekar, S. R. (2012a). Technology assessment for wastewater treatment using multiple-attribute decision-making. *Technology in Society*, *34*, 295–302. https://doi.org/10.1016/j.techsoc.2012.10.001

Kalbar, P. P., Karmakar, S., & Asolekar, S. R. (2012b). Selection of an appropriate wastewater treatment technology: A scenario-based multiple-attribute decision-making approach. *Journal of Environmental Management*, *113*, 158–169. https://doi.org/10.1016/j.jenvman.2012.08.025

Keršulienė, V., Zavadskas, E. K., & Turskis, Z. (2010). Selection of rational dispute resolution method by applying new step-wise weight assessment ratio analysis (SWARA). *Journal of Business Economics and Management*, *11*, 243–258. DOI:10.3846/jbem.2010.12

Kim, K. K., Yeon, J., Lee, H. J., & Yeon, K. S. (2019). Strength development characteristics of SBR-modified cementitious mixtures for 3-dimensional concrete printing. *Sustainability*, *11*, Article 4164. https://doi.org/10.3390/su11154164

Lin, C., & Wu, W. (2008). A causal analytical method for group decision-making under fuzzy environment. *Expert Systems with Applications*, *34*, 205–213. https://doi.org/10.1016/j.eswa.2006.08.012

Mahjouri, M., Ishak, M. B., Torabian, A., Manaf, L. A., & Halimoon, N. (2017). The application of a hybrid model for identifying and ranking indicators for assessing the sustainability of wastewater treatment systems. *Sustainable Production and Consumption*, *10*, 21–37. https://doi.org/10.1016/j.spc.2016.09.006

Muga, H. E., & Mihelcic, J. R. (2008). Sustainability of wastewater treatment technologies. *Journal of Environmental Management*, 88, 437–447. https://doi.org/10.1016/j.jenvman.2007.03.008

Murray, A., Ray, I., & Nelson, K. L. (2009). An innovative sustainability assessment for urban

wastewater infrastructure and its application in Chengdu, China. *Journal of Environmental Management*, *90*, 3553–3560. https://doi.org/10.1016/j.jenvman.2009.06.009

Nowrouzi, M., Abyar, H., & Rostami, A. (2021). Cost coupled removal efficiency analyses of activated sludge technologies to achieve the cost-effective wastewater treatment system in the meat processing units. *Journal of Environmental Management*, *283*, Article 111991. https://doi.org/10.1016/j.jenvman.2021.111991

Nuhu, M., Smith, J., & Doe, A. (2020). Scenario-based assessments using fuzzy methods for decision-making. *International Journal of Decision Support Systems*, *15*(3), 201-215. https://doi.org/10.1016/j.ijdss.2020.321654

Opricovic, S., & Tzeng, G. H. (2007). Extended VIKOR method in comparison with outranking methods. *European Journal of Operational Research*, 178, 514–529. https://doi.org/10.1016/j.ejor.2006.01.020

Pardey, A., Sapkal, V. S., & Sapkal, R. S. (2017). A review on membrane bioreactor (MBR) technology: Its commercial applications and possibilities of hybridization with other membrane techniques to recover valuable industrial by-products for sustainable development and environmental protection. *IRA-International Journal of Technology & Engineering*, *7*, 202–213. https://doi.org/10.21013/jte.icsesd201720

Prajapati, H., Kant, R., & Shankar, R. (2019). Prioritizing the solutions of reverse logistics implementation to mitigate its barriers: A hybrid modified SWARA and WASPAS approach. *Journal of Cleaner Production*, *240*, Article 118219. https://doi.org/10.1016/j.jclepro.2019.118219

Pranoto, K., Pahilda, W. R., Abfertiawan, M. S., Elistyandari, A., & Sutikno, A. (2019). Activated sludge technology to treat wastewater from offices and residential areas PT Kaltim Prima Coal. *Indonesian Mining Professional Journal*, *1*, 61–66. https://doi.org/10.36986/impj.v1i1.14

Purkait, M. K., Bhunia, P., Saha, B., & Khilari, S. (2023). A comprehensive review of advanced wastewater treatment techniques in the steel industry: Focus on ozonation and electrocoagulation. *Environmental Engineering Research*, *28*(1), 115–134. https://doi.org/10.1107/s11356-023-3467

Ren, J., & Ren, X. (2018). Sustainability ranking of energy storage technologies under uncertainties. *Journal of Cleaner Production*, *170*, 1387–1398. https://doi.org/10.1016/j.jclepro.2017.09.229

Santos, P. G., Scherer, C. M., Fisch, A. G., & Rodrigues, M. A. S. (2020). Petrochemical wastewater treatment: Water recovery using membrane distillation. *Journal of Cleaner Production*, *267*, Article 121985. https://doi.org/10.1016/j.jclepro.2020.121985

Sayadi, M. K., Heydari, M., & Shahanaghi, K. (2009). Extension of the VIKOR method for decision-making problems with interval numbers. *Applied Mathematical Modelling*, *33*, 2257–2262. https://doi.org/10.1016/j.apm.2008.06.002

Singhirunnusorn, W., & Stenstrom, M. K. (2009). Appropriate wastewater treatment systems for developing countries: Criteria and indicator assessment in Thailand. *Water Science and Technology*, *59*, 1873–1884. https://doi.org/10.2166/wst.2009.215

Singh, A., Kumari, S., & Bhattacharya,

S. (2023). Sustainability indicators for wastewater treatment technologies: A systematic review. *Sustainable Production and Consumption*, *35*, 756–765.

Sinha, S. K., Sinha, K., Pandey, S. K., & Tiwari, A. (2014). A study on the wastewater treatment technology for the steel industry: Recycle and reuse. *American Journal of Engineering Research*, *3*, 309–315.

Turskis, Z., Goranin, N., Nurusheva, A., & Boranbayev, S. (2019). A fuzzy WASPAS-based approach to determine critical information infrastructures of EU sustainable development. *Sustainability*, *11*, 1–25. https://doi.org/10.3390/su11010001

Yücenur, G. N., & Şenol, K. (2021). Sequential SWARA and fuzzy VIKOR methods in elimination of waste and creation of lean construction processes. *Journal of Building Engineering*, *44(2), 103196*. https://doi.org/10.1016/j.jobe.2021.103196

Wang, L., Wu, M., & Lee, C. (2022). Comparative assessment of wastewater treatment technologies in heavy industries with a focus on economic and environmental performance. *Journal of Cleaner Production*, *351*, Article 131564. https://doi.org/10.1016/j.jclepro.2022.131564

Zadeh, L. A. (1965). Fuzzy sets. *Information and Control*, *8*, 338–353. https://doi.org/10.1016/S0019-9958(65)90241-X

Zhang, X., & Ju, Y. (2021). A fuzzy AHP and TOPSIS approach for technology comparison in sustainable practices. *Journal of Cleaner Production*, *123*(2), 456-467. https://doi.org/10.1016/j.jclepro.2021.123456

Zhou, Q., Zhang, D., & Wang, Y. (2023). Sustainability in steel production: Challenges and wastewater management solutions. *Environmental Science and Pollution Research*, *30*(4), 4550–4562. https://doi.org/10.1007/s11356-022-20676-7

Original Article

Journal of Drought and Climate change Research (JDCR)

Winter 2025, Vol. 2, No. 8, pp 85-102

10.22077/jdcr.2024.7376.1061

Efficiency of Machine Learning Techniques for Predicting Vapor Pressure Deficit in Arid and Semi-Arid Regions (Case Study: South Khorasan Province)

Elham Ghochanian Haghverdi[1*], Hossein Khozeymeh Nezhad[2], AliReza Moghri Friz[3], Omid Khorashadizadeh[4]

1- Department of Water Science and Engineering, Faculty of Agriculture, University of Birjand, Birjand, Iran.
2- Department of Water Science and Engineering, Faculty of Agriculture, University of Birjand, Birjand, Iran.
3- Department of Soil and Water Research Department, South Khorasan Agriculture and Natural Resources Research and Education Center, AREEO, Birjand, Iran.
4- Regional Water Company of south Khorasan, Water Resources Management Company, Birjand, Iran.
*** corresponding author: e.ghochanian@areeo.ac.ir**

Keywords:
Vapor pressure deficit, GAM, Climate change, Machine learning, Drought

Received:
02 March 2024

Revised:
28 April 2024

Accepted:
11 May 2024

Abstract

Climate change, as one of the global challenges of the present century, has profound impacts on water resources and agriculture. Increase in temperature and decrease in rainfall in arid and semi-arid regions have made the optimal water resource management a top priority. In countries facing climate change and drought, accurate estimation of evapotranspiration plays a vital role in water resource management and ensuring food security. One of the key factors affecting evapotranspiration is the vapor pressure deficit (VPD), which significantly impacts the accuracy of related calculations. This study focuses on predicting the vapor pressure deficit using advanced machine learning techniques. The methods employed include Linear Regression (LR), Generalized Additive Model (GAM), Random Subspace (RSS), Random Forest (RF), and M5 Pruned model (M5P). In this study, monthly average data, including temperature, humidity, precipitation, and vapor pressure deficit, were extracted from the Japanese 55-year Reanalysis (JRA-55) database for the period from 1958 to 2023. The analysis on the vapor pressure deficit data in Birjand, Sarayan, Qaen, and Tabas showed that the annual average VPD increased by 6 Pa, 10 Pa, 4 Pa, and 5 Pa, respectively. In the next step, the extracted data for temperature, precipitation, and humidity were

How to cite this article:
Ghochanian Haghverdi, E., Khozeymeh Nezhad, H., Moghri Friz, A. & Khorashadizadeh, O. (2024). Efficiency of Machine Learning Techniques for Predicting Vapor Pressure Deficit in Arid and Semi-Arid Regions (Case Study: South Khorasan Province). *Journal of Drought and Climate change Research* (JDCR), 2(8), 85-102. 10.22077/jdcr.2024.7376.1061

used as input variables, and VPD was used as the target variable in machine learning algorithms. Model performance was evaluated using root mean square error (RMSE), mean absolute error (MAE), Pearson correlation coefficient (CC), and Kling-Gupta efficiency (KGE). Results showed that the GAM model outperformed other models in all regions. The evaluation indices for each region were as follows: Birjand [RMSE=0.308, MAE=0.247, KGE=0.914, and CC=0.920], Sarayan [RMSE=0.401, MAE=0.303, KGE=0.937, and CC=0.951], Qaen [RMSE=0.072, MAE=0.055, KGE=0.987, and CC=0.997] and Tabas [RMSE=0.230, MAE=0.184, KGE=0.920, and CC=0.942]. Predictions showed that, over the next 10 years, the annual average VPD in the studied regions will significantly increase. This increment is as follows: Birjand 9 Pa, Sarayan 10 Pa, Qaen 7 Pa, and Tabas 5 Pa. This increase signifies serious challenges for water resources and an increase in water consumption. Eventually, this study suggests the GAM model as an effective tool for future research, especially for use in the development of smart irrigation systems, which play a crucial role in sustainable water resource management.

Introduction

Agriculture consumes the most water, using 70 % of all freshwater withdrawals on average. However, in some underdeveloped nations, this percentage can reach 95 % (Wada & Bierkens., 2014). To ensure future food security, improving irrigation efficiency is essential to produce more crops using less water (Smidte et al., 2016). Even with advanced biotechnology and conventional breeding techniques, achieving significant yields is only possible with sufficient water and proper crop and soil management (Ahmar et al., 2020). Vapor pressure deficit (VPD) is a critical parameter in precise agricultural water management, impacting moisture flow from the surface to the atmosphere and the water balance at national and global levels (Kimball et al., 1997; Qiu & Katul., 2020). It affects plant physiology and significantly influences plant water requirements and evapotranspiration (Grossiord et al., 2020; Qiu et al., 2019; Yuan et al., 2019). Multiple studies show that VPD significantly impacts evaporation and transpiration (Zhang et al., 2018). The amount of vapor pressure deficit represents the difference between saturation and actual pressures (Rawson et al., 1977). According to the Clausius-Clapeyron equation (Iribarne & Godson, 1981; Bolton, 1980), the saturation vapor pressure of water increases by approximately 7% for each degree Kelvin increases in atmospheric temperature. If the increase in saturation vapor pressure does not correspond with the actual atmospheric water vapor concentration, the vapor pressure deficit

will increase. Relative humidity, which measures the difference between the actual vapor pressure of water and the saturation pressure, fluctuates significantly in humid areas and inland regions (Pierce et al., 2013). Although the long-term trend of the global average relative humidity at the earth's surface is low. (Willett et al., 2008; Dai, 2006) a significant decrease has been observed after 2000 (Simmons et al., 2010; Willett et al., 2014), indicating a severe increase in the vapor pressure deficit at the surface. Recent research has shown that the increase in vapor pressure deficit, rather than changes in precipitation, significantly impacts crop yields, plant transpiration, and evaporation (Konings et al., 2017; Ding et al., 2018; Restaino et al., 2016; Carnicer et al., 2013). Furthermore, the increase in vapor pressure deficit alters plant stomatal activity, reducing vegetation cover over vast areas of land (Fletcher et al., 2007). VPD has a significant impact on plant production in forested areas and lands with trees and shrubs, whereas soil moisture plays a more critical role in rangelands (Sun et al., 2024). Currently, the earth is experiencing atmospheric drying across the globe due to increased vapor pressure deficiency, and it is predicted that this condition will worsen with the decline in global climate quality. (Dai et al., 2018; Ficklin & Novick, 2017; Liu & Sun., 2017; Wang et al., 2012). This effect is mainly due to the increase in saturated vapor pressure, which raises global temperatures, and the decrease in actual vapor pressure, which affects various hydrological phenomena (Ficklin & Novick., 2017). As a result of the increased vapor pressure deficit in agricultural and non-agricultural plants (Otieno et al., 2012), we are witnessing a decrease in plant productivity, which in turn leads to an increase in adverse climatic events such as droughts. In arid and semi-arid regions, the lack of atmospheric vapor pressure reduces the quality and productivity of agricultural products during the spring and summer growing seasons, especially in greenhouses. According to previous studies, increased humidity reduces leaf area and thickness (Devi et al., 2018). If the vapor pressure deficit is high, it delays leaf growth; if the atmosphere is humid, leaf wilting and disruption of xylem function may occur during the tree's growth period (Sellin et al., 2019). Actual VP (e_a) and standard VP (e_s) are widely used to determine the level of vapor pressure deficit. The present study's findings are essential for guiding future research in these areas and attracting policymakers' attention to the impact of vapor pressure deficit on vegetation and the overall hydrological cycle. Most studies have used vapor pressure deficit as one of the input variables similar to the model of the present study to develop machine learning-based models for predicting various hydro-climatic variables and

estimating the water needs of vegetation, which emphasizes the importance of improving their prediction accuracy and precision. (Feng et al., 2019; Huntington et al., 2020; khosravi et al., 2021; Mokhtar et al., 2021; Emami et al., 2022). In South Khorasan, more than 90 percent of water is used for agriculture. Therefore, accurately estimating the evapotranspiration for agricultural products is essential to achieve sustainability under climate change conditions and Iran's limited water share. Monthly vapor pressure deficits can be helpful tools for scheduling irrigation, as they reflect the atmospheric demand for water by plants. The goal of irrigation scheduling is to use the appropriate amount of water at the right time to meet crops' water needs and optimize yield while minimizing water consumption. As mentioned, the vapor pressure deficit is the difference between the amount of moisture in the air and the maximum amount of moisture the air can hold. This index is influenced by temperature and relative humidity and can be calculated using meteorological data. High values of vapor pressure deficit indicate a high atmospheric demand for water. This means that plants release water into the atmosphere more quickly and may require more water. Farmers can monitor their area's vapor pressure deficit values and adjust their irrigation practices to utilize the predicted monthly vapor pressure deficit for irrigation scheduling. For example, when the vapor pressure deficit is high, farmers may need to irrigate more to ensure the plants have enough water. Conversely, farmers can reduce water consumption when the vapor pressure deficit is low while maintaining optimal crop growth. The predicted monthly vapor pressure deficit can also be used to schedule irrigation in advance. Farmers can predict periods of high atmospheric demand for water by monitoring the forecast of vapor pressure deficit and schedule irrigation accordingly. This method can help farmers optimize water consumption and prevent over- or under-irrigation, which may lead to reduced crop yields and water wastage. The predicted monthly vapor pressure deficit can be a helpful tool for irrigation scheduling, allowing farmers to optimize water use and increase crop yields while minimizing water waste. To obtain accurate parameters such as soil moisture, soil temperature, and climatic parameters, the JRA-55 database can be used. In Iran, no studies or research have yet been conducted in the field of agriculture using JRA-55 data. (Mollasharifi et al., 2019) in their study of the impact of the North Atlantic Oscillation on the relationship between the North Atlantic storm tracks and the Mediterranean, have used NCPE/NCAR and JRA-55 data. In another study, (Azarm et al., 2022) have used the JRA-55 database for climatology of Bandal

events. However, this database has not yet been used in the fields of agriculture, water resources and climate change, which highlights the importance of this study. Considering the negative impacts of climate change in South Khorasan and the limitations of water resources in this province, the development of new methods and the use of machine learning algorithms instead of traditional irrigation methods must receive more attention from researchers to maintain sustainable agriculture and improve water use efficiency.

In this study, the prediction of the VPD parameter using machine learning algorithms was examined, marking the beginning of a path for future research aimed at developing intelligent irrigation systems to mitigate the effects of climate change and adapt drought conditions. The aim of this research is to assess the long-term predictive capabilities of several algorithms such as Linear Regression (LR), General Additive Model (GAM), Random SubSpace (RSS), Random Forest (RF), and M5P for Vapor Pressure Deficit (VPD) values in four regions of South Khorasan, including Tabas, Birjand, Qaen, and Sarayan, facing serious water resource limitations.

Additionally, selecting the best machine learning model for predicting VPD based on statistical indicators such as accuracy, high performance, and low statistical errors is another goal. Moreover, this paper aims to familiarize water resource researchers with the JRA-55 database system, particularly in the context of agricultural approaches and vapor pressure deficit.

Materials and Methods

Study area

South Khorasan Province is one of the easternmost provinces of Iran, covering an area of approximately 150,000 square kilometers, which accounts for 22.6% of the country's total area. The province is located between 57 degrees and 1 minute to 60 degrees and 57 minutes of eastern longitude, and between 30 degrees and 32 minutes to 34 degrees and 36 minutes of northern latitude. According to the latest administrative divisions, the province currently includes 12 counties, 32 cities, 28 districts, and 66 rural districts. Due to the province's location between deserts and scattered mountain ranges, the climate in the southern and southwestern regions is hot and dry, while the climate in the northern and northeastern mountainous areas is semi-arid, mild, and cold. The mountain ranges, with their northwestern-southeastern orientation, contribute to the diversity and extreme fluctuations in the region's climate. The province has 35 study areas for water resource management, of which 8 are classified as critical prohibited areas, 18 as critical areas, and 9 as accessible areas. According to recent statistics, the long-term average

annual rainfall in the province is about 113 millimeters, indicating a severe shortage of water resources. This climatic condition and the limitation of water resources significantly affect agriculture and the livelihood of the local population. In this province around 88% of groundwater resources are used for agricultural purposes. This comes from three primary sources: wells (73%), qanats (23%), and springs (4%). The province has been dealing with over two decades of continuous drought and significant reductions in rainfall, which have severely affected both surface and groundwater resources. This heavy reliance on groundwater underscores the critical need for sustainable water management and policies to combat the ongoing water scarcity crisis

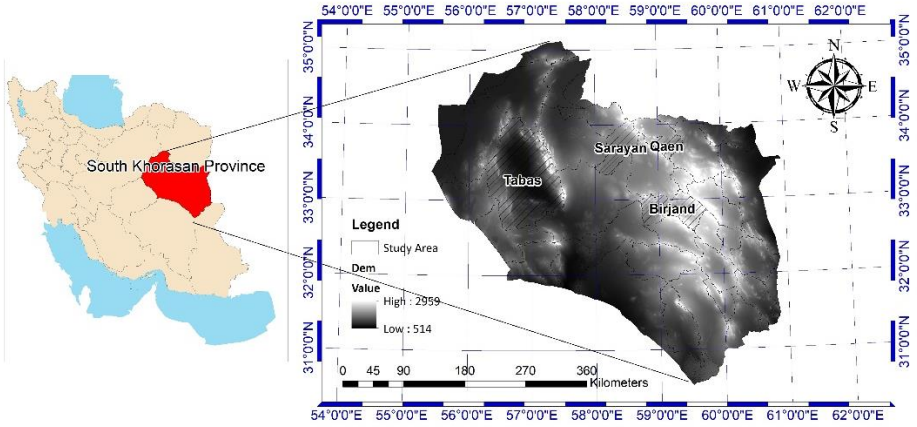

Fig 1. Study area

Introducing the Japanese 55-year Reanalysis

JRA-55 (Japanese 55-Year Reanalysis) is a global atmospheric reanalysis dataset developed by the Japan Meteorological Agency (JMA). Spanning the period from 1958 to the present, it is a crucial resource for studying climate variability and long-term changes. JRA-55 was designed to enhance previous versions, such as JRA-25, by addressing issues like model biases and gaps in observational data. Key features of JRA-55 include:

1. **Data Sources:** It incorporates diverse observational data from sources like weather stations, satellites, and aircraft, ensuring a consistent and comprehensive atmospheric dataset.
2. **Spatial and Temporal Coverage:** With more than five decades of data, JRA-55 provides detailed climate information applicable to various fields, including climate research, weather forecasting, and hydrology.
3. **Improvements:** Enhancements in areas such as temperature analysis, long wave radiation schemes, and the representation of oceanic fronts make

JRA-55 more accurate than earlier reanalysis products.

4. **Applications:** Widely used in atmospheric studies, climate modeling, and global trend assessments, JRA-55 is particularly valuable for research on climate variability and hydrological cycles.

This dataset supports climate scientists, meteorologists, and researchers in better understanding climate systems, evaluating the impacts of climate change, and informing decisions related to environmental policies and resource management. For more detailed information, visit the official JRA-55 website.

Temperature, humidity, precipitation, and vapor pressure deficit data were extracted monthly from the JRA-55 database in NC format files. Then, using the NC files containing monthly statistics for one year (12 months), the Make NetCDF Raster Layer tool in ArcMap software was used to convert these files into raster format. Subsequently, using the Zonal Statistics as Table tool and the boundary layer of the study areas, including Qaen, Birjand, Sarayan, and Tabas, the average data within the borders of these areas were calculated. (Fig 2 shows the process of extracting data from JRA-55 using ArcMap software).

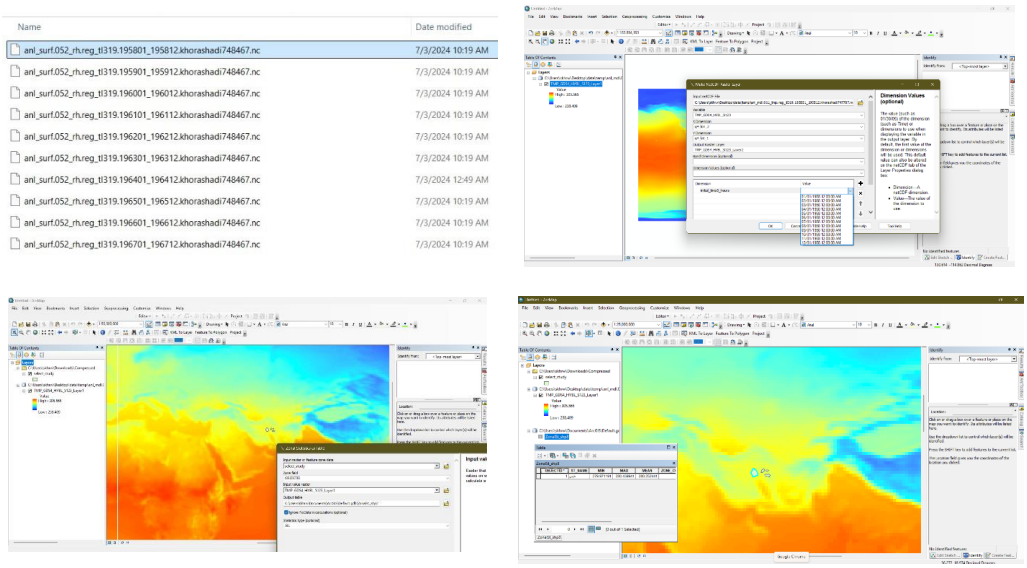

Fig 2. The process of extracting data from the JRA-55 database using ArcMap software.

Machine learning Model description

The present study examines the performance of machine learning models in estimating monthly vapor pressure deficit (VPD) in four study areas of South Khorasan Province. MATLAB software was used to run the models. The data for this region is divided into two sections. The first group consists of 70% for training, and the second group consists of 30% for testing. This study analyzes five machine learning models: linear

regression, generalized additive model, random subset, random forest, and M5P model. The following sections provide a complete explanation of these models.

1. Linear regression (LR)

Linear regression is one of the simplest and most widely used statistical modeling methods, which models the linear relationship between a dependent variable and one or more independent variables. In multiple linear regression, where there is more than one independent variable, the model is expanded as follows:

$$y = \beta_0 + \beta_1 x_1 + \beta_2 x_2 + \cdots + \beta_p x_p \quad (1)$$

$x_1, x_2, \ldots, x_p$: Independent variables

are regression coefficients for each independent variable indicate the effect of changes in each of these variables on y.

2. General additive model (GAM)

GAM is a combination of generalized linear models with additive models. These models have been presented to create a unified method for statistical models such as linear, logistic, and Poisson regression. The general idea of this method is that instead of assuming various functions in the mentioned regressions, knowing the data distribution—which generally comes from a logical assumption of the problem—one can obtain their estimate for the model. This model consists of three components:

1- A distribution for the target variable y, which is usually chosen from the exponential family with dispersion parameter.

$$f_Y(yI\theta,\tau) = h(y,c)\exp\left(\frac{b(\theta)^T T(y) - A(\theta)}{d(\tau)}\right) \quad (2)$$

Pre-dispersion is used for modeling high and low variances

$$\eta = X\beta \quad (3)$$

Pre-dispersion is used for modeling high. The link function g is a strictly monotonic function that connects the two above components with low variances.

3. Random Sub Space (RSS)

The RSS model trains and integrates multiple categories in spaces with different features. This framework categorizes several subsets of data for training, which later serves as the basis for training and considers clustering and self-supervised approaches. While utilizing artificial neural networks, decision trees, or other algorithms, this framework demonstrates nonlinear relationships. This system's classification is developed according to the RSS framework and is related to specific data features. The output of all classifications is easily combined by the voting system in the model. This method improves the ability of each weak classifier. (Skurichina & Duin., 2002) presented the RSS algorithm as follows.

$$\gamma(S) = argmax \sum \delta_{sgn(c^d(s),y} \quad (4)$$

In this formula, $C^d(S)$ represents the classifier (d = 1,2…D); $\delta_{i,j}$ denotes the Kronecker delta, and y = (-1,1) signifies the class label or classification decision

4. Random Forest (RF)

Random forest is a type of ensemble learning algorithm that combines multiple decision trees for prediction. Each decision tree in the random forest is trained on a random subset of the training data and a random subset of the features. Then, the random forest is determined by aggregating the predictions of all the decision trees. This approach allows the random forest to be very accurate and resistant to the problem of overfitting (a common issue in machine learning where the model performs well on training data but poorly on new data).

$$d(x,y) = \sqrt{I - s(x,y)} \quad (5)$$

The RF technique can significantly enhance the estimation efficiency of the system with minimal possible errors and the least noise. RF can effectively work with large-scale datasets with high dimensions (Khosravi et al., 2019; Li et al., 2022)

5.M5 Pruned (M5P)

Reconstructing the M5 Quinlan algorithm helps in generating the M5P model tree. The M5P algorithm is reconstructed to the leaf nodes with a convolution decision tree and a linear regression function (Blaifi et al., 2018). The M5P model algorithm is based on a numerical prediction system. The linear regression model is stored in each leaf, which helps identify the corresponding point cluster value that reaches the leaf. (Shamshirband et al., 2020) identify the best feature split criterion for partitioning a specific section (T) of training data related to a specific node. The standard deviation of the batch related to T is measured as the error for that node. In addition, the reduction of potential error is determined by making estimates at each node. The selection of features used for splitting increases the potential error reduction of the associated node. Minimizing the expected error with standard deviation reduction (SDR) is performed as follows.

$$SDR = sd(T) - \sum \frac{|T_i|}{T} \times sd(T_i) \quad (6)$$

In this formula, T_i corresponds to T_1, T_2, T_3, ... obtained from the division of nodes based on selected features.

Table 1 and Figure 3 shows the workflow diagram related to data collection, processing, and modeling of vapor pressure deficit based on machine learning algorithms from 1955 to 2023.

Table 1. The parameters of the machine learning algorithm used for modeling VPD in the study regions.

Model name	Description of parameters	Cross-validation	Input	Target
Linear regression (LR)	Batch size-100, Debug = False, Eliminate Collinear Attribute =True, Minimal = False	K – fold;k=5	Temp Wind Humidity Precipitation	VPD
Random Subspace (RSS)	Batch size-100, Classifier = REPTree, random seed-1, subspace size = 0. 5, numbers of executions slots = 1, number of iterations= 10			
M5 Pruned (M5P)	Batch size-100, Minimum number of instances = 4			
General additive model (GAM)	Batch size-100, Name-value arguments=optimize Hyper parameters, parameters to optimize=auto,			

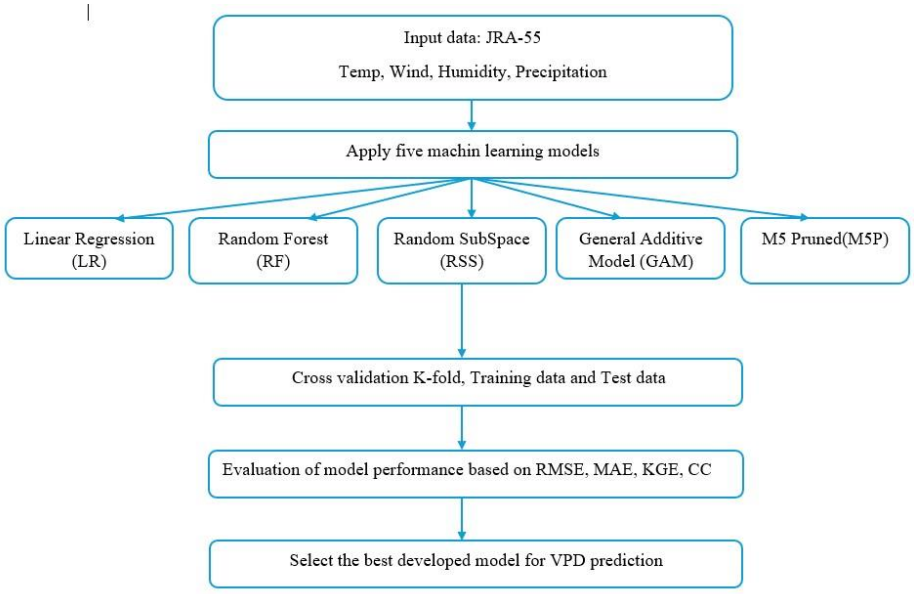

Fig 3. Workflow diagram related to data collection, processing, and modeling of vapor pressure deficit based on machine learning algorithms

Evaluation of model performance

The performance of machine learning models has been evaluated using the following four performance metrics: Correlation Coefficient (CC), Mean Absolute Error (MAE), Root Mean Square Error (RMSE), and Kling-Gupta Efficiency (KGE). These indices have been calculated using the following equations: where N is the total number of measurements, X_a is the observed values, Y_a is the estimated values, is the mean of the observed values in the X variables, and is the mean of the estimated values in the Y variables.

$$CC = \frac{\sum_a^N (X_a - \bar{X})(Y_a - \bar{Y})}{\sqrt{\sum_a^N (X_a - \bar{X})^2 \sum_a^N (Y_a - \bar{Y})^2}} \quad (7)$$

$$MAE = \frac{1}{N}\sum_a^N |X_a - Y_a| \quad (8)$$

$$RMSE = \sqrt{\frac{1}{N}\sum_a^N (X_a - Y_a)^2} \quad (9)$$

$$KGE = 1 - \sqrt{(r-1)^2 + (\alpha - 1)^2 + (\beta - 1)^2} \quad (10)$$

Results and Discussion

Evaluation of the statistical performance of machine learning models based on VPD prediction. The graph of vapor pressure deficit changes from 1958 to 2023 for the regions of Birjand, Qaen, Sarayan, and Tabas is shown in Figure 4.

According to the figure 4, the average increase in vapor pressure deficit is 6 Pa in Birjand, 10 Pa in Sarayan, 4 Pa in Qaen, and 5 Pa in Tabas.The performance of the LR, GAM, RSS, RF, and M5P models for monthly vapor pressure deficit prediction

Fig4. Comparison chart of conversion in vapor pressure deficit

using temperature, precipitation, wind speed, and humidity data was evaluated. In the process of model implementation, the Cross-Validation K-fold statistical technique was used to assess the models' performance and reduce issues caused by overfitting or underfitting. This method helps ensure that the model performs well on new data. In this method, the data is divided into K subsets (folds). In each iteration, one of these subsets is used as test data, and the remaining subsets are used as training data. Four statistical indices, CC, MAE, RMSE, and KGE, were used to evaluate the models for the regions of Birjand, Qaen, Sarayan, and Tabas during both training and testing stages. The criterion for selecting the best model was the lowest error value in the test phase. In the Birjand region, the results showed that the GAM model had the best performance for all evaluation indices, with the highest values for CC and KGE and the lowest values for MAE and RMSE. The performance of GAM, in terms of these statistics, was better than the other models. The LR model was the second best model, with the lowest RMSE and MAE values and the highest KGE and CC values. The third model, which showed good performance for predicting vapor pressure deficit, was the RF model. The performance of the RSS model was average, and the M5P model showed poor performance in predicting VPD (Table 1). In the Qaen region, by evaluating the performance of the models in the test phase, it was found that the GAM model had the best performance, with the highest value for CC and the lowest values for MAE, RMSE, and also a KGE close to 1. In this region, after the GAM model, the RF and LR models were selected as the best models, and the performance of the

Table 2. Performance of the models under training and testing conditions (Birjand)

Model	Training period (1958-2003)				Testing period (2003-2023)			
	RMSE	MAE	KGE	CC	RMSE	MAE	KGE	CC
LR	0.291	0.231	0.914	0.939	0.312	0.252	0.928	0.931
GAM	0.237	0.183	0.934	0.960	0.259	0.206	0.943	0.952
RSS	0.453	0.326	0.729	0.930	0.462	0.358	0.727	0.907
RF	0.171	0.13	0.968	0.979	0.352	0.264	0.911	0.912
M5P	0.781	0.394	0.563	0.666	1.213	0.965	-0.066	-0.027

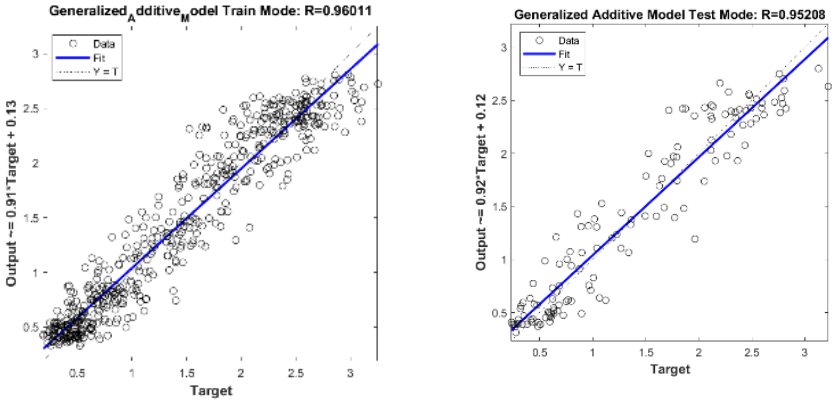

Fig 5. Graph of the correlation results taken from GAM model for the Birjand region.

RSS model was average, while the M5P model had a poor performance compared to the other models.

By evaluating the performance of the models in the Sarayan region, the GAM model was selected as the best model in both the test phases, with the maximum values for KGE and CC and the minimum values for MAE and RMSE. In this region, the second-best model was LR. The RF

Table3. Performance of the models under training and testing conditions (Qaen)

model	Training period (1958-2003)				Testing period (2003-2023)			
	RMSE	MAE	KGE	CC	RMSE	MAE	KGE	CC
LR	0.045	0.035	0.999	0.999	0.083	0.059	0.994	0.996
GAM	0.035	0.027	0.999	0.999	0.077	0.058	0.996	0.997
RSS	0.214	0.134	0.888	0.984	0.200	0.146	0.889	0.990
RF	0.192	0.156	0.968	0.978	0.189	0.152	0.960	0.980
M5P	0.704	0.360	0.598	0.754	0.836	0.648	0.514	0.683

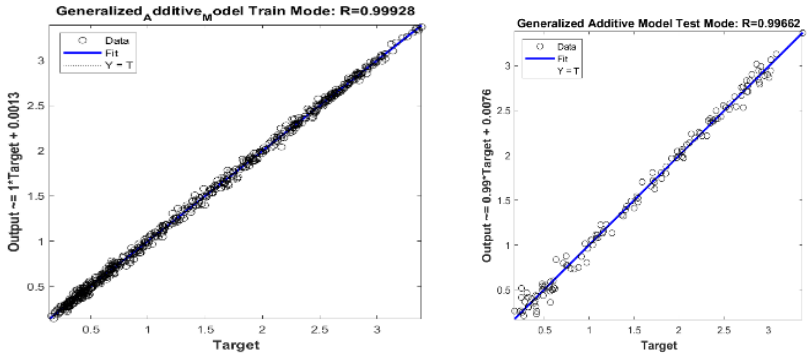

Fig 6. Graph of the correlation results in the GAM model for the Qaen region

model ranked third with a slight difference in performance. The RSS model showed average performance, similar to the other regions. The M5P model was also selected as a model with poor performance.

In the Tabas study area, the GAM model with the following error values [RMSE = 0.226, MAE = 0.180, KGE = 0.915, CC = 0.945, was selected as the best model. The second model, which showed good performance for predicting vapor pressure deficit, was the LR model, with a very slight difference from the RF model. As a result, the RF model was chosen as the third model. Additionally, the RSS model showed average performance, and the M5P model had poor performance in this region.

Table 4. Performance of the models under training and testing conditions (Sarayan)

model	Training period (1958-2003)				Testing period (2003-2023)			
	RMSE	MAE	KGE	CC	RMSE	MAE	KGE	CC
LR	0.424	0.341	0.919	0.942	0.393	0.312	0.924	0.952
GAM	0.284	0.223	0.958	0.975	0.378	0.290	0.953	0.956
RSS	0.565	0.406	0.756	0.952	0.567	0.435	0.778	0.945
RF	0.205	0.160	0.976	0.987	0.440	0.338	0.929	0.942
M5P	1.156	0.586	0.492	0.644	1.609	1.229	0.079	0.165

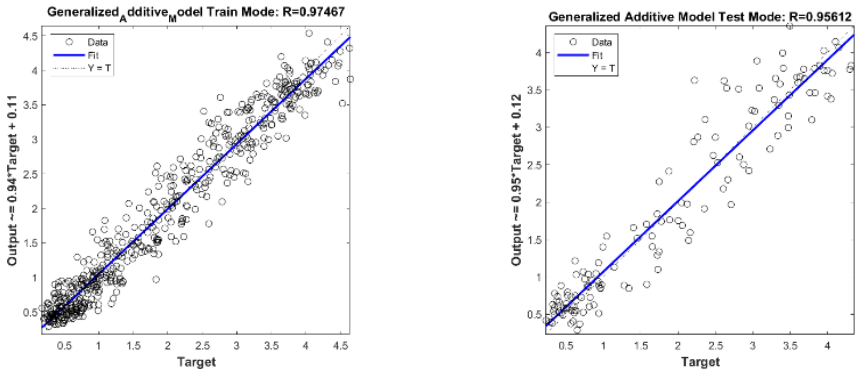

Fig 7. Graph of the correlation results in the GAM model for the Sarayan region

Table 5. Performance of the models under training and testing conditions (Tabas)

model	Training period (1958-2003)				Testing period (2003-2023)			
	RMSE	MAE	KGE	CC	RMSE	MAE	KGE	CC
LR	0.248	0.199	0.910	0.937	0.275	0.221	0.914	0.919
GAM	0.166	0.132	0.949	0.972	0.226	0.180	0.915	0.945
RSS	0.338	0.245	0.766	0.945	0.370	0.289	0.760	0.913
RF	0.135	0.106	0.974	0.982	0.278	0.221	0.912	0.919
M5P	0.615	0.304	0.572	0.686	0.785	0.586	0.318	0.390

Considering the GAM model as the best model for predicting vapor pressure deficit in the Birjand, Qaen, Tabas, and Sarayan regions, predictions for vapor pressure deficit for the next 10 years in these regions were made. The results of the model showed an average annual vapor pressure deficit increase of 10 Pas in Sarayan, 9 Pa in Birjand, 7 Pa in Qaen, and 5 Pa in Tabas. Figure (9). Predicted annual average vapor pressure deficit results in the GAM model for regions a- Sarayan, b- Birjand, c- Tabas, and d- Qaen.

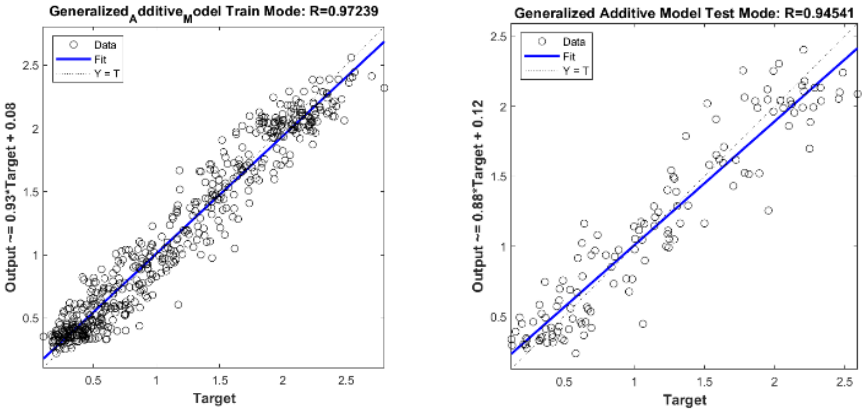

Fig 8. Graph of the correlation results in the GAM model for the Tabas region

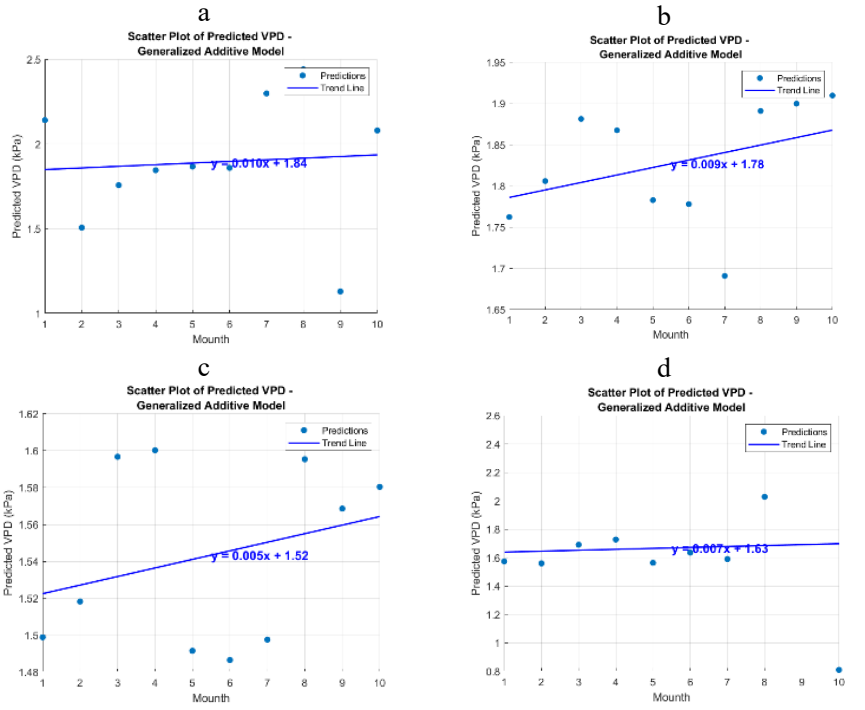

Fig 9. The results of the annual average vapor pressure deficit prediction in the GAM model.

Conclusion

In this study, data extraction process from the JRA-55 database in the regions of Birjand, Qaen, Sarayan, and Tabas were discussed. The data analysis indicated an annual increase in vapor pressure deficit over 65 years in these regions. To predict vapor pressure deficit in these areas, machine learning techniques, including LR, RSS, GAM, M5P, and RF, were used. The results showed that the geographic region did not affect the performance of the machine learning models, as GAM was the best model for estimating vapor pressure deficit across all areas. The GAM model demonstrated high ability to uncover complex, nonlinear relationships between independent and dependent variables,

suggesting that most of the data used in this study had nonlinear relationships. The LR model, on the other hand, is more suitable for simple and linear modeling without deep complexity, which could explain its error weaknesses due to the nonlinear relationships of climatic parameters. The RF model, based on decision trees, uses the combination of multiple trees to reduce variance. Its weakness was its sensitivity to small changes in data (vapor pressure deficit values). The RSS model is useful in analyzing spatial and nonlinear data, but the deep complexity and multiple interactions in the data used in this study posed a limitation for this model. The M5P model, which combines decision tree models and linear regression, is highly effective in uncovering both linear and nonlinear relationships. However, it tends to make errors with highly complex data, leading to the highest error among the models in this study. The GAM model's predictions showed a more significant increase in vapor pressure deficit than the long-term statistics in the studied regions, signaling a potential increase in water consumption in the region's warm and dry climatic conditions. Finally, this study recommends using the GAM model for future research, particularly in smart irrigation systems.

References

Ahmar, S., Gill, R.A., Jung, K.H., Faheem, A., Qasim, M.U., Mubeen, M. & Zhou, W. (2020). Conventional and molecular techniques from simple breeding to speed breeding in crop plants: recent advances and future outlook. *International Journal of Molecular Sciences*. 21(7), 2590. https://doi.org/10.3390/ijms21072590.

Azarm, k., mohebolhojeh, A. & Mirzaie, M. (2022). Climatological Study of Wintertime Blocking Events in the Northern Hemisphere. 20th Iranian Geophysical Conference, Iran.

Blaifi, S.A., Moulahoum, S., Benkercha, R., Taghezouit, B.& Saim, A. (2018). M5P model tree-based fast fuzzy maximum power point tracker. *Solar Energy* 163, 405–424. https://doi.org/10.1016/j.solener.2018.01.071

Bolton, D. (1980). The computation of equivalent potential temperature. *Monthly Weather Review*. 108, 1046–1053. https://doi.org/10.1175/1520-0493(1980)108

Carnicer, J., Barbeta, A., Sperlich, D., Coll, M. & Pe˜nuelas, J. (2013). Contrasting trait syndromes in, angiosperms and conifers are associated with different responses of tree growth to, temperature on a large scale. *Frontiers in Plant Science*. 4, 409. http://doi.org/10.3389/fpls.2013.00409

Dai, G., 2006. Recent climatology, variability, and trends in global surface humidity. *Journal of Climate*. 19(15), 3589–3606.

Dai, A., Zhao, T. & Chen, J. (2018). Climate change and drought: a precipitation and evaporation perspective. *Current Climate Change Reports*, 4 (3), 301–312. http://doi.org/10.1007/s40641-018-0101-6

Devi, M.J., Reddy, V.R. (2018). Effect of temperature under different evaporative demand conditions on maize leaf expansion. *Environmental and Experimental Botany*. 155, 509–517. https://doi.org/10.1016/j.envexpbot.2018.07.024

Ding, J., Yang, T., Zhao, Y., Liu, D., Wang, X., Yao, Y., Peng, S., Wang, T. & Piao, S. (2018). Increasingly important role of atmospheric

aridity on Tibetan alpine grasslands. *Geophysical Research Letters*, 45(6), 2852–2859. https://doi.org/10.1002/2017GL076803

Emami, M., Ahmadi, A., Daccache, A., Nazif, S., Mousavi, S.F. & Karami, H. (2022). County-level irrigation water demand estimation using machine learning: case study of California. *Water*, 14 (12), 1937. https://doi.org/10.3390/w14121937.

Feng, Y., Cui, N., Hao, W., Gao, L.& Gong, D. (2019). Estimation of soil temperature from meteorological data using different machine learning models. *Geoderma* 338, 67–77. https://doi.org/10.1016/j.geoderma.2018.11.044

Ficklin, D.L. & Novick, K.A. (2017). Historical and projected changes in vapor pressure deficit suggest a continental-scale drying of the United States atmosphere. *Journal of Geophysical Research Atmospheres*, 122 (4), 2061–2079. https://doi.org/10.1002/2016JD025855

Fletcher, L., Sinclair, T.R. & Allen Jr., L.H. (2007). Transpiration responses to vapor pressure deficit in well watered 'slow-wilting' and commercial soybean. *Environmental and Experimental Botany*, 61(2), 145–151. https://doi.org/10.1016/j.envexpbot.2007.05.004

Gong, X.W., Qiu, R.J., Sun, J.S., Ge, J.K., Li, Y.B. & Wang, S.S. (2020). Evapotranspiration and crop coefficient of tomato grown in a solar greenhouse under full and deficit, irrigation. *Agricultural Water Management* 235, 106154. https://doi.org/10.1016/j.agwat.2020.106154

Grossiord, C., Buckley, T.N., Cernusak, L.A., Novick, K.A., Poulter, B., Siegwolf, R.T.W., Sperry, J.S. & McDowell, N.G. (2020). Plant responses to rising vapor pressure deficit. *Wiley New Phytologist*. 226 (6), 1550–1566. https://doi.org/10.1111/nph.16485.

Huntington, T., Cui, X., Mishra, U. & Scown, C.D. (2020). Machine learning to predict biomass sorghum yields under future climate scenarios. *Biofuels Bioprod. Bioref.* 14 (3), 566–577. https://doi.org/10.1002/bbb.2087

Iribarne, J.V., and W.L. Godson. 1981. Atmospheric Thermodynamics. D. Reidel, p. 65. Islam, A.R.M., Talukdar, S., Akhter, S., Eibek, K.U., Rahman, M., Pal, S. & Mosavi, A. (2022). Assessing the impact of the farakka barrage on hydrological alteration in the Padma River with future insight. *Sustainability* 14 (9), 5233. https://doi.org/10.3390/su14095233

Khosravi, K., Daggupati, P., Alami, M.T., Awadh, S.M., Ghareb, M.I. & Panahi, M. (2019). Meteorological data mining and hybrid data-intelligence models for reference evaporation simulation: a case study in Iraq. *Computers and Electronics in Agriculture 167*. https://doi.org/10.1016/j.compag.2019.105041

Khosravi, A., Zucchini, M., Giorgi, V., Mancini, A. & Neri, D. (2021). Continuous monitoring of olive fruit growth by automatic extensimeter in response to vapor pressure deficit from pit hardening to harvest. *Horticulturae* 7 (10), 349. https://doi.org/10.3390/horticulturae7100349

Kimball, J.S., Running, S.W. & Nemani, R. (1997). An improved method for estimating surface humidity from daily minimum temperature. *Agricultural and Forest Meteorology*. 85 (1–2), 87–98. http://doi.org/10.1016/S0168-1923(96)02366-0

Konings, A.G., Williams, A.P. & Gentine, P. (2017). Sensitivity of grassland productivity to aridity controlled by stomatal and xylem regulation. *Nature Geoscience*, 10 (4), 284–288. https://doi.org/10.1038/ngeo2903

Kobayashi, S., Ota, Y., Harda, Y., Ebita, A., Moriya, M., Onoda, H., Onogi, K., Kamahori, H., Kobayashi, C., Endo, H., Miyaoka, K. & Gentine, P. (2015). The JRA-55 reanalysis: general specifications and basic characteristics. *Journal of the Meteorological Society of Japan Ser II*.5-48. https://doi.org/10.2151/jmsj.2015-001

Li, Y., Wang, W., Wang, G. & Tan, Q. (2022).

Actual evapotranspiration estimation over the Tuojiang River Basin based on a hybrid CNN-RF model. *Journal of Hydrology*, 610, 127788. https://doi.org/10.1016/j.jhydrol.2022.127788

Liu, W. & Sun, F. (2017). Projecting and attributing future changes of evaporative demand over China in CMIP5 climate models. *Journal of Hydrometeorology*. 18 (4), 977–991. https://doi.org/10.1175/JHM-D-16-0204.1

Maulud, D. & Abdulazeez, A.M. (2020). A review on linear regression comprehensive in machine learning. *Journal of Applied Science and Technology Trends* 1 (4), 140–147. https://doi.org/10.38094/jastt1457

Mokhtar, A., Elbeltagi, A., Maroufpoor, S., Azad, N., He, H. & Alsafadi, K. (2021). Estimation of the rice water footprint based on machine learning algorithms. *Computers and Electronics in Agriculture*. 191, 106501. https://doi.org/10.1016/j.compag.2021.106501

Mollasharifi, A., Mohebalhojeh, A. R. & Ahmadi-Givi, F. (2019). A study of the impacts of the NAO on the relation between the North Atlantic and Mediterranean storm tracks using the NCEP/NCAR and JRA-55 reanalysis data. *Journal of the Earth and Space Physics*. 45(2),423-440. https://doi.org/ 10.22059/JESPHYS.2019.267521.1007050

Otieno, D., Lindner, S., Muhr, J. & Borken, W. (2012). Sensitivity of peat land herbaceous vegetation to vapor pressure deficit influences net ecosystem CO2 exchange. *Wetlands,* 32 (5), 895–905. https://doi.org/10.1007/s13157-012-0322-8.

Pierce, W., Westerling, A.L. & Oyler, J. (2013). Future humidity trends over the western United States in the CMIP5 global climate models and variable infiltration capacity hydrological modeling system. *Hydrology and Earth System Sciences Discussions*, 9(12), 13651-13691. https://doi.org/10.5194/hessd-17-18332013

Qiu, R.J., Liu, C.W., Cui, N.B., Wu, Y.J., Wang, Z.C. & Li, G. (2019). Evapotranspiration estimation using a modified Priestley-Taylor model in a rice-wheat rotation system. *Agricultural Water Management* 224, 105755. http://doi.org/10.1016/j.agwat.2019.105755.

Qiu, R.J., Katul, G.G. (2020). Maximizing leaf carbon gain in varying saline conditions: an optimization model with dynamic mesophyll conductance. *The Plant Journal*. 101 (3), 543–554. https://doi.org/10.1111/tpj.14553

Rawson, H.M., Begg, J.E., Woodward, R.G. (1977). The effect of atmospheric humidity on photosynthesis, transpiration and water use efficiency of leaves of several plant species. *Planta* 134, 5–10. https://doi.org/10.1007/BF00390086.

Restaino, M., Peterson, D.L. & Littell, J. (2016). Increased water deficit decreases Douglas firgrowth throughout western US forests. *Proceedings of the National Academy of Sciences*. 113(34), 9557–9562.https://doi.org/10.1073/pnas.1602384113

Sangin´es de C´arcer, P., Vitasse, Y., Pe˜nuelas, J., Jassey, V.E.J., Buttler, A. & Signarbieux, C. (2018). Vapor–pressure deficit and extremeclimatic variables limit tree growth. *Global Change Biology*. 24 (3), 1108–1122. https://doi.org/10.1111/gcb.13973.

Sellin, Taneda, H. & Alber, M. (2019). Leaf structural and hydraulic adjustment with respect to air humidity and canopy position in silver birch (Betula pendula). *Journal of Plant Research*, 132, 369–381. https://doi.org/10.1007/s10265-019-01106-w.

Shamshirband, S., Hashemi, S., Salimi, H., Samadianfard, S., Asadi, E., Shadkani, S. & Chau, K.W.(2020). Predicting standardized stream flow index for hydrological drought using machine learning models. *Engineering Applications of Computational Fluid Mechanics*. 14 (1), 339–350. https://doi.org/10.1080/19942060.2020.17158

44
Simmons, J., Willett, K.M., Jones, P.D., Thorne, P.W. & Dee, D.P. (2010). Low-frequency variations in surface atmospheric humidity, temperature, and precipitation: Inferences fromreanalyses and monthly gridded observational data sets. *Journal of Geophysical Research Atmospheres*. 115(1), https://doi.org/10.1029/2009JD012442
Skurichina, M. & Duin, R.P. (2002). Bagging, boosting and the random subspace method for linear classifiers. *Pattern Analysis & Applications*. 5 (2), 121–135. https://doi.org/10.1007/s100440200011
Smidte, S.J., Haacker, E.M.K., Kendall, A.D., Deines, J.M., Pei, L., Cotterman, K.A., Li, H., Liu, X., Basso, B. & Hyndman, D.W. (2016). Complex water management in modern agriculture: Trends in the water–energy–food nexus over the High Plains aquifer. *Science of the Total Environment*. 566–567, 988–1001. https://doi.org/10.1016/j.scitotenv.2016.05.127
Sun, X., Lai, P., Wang, S., Song, L., Ma, M. & Han, X. (2022). Monitoring of extreme agricultural drought of the past 20 years in southwest china using gldas soil moisture. remote sensing. 14, 13-23. https://doi.org/10.3390/rs14061323.
Wada, Y., Bierkens, M.F.P. (2014). Sustainability of global water use: past reconstruction and future projections. *Environmental Research Letters*, 9(10), 104003. https://doi.org/10.1088/1748-9326/9/10/104003.
Wang, K., Dickinson, R.E. & Liang, S. (2012). Global atmospheric evaporative demand over land from 1973 to 2008. *Journal of Climate*. 25 (23), 8353–8361. https://doi.org/10.1175/JCLI-D-11-00492.1
Willett, K.M., Jones, P.D., Gillett, N.P. & Thorne, P.W. (2008). Recent changes in surface humidity: development of the HadCRUH dataset. *Journal of Climate*, 21(20), 5364–5383. https://doi.org/10.1175/2008jcli2274.1.
Willett, K.M., Dunn, R.J.H., Thorne, P.W., Bell, S., de Podesta, M., Parker, D.E., Jones, P. D. & Williams Jr., C.N. (2014). HadISDH land surface multi-variable humidity and temperature record for climate monitoring. *Climate of the Past,* 10(6), 1983–2006. https://doi.org/10.5194/cp-10-1983-2014.
Yuan, W., Zheng, Y., Piao, S., Ciais, P., Lombardozzi, D., Wang, Y. & Yang, S. (2019). Increased atmospheric vapor pressure deficit reduces global vegetation growth. *Science Advances*, *5*(8), eaax1396. https://doi.org/10.1126/sciadv.aax1396.
Zhang, D., Liu, Y., Li, Y., Qin, L., Li, J. & Xu, F. (2018). Reducing the excessive evaporative demand improved the water-use efficiency of greenhouse cucumber by regulating the trade-off between irrigation demand and plant productivity. *HortScience*, 53(12), 1784–1790. https://doi.org/10.21273/HORTSCI13129-18.

Original Article

Journal of Drought and Climate change Research (JDCR)

Winter 2025, Vol. 2, No. 8, pp 103-120

10.22077/jdcr.2025.8632.1097

Optimizing Water Use for Wheat Production under Drought Conditions

Bijan Haghighati[1*]

1- Soil and Water Research Department, Chaharmahal and Bakhtiari Agricultural and Natural Resources Research and Education Center, Agricultural Research, Education and Extension Organization (AREEO), Shahrekord, Iran.

*** corresponding author: bhaghighati@yahoo.com**

Keywords:
Water productivity, Biological yield, Grain yield, Water use efficiency.

Received:
28 Dec 2024

Revised:
21 Jan 2025

Accepted:
27 Jan 2025

Abstract

In order to compare new wheat cultivars and lines, an experiment was implemented in the form of split plots (randomized complete blocks) with three replications for two years at the Chahartakhte research station, Shahrekord, located in the agricultural and natural resources research center of Chaharmahal and Bakhtiari Province. The main treatments included three levels of irrigation, corresponding to (FI) 100%, (I80) 80%, and (I65) 65% soil moisture deficiency, while the subplots featured six wheat cultivars (Mihan, Heydari, line CD-94-9, line CD-94-8, Oroom, and Pishgam). The results of analysis of variance showed that the effect of irrigation levels on grain yield, total yield, plant height, harvest index, 1000 grams grain weight, spike length, water use efficiency and water productivity were significant at 1% level. The highest amount of grain yield was obtained from the Mihan cultivar with FI treatment with 7.85 tons/ha, which was placed in the same statistical group with the yield of two cultivars, Heydari and Pishgam. The lowest amount of grain yield was obtained from the Heidari cultivar treatment with the I65 irrigation level with 2.81 tons per hectare. The highest water use efficiency and water productivity were 2.06 and 1.83 kg/m^3, respectively, obtained from the Mihan cultivar treatment in FI irrigation management. The lowest water

How to cite this article:
Haghighati, B. (2024). Optimizing Water Use for Wheat Production under Drought Conditions. *Journal of Drought and Climate change Research* (JDCR), 2(8), 103-120. 10.22077/jdcr.2025.8632.1097

use efficiency and water productivity were 1.13 and 1.01 kg/m^3, respectively, obtained from the Heydari cultivar and I65 treatments. Therefore, in order to improve water efficiency with the aim of producing more for less water used, using cultivars with high yield potential and drought tolerance (the cultivars used in the present research), including the Mihan cultivar, can be some of the most important saving solutions for water used.

Introduction

In recent years, the demand for food has increased, through increasing the of world population. However, climate change has created many challenges, like pests, environmental pollution, etc. These factors can affect agricultural production and grain quality. Wheat (*Triticum aestivum* L.) is one of the most important food crops in the world (Asseng *et al*., 2020) and is a source of energy for more than half of the world's population (Lian *et al*., 2020). The area under wheat cultivation in 2020 in Iran and the world was six million hectares and 219 million hectares, respectively. The average wheat yield in the world is 3.68 tons per hectare, but in Iran, it is 1.66 tons per hectare (FAO, 2022). Abiotic stresses such as salinity, ultraviolet rays, high and low temperatures, drought and heavy metals can affect different stages of the plant's life cycle. These stresses have a significant impact on plant morphology, growth and production (AL-Quraan *et al*., 2019). Wheat production is seriously affected by global climate changes and rainfall patterns. With the decrease of rainfall, evapotranspiration and air temperature increase, as a result, the water requirement of wheat increases. So far, extensive studies have been conducted to investigate the effect of drought stress on the yield of crops, especially wheat, worldwide, including in Iran. Among environmental stresses, drought stress is the most important factor that leads to a significant decrease in wheat grain yield through closing the stomata and as a result, reducing the amount of photosynthesis. In short, this stress often occurs during the reproductive period of wheat (Rebetzke *et al*., 2008). Less irrigation or water saving can be an effective method of water management in the field, increasing the area under cultivation and helping determine optimal cultivation patterns. The results of many researchers showed that moisture stress in different stages of wheat development has caused a decrease in biological yield, grain yield, harvest index, and yield components of wheat grain, inside and outside the country (Emam *et al*., 2007; Gooding *et al*., 2003). Akbari Moghaddam *et al*. (2002) showed that the interruption of irrigation at the stage of spike emergence reduced grain yield and biomass yield by 36% and 20%, respectively. Shanazari *et al*. (2021)

conducted an experimented to evaluate the tolerance of drought stress in bread wheat (Tritipyrum and Terticale genotypes) in two regions of Isfahan and Shiraz provinces. The results showed that triticale lines had the highest drought tolerance. Saba et al. (2018) showed that increase in plant height caused to increase in length of the grain filling period and reducing the number of days to spike. Also, Spike length increases the number of spikes per plant and the weight of one thousand grains and reduces the selection criteria for high grains. Hosseinalipour *et al*. (2020) showed that drought stress in soil water potential lower than -5 bar causes a significant decrease in root growth parameters. Also, there was a genetic difference between cultivars regarding root growth and response to drought stress, and drought-tolerant and sensitive cultivars showed different responses to drought stress. Therefore, an important factor in the drought tolerance of the wheat plant is the reaction and development of the root system, which can be affected by drought stress, and the difference between cultivars, in terms of root growth characteristics, may reveal their difference in resistance to drought stress. Additionally, Ahmed et al. (2020) showed that when drought stress is applied to wheat, the photosynthetic pigment content of the crop diminishes, whereas the tolerant genotypes exhibit higher levels of chlorophyll. The basic solution to eliminate or minimize the effects of environmental stresses, including drought stress, is to find genotypes that, by having a set of desirable traits and high heritability, can tolerate such stresses with minimal yield reduction.

Wheat is one of the leading products of Chaharmahal and Bakhtiari Province. However, wheat production is seen as one of the significant obstacles in the province of Chaharmahal and Bakhtiari. Under such conditions, it is essential to explore various methods to enhance production relative to the water used. Different wheat cultivars have been cultivated in the province, with some being studied. However, comprehensive information about their responses to water stress is lacking. Investigating the reactions of suitable cultivars with high yield potential and desirable quality under low irrigation and drought stress management is crucial. This research aims to develop effective and practical management strategies for improving water use efficiency and irrigation water productivity, representing a fundamental and significant challenge in irrigated agriculture. Therefore, in order to make the research comprehensive and to answer the questions raised in this field, the practical and affected factors of deficit irrigation and drought stress should be considered, which play a decisive role in choosing the best option. For this reason, the present study was conducted to

Optimize water use for wheat production under drought conditions in Shahrekord province, Iran.

Materials and Methods

Study Area

The current research was carried out for two years (2018-2019) at the Chahartakhte research station of Shahrekord, located in the agricultural and natural resources research center of Chaharmahal and Bakhtiari province, (32°N latitude and 55°E longitude). It was implemented at altitude of 2090 meters above sea level and with a semi-humid regional climate with a mild summer and a very cold winter. Figure 1 shows the location of the intended research farm.

Fig 1. Studied location

Soil characteristics of the study area

To determine some physical and chemical characteristics of the soil, compound samples of the soil of the project were prepared from the depths of 0-30 and 30-60 cm, before soil preparation stages, at the beginning of October for two years. The samples were transferred to the soil and water research department laboratory and their various characteristics were measured. The results of these measurements are presented in Tables 1 and 2.

Table 1. Physical soil properties

Year	Soil depth (cm)	Texture	Bulk density ($g.cm^{-3}$)	F.C (θ_m%)	P.W.P (θ_m%)
2018	0-30	Loam	1.36	24.01	9.3
	30-60	Silt Loam	1.41	25.20	8.3
2019	0-30	Loam	1.34	26.8	9.1
	30-60	Silt Loam	1.39	23.5	8.2

Table 2. Chemical soil properties

Year	Soil depth (cm)	E.C (dS.m^{-1})	pH	O.C (%)	P ava. (mg.kg^{-1})	K ava. (mg.kg^{-1})	N (%)
2018	0-30	0.709	7.73	0.838	6.3	265	0.081
2019	0-30	0.801	7.77	0.912	9.1	284	0.086

Characteristics of irrigation water

The water used in the research farm was supplied from a well. In order to determine the quality of irrigation water, water sample was taken from the outlet of the well and transported to the laboratory to measure its chemical properties. The results of chemical analysis of water are shown in Table 3.

Table 3. Some chemical properties of water used in this study

pH	EC	Na^+	K^+	Ca^{2+}	Mg^2	Cl^-	HCO_3^-	CO_3^{2-}	SO_4^{2-}	Cd	Fe^{2+}	Cu^+	Zn^+
	µS/cm	(meq/L)								(mg/L)			
7.20	325	0.17	0.05	5.01	2.81	0.52	7.35	0	0.01	0	0.03	0.01	0.01

Stages of preparation and implementation of the plan

In order to prepare the soil, plowing and disc harrowing were carried out, in early October, for two years. Land leveling was carried out to prepare the soil, before planting. Based on the results of soil compound samples, the required amount of fertilizers was determined according to the soil test method, in each year. The required phosphorus and potassium fertilizers were from triple superphosphate and potassium sulfate sources, given to the soil respectively, before cultivation. The required nitrogen was supplied to the plant from the urea source in four stages: before cultivation, tillering stage, stem growth and before spike emergence. Iron, zinc, copper and manganese micronutrient elements were obtained from iron sulfate, zinc sulfate, copper sulfate and manganese sulfate, respectively, and used before planting. Wheat grains were disinfected before sowing (Table 4). Planting operations were carried out in the first decade of November every year. Following planting, pipes and drip irrigation equipment were installed in the field. Planting operations were carried out in the first decade of November and harvesting in early June.

Experimental design

An experiment was conducted using a split-plot design within a randomized complete block framework, with three replications, to compare wheat cultivars and lines under different irrigation levels. The study was carried out on a 1,000 square-meter plot over two consecutive cropping years. The main plots included treatments for drought stress and deficit irrigation, which were as

Table 4. Types and amounts of fertilizers used in the two years of the experiment (kg/hec)

year	Fertilization time	Nitrogen	Phosphorus	Potassium	Iron	zinc	copper	Manganese
2018	Before planting	100	150	0	40	30	15	20
	Soiling stage	100	0	0	0	0	0	0
	Before flowering	100	0	0	0	0	0	0
2019	Before planting	100	150	150	40	30	15	20
	Soiling stage	100	0	0	0	0	0	0
	Before flowering	100	0	0	0	0	0	0

follows:

FI = full irrigation (without stress)

I80 = providing 80% of the soil moisture deficiency of the complete irrigation treatment for this treatment in each irrigation (mild tension)

I65 = providing 65% of the soil moisture deficiency of the full irrigation treatment for this treatment in each irrigation (severe stress)

The treatments in this research included: 1- six cultivars and lines of wheat 2- three levels of irrigation and moisture drainage. Sub-treatments include new cultivars and lines of wheat, which include: V1 =Mihan, V2 = Heydari (New cultivar), V3 = promising line CD-94-9 is expected to have more tolerance to drought stress, V4 = promising line CD-94-8 is expected to be more tolerant to drought stress, V5 = Oroom, V6= Pishgam.

In this research, the number of treatments was 18 (3 * 6) with three replications, which formed 54 experimental plots. The dimensions of the sub-plots were considered to be 2 * 5 meters. The sub-plots were separated by 1 meter, the main plots by 1 meter and the replications by 3 meters. Grains (with a density of 450 grains per square meter) after disinfection were planted in plots with an area of 10 square meters in a line with a distance of 15 cm, In the first decade of November every year. All the operations of land preparation, planting, were carried out uniformly according to the practice of the region. The irrigation method in this research was drip tape which was installed on the soil at a distance of 50 cm. In the strip drip irrigation method, drip tapes 36 meters long with a diameter of 16 mm and a distance of water outlet channels of 20 cm were used for each crop row. The amount of irrigation water in each treatment was measured and controlled by shut-off valves and a volume meter installed on polyethylene pipes for water transfer. In this research, the amount of irrigation water in each irrigation interval was calculated by measuring the soil moisture during irrigation (Using a portable moisture measuring device) and in the full irrigation treatment according to the area of each plot and applying the irrigation efficiency of the volume of water used for each method. The amount of water used for the

deficit irrigation management treatments was set as a coefficient of its amount in the full irrigation treatment. The irrigation interval for all treatments was considered constant in the full irrigation treatment and the maximum daily evaporation and transpiration rate of the experimental site was considered for 7 days so that no stress is applied to the plant in the full irrigation treatment. In this way, in the full irrigation treatment, the amount of soil moisture was always higher than the amount of easily accessible moisture during irrigation. The studied traits included spike length, grain yield, biological yield, harvest index, and thousand grain weight. In the end, the obtained data were subjected to simple and compound variance analysis based on the statistical design using SAS software, and Tukey's test was used to compare the means of the treatments, and finally, the most tolerant genotype to water stress conditions during the season was the basis of grain yield, grain protein and water use efficiency for use in Shahrekord city and similar areas were identified and introduced. The total water used was calculated based on the National Water in Agriculture Document. Equations 1, 2 and 3 calculate water use efficiency, water productivity and harvest index.

$$WUE = \frac{Yield}{ET_c} \quad (1)$$

$$WP = \frac{amount\ of\ product\ produced}{amount\ of\ water\ used} \quad (2)$$

$$\text{harvest index} = \frac{grain\ Yield}{total\ Yield} \quad (3)$$

Water use efficiency ($Kg.mm^{-1}$), Yield ($Kg.\ ha^{-1}$), Plant evapotranspiration ($mm.\ ha^{-1}$) and : Water Productivity.

Results and discussion

The amount of applied water

The net irrigation water requirement for the treatment of maintaining 100% of soil moisture deficiency was calculated and applied during each irrigation interval. The goal was to replenish soil moisture in the root development zone up to field capacity. To calculate the gross requirement of irrigation water, the application efficiency was obtained on average for two years of research during the growing season of the plant in the drip tapes irrigation method, according to the uniformity coefficient of water distribution and the efficiency reduction factor, the water application efficiency was 89%. The average values of the net and gross requirement of irrigation water used for the experimental treatments in the two years of the research are presented in Table 5.

Yield and yield components

The summary of the results of the compound variance analysis of the effect of cultivar and irrigation levels on the yield and yield components of wheat in two years of the research is presented in Table 6.

Table 5. Water volume required and consumed for different drought stress treatments during the wheat growing season

Levels of irrigation	FI	I_{80}	I_{65}
Water volume required (m^3/ha)	3814	3051	2479
Water volume consumed (m^3/ha)	4285	3428	2785

Table 6. Results of the combined analysis of variance of measure properties of wheat crop under irrigation treatment in two crop years

Source of variation	df	Mean of squares					
		Grain yield	Biological performance	Plant height	Harvest index	Weight of a thousand grains	Spike length
Year (y)	1	2832^{ns}	13125^{ns}	156^{ns}	33699^{ns}	681^{ns}	12.07^{ns}
Error y	4	1840	2220	5.34	0.32	1.08	0.2
Levels of irrigation	2	1429560**	3566431**	95.21**	502**	951.38**	16.63**
Year ×Levels of irrigation	2	8601**	1798^{ns}	4.25^{ns}	487**	8.86**	0.01^{ns}
Error a	8	530	1701	2.41	2.19	0.49	0.1
Cultivar	5	24839**	270952**	106.15**	5.33**	19.07**	10.59**
Year ×Cultivar	5	2866**	4633**	0.86	5.39^{ns}	10.52**	0.34**
Levels of irrigation × Cultivar	10	11071**	49847**	33.11**	17.96**	9.90**	0.37**
Year ×Levels of irrigation× Cultivar	10	2653**	8742**	2.32^{ns}	17.99**	5.60**	0.02^{ns}
Error b	60	744	1319	2.94	1.86	0.74	0.1
CV		5.02	2.38	2.03	7.57	2.63	3.05

ns, * and **: not significant, significant at 5% and 1% probability levels, respectively.

Grain yield

In general, the results of compound variance analysis (Table 6) showed that the effect of year was not significant on grain yield. The effect of irrigation levels was significant at level of 1% level on grain yield. The maximum and minimum grain yields were obtained at 7.05 and 3.30 tons per hectare for FI and I65 treatments, respectively (Table 7). The effect of cultivar on grain yield was significant at the level of 1%, so that the maximum and minimum grain yield per unit area was 5.75 and 4.82 tons per hectare, respectively, for Mihan cultivar and line CD-94-8 (Table 7). The interaction effect of cultivar and irrigation levels on grain yield was significant (Table 6). The mean comparison of grain yield in wheat cultivars under different irrigation levels showed the highest grain yield in Mihan cultivar with FI treatment (7.85 tons per hectare) and the lowest grain yield in Heydari cultivar with I65 irrigation level (2.81 tons per hectare) (Figure 2). In this study, the I_{80} treatment decreased the grain yield by 20%, but the I_{65} treatment decreased the grain yield by 56%. This reduction in yield can be attributed to the long-term stress applied to the plant, which reduces the photosynthetic level of the plant, thereby reducing plant growth and ultimately reducing yield. Ahmadi Lahijani and Emam (2013) indicated that grain yield under normal irrigation

conditions and drought stress had a positive and significant correlation with all traits except for thousand grain weight. The reduction of grain yield due to drought stress has been reported in other studies (Emam *et al*., 2007). Also, results showed that by increasing amount of irrigation water to the full irrigation, grain yield can increase near the production potential and full irrigation treatment had the highest grain yield, but severe stress on the plant caused a significant reduction in the yield. The cultivars used in this research have a high yield. (Table 7), which is due to the high potential and compatibility with the growing environment of these cultivars. The aims of cultivar selection are different in different countries, but in all programs, it is cultivar selection will likely be effective for high yield, and their suitability for specific uses, resistance to living and non-living stresses, less water requirement, better use of nutrients such as nitrogen and phosphorus. In short, new cultivars should have high yield. In this regard, new cultivars should be evaluated for different traits in the country. Therefore, for the optimal use of water and increased production per unit of water used, it is necessary to modify and select suitable plant cultivars according to the environmental conditions of plant growth and apply appropriate management of low irrigation. Also, the grain yield in all drought stress management treatments was higher in Mihan cultivar than other cultivars. Due to the limitation of water resources in arid and semi-arid regions, methods should be adopted to obtain optimal productivity from available water resources and also not to harm the sustainability of the production of this product. One of the possible methods in the optimal use of available water resources is to introduce cultivars that are less sensitive to irrigation reduction and have acceptable yield in low irrigation conditions.

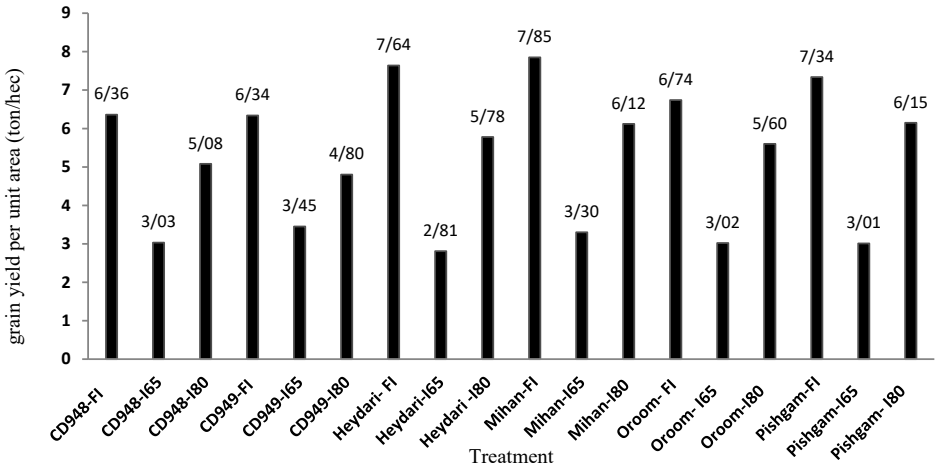

Fig 2. Interaction effect of cultivar and irrigation levels on wheat grain yield

Biological function

In general, the results of compound variance analysis (Table 6) showed that the effect of year on biological yield was insignificant. The effect of irrigation levels on biological yield was significant at the 1% level (Table 6). The maximum and minimum biological yield were obtained at 17.07 and 10.85 tons per hectare for FI and I_{65} treatments, respectively (Table 8). Emam *et al*., (2011) and Pireivatlou *et al*., (2010), also reported similar results of reduced biological yield due to drought stress. The effect of cultivar on biological yield per unit area was significant at the level of 1% (Table 6). The highest amount of biological yield per unit area was obtained for the Mihan cultivar (15.71 tons per hectare). The interaction effect of cultivar and irrigation levels on biological performance was significant (Table 6). Comparison of biological yield in wheat cultivars under different levels of irrigation showed that the highest biological yield per unit area was in the Pishgam cultivar with FI treatment amounting to 18.49 tons per hectare, which was in the same statistical group with Mihan and Heydari cultivars (Figure 3). The lowest amount of biological yield per unit area was obtained in Heydari cultivar with I_{65} irrigation level of 10.25 tons per hectare (Figure 3). The results showed that biological yield reduced with the decrease in the amount of irrigation water. The I_{65} treatment reduced biological yield by 36% compared to FI. In mild drought stress, Mild drought stress primarily reduces transpiration, whereas severe stress significantly impairs photosynthesis, leading to a sharp decline in biological yield. Therefore, for optimal use of water and increase production per unit of water used, it is necessary, modify and select suitable plant cultivars according to the environmental conditions of plant growth.

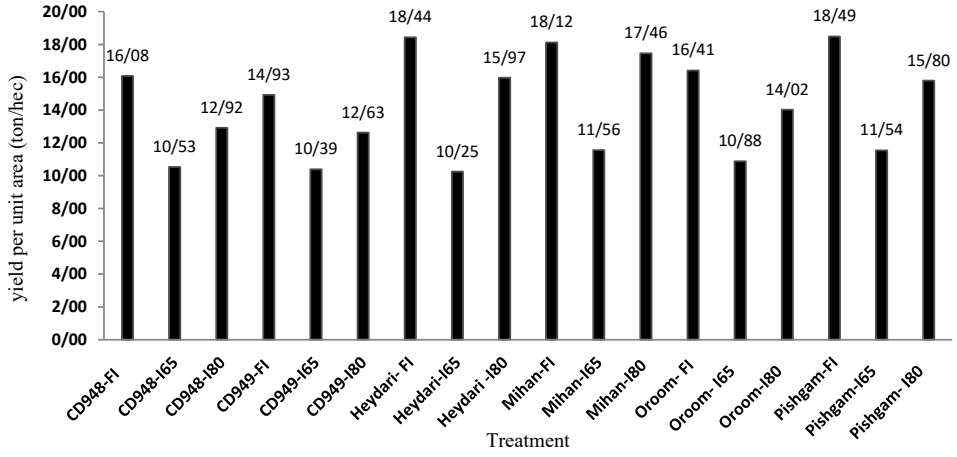

Fig 3. Interaction effect of irrigation levels in cultivar on biological yield of wheat

Plant height

In general, the results of compound variance analysis (Table 6) showed that the effect of year on plant height was insignificant. The effect of irrigation levels on plant height was significant at the 1% level (Table 6). Also, by increasing the amount of irrigation water from 65% to 100%, the height of the plant increased from 82.91 to 86.15 cm (Table 7). Plant height is one of the characteristics that is influenced by genetic and environmental factors. The increase in plant height is usually the most noticeable change caused by plant growth. Height can be considered an advantage in terms of competition with other plants in a plant community. Generally, biological yield is the sum of grain yield and straw yield. The higher the plant height, the higher the straw yield, and thus the higher the total yield.

The effect of the cultivar on plant height was significant at the 1% level (Table 6). The highest height of the plant was obtained for the Oroom cultivar (87.8 cm) (Table 7). The interaction effect of cultivar and irrigation levels on plant height was significant at the 1% level (Table 7). The mean comparison of plant height in wheat cultivars under different irrigation levels showed that the highest plant height was obtained in Oroom cultivar with FI treatment at a height of 90.32 cm and the shortest plant height in Mihan with I_{65} irrigation treatment at height of 77.98 cm. (Figure 4).

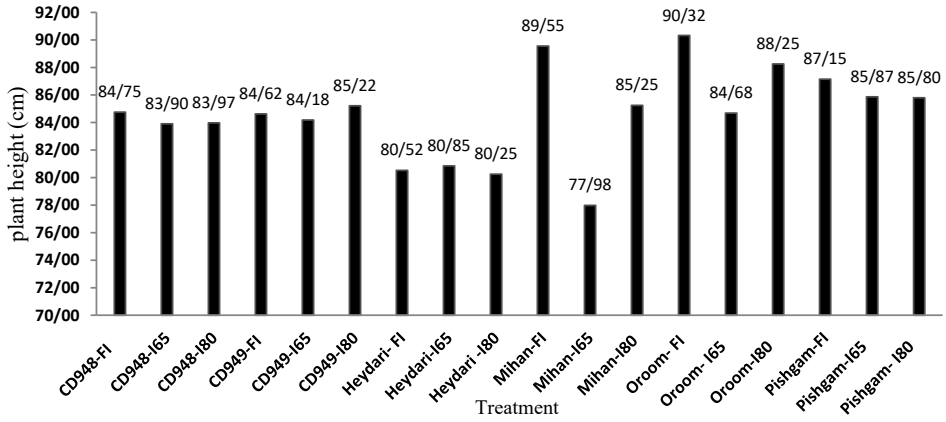

Fig 4. Interaction effect of irrigation levels and cultivar on wheat plant height

Table 7. Comparison of means in different traits of

Treatment		Grain yield (ton/ha)	Biological performance (ton/ha)	Plant height (cm)	Harvest index	Thousand grain weight (gr)	Spike length (cm)
Year	Year 1	5.29a	14.35a	85.81a	0.36a	35.44a	10.67a
	Year 2	5.19a	14.13a	83.41a	0.36a	33.76a	10.00a
Levels of irrigation	FI	7.05a	17.07a	86.15a	0.42 a	38.03a	11.03a
	I_{80}	5.58b	14.8b	84.79b	0.37b	33.01b	10.31b
	I_{65}	103.10c	10.85c	82.91c	0.3c	27.75c	9.67c
Cultivar	Mihan	5.76a	15.71a	384.3c	0.35b	32.2d	10.1c
	Oroom	5.13c	13.77d	87.8a	0.35b	31.6e	11.3a
	CD-94-8	4.82d	13.17e	84.2c	0.36b	33.3bc	10.7b
	CD-94-9	4.86d	12.65f	84.7c	0.4a	32.7acd	10.6b
	Heydari	5.41b	14.89c	80.5d	0.34b	33.41b	10.2c
	Pishgam	5.50b	15.27b	86.3b	0.36b	34.48a	9.0d

Means in each column having at least one similar letter are not significantly different at 5% probability.

Harvesting index

In general, the results of compound variance analysis (Table 6) showed that the effect of year on harvesting index was not significant. The results showed that the effect of irrigation levels on the harvesting index was significant at the 1% level (Table 6). The lowest and highest harvest index at different irrigation levels were 0.30 and 0.42, respectively (Table 8). The effect of cultivar on harvesting index was significant at the level of 1%. The lowest harvesting index (0.34) was obtained from Heydari cultivar and the highest harvesting index (0.40) from CD-94-9 line (Table 7). According to the harvesting index calculation equation (3), when the grain yield is higher, the harvesting index value increases.

Soleimani (2016) indicated that the effect of drought stress treatments on the harvesting index was significant. The interaction effect of cultivar and irrigation levels on harvesting index was significant at the level of 1% (Table 6). The mean comparison of the harvesting index in wheat cultivars under different irrigation levels showed that the highest harvesting index was obtained in Mihan cultivar with FI treatment at the rate of 0.43 and the lowest harvesting index was obtained in Pishgam, Heydari and Oroom cultivars with I_{65} irrigation treatment at the rate of 0.27 (Fig 5).

Thousand grains Weight

In general, the results of compound variance analysis (Table 6) showed that the effect of year on the weight of one thousand grains was insignificant. The results showed that the effect of irrigation levels on the weight of 1000 grains was significant at the level of 1%, so that the maximum weight of 1000 grains (1803 grams) was related to the FI treatment and the minimum weight of 1000 grains (27.75 grams) was related

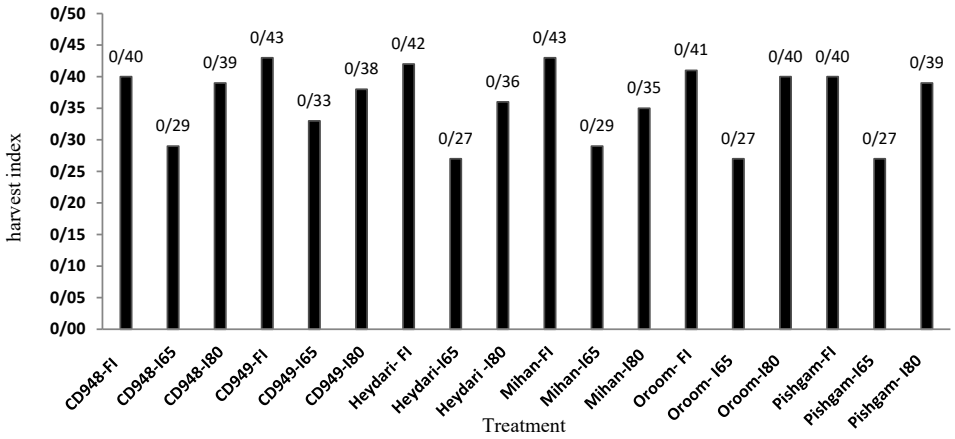

Fig 5. Interaction effect of irrigation levels and cultivar on harvesting index

to the I65 treatment (Table 7). The effect of cultivar on the weight of 1000 grains was significant at the level of 1% (Table 6). The lowest weight of 1000 grains (31.6 grams) were obtained from the Oroom cultivar and the highest weight of 1000 grains (34.48 grams) was obtained from the Pishgam (Table 7). Marc *et al*. (1985) reported that post-flowering drought stress reduced the number of endosperm cells at the base and apex of the spike and ultimately reduced the 1000 grain weight. The interaction effect of cultivar and irrigation levels on the weight of 1000 grains was significant at the 1% level (Table 6). Results of the mean comparison of the weight of 1,000 grains in different wheat cultivars for different irrigation levels showed that the Pishgam cultivar with FI irrigation management treatment had the maximum 1,000 grain weight (41.27 grams) and the Oroom cultivar with I65 irrigation level had the minimum 1,000 grain weight (35. 26 gr) (Figure 6). In general, as grain yield decreases, harvesting index and water use efficiency decrease.

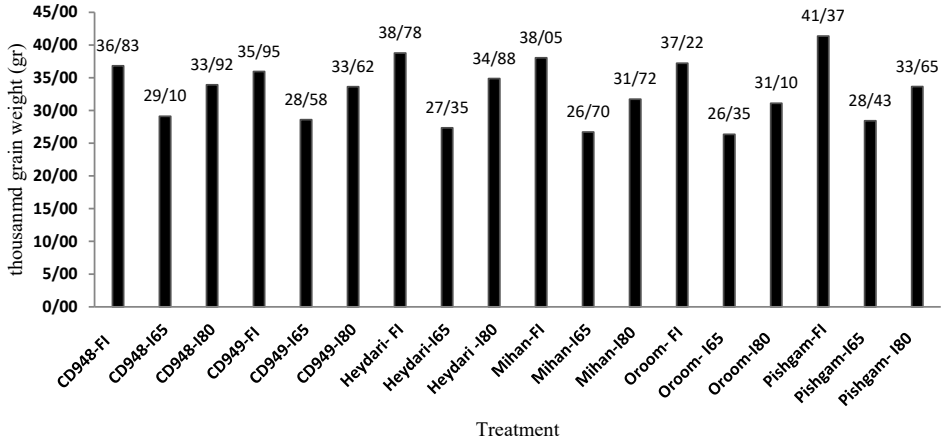

Fig 6. Interaction effect of irrigation levels and cultivar on thousand grain weight

Spike length

In general, the results of compound variance analysis (Table 6) showed that the effect of year on spike length was insignificant. The effect of irrigation levels on spike length was significant at the level of 1% (Table 6), so that by increasing the amount of irrigation water from 65% to 100%, spike length increased from 9.67 to 11.03 cm (Table 7). The effect of cultivar on spike length was significant at the 1% level (Table 6). The longest spike length was obtained from Oroom cultivar (11.30 cm) and the shortest spike length was obtained from Pishgam cultivar (0.9 cm) (Table 7). The interaction effect of the cultivar and irrigation levels on spike length was significant at the 1% level (Table 6). The results of mean comparison of spike length in wheat cultivars under different irrigation levels showed that the longest spike length in Oroom cultivar with FI treatment was 12.07 cm and the shortest spike length was 8.58 cm in Pishgam cultivar with I65 irrigation treatment (Fig 7).

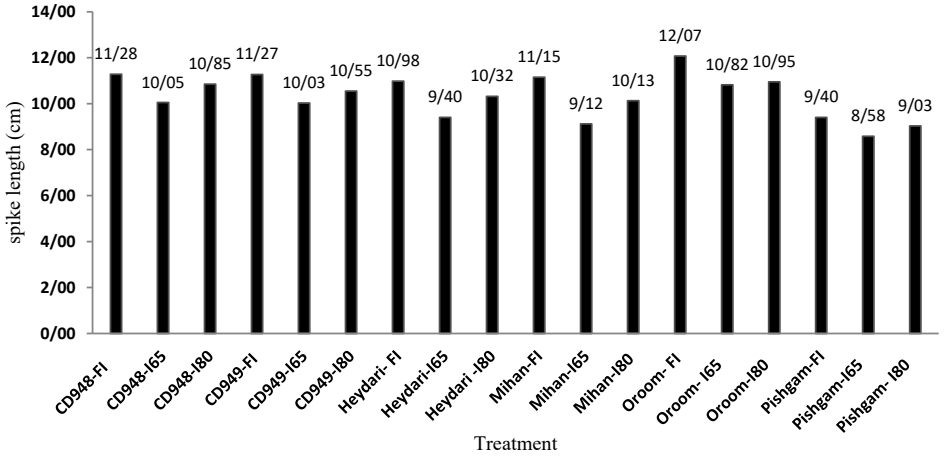

Fig 7. Interaction effect of irrigation levels and cultivar on spike length

Effect of drought stress management on water use efficiency and water productivity

The summary of the results of the compound variance analysis of the effect of cultivar and irrigation levels on the water use efficiency and water productivity in two years of research is presented in Table 7. The results of the analysis of the variance table (Table 8) showed that the effect of irrigation levels on the water use efficiency and water productivity was significant at the level of 1%. In general, the results of the mean comparison showed that the highest water use efficiency and water productivity were 1.85 and 1.64 kg per cubic meter, respectively, which were related to the FI irrigation management treatment, and the lowest water use efficiency and water productivity were 1.25 and 1.12 kg, respectively. per cubic meter in I65 (Table 9). Liu *et al*. (2016)

stated that with the increase in the intensity of drought stress, the water use efficiency for total dry matter and grain yield increases, so that mild stress creates a significant difference compared to the control treatment (no stress). The effect of cultivar on water use efficiency and water productivity was significant at the level of 1% (Table 8). The results of the mean comparison showed that the highest water use efficiency and water productivity were 1.80 and 1.60 kg/m^3, respectively, for Mihan (Table 9). The lowest water use efficiency and water productivity were 1.52 and 1.35 kg/m^3, respectively, in the CD-94-8 line (Table 9). The interaction effect of cultivar and irrigation levels on water use efficiency was significant at the level of 1% (Table 8). The mean comparison of water use efficiency in wheat cultivars under different irrigation levels showed the maximum water use efficiency in Mihan cultivar with FI treatment with 2.06 kg/m^3 and the lowest water use efficiency in Heydari cultivar with I65 treatment 1.13 kg/m^3 (Figure 8). The mean comparison of water productivity in two cultivars under different irrigation levels showed that the maximum water productivity in Mihan cultivar with FI treatment was 1.83 kg/m^3 and the lowest water productivity was obtained in Heydari cultivar with I_{65} treatment at 1.01 kg/m^3 (Fig. 9). In drip irrigation, because water is provided exactly according to the plant's needs and water efficiency is very high, it is recommended that all the water needed be provided for it and deficit irrigation is not recommended.

Table 8. Results of the combined analysis of variance of water use efficiency and water efficiency of wheat crop in two crop years

Source of variation	df	Mean of squares	
		Water Use Efficiency	Water efficiency
Year (y)	1	0.13^{ns}	0.11^{ns}
Error y	4	0.02	0.01
Levels of irrigation	2	4.13**	3.28**
Levels of irrigation× Year	2	0.12^{ns}	0.09^{ns}
Error a	8	0.001	0.001
Cultivar	5	0.21	0.16**
Cultivar× Year	5	0.03^{ns}	0.02^{ns}
Cultivar× Levels of irrigation	10	0.11**	0.09**
Year × Levels of irrigation× Cultivar	10	0.03^{ns}	0.02^{ns}
Error b	60	0.01	0.01
CV		5.41	5.45

ns, * and **: not significant, significant at 5% and 1% probability levels, respectively.

Table 9. Mean of water use efficiency and water efficiency in two crop years

Treatment		Water use efficiency (kg/m^3)	Water efficiency (kg/m^3)
Year	Year 1	1.67a	1.49 a
	Year 2	1.60 a	1.43 a
Levels of irrigation	FI	1.85a	1.64a
	I_{80}	1.83a	1.63a
	I_{65}	1.25b	1.12b
Cultivar	Mihan	1.80a	1.60a
	Oroom	1.61c	1.43b
	CD-94-8	1.52d	1.35d
	CD-94-9	1.54d	1.37d
	Heydari	1.68b	1.49b
	Pishgam	1.72b	1.53b

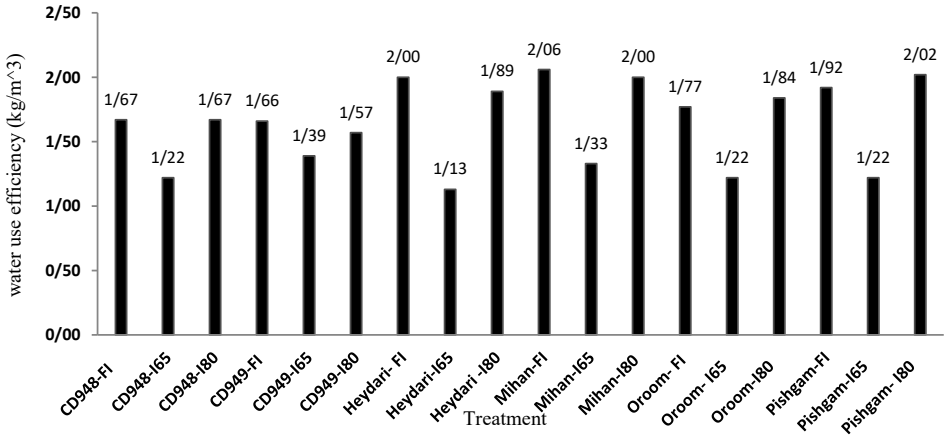

Fig 8. Interaction effect of cultivar and irrigation levels on wheat water use efficiency

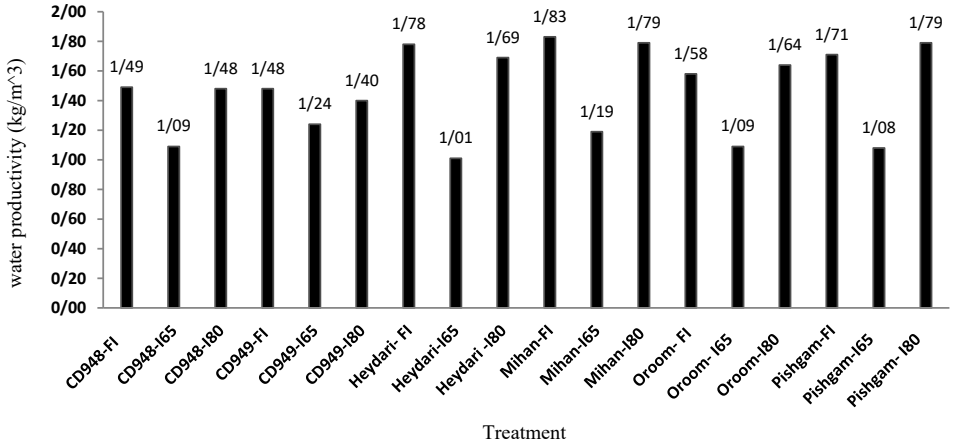

Fig 9. Interaction effect of irrigation levels and cultivar on wheat water productivity

Conclusion

To address the challenge of improving water use efficiency, it is essential to increase crop yield (the numerator of the efficiency index) while simultaneously reducing water used (the denominator). The effectiveness of measures aimed at enhancing water use efficiency is realized when these actions lead to simultaneous improvements—an increase in the numerator and a decrease in the denominator of the efficiency index. In other words, solving the problem of increasing water use efficiency requires a broader perspective that goes beyond focusing solely on the water sector. A special emphasis should also be placed on other areas, such as agriculture and plant nutrition. These findings support national development programs aiming to improve water use efficiency and food security under water-scarce conditions. To optimize water use and increase production per unit of water consumed, it is essential to adapt and using cultivars with high yield potential (cultivars used in the present study), including Mihan cultivar. Also, due to the limited water resources of the country and the need to plant wheat as an agricultural product that creates employment and provides food security and eradicates poverty in the world, it requires that the use of new technologies for the irrigation of this product be taken into consideration, and it seems that the drip tapes irrigation method and cultivars tested in this research, by reducing water used, is one of the ways to fight against water scarcity for the cultivation of this crop in arid and semi-arid regions of Iran.

References

Ahmed, H. G. M. D., Zeng, Y., Yang, X., Anwaar, H. A., Mansha, M. Z., Hanif, C. M. S. & Alghanem, S. M. S. (2020). Conferring drought-tolerant wheat genotypes through morpho-physiological and chlorophyll indices at grainling stage. *Saudi Journal of Biological Sciences*, 27, 2116-2123. DOI: 10.1016/j.sjbs.2020.06.019

Ahmadi Lahijani. M.J., & Emam, Y. (2013). Investigating the response of wheat genotypes to drought stress at the end of the season using physiological indicators. J*ournal Of Production And Processing Of Agricultural And Horticultural Products*, 3 (9), 163-175. [In Persian]

Akbari Moghaddam, H., Etesam, G.H., Koohkan, R., Rostami, Sh.A. & Keikha, Gh.A. (2002). Effect of moisture stress in different growth stages on grain yield in wheat cultivars. *Proceedings of the 7th Iranian Crop Science Congress.* Karaj, Iran. [In Persian]

AL-Quraan N.A., AL-Ajlouni Z.I. & Obedat D.I. (2019). The GABA shunt pathway in germinating grains of wheat (*Triticum aestivum* L.) and barley (*Hordeum vulgare* L.) under salt stress. *Grain Science Research*, 1-11. DOI:10.1017/S0960258519000230

Asseng, S., Guarin, J.R., Raman, M., Monje, O., Kiss, G., Despommier, D.D., Meggers, F.M. & Gauthier, P.P.G. (2020). Wheat yield potential in controlled-environment vertical farms. *Proceedings of the National Academy of Sciences*, 117, 19131-19135. DOI:10.1073/pnas.2002655117

Emam, Y., Ranjbari, A.M. & Bahrani,

M.J. (2007). Evaluation of yield and yield components in wheat genotypes under post-anthesis drought stress. *Journal of Science and Technology of Agriculture and Natural Resources* 11, 317-328. [In Persian]

Emam, Y. & Niknejhad, M. (2011). An introduction to the physiology of crop yield. shiraz university press. [In Persian]

FAO. 2022. https://www.fao.org/faostat/en/#data/QCL.

Gooding, M.J., Ellis, R.H., Shewry, P.R. & Schofield, J. D. 2003. Effects of restricted water availability and increased temperature on the grain filling, drying and quality of winter wheat. *Journal of Cereal Science,* 37, 295-309. DOI:10.1006/jcrs.2002.0501

Hosseinalipour, B., Rahnama, A. & Farrokhian Firouzi, A. (2020). Effect of drought stress on wheat root growth and architecture at vegetative growth stage. *Iranian Journal of Field Crop Science,* 51 (1), 63-75. [In Persian] DOI: 10.22059/ijfcs.2019.266586.654531

Lian, J., Wu, J., Xiong, H., Zeb, A., Yang, T., Su, X. & Sua, L.W. (2020). Impact of polystyrene nanoplastics (PSNPs) on grain germination and grainling growth of wheat (*Triticum aestivum* L.). *Journal of Hazardous Materials*, 358, 121620. DOI: 10.1016/j.jhazmat.2019.121620

Liu, E.K., Mei, X.R., Yan, C.R.., Gong, D.Z. & Zhang, Y.Q. (2016). Effects of water stress on photosynthetic characteristics, dry mattertranslocation and WUE in two winter wheat genotypes. *Agricultural Water Management*, 167, 75-85. DOI:10.1016/j.agwat.2015.12.026

Marc, E.N., Roslyn, M.G. & Dalling, M.J. (1985). Effect of post-anthesis drought on cell division and starch accumulation in developing wheat grains. *Annals of Botony,* 55, 433-444.

Pireivatlou, A.S., Dehdar Masjedlou, B. & Ramiz, T. A. (2010). Evaluation of yield potential and stress adaptive trait in wheat genotypes under post anthesis drought stress conditions. *African Journal of Agricultural Research,* 5, 2829-2836. DOI: 10.5897/AJAR.9000329

Rebetzke, G.J., Van Herwaarden, A.F., Jenkins, C., Weiss, M., Lewis, D., Ruuska, S., Tabe, L., Fettell, N. A. & Richards, R. A. (2008). Quantitative trait loci for water- soluble carbohydrates and associations with agronomic traits in wheat. *Journal of Agricultural Research*, 59, 891-905. DOI:10.1071/AR08067

Saba, J., Tavana, Sh., Qorbanian, Z., Shadan, E., Shekari, F. & Jabbari, F. (2018). Canonical correlation analysis to determine the best traits for indirect improvement of wheat grain yield under terminal drought stress. *Journal of agricultural science and technology*, 20, 1037-1048. [In Persian] DOR: http://dorl.net/dor/20.1001.1.16807073.2018.20.5.10.0

Shanazari, M., Golkar, P., Mirmohammady Maibody, S.A.M. & Shahsavand-Hassani, H. (2021). Using drought tolerance indices in evaluation of some wheat, triticale and tritipyrum genotypes. *Journal of Crop Production and Processing*, 10 (4), 45-68. [In Persian]

Soleimani, A. (2016). Investigating the impact of drought stress on wheat yield and yield components using the FT-HS model. *Environmental stress in agricultural sciences*, 9 (3), 205-215. [In Persian] DOI: 10.22077/escs.2016.412

Zamani, A., Mortazavi, S.A. & Balali, H. (2014). Investigating the economic efficiency of water in different crops in Dasht Bahar. *Journal of water research in agriculture*, 28 (1), 51-61. [In Persian] DOI: 10.22092/jwra.2015.101065

Original Article

Journal of Drought and Climate change Research (JDCR)

Winter 2025, Vol. 2, No. 8, pp 121-140

10.22077/jdcr.2025.8636.1098

Development of Intensity-Duration-Frequency Curves at Basin Scale using the ERA5 Reanalysis Product

Ameneh Mianabadi[1], Javad Omidvar[2], Mohsen Pourreza-Bilondi[3*]

1- Department of Ecology, Institute of Science and High Technology and Environmental Sciences, Graduate University of Advanced Technology, Kerman, Iran.
2- Department of Water Sciences and Engineering, Faculty of Agricultural, Ferdowsi University of Mashhad, Mashhad, Iran.
3- Department of Water Engineering, University of Birjand, Birjand, Iran.
*** corresponding author: Mohsen.pourreza@birjand.ac.ir**

Keywords:
Annual Maximum Precipitation, Bias Correction, Climate Change, Flood Management, Karkheh River Basin.

Received:
25 Dec 2024

Revised:
5 Feb 2025

Accepted:
7 Feb 2025

Abstract

Intensity-Duration-Frequency (IDF) curves are essential for hydrological modeling, infrastructure design, and flood risk management. However, traditional methods of IDF curve development relying on ground-based observations face significant limitations, including sparse spatial coverage, short temporal records, and the stationary assumption, particularly in the context of climate change. Accordingly, this study addresses these challenges by utilizing ERA5 reanalysis data to develop basin-scale IDF curves for the Karkheh River Basin (KRB) in Iran. The Annual Maximum Precipitation (AMP) series for durations of 6-, 12-, 18-, and 24-hours were extracted from ERA5 data and corrected for bias using observed precipitation from seven synoptic stations. The bias correction significantly improved ERA5 estimates, especially in high-altitude regions. A relationship between elevation and bias factors was established to extend the correction across the basin. The corrected AMP data were then modeled using the Generalized Extreme Value (GEV) distribution, considering both stationary and non-stationary conditions, to construct spatially distributed IDF curves based on 82 grid points across the basin. The spatial maps of IDF indicate that rainfall intensity varies

How to cite this article:
Mianabadi, A., Omidvar. J., & Pourreza-Bilondi. M. (2024). Development of Intensity-Duration-Frequency Curves at Basin Scale using the ERA5 Reanalysis Product. *Journal of Drought and Climate change Research* (JDCR), 2(8), 121-140. 10.22077/jdcr.2025.8636.1098

significantly across the basin, with higher intensities observed in elevated regions. These maps provide detailed and reliable rainfall intensity estimates compared to traditional station-based methods. This work highlights the potential of ERA5 data, combined with robust bias correction, to enhance hydrological analysis in data-scarce regions.

Introduction

Accurate estimation of extreme rainfall events is crucial for the design and planning of various critical infrastructures, including urban drainage systems, dams, and bridges (Venkatesh et al., 2022). These structures must be designed to withstand the impacts of intense rainfall events, which can lead to flooding and other significant consequences. Intensity-Duration-Frequency (IDF) curves provide a valuable tool for characterizing these extreme events by relating rainfall intensity to its duration and return period (Koutsoyiannis et al., 1998). Traditional methods for developing IDF curves primarily rely on historical rainfall data collected from ground-based rain gauges (Marra et al., 2017; Noor et al., 2021; Venkatesh et al., 2022). However, these methods often face significant limitations. Firstly, the spatial coverage of ground-based rain gauges is typically sparse, leading to inadequate representation of rainfall variability across a basin. This spatial sparsity can result in significant uncertainties in the derived IDF curves, particularly in regions with limited gauge networks (Noor et al., 2021). Secondly, the temporal record of ground-based observations is often relatively short, limiting the ability to capture the full range of extreme rainfall events, especially for the longer return periods (Marra et al., 2017). Thirdly, the assumption of stationary, which assumes that the statistical properties of rainfall remain constant over time, may be rendered invalid due to the impacts of climate change (IPCC, 2021). Finally, the distance of the designed infrastructures from the gauges' location decreases the effectiveness of the gauge-acquired IDF curves (Marra et al., 2017). These limitations lead the researcher to apply alternative data sources such as global gridded precipitation products for IDF development (Wambura, 2024).

In addition to the mentioned challenges, the point-based IDF curves may not adequately capture spatial variations in rainfall intensity, especially in large or topographically diverse regions (Marra et al., 2017). To overcome this issue, the development of spatially-distributed IDF curves has gained attention. Spatial IDF curves utilize gridded datasets to provide continuous coverage over a region, offering more detailed and reliable information for infrastructure design and flood management. The emergence of high-resolution reanalysis datasets, such as

ERA5 (Hersbach et al., 2020), has provided a promising alternative for developing IDF curves (Hersbach et al., 2023). The ERA5 dataset, produced by the European Centre for Medium-Range Weather Forecasts (ECMWF), provides a globally consistent and spatially comprehensive record of atmospheric variables, including precipitation. The high temporal resolution of this product (hourly to daily available data) , make it suitable for developing IDF curves in data-scarce basins (Tarek et al., 2020).

Few studies used the ERA5 data to develop the IDF curves at global (Courty et al., 2019) and regional scales (Jalbert et al., 2022; Wambura, 2024; Zambrano-Bigiarini et al., 2024). Among them, Jalbert et al. (2022) provided a map of spatial rainfall intensity for 25-year return period for 30-min rainfall. This study aims to assess the feasibility and accuracy of utilizing ERA5 reanalysis data for IDF curve development at the basin scale by establishing an explicit relationship between elevation and bias factor as describe in Materials and Methods section. The study also investigates potential improvements in spatial coverage and characterization of extreme rainfall events in regions with complex topography. Such integration of elevation-based corrections with ERA5 data and providing the spatial distribution of rainfall intensity for different durations and return periods have not been widely explored. Hence, this study represents a significant advancement in this filed.

Materials and Methods

Study Area

The Karkheh River Basin (KRB) with an area of approximately 51,000 km^2 is located in the southwest of Iran (Figure 1). The mean annual precipitation over the basin varies between about 250 mm in the southern part and up to 700 mm in the northern part (Ashraf Vaghefi et al., 2014). The Karkheh River originates from the Zagros mountains and goes firstly, to Hoor-Al-Azim Swamp (a transboundary wetland shared between Iran and Iraq), and then to Persian Gulf by connecting to Arvand Rud. The KRB holds great significance in the realms of both agriculture activities and energy generation. Karkheh Dam as the largest reservoir of Iran (> 5 billion cubic meters (BCM), has been constructed to provide water for these purposes (Davtalab et al., 2017).

ERA5 Data

ERA5, as the Fifth Generation of the European Centre for Medium-Range Weather Forecasts (ECMWF) Reanalysis, provides various meteorological variables data at global scale. The data are available from 1940 to present with a 0.25°×0.25° resolution (Hersbach et al., 2023). The hourly ERA5 precipitation data were downloaded from https://cds.climate.copernicus.eu/ (last access: 20/09/2023)

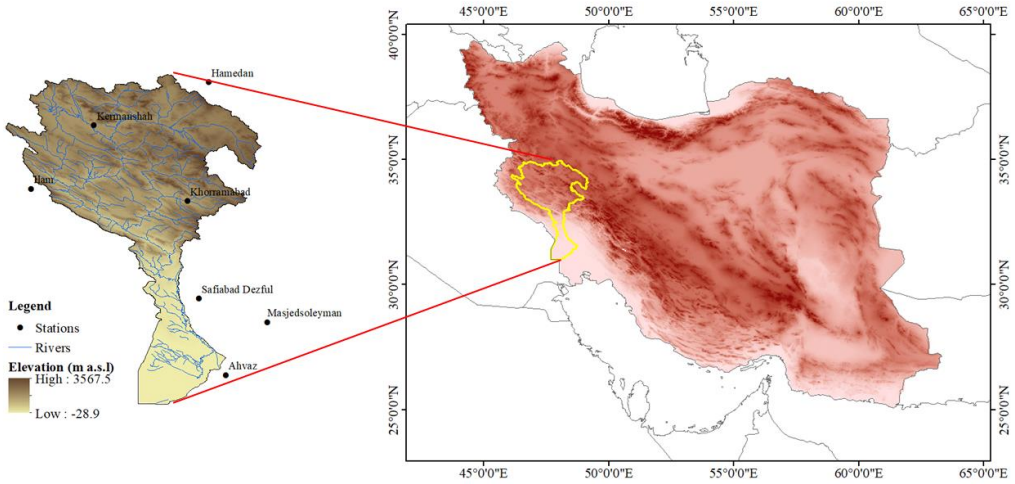

Fig 1. Geographical characteristics of the case study and the synoptic stations.

and then aggregated to the 6-, 12-, 18-, and 24-hourly precipitation data.

Observed Data

To validate the ERA5 data, we acquired the precipitation data from seven synoptic stations, within and around the watershed. The location of these stations has been shown in Figure 1. Due to limited access to the data, the quality-controlled 6-hourly precipitation data from 1996 to 2020 (25 years) were used for the analysis. The 12-, 18-, and 24-hourly precipitation data were acquired from the 6-hourly precipitation data.

Bias Correction

Previous investigations have demonstrated that the reanalysis products exhibit both random and systematic errors, particularly for heavy precipitation estimation (Frank et al., 2018; Garibay et al., 2021; Hersbach et al., 2020; Parker, 2016; Probst & Mauser, 2022). Hence, it is necessary to rectify the bias associated with extreme precipitation values. To achieve this, the Annual Maximum Precipitation (AMP) series for 6-h, 12-h, 18-h and 24-h durations were extracted from both observed and ERA5 data. Then, the AMP series were subsequently arranged in descending order. The bias correction factor (f_{bc}) is established as the proportion of the th observed AMP ($\mathrm{AMP}_{Obs(i,j,l)}$) to the th ERA5 AMP ($\mathrm{AMP}_{ERA5(i,j,l)}$), as shown in the following Equation:

$$f_{bc} = \frac{\mathrm{AMP}_{Obs(i,j,l)}}{\mathrm{AMP}_{ERA5(i,j,l)}} \quad (1)$$

In this equation, i and j indicate the given station and duration, respectively. Afterward, the average factor is multiplied by the original ERA5 AMP data and the bias-corrected ERA5 AMP is obtained. By the above-mentioned method, the bias factors are estimated for the seven synoptic stations. However, we need the bias factor for each grid of the ERA5 data to have

a map of the IDF curves over the basin. As proposed by Noor et al., (2021), the obtained bias correction factor for the gauge stations can be related to the physiographic factors such as elevation. This relationship then can be applied for the ungauged areas based on their topography. Accordingly, in this study, a relationship between the bias factors and the elevations of the stations were developed. Then using the developed relationship and the elevations of the grid points, the bias factors for each grid point were estimated.

GEV Distribution

The Generalized Extreme Value (GEV) distribution is a widely employed statistical model in hydrology and extreme value analysis. The GEV distribution is a three-parameter family of continuous probability distributions which is defined as follows:

$$F(x) = \exp\left[-\left(1 + k\frac{(x-\mu)}{\sigma}\right)^{-\frac{1}{k}}\right] \quad (2)$$

where, $1 + k\frac{(x-\mu)}{\sigma} > 0$, k, μ, and σ are the shape, location, and scale parameters, respectively. The parameters have been estimated using the Maximum Likelihood Estimation (MLE) method at 95% confidence level (Hilbe & Robinson, 2013).

The suitability of the GEV distribution for modeling extreme events is rooted in its ability to describe the distribution of block maxima (Coles et al., 2001) including the AMP series. Previous studies have successfully applied the GEV distribution for development of the IDF curves (Cheng & AghaKouchak, 2015; Crévolin et al., 2023; Guhathakurta et al., 2011; Ragno et al., 2018; Shrestha et al., 2017). Recently, it has been used for extreme rainfall events modeling using the gridded rainfall data (Marra et al., 2017, 2019; Mianabadi, 2023; Noor et al., 2021; Ombadi et al., 2018; Venkatesh et al., 2022). Hence, the GEV distribution was also applied in this study, to fit the AMP series to develop the IDF curves.

The three parameters of k, μ, and σ are time-independent for a stationary GEV distribution, while the parameters are changing with time for the non-stationary distribution (Cheng & AghaKouchak, 2015; Coles et al., 2001). Srivastava et al. (2021) suggested that for the non-stationary distribution, the shape parameter is constant and the location and scale parameters is described as follows:

$$\mu(t) = \mu_0 + \mu_1 t \quad (3)$$

$$\sigma(t) = \sigma_0 + \sigma_1 t \quad (4)$$

In these equations, t is time and μ_0, μ_1, σ_0, and σ_1 are the regression coefficients.

It should be noted that the shape parameter of a non-stationary Generalized Extreme Value (GEV) distribution is typically assumed to be constant because it reflects the stable tail behavior of extreme events governed by fundamental physical laws. This assumption simplifies modeling and parameter estimation, while empirical

studies have consistently shown that the shape parameter remains stable over time, despite variability in the location and scale parameters (Barbero et al., 2017; De Leo et al., 2021; Luke et al., 2017).

To distinguish between the stationary and nonstationary GEV distribution, the trends in the AMP series should be analyzed. If the trend in the AMP series is significant/ insignificant at 95% confidence level, the GEV distribution is non-stationary/ stationary (Cheng & AghaKouchak, 2015; Ragno et al., 2018). More details on this issue is provided by Srivastava et al. (2021) and Cheng and AghaKouchak (2015). In this study, the Mann-Kendall (MK) trend test (Kendall, 1975; Mann, 1945) were used for trend analysis. The analysis was conducted by the "extRemes2.0" package in R (Gilleland & Katz, 2016).

Mann-Kendall Test for Trend Analysis

The Mann-Kendall (MK) test is commonly used to analyze the trend in hydrological and climatological time series. As a non-parametric test, it can be applied to all kind of probability distributions, meaning that the assumption of normality is not required for the data series. The Mann-Kendall test statistic is defined as follows:

$$z_{MK} = \begin{cases} \frac{S-1}{\sqrt{V(S)}} & if\ S > 0 \\ 0 & if\ S = 0 \\ \frac{S+1}{\sqrt{V(S)}} & if\ S < 0 \end{cases} \quad (5)$$

in which

$$S = \sum_{k=1}^{n-1} \sum_{j=k+1}^{n} \text{sign}(x_j - x_k) \quad (6)$$

$$V(S) = \frac{[n(n-1)(2n+5) - \sum_{i=1}^{m} t_i(t_i-1)(2t_i+5)]}{18} \quad (7)$$

with x_j and x_k the sequential data values, V(S) the variance of S, t_i the number of ties for the i-th value, n the number of data points, and m the number of tied groups. The positive/negative values of z_{MK} represent increasing/decreasing trends in the data series. The significant trends were considered at 90, 95, and 99% confidence interval, i.e., α=0.1, α=0.05, and α=0.01, respectively. The seasonal effect was considered for the series by seasonal decomposition method, but as the seasonal effect was not significant, we did not include it in the manuscript. Seasonal effect may result in significant trend in AMP series, but the trend is not significant in most areas of the basin and thus, the seasonal variability does not affect the trend in AMP.

Results and Discussion

Bias Correction

To extract the gridded data into the stations' locations, the nearest neighbor interpolation method was applied. Then the extracted data was compared to the measured data of the stations. Figures 2-5 illustrate the Q-Q plots comparing the quantiles of the AMP series before and after bias correction for 6-24 hourly precipitation, respectively. Beside Q-Q plot, the evaluation metrics have been also presented in Table 1. According to the

figures and table, in general, the original ERA5 performs better as the precipitation duration increase, however, the bias correction led to better estimation of AMP values, implying that it can remove a significant part of systematic errors (bias) in the ERA5 data (Ombadi et al., 2018). It leads to better estimation of IDF curves as illustrated in figure 6. As shown in this figure, the IDF curves developed by bias corrected ERA5 data is closer to the ones developed by measured data. It should be mentioned that the ERA5 IDF curves is closer to the measured one for the shorter return periods (i.e., 2, 5, and 10 years). Larger discrepancies for the return periods longer than the length of the data record were also reported by (Marra et al., 2017). Their results indicated the uncertainty for the return periods longer than twice the data record length (in this study, 50 and 100 years) might be up to 125%. The figure also shows that the IDF curves is more reliable for the 12, 18, and 24 h durations. Prein et al. (2015) suggested that ERA5 underestimates precipitation intensities at shorter duration because they are likely to be convective in nature and of limited spatial scale. This is important due to the fact that ERA5 does not directly assimilate any rain-gauge data, but it estimates precipitation through modelling process (Courty et al., 2019; Lavers et al., 2022). Marra et al. (2017) indicated that the gridded precipitation products are reliable for IDF development for 12-24 h durations and 2-10 years return periods, which are more applicable for flood management and infrastructures design. Among the study stations, Ilam, Kermanshah, and Khoramabad show the worst performance of the original ERA5. These stations with high elevations (1337, 1318.5, and 1147.8 m, respectively) receive the highest amount of annual precipitation during 1996-2020 (560, 414, and 478 mm, respectively) in the study area. Hence, it indicates that the ERA5 does not perform well for the high-altitude stations with the high amount of precipitation. Such results also found by Kavyani Malayeri et al., (2021).

Additionally, the discrepancy between measured and simulated extreme precipitation might be due to the smoothing effect (Hamm et al., 2020; Herrera et al., 2012; Merino et al., 2021; Reder et al., 2022; Wati et al., 2022). A grid point of the gridded products has the information of an area, according to the spatial resolution (for ERA5 31km×31km). Averaging the information from that area into a point may affect the amount of estimated precipitation.

Elevation-Bias Factor Relationship

Table 2 shows the elevation and the bias factors of the seven stations. According to this table, the correlation between elevation and bias factors are provided as illustrated in figure 7. The figure shows

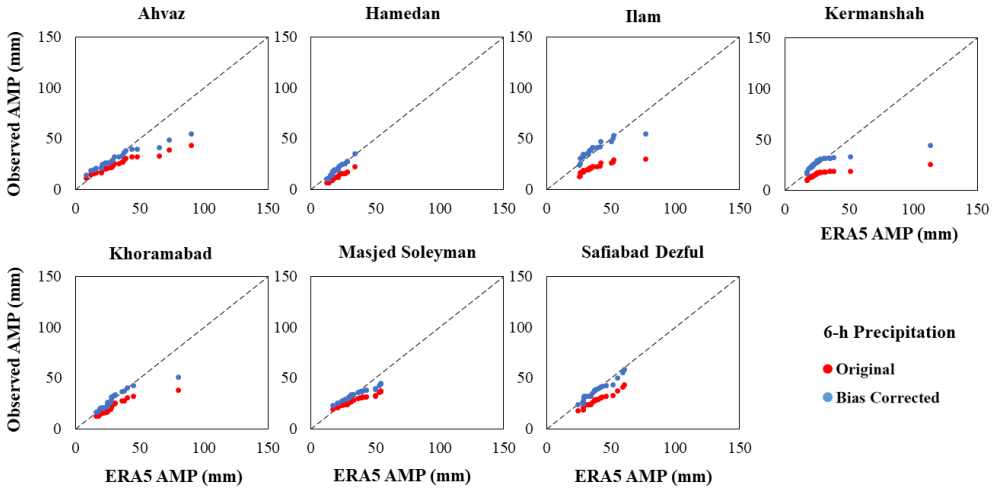

Fig 2. Q-Q plot of observed 6-h AMP vs ERA5 6-h AMP for each station before and after bias correction.

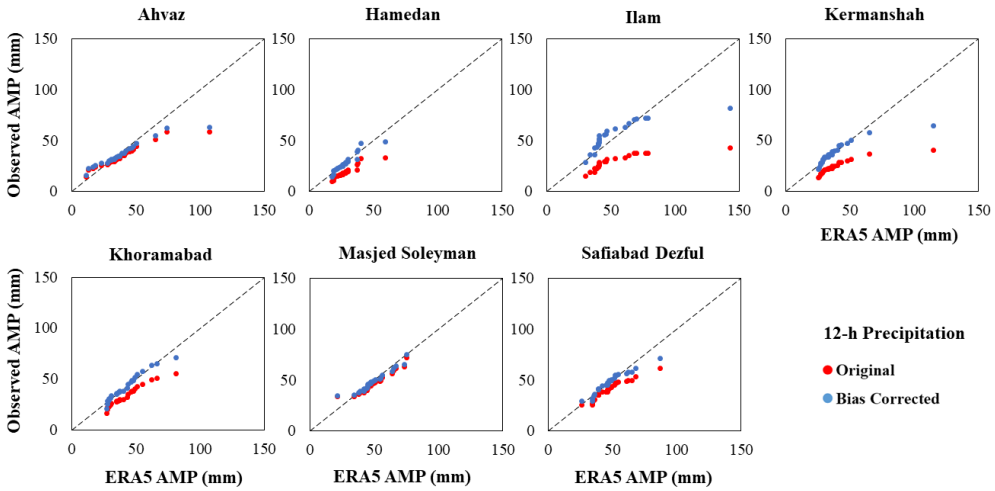

Fig 3. Q-Q plot of observed 12-h AMP vs ERA5 12-h AMP for each station before and after bias correction.

a reasonable correlation as R^2 varies between 0.52 to 0.74 for 6-24 hourly AMP. As indicated by Ombadi et al., (2018), these correlations show that 52 to 74 percent of the variability in the bias is explained linearly by elevation. It can be concluded that the ERA5 precipitation tends to have higher bias in the high-altitude areas. Such results also found by Jiao et al., (2021) and Kavyani Malayeri et al., (2021). The statistical significance of Pearson correlation coefficient has been investigated and presented in Table 2. As shown in Table 2, the Pearson correlation is significant at 95% confidence level (P_value<0.05). Hence, the elevation-bias factor relationship can be applied for all grid points of the basin.

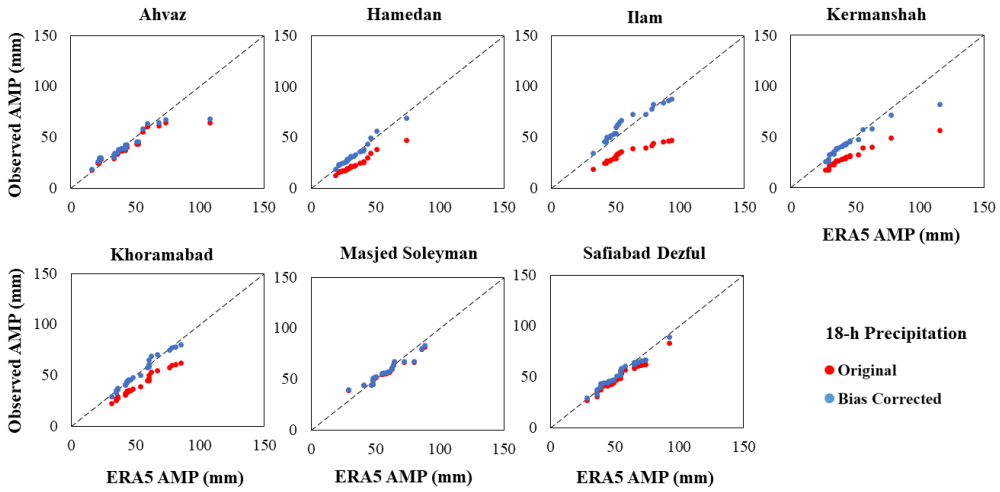

Fig 4. Q-Q plot of observed 18-h AMP vs ERA5 18-h AMP for each station before and after bias correction.

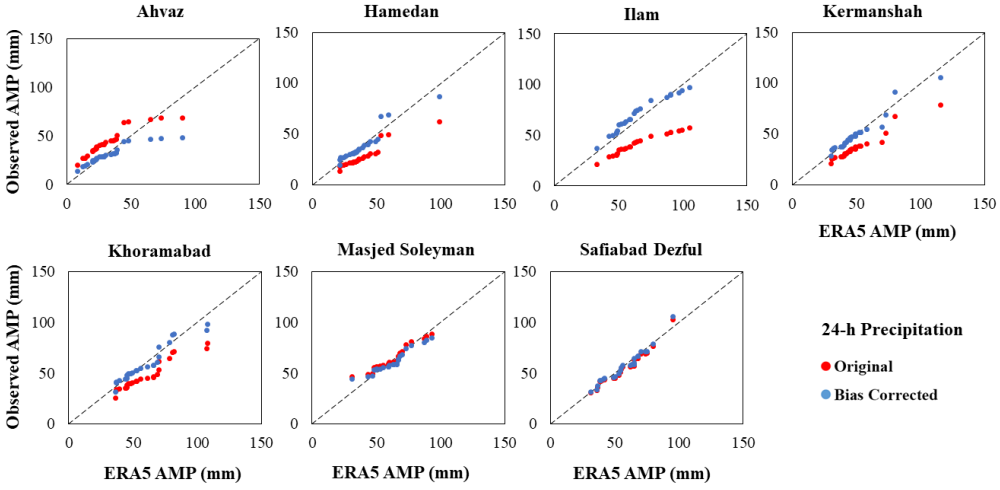

Fig 5. Q-Q plot of observed 24-h AMP vs ERA5 24-h AMP for each station before and after bias correction.

Trend Analysis

As indicated earlier, to choose between the stationary or non-stationary GEV distribution function, it is needed to analyze the trends in the AMP series for each grid point. Figure 8 shows the spatial distribution of the across the KRB. As seen in the figure, some limited grid points in the northeast show significant trends in the 6-h and 12-h AMP series at 95% confidence level. For these grid points the non-stationary GEV distribution function should be fitted to the AMP series. For the other grid points the stationary GEV was applied.

IDF development for the KRB

Spatial distribution of rainfall intensity (mm/h) for different return periods has been illustrated in figures 9-12 for

Table 1- Evaluation metrics for 6-h, 12-h, 18-h, and 24-h AMP series before and after bias correction.

Station	Evaluation Metric	6-h		12-h		18-h		24-h	
		Original	Bias corrected	Original	Bias corrected	Original	Bias corrected	Original	Bias corrected
Ahvaz	MAE	9.0	5.9	6.6	5.1	5.2	4.4	13.1	6.4
	RMSE	14.3	10.3	11.2	9.9	9.7	8.8	13.7	11.0
Hamedan	MAE	7.1	0.9	8.8	1.9	10.5	1.5	10.9	3.4
	RMSE	7.3	1.1	9.7	3.0	11.4	2.1	12.7	5.0
Ilam	MAE	20.3	9.7	30.2	14.6	34.8	15.2	35.0	15.6
	RMSE	34.8	25.8	48.9	33.9	54.7	36.3	54.2	35.3
Kermanshah	MAE	12.8	6.4	14.7	4.2	14.4	3.3	13.1	2.7
	RMSE	20.6	14.5	19.5	10.4	17.6	7.0	14.7	4.4
Khoramabad	MAE	7.4	2.5	8.9	2.0	11.8	1.8	11.8	4.5
	RMSE	10.3	5.9	9.8	2.8	12.5	2.5	13.8	5.6
Masjed Soleyman	MAE	6.9	4.1	3.4	2.1	3.1	3.0	3.9	4.0
	RMSE	8.8	5.2	4.5	3.6	4.3	4.2	5.2	4.9
Safiabad Dezful	MAE	9.8	1.8	6.9	3.1	4.0	2.5	3.3	3.0
	RMSE	10.6	2.3	8.6	4.2	5.1	3.0	4.0	3.7

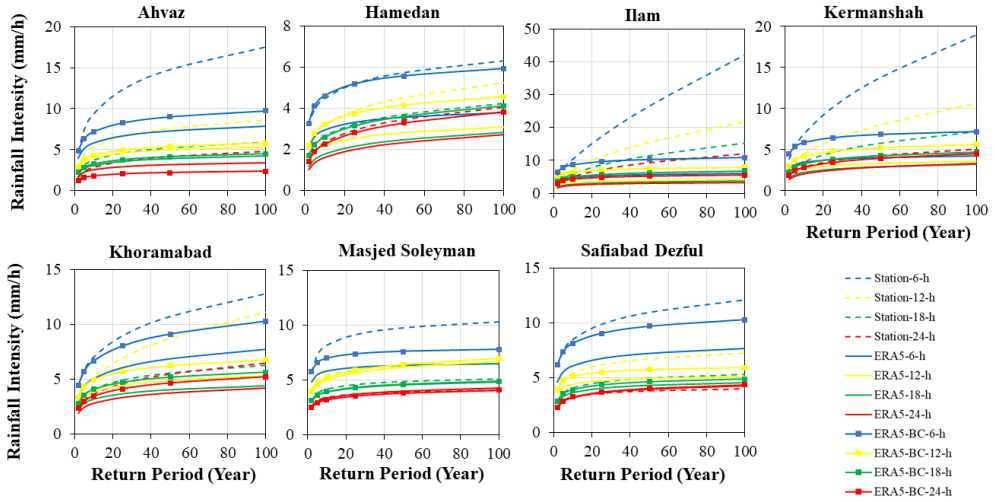

Fig 6. IDF curves developed by measured, ERA5, and ERA5 bias corrected AMP series. The term "BC" indicates the Bias Corrected ERA5.

Table 2- Relationship between elevation and bias factor for each station and precipitation duration.

Station	Elevation (m)	Bias Factor			
		6-h	12-h	18-h	24-h
Ahvaz	22.5	1.25	1.07	1.05	0.69
Hamedan	1740.8	1.56	1.47	1.45	1.40
Ilam	1337	1.82	1.89	1.85	1.70
Kermanshah	1318.5	1.70	1.28	1.45	1.35
Khorramabad	1147.8	1.33	1.58	1.29	1.24
Masjed Soleyman	320.5	1.20	1.04	1.01	0.96
Safiabad Dezful	82.9	1.34	1.16	1.07	1.03

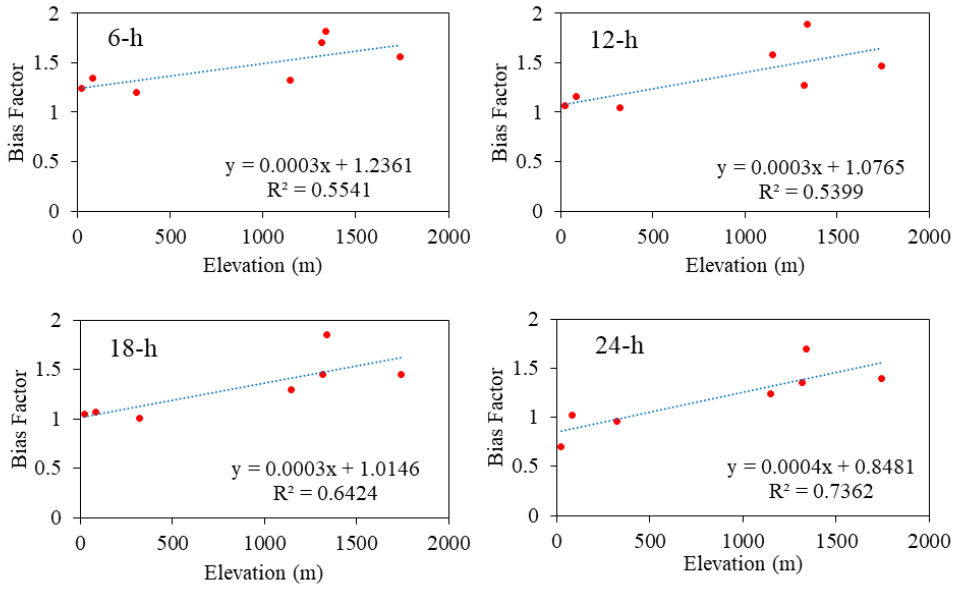

Fig 7. Correlation between elevation and bias factor for different precipitation durations.

Table 2- Statistical significance test of the Pearson correlation between elevation and Bias factor.

Station	Elevation (m)	Bias Factor			
		6-h	12-h	18-h	24-h
Ahvaz	22.5	1.25	1.07	1.05	0.69
Hamedan	1740.8	1.56	1.47	1.45	1.40
Ilam	1337	1.82	1.89	1.85	1.70
Kermanshah	1318.5	1.70	1.28	1.45	1.35
Khorramabad	1147.8	1.33	1.58	1.29	1.24
Masjed Soleyman	320.5	1.20	1.04	1.01	0.96
Safiabad Dezful	82.9	1.34	1.16	1.07	1.03

*: Significant at 95% confidence level.

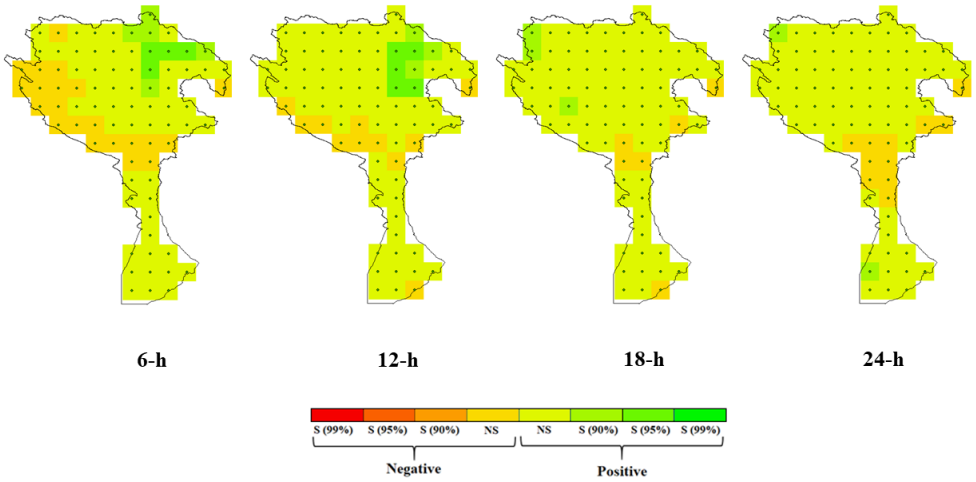

Fig 8. Spatial distribution of the Z_{MK} and significance of the trends in KRB.

6-24 hourly precipitation, respectively. According to these figures, the rainfall intensity has the similar patterns for each duration and return period. The rainfall is more intense in the high-altitude regions of the KRB. Based on these figures, the intensity, duration and return period for each grid point can be acquired. Marra et al. (2017) pointed out that the distance from the rain gauge location reduces the repre-sentativeness of the gauge-acquired IDF curves. Thus, for constructing the infrastructures, the policy makers can use the information of the closer grid points to the location of the infrastructures rather than that of the distant rain gauges.

Spatial analysis of Figures 9 to 12 indicates that the highest rainfall intensities for various durations and return periods are concentrated in the eastern, southeastern, and central parts of the basin, corresponding to the Kashkan sub-basin. This sub-basin, identified by Azadi et al. (2020) as having the highest flood potential in the KRB, underscores the critical importance of accurate IDF estimates in these areas due to their heightened sensitivity to flooding. The comprehensive IDF curves of the KRB is presented in figure 13. As seen in the figure, the curves of each return period are relatively equally spaced. It means the difference between rainfall intensities for different return periods is constant during all rainfall durations. Wambura (2024) believed that this constant difference might be due to using the same probability distribution function for all series, while the series might be fitted with different functions. Since the curves are provided by the bias corrected precipitation data of 82 points, it may be more reliable than the curves acquired from only seven stations within or around the KRB. Moreover, the IDF curves can be developed for each grid point, as it can be more helpful for infrastructures design in each location across the basin.

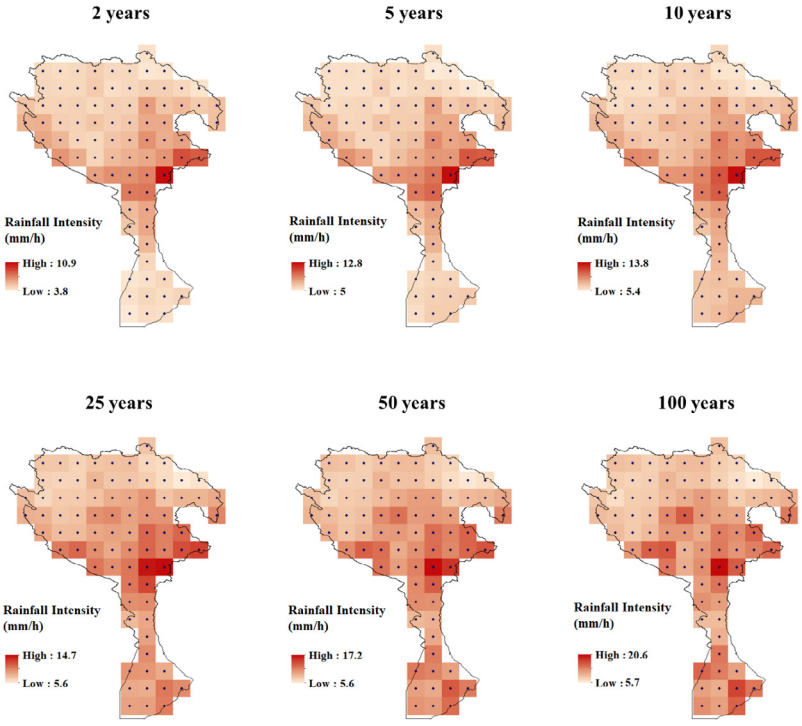

Fig 9. Spatial distribution of 6-h rainfall intensity for different return periods over the KRB.

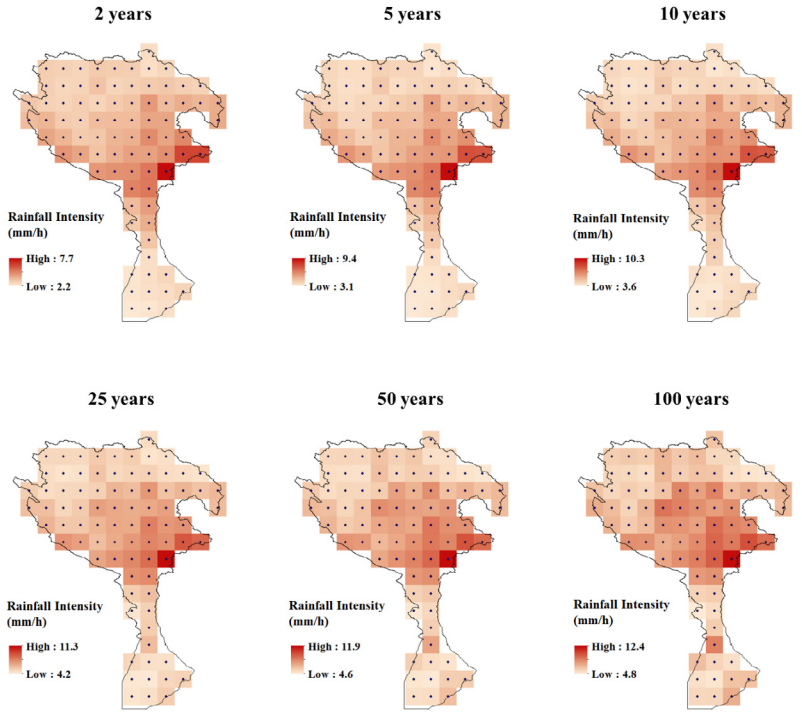

Fig 10. Spatial distribution of 12-h rainfall intensity for different return periods over the KRB.

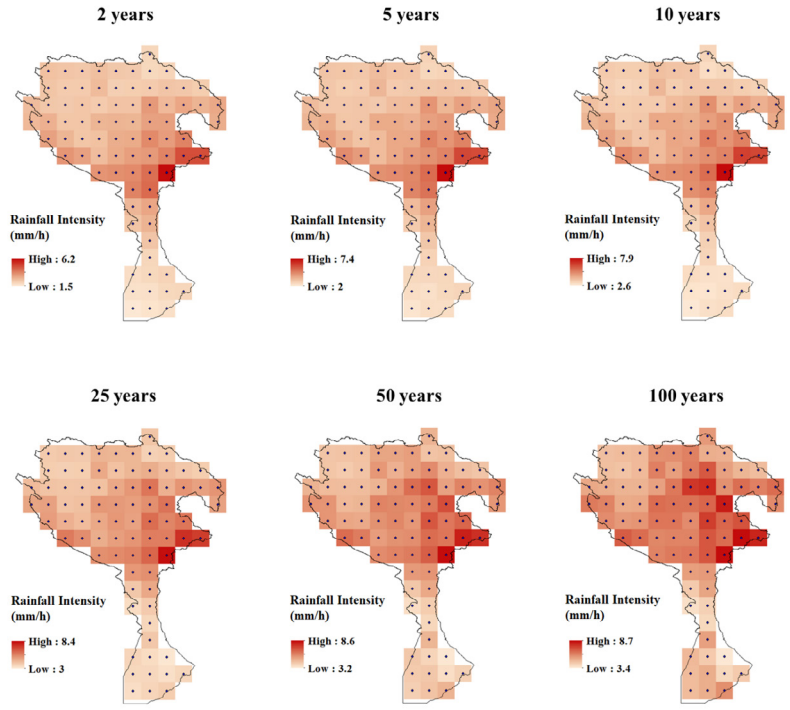

Fig 11. Spatial distribution of 18-h rainfall intensity for different return periods over the KRB.

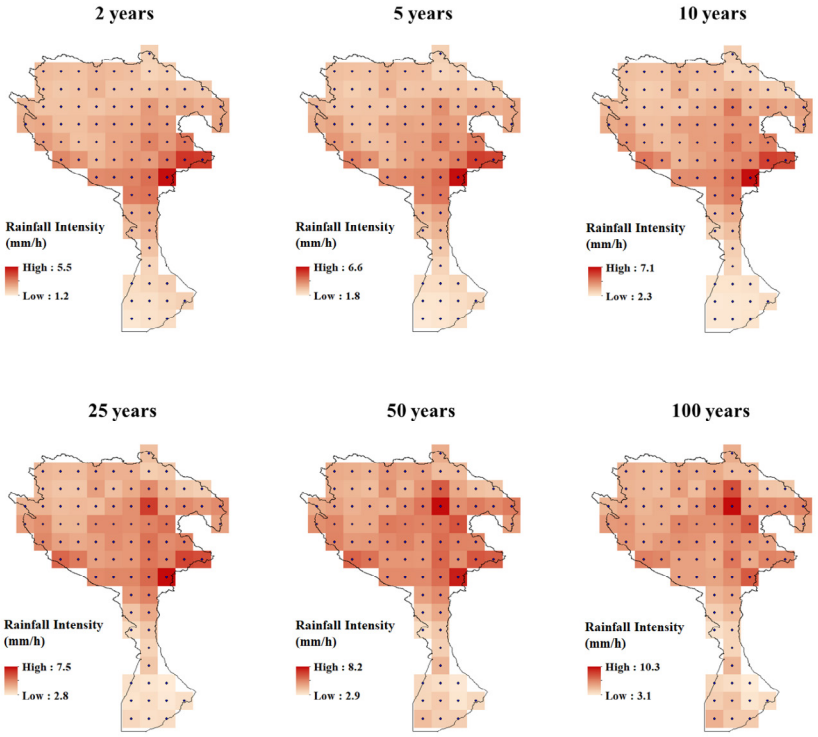

Fig 12. Spatial distribution of 24-h rainfall intensity for different return periods over the KRB.

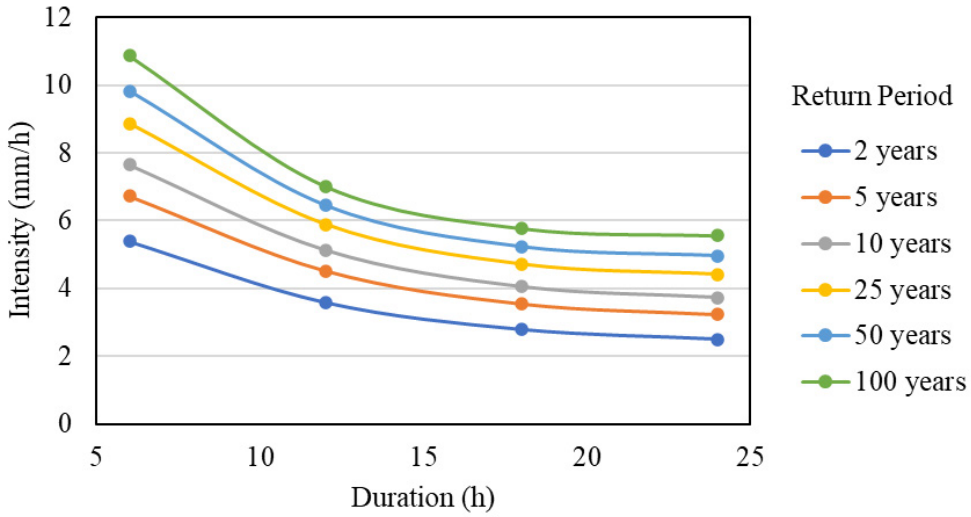

Fig 13. IDF curve of the KRB developed by the ERA5 database.

Conclusion

This study developed Intensity-Duration-Frequency (IDF) curves for the Karkheh River Basin (KRB) using ERA5 reanalysis data, supported by bias correction with observed precipitation data. The analysis revealed that bias correction significantly improves ERA5 estimates, particularly for high-altitude regions prone to systematic errors. The relationship between bias factors and elevation was effectively utilized to extend bias correction across the basin. Furthermore, the use of the Generalized Extreme Value (GEV) distribution, incorporating both stationary and non-stationary trends, provided a robust framework for modeling extreme precipitation.

While this study demonstrates the potential of ERA5 data to enhance hydrological analyses, it acknowledges limitations such as the short observational record (25 years), which reduces the accuracy of rainfall intensity estimates for longer return periods e.g., 50 and 100 years. Future research should address this limitation and uncertainties by extending data records, refining bias correction methods, exploring alternative datasets, and evaluating uncertainties related to interpolation techniques, parameter estimation, and distribution fitting.

By providing a framework for utilizing ERA5 reanalysis data for spatially comprehensive IDF curve development, this study contributes to more reliable flood mitigation strategies, climate-resilient infrastructure planning, and improved adaptation to the impact of climate change particularly in data-scarce regions. Policymakers and engineers are encouraged to utilize these updated IDF curves to inform decision-making processes that enhance resilience against extreme weather events.

References

Ashraf Vaghefi, S., Mousavi, S. J., Abbaspour, K. C., Srinivasan, R., & Yang, H. (2014). Analyses of the impact of climate change on water resources components, drought and wheat yield in semiarid regions: Karkheh River Basin in Iran. Hydrological Processes, 28(4), 2018–2032. https://doi.org/10.1002/hyp.9747

Azadi, F., Sadough, S. H., Ghahroudi, M., & Shahabi, H. (2020). Zoning of flood risk in kashkan river basin using two models WOE and EBF. Journal of Geography and Environmental Hazards, 9(1), 45–60. [In Persian]. https://doi.org/ 10.22067/GEO.V9I1.83090.

Barbero, R., Fowler, H. J., Lenderink, G., & Blenkinsop, S. (2017). Is the intensification of precipitation extremes with global warming better detected at hourly than daily resolutions? Geophysical Research Letters, 44(2), 974–983. https://doi.org/10.1002/2016GL071917

Cheng, L., & AghaKouchak, A. (2015). Nonstationary precipitation intensity-duration-frequency curves for infrastructure design in a changing climate. Scientific Reports, 4(1), 7093. https://doi.org/10.1038/srep07093

Coles, S., Bawa, J., Trenner, L., & Dorazio, P. (2001). An introduction to statistical modeling of extreme values. Springer London. https://doi.org/10.1007/978-1-4471-3675-0

Courty, L. G., Wilby, R. L., Hillier, J. K., & Slater, L. J. (2019). Intensity-duration-frequency curves at the global scale. Environmental Research Letters, 14(8), 084045. https://doi.org/10.1088/1748-9326/ab370a

Crévolin, V., Hassanzadeh, E., & Bourdeau-Goulet, S.-C. (2023). Updating the intensity-duration-frequency curves in major Canadian cities under changing climate using CMIP5 and CMIP6 model projections. Sustainable Cities and Society, 92(September 2022), 104473. https://doi.org/10.1016/j.scs.2023.104473

Davtalab, R., Mirchi, A., Khatami, S., Gyawali, R., Massah, A., Farajzadeh, M., & Madani, K. (2017). Improving continuous hydrologic modeling of data-poor river basins using hydrologic engineering center's hydrologic modeling system: case study of karkheh river Basin. Journal of Hydrologic Engineering, 22(8). https://doi.org/10.1061/(ASCE)HE.1943-5584.0001525

De Leo, F., Besio, G., Briganti, R., & Vanem, E. (2021). Non-stationary extreme value analysis of sea states based on linear trends. Analysis of annual maxima series of significant wave height and peak period in the Mediterranean Sea. Coastal Engineering, 167, 103896. https://doi.org/10.1016/j.coastaleng.2021.103896

Frank, C. W., Wahl, S., Keller, J. D., Pospichal, B., Hense, A., & Crewell, S. (2018). Bias correction of a novel European reanalysis data set for solar energy applications. Solar Energy, 164, 12–24. https://doi.org/10.1016/j.solener.2018.02.012

Garibay, V. M., Gitau, M. W., Kiggundu, N., Moriasi, D., & Mishili, F. (2021). Evaluation of reanalysis precipitation data and potential bias correction methods for use in data-scarce areas. Water Resources Management, 35(5), 1587–1602. https://doi.org/10.1007/s11269-021-02804-8

Gilleland, E., & Katz, R. W. (2016). ExtRemes 2.0: an extreme value analysis package in R. Journal of Statistical Software, 72(8), 1–39. https://doi.org/10.18637/jss.v072.i08

Guhathakurta, P., Sreejith, O. P., & Menon, P. A. (2011). Impact of climate change on extreme rainfall events and flood risk in India. Journal

of Earth System Science, 120(3), 359–373.
Hersbach, H., Bell, B., Berrisford, P., Biavati, G., Horányi, A., Muñoz Sabater, J., Nicolas, J., Peubey, C., Radu, R., Rozum, I., Schepers, D., Simmons, A., Soci, C., Dee, D., & Thépaut, J.-N. (2023). ERA5 hourly data on single levels from 1940 to present. Copernicus Climate Change Service (C3S) Climate Data Store (CDS). https://doi.org/10.24381/cds.adbb2d47
Hersbach, H., Bell, B., Berrisford, P., Hirahara, S., Horányi, A., Muñoz-Sabater, J., Nicolas, J., Peubey, C., Radu, R., Schepers, D., Simmons, A., Soci, C., Abdalla, S., Abellan, X., Balsamo, G., Bechtold, P., Biavati, G., Bidlot, J., Bonavita, M., … Thépaut, J. (2020). The ERA5 global reanalysis. Quarterly Journal of the Royal Meteorological Society, 146(730), 1999–2049. https://doi.org/10.1002/qj.3803
Hilbe, J. M., & Robinson, A. P. (2013). Methods of statistical model estimation. CRC Press.
IPCC. (2021). Technical summary. contribution of working group I to the sixth assessment report of the Intergovernmental panel on climate change. In climate change 2021: The Physical Science Basis.
Jalbert, J., Genest, C., & Perreault, L. (2022). Interpolation of precipitation extremes on a large domain toward IDF curve construction at unmonitored locations. Journal of Agricultural, Biological and Environmental Statistics, 27(3), 461–486. https://doi.org/10.1007/s13253-022-00491-5
Jiao, D., Xu, N., Yang, F., & Xu, K. (2021). Evaluation of spatial-temporal variation performance of ERA5 precipitation data in China. Scientific Reports, 11(1), 17956. https://doi.org/10.1038/s41598-021-97432-y
Kavyani Malayeri, A., Saghafian, B., & Raziei, T. (2021). Performance evaluation of ERA5 precipitation estimates across Iran. Arabian Journal of Geosciences, 14(23), 2676. https://doi.org/10.1007/s12517-021-09079-8
Kendall, M. G. (1975). Rank Correlation Methods. Charles Griffin.
Koutsoyiannis, D., Kozonis, D., & Manetas, A. (1998). A mathematical framework for studying rainfall intensity-duration-frequency relationships. Journal of Hydrology, 206(1–2), 118–135. https://doi.org/10.1016/S0022-1694(98)00097-3
Lavers, D. A., Simmons, A., Vamborg, F., & Rodwell, M. J. (2022). An evaluation of ERA5 precipitation for climate monitoring. Quarterly Journal of the Royal Meteorological Society, 148(748), 3152–3165. https://doi.org/10.1002/qj.4351
Luke, A., Vrugt, J. A., AghaKouchak, A., Matthew, R., & Sanders, B. F. (2017). Predicting nonstationary flood frequencies: Evidence supports an updated stationarity thesis in the <scp>U</scp> nited <scp>S</scp> tates. Water Resources Research, 53(7), 5469–5494. https://doi.org/10.1002/2016WR019676
Mann, H. B. (1945). Nonparametric Tests Against Trend. Econometrica, 13(3), 245–259.
Marra, F., Morin, E., Peleg, N., Mei, Y., & Anagnostou, E. N. (2017). Intensity–duration–frequency curves from remote sensing rainfall estimates: comparing satellite and weather radar over the eastern Mediterranean. Hydrology and Earth System Sciences, 21(5), 2389–2404. https://doi.org/10.5194/hess-21-2389-2017
Marra, F., Nikolopoulos, E. I., Anagnostou, E. N., Bárdossy, A., & Morin, E. (2019). Precipitation frequency analysis from remotely sensed datasets: A focused review. Journal of Hydrology, 574, 699–705. https://doi.

org/10.1016/j.jhydrol.2019.04.081

Mianabadi, A. (2023). Evaluation of long-term satellite-based precipitation products for developing intensity-frequency (IF) curves of daily precipitation. Atmospheric Research, 286(February), 106667. https://doi.org/10.1016/j.atmosres.2023.106667

Noor, M., Ismail, T., Shahid, S., Asaduzzaman, M., & Dewan, A. (2021). Evaluating intensity-duration-frequency (IDF) curves of satellite-based precipitation datasets in Peninsular Malaysia. Atmospheric Research, 248, 105203. https://doi.org/10.1016/j.atmosres.2020.105203

Ombadi, M., Nguyen, P., Sorooshian, S., & Hsu, K. (2018). Developing intensity-duration-frequency (IDF) curves from satellite-based precipitation: Methodology and Evaluation. Water Resources Research, 54(10), 7752–7766. https://doi.org/10.1029/2018WR022929

Parker, W. S. (2016). Reanalyses and Observations: What's the difference? Bulletin of the American Meteorological Society, 97(9), 1565–1572. https://doi.org/10.1175/BAMS-D-14-00226.1

Prein, A. F., Langhans, W., Fosser, G., Ferrone, A., Ban, N., Goergen, K., Keller, M., Tölle, M., Gutjahr, O., Feser, F., Brisson, E., Kollet, S., Schmidli, J., van Lipzig, N. P. M., & Leung, R. (2015). A review on regional convection-permitting climate modeling: Demonstrations, prospects, and challenges. Reviews of Geophysics, 53(2), 323–361. https://doi.org/10.1002/2014RG000475

Probst, E., & Mauser, W. (2022). Evaluation of ERA5 and WFDE5 forcing data for hydrological modelling and the impact of bias correction with regional climatologies: A case study in the Danube River Basin. Journal of Hydrology: Regional Studies, 40, 101023. https://doi.org/10.1016/j.ejrh.2022.101023

Ragno, E., AghaKouchak, A., Love, C. A., Cheng, L., Vahedifard, F., & Lima, C. H. R. (2018). Quantifying changes in future intensity-duration-frequency curves using multimodel ensemble simulations. Water Resources Research, 54(3), 1751–1764. https://doi.org/10.1002/2017WR021975

Shrestha, A., Babel, M., Weesakul, S., & Vojinovic, Z. (2017). Developing intensity–duration–frequency (IDF) curves under climate change uncertainty: The Case of Bangkok, Thailand. Water, 9(2), 1–22. https://doi.org/10.3390/w9020145

Srivastava, A. K., Grotjahn, R., Ullrich, P. A., & Sadegh, M. (2021). Pooling data improves multimodel IDF estimates over median-based IDF estimates: Analysis over the Susquehanna and Florida. Journal of Hydrometeorology, 22(4), 971–995. https://doi.org/10.1175/JHM-D-20-0180.1

Tarek, M., Brissette, F. P., & Arsenault, R. (2020). Evaluation of the ERA5 reanalysis as a potential reference dataset for hydrological modelling over North America. Hydrology and Earth System Sciences, 24(5), 2527–2544. https://doi.org/10.5194/hess-24-2527-2020

Venkatesh, K., Maheswaran, R., & Devacharan, J. (2022). Framework for developing IDF curves using satellite precipitation: a case study using GPM-IMERG V6 data. Earth Science Informatics, 15(1), 671–687. https://doi.org/10.1007/s12145-021-00708-0

Wambura, F. J. (2024). Using reanalysis precipitation data for developing intensity-duration-frequency curves in a poorly gauged city. Journal of Hydrology: Regional Studies, 56, 102005. https://doi.org/10.1016/j.

ejrh.2024.102005

Zambrano-Bigiarini, M., Soto, C., & Tolorza, V. (2024). Spatially-distributed intensity-duration-frequency (IDF) curves for chile using sub-daily gridded datasets. EGU general assembly 2024, Vienna, Austria, 14–19 Apr 2024. https://doi.org/10.5194/egusphere-egu24-21043

Original Article

Journal of Drought and Climate change Research (JDCR)

Winter 2025, Vol. 2, No. 8, pp 141-160

10.22077/jdcr.2025.8683.1102

Evaluating Hybrid Models and Google Earth Engine for Predicting Climate Change Impacts on Runoff in the Kasilian Catchment, Northern Iran

Farhad Hajian[1*], Elham Yousefi[2], Hossein Monshizadeh Naeen[3]

1- Department of Civil Engineering, Neyshabur Branch, Islamic Azad University, Neyshabur, Iran.
2- Department of Environment, Faculty of Natural Resources and Environment, University of Birjand, Iran
3- Department of Computer Engineering, Neyshabur Branch, Islamic Azad University, Neyshabur, Iran..
*** corresponding author: F.hajian@yahoo.com**

Keywords:
Remote sensing, Hybrid models, Google earth engine (GEE), Erosion, Sediment yield.

Received:
31 Dec 2024

Revised:
24 Jan 2025

Accepted:
25 Jan 2025

Abstrsct

This study investigates the effect of climate change on annual rainfall and runoff of Kasilian catchment through two distinct approaches. Firstly, it utilizes hybrid models by integrating the Hydrologic Engineering Center's Hydrologic Modeling System (HEC-HMS) with Artificial Neural Networks (ANN), Support Vector Machines (SVM), Adaptive Neuro-Fuzzy Inference System (ANFIS), and Gene Expression Programming (GEP) separately, as well as employing the Long Ashton Research Station Weather Generator (LARS-WG). Secondly, it employs Google Earth Engine (GEE) to analyze changes in annual rainfall and runoff for the observed period, compensating for incomplete data from hydrometric and climatological stations. The results demonstrate that under the SSP585 scenario, from various climate models in LARS WG and when employing hybrid models, the median annual rainfall is projected to increase in the future compared to the base period, while the median annual runoff is expected to decrease due to rising temperatures and increased evapotranspiration. Consistent with these projections, GEE data from 1981 to 2023 also indicates an increase in annual rainfall and a decrease in annual runoff. Additionally, there is a reduction in annual erosion and sedimentation rates, attributed to the reduced capacity of runoff to transport sediment. These

How to cite this article:
Hajian, F., Yousefi, E. & Monshizadeh Naeen, H. (2024). Evaluating Hybrid Models and Google Earth Engine for Predicting Climate Change Impacts on Runoff in the Kasilian Catchment, Northern Iran. *Journal of Drought and Climate change Research* (JDCR), 2(8), 141-160. 10.22077/jdcr.2025.8683.1102

findings highlight the potential for more extreme rainfall events, increased annual precipitation, and a subsequent decrease in annual runoff and sediment load in the Kasilian catchment, providing essential perspectives for managing water resources.

Introduction

The primary sources of uncertainty in climate change impact studies stem from the structure of Global Climate Models (GCMs) or climate data, the structure of hydrological models, and the parameters used within hydrological models. Different climate models produce varying rainfall patterns, resulting in different runoff magnitudes (Hajian, 2013). For example, Abbaspour et al. (2009) found increased precipitation in northern Iran up to 40% for future periods, while Babaeian et al. (2007) observed a 2% decrease in rainfall for Mazandaran Province for 2010-2039 compared to 1976-2005. The variability in rainfall predictions highlights the necessity of using multiple climate models in climate change impact studies. Many studies have traditionally relied on a single GCM, underscoring the need for diverse model applications to better understand potential impacts on water resources.

Bae et al. (2011) examined uncertainties in climate change impact studies in the Chungju Dam Catchment, South Korea, using three semi-distributed hydrological models (PRMS, SLURP, and SWAT) with multiple potential evapotranspiration methods, and 39 climate change scenarios across two future periods (2011-2040 and 2071-2100). The models performed identically for calibration and validation with observed data, but showed varying runoff results with GCM outputs. Runoff changes were significant during winter (dry period) and minor in other seasons, influenced by model structure, GCM type, and evapotranspiration methods. This highlights the need for careful selection of hydrological models, GCMs, and parameterization methods in climate impact studies, as these choices significantly affect the results.

Shifteh Some'e et al. (2012) analyzed the percent change of annual and seasonal rainfall data for 28 synoptic stations of Iran over the period 1967-2006. The annual rainfall increased by 0-10%, spring rainfall increased by 10%, summer rainfall increased by 0-30%, autumn rainfall increased by 0-10%, and a noticeable decrease of 10-20% in the winter rainfall was observed over the period 1967-2006, for northern parts (southern Caspian Sea coastal area).

The following studies collectively demonstrate the effectiveness of various advanced modeling approaches in accurately predicting and simulating hydrological processes across different regions. One study compared the performance of Gene Expression

Programming (GEP), Adaptive Neuro-Fuzzy Inference System (ANFIS), and Support Vector Machine (SVM) models in simulating rainfall using historical data from the Kiyav-Chay River basin in Iran. The GEP model outperformed the ANFIS and SVM models, achieving the highest R^2 value and the lowest RMSE and MAE values, concluding that GEP is a reliable and accurate method for rainfall simulation in this region (Tabatabaei et al., 2021). Another study reviewed LS-SVM, GEP, and ANFIS-PSO models for simulating rainfall-runoff in the Halil River, determining that the ANFIS-PSO model outperformed others with the lowest RMSE (0.35) and highest R^2 (0.92) values (Kavoosi & Khozeymehnezhad 2021). Different studies in the Anandpur and Champua catchments of the Baitarani catchment, India, evaluated ANN, ANFIS, and SRC models, with ANN and ANFIS models performing best for sediment load simulation (Kumaret al., 2019).

A study introduced a hybrid model named Ia-LSTM, which combines the physical-based HEC-HMS model with the data-driven LSTM model to optimize the "initial loss" (Ia) and accurately capture the rainfall-runoff relationship. This model was tested in the Yufuhe basin in Jinan City, Shandong province, China. The Ia-LSTM model consistently demonstrated superior performance compared to the individual HEC-HMS and LSTM models. It achieved impressive average Nash-Sutcliffe Efficiency (NSE) values of 0.873 and 0.829, and average R^2 values of 0.916 and 0.870 during calibration and validation, respectively (Zhang et al., 2022).

Asadi and Santos (2022) created a hybrid model that integrates artificial intelligence (ANN) with the SWAT semi-distributed hydrological model, achieving high accuracy with NSE values of 0.85 for calibration and 0.82 for validation. This research was conducted in the Upper Sabarmati River Basin in Gujarat, India. In another study, Gebremichael and Hailu (2024) compared the HEC-HMS model with machine learning models (SVM, ANN, and ANFIS) for rainfall-runoff prediction, discovering that the ANFIS model outperformed the others with NSE values of 0.88 for calibration and 0.85 for validation. This study took place in the Rappahannock River basin near Fredericksburg, Virginia, USA.

This study seeks to improve the performance of the HEC-HMS model by integrating it with Artificial Neural Networks (ANN), Gene Expression Programming (GEP), Support Vector Machines (SVM), and Adaptive Neuro-Fuzzy Inference Systems (ANFIS). These integrated approaches, collectively known as hybrid models, will then be applied to climate change studies. The objectives of this study are:

1. To evaluate the accuracy of these

hybrid models in simulating rainfall-runoff processes in the Kasilian Catchment.

2. To evaluate the effect of climate change on runoff in the Kasilian Catchment by applying these hybrid models. While the integration of conceptual model like HEC-HMS with machine learning models are commonly used to improve model performance, limited research has explored their application in assessing climate change effects on water resources.
3. To validate the future projections generated using the hybrid and LARS-WG models with observational data from Google Earth Engine (GEE), considering the trend of change. This additional validation step confirmed the future projections to a significant extent by analyzing changes in annual rainfall, annual runoff, and annual sediment load based on observed data.

Material and Methods

Study area

The Kasilian Watershed, situated in Mazandaran Province in northern Iran, spans coordinates 53°18′ to 53°30′E and 35°58′ to 36°07′N (Figure 1). Covering an area of 65.7 km² above the Valikbon hydrometric station, the watershed flows northward into the Caspian Sea with its longest flow path extending 17.8 kilometers. Approximately 80% of the area is forested, while the lower regions have been cleared for agriculture. The geology consists of shale, sandstone, marl, and siltstone (Hajian, 2013). The Sangdeh meteorological station records daily rainfall and temperature, and the Valikbon station monitors river discharge (Figure 1). From 1977 to 1996, the average annual rainfall was about 756 mm, and the average annual runoff from 1980 to 1996 was 229 mm (Hajian, 2013).

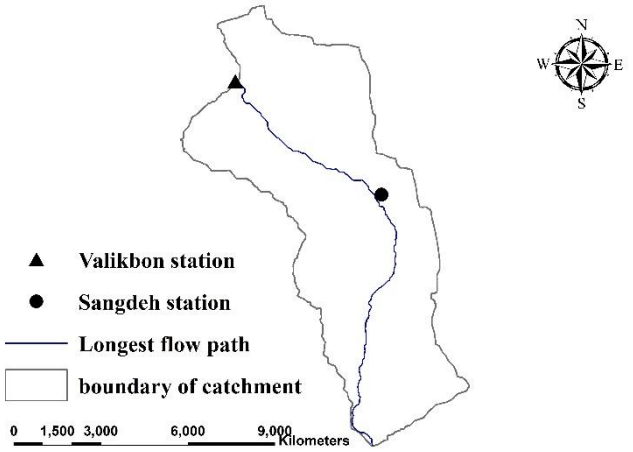

Fig 1. Study area.

Modeling the Rainfall-Runoff Process with HEC-HMS

In this study, the HEC-HMS model, developed by the US Army Corps of Engineers, was used to evaluate hydrological processes within the Kasilian Catchment. Due to limited data availability, the Thornthwaite method was employed to estimate potential evapotranspiration (PET) using temperature data. The study found that uncertainties in PET had a smaller impact on runoff simulations compared to variations arising from different types of General Circulation Models (GCM) or future climate scenarios. The HEC-HMS model, which utilizes 23 parameters, was optimized using the Nelder-Mead method. Initial parameter values were derived from geological, soil, and land use maps, as well as existing literature (Hajian, 2013). The calibration-validation process indicated poor performance, with Nash and Sutcliffe coefficients of -0.293 during the calibration period (September 23, 2007, to March 20, 2018) and 0.060 during the validation period (September 23, 2018, to September 22, 2021). The inadequate performance of HEC-HMS in estimating seasonal runoff volumes is attributed to seasonal variations in parameter values such as maximum infiltration rate and surface storage. To achieve accurate estimations, seasonal optimization might be required; however, the lumped HEC-HMS model cannot accommodate such adjustments, thus limiting its accuracy in simulating seasonal rainfall-runoff dynamics.

Hybrid modelling approach (Integrating machine learning (ML) with HEC-HMS conceptual model)

Improving the precision of runoff predictions can be achieved by combining conceptual hydrological models with machine learning (ML) techniques. Methods such as artificial neural networks (ANN), gene expression programming (GEP), Support Vector Machines (SVM), and the Adaptive Neuro-Fuzzy Inference System (ANFIS) offer powerful tools for refining forecast accuracy. Incorporating streamflow estimates from conceptual models as input for ML algorithms greatly enhances runoff forecasting precision. Research by Farfan et al., (2020) and Hitokoto & Sakuraba (2020) has demonstrated the effectiveness of this method, leading to significantly improved streamflow predictions. These findings highlight the advantages of integrating conceptual models with ML techniques for more accurate and dependable runoff estimations. These studies underscore the potential of combining conceptual models with ML techniques for more precise and reliable runoff predictions. The ML methods use discharge estimates from HEC-HMS (Q_t), along with estimates from one-day (Q_{t-1}) and two-day (Q_{t-2}) lags, representing previous days' discharge. As

highlighted in Table 1, the integration of SVM with HEC-HMS outperformed other hybrid models and the standalone HEC-HMS model. Nonetheless, the impact of climate change on runoff was examined across all hybrid models, regardless of their individual performance.

Table 1. The performance evaluation of different hybrid models.

Integration HEC HMS & ANN (3,3,1) with Tansig activation function		**Integration HEC HMS & GEP**		**Integration HEC HMS & SVM with RBF kernel and gamma=10 and σ^2 = 0.2**		**Integration HEC HMS & ANFIS**	
NSE train	NSE test	NSE train	NSE test	NSE train	NSE test	NSE train	NSE test
0.253	0.11	0.261	0.153	0.514	0.072	0.16	0.146

Artificial Neural Network (ANN)

Complex biological systems, with their intricate networks of interconnected processing units, demonstrate remarkable capabilities in information processing and pattern recognition. Individual processing units, while limited in their computational capacity, collectively engage in sophisticated tasks. These systems learn from their environment and establish connections that facilitate information flow through input pathways, processing stages, and output pathways. Artificial Neural Networks (ANNs) are computational models inspired by the architecture of such biological systems. They mimic the interconnected network of processing units for a range of tasks, including classification, pattern recognition, and regression. In ANNs, inputs are analogous to the input pathways, connection weights to the strength of inter-unit connections, activation functions to the influence of the processing units, and outputs to the output pathways.

ANNs typically comprise interconnected layers of artificial neurons. A crucial feature is the inclusion of hidden layers positioned between the input and output layers. These hidden layers enable ANNs to capture complex non-linear relationships and patterns within the data, functioning through multiple processing stages. Each artificial neuron is a mathematical construct involving inputs, associated weights, a bias term, an activation function, and an output. Mathematically, the output of a single neuron can be expressed as

$$y_j = f\left(\sum_{i=1}^{n} w_{ij} x_i + b_j\right) \quad (1)$$

Where is the output of the th neuron, is the th input to the neuron. is the weight connecting the th input to the th neuron, is the bias term of the th neuron neuron, and is the number of inputs to the neuron. The activation function introduces non-

linearity into the model, allowing ANNs to model complex mappings that are not linearly separable (Glorot et al. 2010).

ANNs are particularly well-suited for regression tasks, which involve the prediction of continuous-valued outputs and the modeling of intricate input-output relationships, rendering them invaluable across various practical domains. Among different ANN architectures, feed-forward backpropagation networks, optimized with the Levenberg-Marquardt algorithm, have demonstrated effective training performance, making them widely applicable.

This study utilizes a feed-forward backpropagation artificial neural network (ANN) model, with weight optimization achieved through the Levenberg-Marquardt algorithm. In many nonlinear problems, a single hidden layer is often sufficient to achieve reliable results. Increasing the number of hidden layers beyond two generally does not lead to significant performance improvements and may introduce issues like overfitting or vanishing gradients (Pashazadeh & Javan, 2019; Kisi et al., 2013). In this study, after evaluating various ANN configurations, it was found that a single hidden layer offered the best performance. Specifically, the Tansig activation function with three neurons in the hidden layer produced optimal results. The final optimal ANN architecture for investigating climate change impacts was determined to be ANN (3,3,1), comprising three input neurons, three hidden layer neurons, and one output neuron (Table 1). The ANN model, combined with a calibrated HEC-HMS model, was trained and tested with different configurations. However, the study does not detail the results for other configurations, such as varying activation functions and different numbers of hidden layer neurons.

Gene Expression Programming (GEP)

Gene Expression Programming (GEP) extends traditional evolutionary algorithms by representing solutions as expression trees. These expression trees offer a transparent and mathematically explicit relationship between inputs and outputs. This characteristic of clarity makes GEP particularly valuable for applications such as runoff prediction, where interpretability of the model is a crucial requirement. The GEP process commences with the definition of a fitness function.

In Gene Expression Programming (GEP) modeling, the initial step involves selecting an appropriate fitness function (Kisi et al., 2013). This study employed the Root Mean Square Error (RMSE) as the fitness function, which guided the evolutionary process of the expression trees by evaluating the differences between predicted and observed values. Various functional and terminal nodes

were utilized to construct the expression trees. The default functions provided by GeneXpro were used, including addition, subtraction, multiplication, division, power, square root, exponential, natural logarithm, absolute value, inverse, cube root, sine, cosine, tangent, cotangent, cosecant, secant, arcsine, arccosine, arctangent, arc cotangent, arc cosecant, arc secant, hyperbolic tangent, and other linking functions. These functions are combined to generate equations that relate input features to the target variables. The general form of a GEP-derived equation can be represented as:

$$y = \sum_{j=1}^{g} c_j f_j(X) \quad (2)$$

Here is the output variable, represents the th functional node, is the coefficient associated with the j-th functional node, is the vector of input variables, and is the number of genes in the model.

This example illustrates how GEP integrates both linear and nonlinear relationships and domain-specific information into a predictive model. The structure of these equations can help to understand the relationships learned between the input and output variables.

A key advantage of combing HEC-HMS with Gene Expression Programming (GEP) is GEP's ability to derive explicit mathematical relationships between input and output variables—something that traditional models like ANN and ANFIS often lack (Kisi et al., 2013). The GEP-derived expression formulated in this study for the model presented in Table 1 is:

$$y = cos\left(cos\left(cos\left(\sqrt[3]{d_2} - d_0 - 1.32938895082628\right)\right)\right) + \left(\frac{(d_2 - d_0) \times d_0 \times acot(-7.12454252754295)}{\cos(\cos(d_2))}\right) + \left(\frac{1}{\tan\left(\sqrt{e^{1.34469875637074} - d_0}\right) - \frac{1}{59.299337086763 - (-7.57133701590014)}}\right) \quad (3)$$

Here, d_0 denotes the discharge estimates from HEC-HMS at time t (Q_t), and d_2 refers to discharge estimates from HEC-HMS two days prior (Q_{t-2}). The genetic operators utilized for the HEC-HMS and GEP integration, as detailed in Table 1, are as follows: chromosome count: 30, head size: 7, gene count: 3, linking function: addition, fitness function: RMSE, Mutation rate: 0.00138, inversion rate: 0.00546.

Support Vector Machine (SVM)

Support Vector Machines (SVMs) are powerful supervised learning algorithms that have been widely applied in hydrological modeling due to their capacity to handle nonlinear relationships and high-dimensional datasets (Mountrakis et al., 2011). The fundamental principle of SVMs involves identifying an optimal hyperplane that separates data points of different classes (or, in the case of regression, accurately models continuous outputs) by maximizing the margin between them. For regression tasks, the SVM algorithm employs the concept of ε-insensitive loss, focusing primarily on predictions that

deviate from actual values by more than a specified tolerance, ε (Smola et al., 2004). This approach allows for more robust and generalized model predictions. For an input vector x and corresponding output y, the SVM regression function can be represented as:

$$y(x) = \sum_{i=1}^{N} \alpha_i K(x, x_i) + b \quad (4)$$

Where represents the support vector coefficients, is the kernel function that defines the similarity between the input vector and the support vectors , is the number of support vectors, and is the bias term.

The kernel function, , is a critical component of SVM, enabling it to map data into higher-dimensional spaces to capture complex nonlinearities. In this study, the Radial Basis Function (RBF) kernel was primarily utilized, alongside linear and polynomial kernels. The RBF kernel, also known as Gaussian kernel, is defined as:

$$K(x, x_i) = \exp(-\gamma \parallel x - x_i \parallel^2) \quad (5)$$

Where is the kernel parameter that controls the width of the Gaussian function, and consequently affects the influence of each support vector.

Parameter optimization is crucial to the performance of SVM models. This includes optimizing the penalty parameter, which controls the balance between minimizing training error and maximizing the margin, and the kernel-specific parameters, such as for the RBF kernel and the degree of the polynomial for the polynomial kernel.

In this study, linear kernel, polynomial kernel, and RBF kernel were used in SVM integration with the HEC-HMS model. The gamma parameter (γ) was optimized through a systematic trial-and-error process for all kernels, with γ values tested over a range of {10^{-3}, 10^{-2}, 10^{-1}, 1, 10, 20, 50, 100}. An additional sigma squared parameter (σ^2) for the RBF kernel was also determined through a similar trial-and-error process, with σ^2 varied in steps including {0.1, 0.2, 0.3, 0.4, ..., 10}. Specifically, the RBF kernel with $\gamma = 10$ and $\sigma^2 = 0.2$ provided the best results in terms of the NSE coefficient (Table 1). The selected values minimized the validation error and achieved a good balance between model complexity and generalization, thereby optimizing the model's performance. The SVM model was configured for function approximation (type f), as shown in Table 1.

Adaptive Neuro-Fuzzy Inference System (ANFIS)

The Adaptive Neuro-Fuzzy Inference System (ANFIS) is a hybrid computational model that combines the strengths of fuzzy logic and neural networks. This integration makes ANFIS particularly effective for modeling nonlinear and

complex relationships, such as those commonly found in hydrology (Fahimi et al. 2017). ANFIS utilizes fuzzy IF-THEN rules to mimic human-like reasoning and refines these rules through neural network training techniques to optimize predictive performance. As a result, the model is both interpretable, due to the fuzzy logic component, and capable of learning complex patterns, thanks to the neural network component.

The ANFIS model is based on a Sugeno-type fuzzy inference system, where the output is a linear combination of input variables within each fuzzy rule. A typical fuzzy IF-THEN rule in ANFIS can be expressed as:

(6)

IF is AND is ... AND is THEN

$y = p_0 + p_1 x_1 + p_2 x_2 + \cdots + p_n x_n$

Where represents the input variables, are the membership functions (MFs) associated with each input variable, is the output variable, and are the consequent parameters.

The membership functions (MFs) quantify the degree to which each input variable belongs to a particular fuzzy set. These functions, such as Gaussian or Generalized Bell (GBellMF) functions, mathematically define the degree of membership. The mathematical form of the Generalized Bell membership function (GBellMF) is:

$$\mu_A(x) = \frac{1}{1 + \left|\frac{x - c}{a}\right|^{2b}} \quad (7)$$

Where a, b, and c are parameters that control the shape of the membership function, and represents the degree of membership of in the fuzzy set . Training ANFIS involves optimizing the parameters of the membership functions (a, b, c) and the consequent parameters (). A hybrid optimization method is typically used to refine these parameters, combining gradient descent to adjust the membership function parameters and least squares estimation to determine the consequent parameters.

In this study, an ANFIS model was trained and tested using a hybrid optimization method with three input membership functions (MFs) set to the GBellMF type and a linear output MF type (Table 1). The use of multiple membership functions allows the model to capture a wide range of input variable behaviors. The GBellMF type has been shown to perform well in these contexts.

Future climate scenario projections

LARS-WG was selected for its excellent performance and ability to downscale GCM outputs for the Sangdeh station area. The tool's effectiveness was assessed by replicating observed daily data from 1985 to 2005 and producing 300 years of synthetic data, which mirrored the statistical properties of the observed data. LARS-WG then generated daily datasets for six models (ACCESS-

ESM1-5, CNRM-CM6-1, GFDL-ESM4, HADGEM3-GC31-LL, MPI-ESM1-2-LR, MRI-ESM2-0) under the SSP585 scenario for the periods 2031-2050 and 2051-2070. This scenario is appropriate for Iran due to the nation's high fossil fuel consumption and slow transition to renewable energy, leading to projections of more extreme weather events (Horanyi , 2023). These climate data allow for the comparison of future runoff conditions with data recorded from 2007-2018.

Results and discussion

Future Projections and Managing Uncertainty from Various Climate Model Forecasts

Climate models vary in their predictions of rainfall and runoff patterns. For example, some models within the LARS-WG framework project an increase in mean annual rainfall in certain areas, while others foresee a decrease in those same regions (Semenov et al. 1998). Utilizing a range of climate models is essential for accurate climate change impact assessments. To illustrate the uncertainty in these predictions, two box plots were created using future mean annual values of climatic variables (rainfall) and hydrological variables (runoff) from all General Circulation Models (GCMs). These future values are then compared with historical data. The box plots show the 25th and 75th percentiles, the median (50th percentile), and the minimum and maximum values (Semenov & Shewry, 2011). Figures 2 and 3 display the annual changes in rainfall and runoff for two future periods.

Throughout the calibration period from 2007 to 2018, the mean annual rainfall was 788 mm. When integrating HEC-HMS with ANN, GEP, ANFIS, and SVM, the mean annual runoff values were 174.23 mm, 183.29 mm, 164.62 mm, and 169.79 mm, respectively. The projected annual rainfall shows an increasing trend over the coming decades. From the calibration period, where the mean annual rainfall was 788 mm, there is a projected increase to a median annual rainfall of 807.4 mm in 2031-2051, representing a 2.46% rise. This trend continues, with the median annual rainfall expected to reach 834.9 mm in 2051-2070, marking a 5.95% increase from the calibration period. The projected median annual runoff using the integration of HEC-HMS with SVM shows a decreasing trend over the coming decades. For the period from 2031-2051, the median annual runoff is expected to be 163.81 mm, representing a 3.53% decrease from the calibration period's mean of 169.79 mm. In the period from 2051-2070, the median annual runoff is projected to rise slightly to 167.61 mm, which is a 1.28% decrease from the calibration period. It is crucial to recognize that integrating HEC-HMS with ANFIS, ANN, and GEP

models shows a projected decline in runoff compared to the calibration period. These trends indicate a decrease in annual runoff, highlighting the necessity for adaptive water management strategies to address potential variations in water availability (Figure. 2 and 3). Increased temperatures and higher evapotranspiration rates are anticipated to further lower median annual runoff.

The IPCC Sixth Assessment Report (2023) underscores that anthropogenic global warming of 1.1°C has precipitated unprecedented alterations in Earth's climate, manifesting as more extreme weather events and heightened rainfall in numerous regions. The report stresses that each additional 0.5°C rise in global temperature will trigger more frequent and intense heat extremes, heavy rainfall, and regional droughts. Similarly, Ripple et al. (2024) point out that escalating greenhouse gas emissions are driving more extreme weather events, with human-induced carbon dioxide emissions being the principal contributors to climate change, resulting in increased rainfall and more frequent extreme weather phenomena.

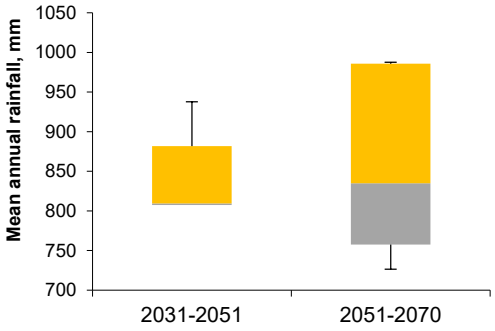

Fig 2. Box plots created from the average annual rainfall data derived from various climate models for the SSP585 scenario and projected future period.

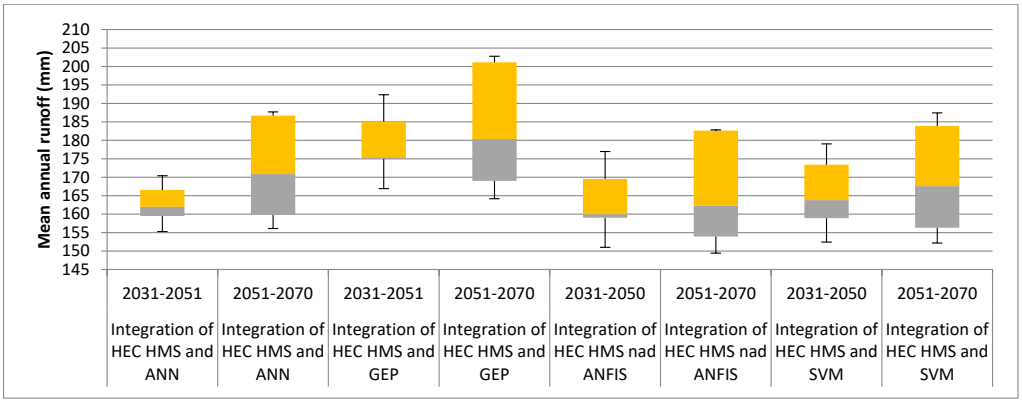

Fig 3. Box plots created using the average annual runoff values derived from various climate models for the SSP585 scenario and projected future period.

Google Earth Engine analysis to investigate the impact of climate change on rainfall and runoff

Over the past decade, extensive research has highlighted the effective use of remote sensing and the Google Earth Engine (GEE) platform for runoff and flood risk calculations. Studies by Yousefi et al. (2022 & 2024) and Tiwari et al. (2020) underscore GEE's capability in estimating runoff, sediment, and mapping flood inundation areas.

Additionally, we utilized Google Earth Engine to analyze climate change impacts using observational data, compensating for the incomplete datasets from the Valikbon Hydrometric Station and the Sangdeh Meteorological Station.

This study utilized Google Earth Engine to analyze annual precipitation trends using the CHIRPS dataset. We centered the region of interest (Kasilain catchment) on the map and aggregated daily CHIRPS precipitation data into annual sums for the years 1981 to 2023. The mean annual precipitation for the Kasilain catchment can be calculated by averaging these annual sums. The resulting data was visualized with a chart, depicting year-to-year variations in annual precipitation and providing insights into long-term climate trends and variability (Figure 4).

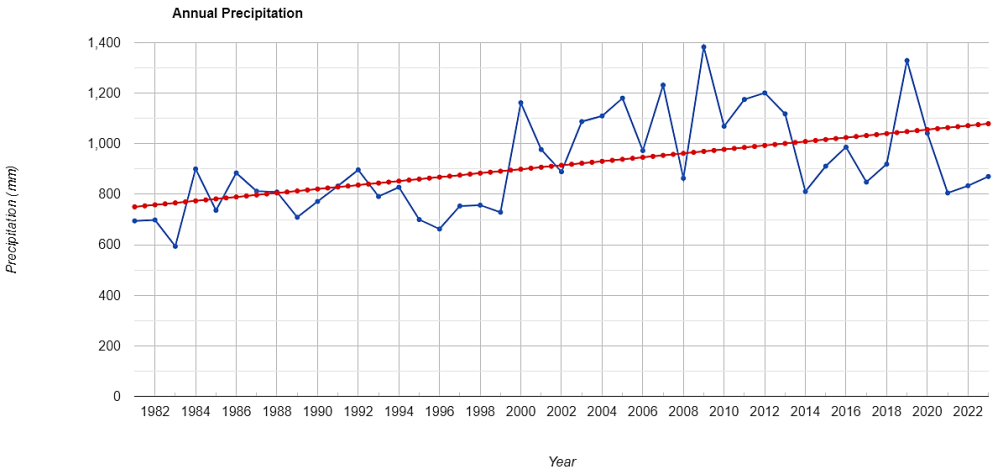

Fig 4. Annual Precipitation in the Kasilian catchment analyzed using Google Earth Engine, blue line: Annual precipitation data points, Red dashed line: Trend line indicating overall precipitation trend

A different code in Google Earth Engine (GEE) was used to analyze and visualize annual runoff data for the Kasilian catchment from 1981 to 2023, utilizing the IDAHO_EPSCOR/TERRACLIMATE dataset. Runoff data is filtered by spatial and temporal bounds, selecting only the runoff ('ro') band. The code then calculates annual runoff by summing the monthly runoff for each year and creates an image collection with each year's total runoff. This data is visualized through a time series

chart, plotting annual runoff over time and including a trendline to highlight long-term patterns. The chart, titled "Annual runoff Kasilian catchment," displays years on the x-axis and runoff values in millimeters on the y-axis, providing valuable insights into the hydrological behavior and trends of the Kasilian catchment over four decades (Figure 5).

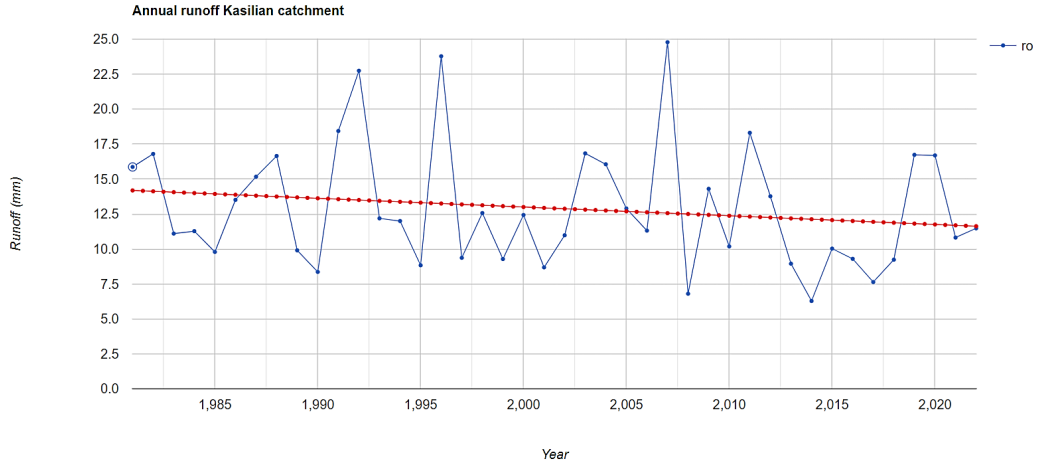

Fig 5. Annual runoff in the Kasilian catchment analyzed using Google Earth Engine, blue line: Annual runoff data points, Red dashed line: Trend line indicating overall runoff trend

A Google Earth Engine code visualizes annual Potential Evapotranspiration (PET) for the Kasilian catchment from 2000 to 2023 (Figure 6). This code centers the map on the catchment, specifies the time range, retrieves the MODIS PET product, and calculates the annual sum of PET. It then generates a time series chart of annual PET values, including axis titles and a trend line. Unfortunately, the MODIS PET data does not extend before 2000 but continues to be updated periodically up to the present. This visualization helps monitor changes in annual PET over time for the Kasilian catchment.

Sediment load and soil loss in Kasilian catchment

The Revised Universal Soil Loss Equation (RUSLE) is a highly used model demonstrating the connection between rainfall and soil erosion. In this equation (Eq. 8), R signifies the rainfall erosivity factor, K represents the soil erodibility factor, LS is the slope length and steepness factor (dimensionless), C denotes the cover management factor, P is the support practice factor (ranging from 0 to 1), and A represents the estimated soil loss ($ton \cdot hectare^{-1} \cdot annum^{-1}$) (Islam 2022, Benavidez et al. 2018, Sakhraoui & Hasbaia 2023).

It is important to note that various formulas from Islam (2022), Benavidez et al. (2018), and Sakhraoui & Hasbaia (2023) were utilized to estimate the C factor, K factor, R

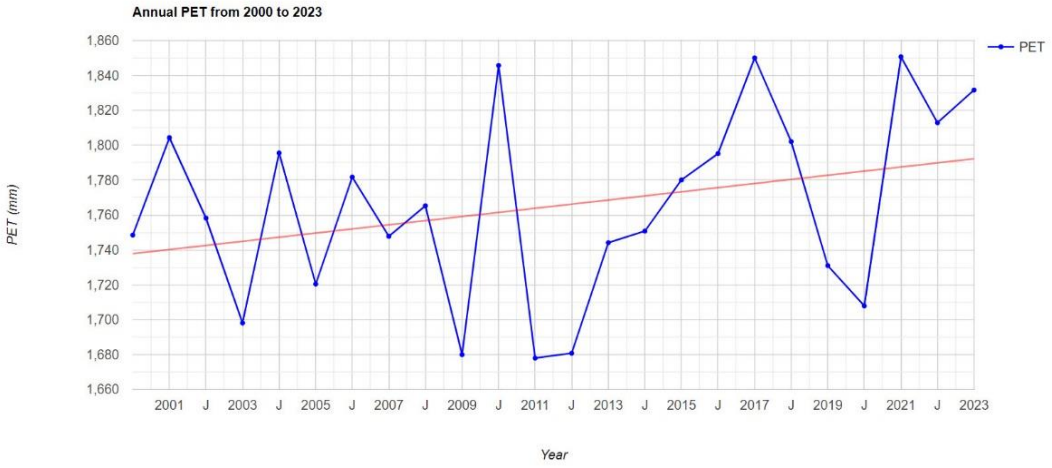

Fig 6. Annual potential evapotranspiration in the Kasilian catchment analyzed using Google Earth Engine, blue line: Annual potential evapotranspiration data points, Red dashed line: Trend line indicating overall potential evapotranspiration trend

factor, and LS factor in order to determine the actual value of mean sediment load for the Kasilian catchment. Ultimately, equations 10 to 15 were identified as the most accurate for estimating the true mean sediment load of the Kasilian catchment.

$$A = R \times K \times LS \times C \times P \quad (8)$$

The sediment delivery ratio (SDR) quantifies the proportion of eroded soil that is carried away from a specific land area over a certain period. This concept is mathematically represented as (Hajian 2013):

$$SDR = sediment\frac{yield}{soil\ erosion} \quad (9)$$

Rainfall factor (R):

$$MFI = \sum_{I=1}^{12} \frac{P_I^2}{p} \quad (10)$$

MFI: the Modified Fournier Index; Pi: the monthly precipitation; P: the annual precipitation;

The R factor is calculated as:

$$R = 0.07397 \times MFI^{1.847} \quad (11)$$

Soil factor (K):

The K factor was determined using Equation 12:

$$K = [0.2 + 0.3 \times exp - 0.0256 \times SAN \times (1 - \frac{SIL}{100}) \times \left[1 - \frac{0.25 \times CLA}{CLA + \exp(3.72 - 2.95 \times CLA)}\right] \quad (12)$$

where SAN represents the percentage of sand, SIL indicates the percentage of silt, and CLA denotes the percentage of clay.

LS factor (LS):

The LS factor was determined using Equation 13 and serves as an accelerating factor for rainfall erosion:

$$LS = \left(\frac{l}{22}\right)^{0.5} \times (0.065 + 0.045s + 0.0065s^2) \quad (13)$$

l: slope length (m)

s: slope steepness (%)

Cover management factor (C):

This relates to cover management, calculated using the Normalized Difference Vegetation Index (NDVI) (Equation 14):

$$\mathrm{NDVI} = \frac{(\mathrm{NIR} - RED)}{(\mathrm{NIR} + \mathrm{RED})} \quad (14)$$

NIR denotes the reflectance value in the near-infrared band, while RED indicates the reflectance value in the red band.

Equation 15 was utilized to determine the C factor, which is dependent on NDVI.

$$\mathrm{C\ factor} = \mathrm{e}^{\frac{-2\mathrm{NDVI}}{1-\mathrm{NDVI}}} \quad (15)$$

This methodology utilizes various satellite datasets to derive the factors of the Revised Universal Soil Loss Equation (RUSLE). Specifically, the C factor is obtained from MODIS NDVI data covering the period from January 1, 2000, to December 31, 2023. The LS factor is calculated using SRTM 30-meter Digital Elevation Model (DEM) data. Soil property data from OpenLandMap is used to estimate the K factor. Additionally, the CHIRPS daily precipitation dataset, spanning from January 1, 2000, to December 31, 2023, is employed to determine the R factor. By integrating these datasets with the appropriate formulas, a comprehensive model for estimating soil erosion is developed. The sediment load analysis is limited to the period from 2000 to 2022 due to the availability of NDVI data from the MODIS sensor (MODIS/006/MOD13A2), which was launched on December 18, 1999 (Figure 7). Therefore, prior to 2000, NDVI data necessary for estimating the C factor was unavailable.

Considering the sediment delivery ratio (SDR) of the Kasilian catchment obtained as 0.763 from Hajian (2013), the estimated mean annual sediment load of the Kasilian catchment using GEE (631.667 t km^{-2} yr^{-1}) closely matched the observed value for the Talar catchment (532 t km^{-2} yr^{-1}), of which Kasilian is a subcatchment. Therefore, the sediment load derived from GEE seems to more accurately reflect the sediment load conditions in the Kasilian catchment (Hajian, 2013).

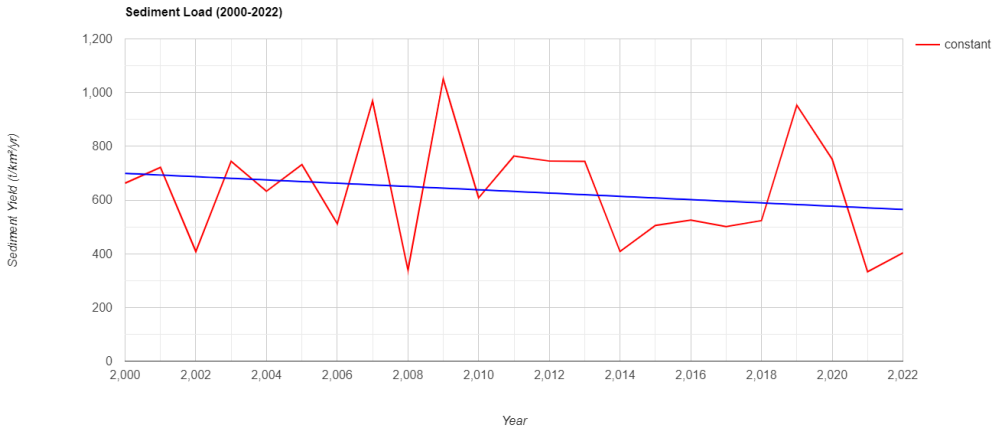

Fig 7. Annual sediment load in the Kasilian catchment analyzed using Google Earth Engine, blue line: Annual sediment load data points, Red dashed line: Trend line indicating overall sediment load trend

The increase in extreme rainfall events has led to higher annual rainfall, while rising temperatures and greater annual potential evapotranspiration have reduced annual runoff. This reduction in runoff has decreased sediment load due to the diminished capacity of streams to transport sediment. From 1981 to 2023, annual rainfall has increased, but annual runoff has decreased, as shown in Figures 4 and 5, consistent with Figures 2 and 3. The increase in rainfall enhances soil moisture, promotes vegetation growth, stabilizes the soil, reduces erosion, and leads to greater infiltration, which decreases erosion and sedimentation rates. Despite the rise in rainfall, the overall impact is a complex interplay of factors affecting hydrological and sedimentation processes in the catchment area.

Research by Cho et al. (2011) and Bae et al. (2008) shows that annual precipitation and mean air temperature significantly impact annual runoff. Higher temperatures increase evapotranspiration, reducing runoff despite higher precipitation. This underscores the necessity to consider temperature effects in water resource management and climate adaptation strategies. Future projections indicate increased rainfall but decreased runoff due to heightened evapotranspiration, stressing the need for integrating these climatic changes into water management strategies.

Conclusions

The integration of Support Vector Machine (SVM) and Hydrologic Engineering Center's Hydrologic Modeling System (HEC-HMS) models has shown superior performance over other hybrid models in simulating rainfall-runoff processes. Despite this, all hybrid models were used to evaluate the impact of climate change on runoff. Combining stream flow forecasts from conceptual models with machine learning techniques like ANN, GEP, SVM, and ANFIS improves runoff prediction accuracy and is highly effective for assessing the impacts of climate change on water resources. In the Kasilian Catchment and northern Iran, climate change is anticipated to result in more extreme rainfall events and increased annual rainfall. However, rising annual evapotranspiration rates are expected to decrease annual runoff. The increase in mean rainfall is likely driven by these extreme events. The annual sediment load likely decreased due to reduced runoff. This reduction in runoff diminished the ability of the streams to transport sediment, leading to lower sediment load. Observed data from the Google Earth Engine platform showed an increase in annual rainfall and a decrease in annual runoff, consistent with future analysis results using hybrid models and LARS-WG.

Author Contributions

The first author was responsible for all aspects of the study, including calculations and writing, as well as other related tasks. The second and third authors provided guidance and support throughout the research process.

References

Abbaspour K.C., Faramarzi M., Ghasemi S.S., & Yang H. (2009). Assessing the impact of climate change on water resources in Iran, *Water Resources*, 45, W10434. Doi:10.1029/2008WR007615.

Asadi, H., & Santos, C.A.G. (2022). A hybrid artificial intelligence and semi-distributed model for runoff prediction, *Water Supply*, 22(7), 6181-6195. doi: https://doi.org/10.2166/ws.2022.123

Babaeian I., Najafinik Z., Zabolabasi F., Habibinokhandan M., Adab H., & Malbosi S. (2007). Climate change investigation of Iran for 2010-2039 using downscaled output of ECHO-G climate model, *Geography and Development Iranian Journal*, 16, 135-152. [in Persian]. https://doi.org/10.22111/gdij.2009.1179.

Bae D.H., Jung W., & Chang H. (2008). Potential changes in Korean water resources estimated by high-resolution climate resolution, *Climate Research*, 35, 213-226. https://doi.org/10.3354/cr00704.

Bae D.H., Jung W., & Lettenmaier D.P. (2011). Hydrologic uncertainties in climate change from IPCC AR4 GCM simulations of the Chungju Catchment, Korea, *Journal of Hydrology*, 401, 90–105. https://doi.org/10.1016/j.jhydrol.2011.02.012

Benavidez, R., Jackson, B., Maxwell, D., & Norton, K. (2018). A review of the (Revised) Universal Soil Loss Equation ((R)USLE): with a view to increasing its global applicability and improving soil loss estimates. *Hydrology and Earth System Sciences*, 22(11), 6059-6086. doi:10.5194/hess-22-6059-2018.

Cho, J., Komatsu, H., Pokhrel, Y. et al.(2011). The effects of annual precipitation and mean air temperature on annual runoff in global forest regions. *Climatic Change,* 108, 401–410. https://doi.org/10.1007/s10584-011-0197-3.

Fahimi, F., Yaseen, Z. M., & El-shafie, A. (2017). Application of soft computing based hybrid models in hydrological variables modeling: a comprehensive review. *Theoretical and applied climatology*, 128, 875-903. doi: https://doi.org/10.1007/s00704-016-1735-8

Farfan, J.F., Palacios, K., Ulloa, J., & Avilés, A. (2020). A hybrid neural network-based technique to improve the flow forecasting of physical and data-driven models: Methodology and case studies in Andean watersheds. *Journal of Hydrology: Regional Studies, 27*, 100652. https://doi.org/10.1016/j.ejrh.2020.100652.

Gebremichael, M., & Hailu, A. (2024). Comparative analysis of HEC-HMS and machine learning models for rainfall-runoff prediction, *Hydrology Research*, 55(3), pp. 456-470. doi: https://doi.org/10.2166/nh.2024.032

Glorot, X., & Bengio, Y. (2010). Understanding the difficulty of training deep feed forward neural networks. In Proceedings of the thirteenth international conference on artificial intelligence and statistics, *JMLR Workshop and Conference Proceedings.*

Hajian, F. (2013). Effects of land cover and climate changes on runoff and sediment yield

from a forested catchment in northern Iran. PhD thesis. Kingston University.

Hitokoto, M., & Sakuraba, M. (2020). Hybrid deep neural network and distributed rainfall-runoff model for real-time river-stage prediction, *Journal of Japan Society of Civil Engineers (JSCE)*, 8(1), 46–58. https://doi.org/10.2208/journalofjsce.8.1_46

Horanyi, A. (2023). CMIP6: Global climate projections. European Centre for Medium-Range Weather Forecasts (ECMWF). https://confluence.ecmwf.int/display/COPSRV/CMIP6%3A+Global+climate+projections.

IPCC. (2023). Climate Change 2023: Synthesis Report. Contribution of Working Groups I, II and III to the Sixth Assessment Report of the Intergovernmental Panel on Climate Change [Core Writing Team, H. Lee and J. Romero (eds.)]. IPCC, Geneva, Switzerland. doi:10.59327/IPCC/AR6-9789291691647.

Islam, Z. (2022). Soil loss assessment by RUSLE in the cloud-based platform (GEE) in Nigeria. *Modeling Earth Systems and Environment*, 8, 4579-4591. doi:10.1007/s40808-022-01467-7.

Kavoosi, M., & Khozeymehnezhad, H. (2021). Review and compare performance of 4 modeling methods LS-SVM, NN, GEP, and ANFIS-PSO in simulation of rainfall-runoff (Study Area: Halil River - Jiroft Dam). *Iranian Journal of Ecohydrology*, 8(2), 123-135. doi:10.22125/iwe.2021.128115.

Kisi, O., Shiri, J., & Tombul, M. (2013). Modeling rainfall-runoff process using soft computing techniques, *Computers & Geosciences*, 51, 108–117. doi: https://doi.org/10.1016/j.cageo.2012.07.001

Kumar, A., Kumar, P., & Singh, V. K. (2019). Evaluating different machine learning models for runoff and suspended sediment simulation. *Water Resources Management*, 33(4), 1217-1231. doi:10.1007/s11269-018-2178-z.

Mountrakis, G., Im, J., & Ogole, C. (2011). Support vector machines in remote sensing: A review. *ISPRS journal of photogrammetry and remote sensing*, 66(3), 247-259. doi: https://doi.org/10.1016/j.isprsjprs.2010.11.001

Pashazadeh, A., & Javan, M. (2019). Comparison of the gene expression programming, artificial neural network (ANN), and equivalent Muskingum inflow models in the flood routing of multiple branched rivers, *Theoretical and Applied Climatology*, doi: https://doi.org/10.1007/s00704-019-03032-2.

Ripple, W. J., Wolf, C., Gregg, J. W., Rockström, J., Mann, M. E., Oreskes, N., Lenton, T. M., Rahmstorf, S., Newsome, T. M., Xu, C., Svenning, J.-C., Pereira, C. C., Law, B. E., & Crowther, T. W. (2024). The 2024 state of the climate report: Perilous times on planet Earth. *BioScience, 74*(10), 1-13. doi:10.1093/biosci/biae087.

Sakhraoui, F., & Hasbaia, M. (2023). Evaluation of the sensitivity of the RUSLE erosion model to rainfall erosivity: A case study of the Ksob watershed in central Algeria. *Water Supply, 23*(8), 3262-3284. https://doi.org/10.2166/ws.2023.207.

Semenov M.A., Brooks R.J., Barrow E.M., & Richardson C.W. (1998). Comparison of the WGEN and LARS-WG stochastic weather generators for diverse climates, *Climate Research*, 10, 95–107.

Semenov, M., & Shewry, P.R. (2011). Modelling predicts that heat stress, not drought, will increase vulnerability of wheat in Europe, *Scientific Reports*, 1, 66. doi: https://doi.org/10.1038/srep00066

Shifteh Some'e B., Ezani A., & Tabari H. (2012). Spatiotemporal trends and change point of precipitation in Iran, Atmospheric Research, 113, 1-12. https://doi.org/10.1016/j.atmosres.2012.04.016.

Smola, A. J., & Schölkopf, B. (2004). A tutorial on support vector regression. *Statistics and computing*, 14, 199-222. doi: https://doi.org/10.1023/B:STCO.0000035301.49549.88

Tabatabaei, S. M., Nazeri Tahroudi, M., & Hamraz, B. S. (2021). Comparison of the performances of GEP, ANFIS, and SVM artificial intelligence models in rainfall simulation. *IDŐJÁRÁS / Quarterly Journal of the Hungarian Meteorological Service*, 125(2), 195-209. doi:10.28974/idojaras.2021.2.21.

Tiwari V, Kumar V, Matin MA, Thapa A, Ellenburg WL, Gupta N, et al. (2020). Flood inundation mapping- Kerala 2018; Harnessing the power of SAR, automatic threshold detection method and Google Earth Engine. PLoS ONE, 15(8): e0237324. https://doi.org/10.1371/journal.pone.0237324

Yousefi, E., Kaffash, M., & shariati, M. (2024). Spatial analysis of flood risk in Tabas watershed using satellite images and geographic information system (GIS). *Journal of Drought and Climate change Research*, 2(2), 105-118. doi: 10.22077/jdcr.2024.7489.1066

Yousefi, E., Sayadi, M. H., & Chamenhpour, E. (2022). Google Earth Engine platform to calculate the hydrometeorology and hydrological water balance of wetlands in arid areas and predict future changes. *Journal of Applied Research in Water and Wastewater*, 9(1), 52-68. doi: 10.22126/arww.2022.7033.1228

Zhang, Y., Li, X., & Wang, J. (2022). A Hybrid Rainfall-Runoff Model: Integrating Initial Loss and LSTM for Improved Forecasting. *Journal of Hydrology, 610*, 127-139. doi:10.1016/j.jhydrol.2022.127139.

Original Article

Journal of Drought and Climate change Research (JDCR)

Winter 2025, Vol. 2, No. 8, pp 161-184

10.22077/jdcr.2025.8565.1095

A Review of Participatory Management's Role in Reducing Vulnerability and Enhancing Resilience to Climate Change and Drought (2006-2024)

Moein Tosan[1], Raziyeh Shamshirgaran[2], Malihe Falaki[3,4*]

1- Department of in Water Resources, University of Birjand, Birjand, Iran.
2- Department of in Water Resources Management and Engineering, University of Birjand, Birjand, Iran.
3- Department of Plant Production and Genetics Engineering, University of Birjand, Birjand, Iran.
4- Department of Drought and Climate Change Research Group, University of Birjand, Birjand, Iran.
*** corresponding author: falaki@birjand.ac.ir**

Keywords:
Community resilience, Crisis adaptation, Local governance, Crisis prediction models, Sustainable water resources.

Received:
02 March 2024

Revised:
28 April 2024

Accepted:
11 May 2024

Abstract

Given the escalating challenges posed by climate change and the increasing frequency of droughts, participatory management has emerged as a critical strategy for enhancing resilience and mitigating vulnerability within the governance frameworks of water resources. This includes influencing decision-making processes, policies, and institutional arrangements related to water management. This study critically examines the role of participatory management in mitigating vulnerability and enhancing resilience to climate change and drought, utilizing bibliometric analysis of articles published between 2007 and 2024, sourced from the Web of Science. Analysis of the data using advanced tools such as VOSviewer and Biblioshiny revealed a marked increase in participatory management research within the context of climate and drought resilience, particularly since 2015. Key themes emerging from the literature include resilience, vulnerability, and the integration of public participation in water resource management decision-making processes. The transition from conceptual to applied research has been accompanied by the growing incorporation of cutting-edge technologies, including remote sensing, Geographic Information Systems (GIS), and machine learning models. These technologies have been proven instrumental in facilitating data sharing,

How to cite this article:
Tosan, M., Shamshirgaran, R. & Falaki, M. (2024). A Review of Participatory Management's Role in Reducing Vulnerability and Enhancing Resilience to Climate Change and Drought (2006-2024). *Journal of Drought and Climate change Research* (JDCR), 2(8), 161-184. 10.22077/jdcr.2025.8565.1095

modeling climate change impacts, and enhancing participatory decision-making frameworks. Geographically, there is a global trend toward strengthening local community engagement in water resource governance, with such participatory efforts playing a pivotal role in building resilience and developing sustainable water crisis management strategies. This study identifies key research gaps including the development of predictive resilience models, enhancement of local participation, and effective use of real-time data and advanced technologies to improve water resource management under changing climate conditions.

Introduction

Climate change and the crises arising from droughts represent some of the most significant challenges faced by human societies in the contemporary era (Ewane et al., 2023). These crises, particularly in arid and semi-arid regions, are increasingly impacting the quality of life and well-being of communities through heightened drought frequency and severity, reduced water resources, and significant environmental and economic threats (Kapica et al., 2024). In this context, climate change is a primary driver of many water-related challenges, as shifts in precipitation patterns, rising temperatures, and altered evaporation rates exacerbate water crises and drought events (Yassebi Naeini et al., 2016). Specifically, in water-scarce and semi-arid regions, these changes lead to a reduction in both surface and groundwater resources, extended drought periods, and threats to food security (Johnson et al., 2020). Therefore, effective water resource management in the face of these challenges is crucial for ensuring the sustainability and resilience of communities and ecosystems.

In response to these crises, various management approaches have been employed to address the impacts of droughts and climate change, particularly in the domain of water resources management and climate change adaptation (Tosan & Beyranvand, 2023). Traditionally, top-down, centralized approaches to water management have been prevalent, often focusing on technical solutions such as large-scale infrastructure projects.

However, these traditional approaches have often proven inadequate in addressing the complex and multifaceted challenges of climate change and drought. They often fail to consider the specific needs and knowledge of local communities, leading to ineffective or unsustainable outcomes. Furthermore, they can exacerbate social inequalities and undermine local resilience.

Among the more effective solutions are the adoption of "participatory management" models and "multi-stakeholder governance" frameworks, which have increasingly gained prominence in the management

of natural resources, especially water resources, in the face of drought and climate change challenges (Salvador et al., 2020; Tosan et al., 2024). These approaches emphasize enhancing synergies and fostering collaboration between local communities, various stakeholders, and governmental and non-governmental entities in decision-making and planning processes for water resource management and climate change adaptation (Rezvani Moghaddam et al., 2016). This form of governance, which is bottom-up and inclusive of all stakeholders in making key decisions, is increasingly recognized as a sustainable and effective strategy for addressing crises and droughts (Feizi & Tosan, 2016). Participatory management, as a governance model, holds significant potential for strengthening the resilience of communities in the face of crises. This approach is particularly crucial in the management of water resources under climate change, as active community participation in decision-making processes can significantly contribute to reducing vulnerabilities and enhancing resilience to climate change impacts (Markowska et al., 2020).

Therefore, understanding the role and impact of participatory management in addressing drought and climate change, especially in the areas of "drought risk management", "drought adaptation", "governance and participatory governance" and "water resource management under climate change," is of paramount importance (Savari et al., 2022; Yuan et al., 2023). These approaches are especially critical given the need for collective decision-making and participatory strategies that incorporate both indigenous knowledge and scientific expertise, thereby contributing to addressing drought and climate change crises (Hedayat & Kaboli, 2024).

This paper presents a bibliometric analysis of the literature concerning the role of participatory management in tackling drought and climate change challenges. The aim of this study is to explore research trends, recent advancements, and evaluate the impact of participatory approaches in addressing water crises and climate change. Additionally, this study analyzes various models of participatory governance at both the local and national levels and examines how these approaches can serve as effective tools for enhancing resilience to drought and climate change crises. Our bibliometric analysis reveals key trends in this research area, including a significant increase in publications since 2015 and a growing emphasis on specific themes such as resilience, co-management, and the use of advanced technologies. Ultimately, the paper emphasizes the importance of "participatory decision-making processes", "water resource management," and "climate change adaptation" at various levels

of governance and local communities, illustrating the positive changes that can result from employing these approaches in water resource management and mitigating the effects of droughts.

Materials and Methods

To investigate the role of participatory management in reducing vulnerability and enhancing resilience to climate change and drought, research data were collected from the reputable Web of Science (Pranckutė, 2021) database. This database is one of the leading global sources that provides access to scholarly articles, books, conference papers, and other academic resources across various disciplines, offering comprehensive data extraction capabilities (Akbarpour et al., 2024; Tosan et al., 2024). Given its vast coverage and accuracy in sourcing relevant information, the Web of Science was selected as the primary data source for this study. The data collection process was completed on December 8, 2024, and all extracted data pertained to publications spanning the years 2007 to 2024.

In selecting keywords for this study, an initial review of literature on participatory management and climate change was conducted. The primary aim was to analyze and assess the role of participatory management in reducing community vulnerability and enhancing resilience against the challenges of drought and climate change. Keywords were specifically chosen to emphasize concepts related to water resource management and community resilience in the context of environmental crises. These keywords were categorized into two main groups. The first category pertains to participatory management and local governance, including terms such as "Participatory management", "Community-based management", "Collaborative management", "Stakeholder involvement", "Participatory decision-making" and "Local governance." These terms focus on the significance of social collaboration and shared decision-making processes across various levels of governance. This category underscores the importance of cooperation among diverse stakeholders and local governance for the effective management of resources and enhancing community resilience in the face of crises. The second category includes keywords related to drought management and resilience to climate change, encompassing terms such as "Drought management," "Drought resilience," "Drought adaptation," "Drought mitigation," "Water scarcity and drought," and "Climate change adaptation." These keywords address the challenges and strategies associated with managing droughts and mitigating the impacts of climate change. The focus of this category is on the development of strategies for adaptation and reducing the adverse

effects of climate change and drought on water resources and community resilience. To analyze the research content and identify emerging patterns in the literature, two advanced software tools, VOSviewer 1.6.20 (Arruda et al., 2022) and Biblioshiny 2.0 (Rógora Kawano, 2024), were employed. These tools are powerful instruments for bibliometric analysis and the examination of co-authorship, citation networks, and keyword clustering (Tosan et al., 2024). VOSviewer is widely used for visualizing data and analyzing scientific networks, allowing for the graphical representation of relationships between articles, authors, keywords, and other scientific indicators (Van Eck & Waltman, 2010; Van Eck & Waltman, 2011). This methodology facilitates the identification of research trends, international collaborations, and the impact of various publications. Additionally, Biblioshiny, operating within the R software environment, was used for the precise bibliometric analysis (Derviş, 2019), enabling the evaluation of citation trends and the clustering of relevant keywords in this field (Aria & Cuccurullo, 2017).

Results and Discussion

Analysis of Scientific Publication Trends on Participatory Management in Addressing Climate Change and Drought

The initial data extracted from the Web of Science (WoS) regarding the role of participatory management in addressing the challenges of drought and climate change include 247 publications from 2007 to 2024, spread across 158 different journals (Figure 1). The collected articles exhibit an average publication rate of 12.73 per year, with an average of 22.76 citations per article. The extracted data comprised 219 journal articles, two book chapters, 17 review papers, 10 conference proceedings, and 8 other types of publications. Furthermore, the research field is characterized by 585 indexed keywords (Keyword Plus), 782 author keywords, and 896 individual authors contributing to the body of work.

The publication trend in the Web of Science from 2007 to 2024 in the field of participatory management's role in mitigating drought and climate change challenges reflects a scientific growth and evolution in this domain. Analysis of this trend shows that participatory management has gradually became a central theme in water resource management research.

In the early years of the research period, the number of publications was relatively limited, indicating the novelty of the field and global awareness being in its nascent stages regarding the effects of climate change and drought. However, the early papers laid the theoretical foundations for

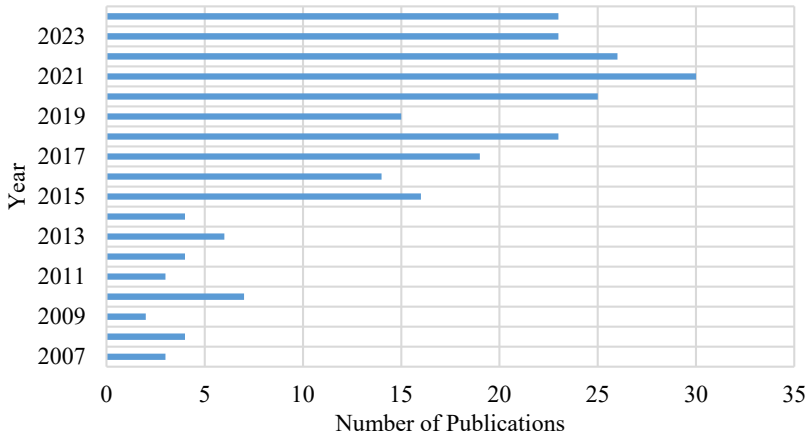

Fig 1. Distribution of articles on the role of participatory management in reducing vulnerability and increasing resilience to climate change and drought.

participatory management and highlighted the relationship between this approach and resilience against climate crises. From the mid-2010s, a significant increase in publications marked the growing convergence between global needs for sustainable resource management and the influence of participatory climate policies. The increase, from 6 publications in 2013 to 30 publications in 2021, reflects global efforts to develop management frameworks that integrate local communities and stakeholders directly into decision-making processes. This shift in perspective is largely due to the exacerbation of climate and drought crises across many regions, necessitating participatory, localized approaches to water management.

Published research in this area has gradually shifted from theoretical studies to more applied, data-driven research. Emerging technologies, such as Geographic Information Systems (GIS), remote sensing, and machine learning models, have increasingly been integrated into these studies to facilitate participatory management. The role of these technologies in enabling data sharing platforms, modeling climate change impacts, and fostering effective community engagement has been particularly significant. These technological innovations have provided robust tools for collaborative decision-making, allowing for more precise assessments of climate vulnerability and drought resilience. Furthermore, they have enhanced the ability to monitor and manage resources effectively, supporting the development of participatory strategies that are increasingly aligned with scientific advancements and practical, real-world applications.

This progression demonstrates the growing interdisciplinary nature of participatory management in the context of environmental crises, positioning

it as a key approach in contemporary water resource management and climate resilience research.

Analysis of Key Publications and Scholarly Sources

Figure 2 presents the top 20 publications with the highest number of articles published on the role of participatory management in mitigating vulnerabilities and enhancing resilience against climate change and droughts, as reflected in the Web of Science database. This indicates the breadth and diversity of research within this domain. These sources represent leading journals that focus specifically on natural resource management, climate change, and drought-related challenges. Among these, the journal *Sustainability* stands out with 12 articles published on this topic, making it a primary source for participatory management and climate change studies. *Sustainability* regularly addresses issues of sustainable development, natural resource management, and various strategies for dealing with environmental crises. The articles published here often propose innovative models and approaches aimed at advancing participatory management to tackle droughts and climate change. Given that *Sustainability* focuses on analyzing various aspects of sustainability, especially in water and natural resource management, it plays a crucial role in shaping policy recommendations for adapting local communities to climate change impacts.

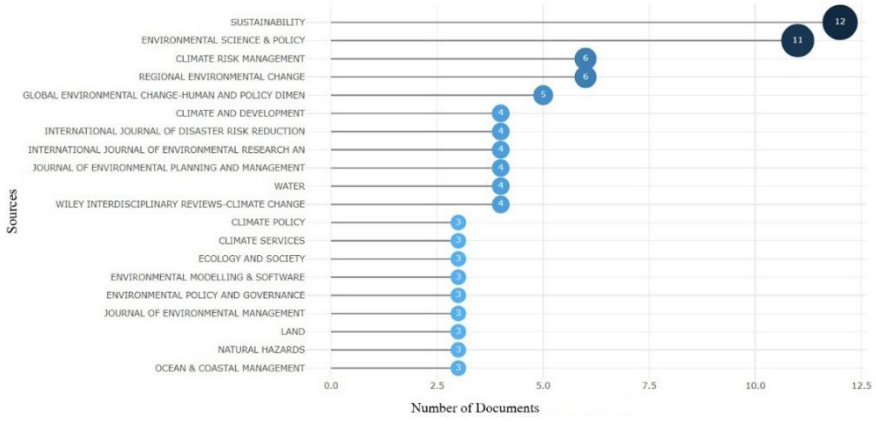

Fig 2. Number of published articles on the role of participatory management in reducing vulnerability and increasing resilience to climate change and drought in the top 20 journals.

Another prominent source is *Environmental Science & Policy*, which has published 11 articles within this field. This journal focuses on the policies and management strategies designed to confront the challenges posed by droughts and climate change. It primarily discusses the legal, policy-making, and governance aspects of natural resource management, with a significant emphasis on participatory

management's role in addressing environmental crises. It remains an essential reference for scholars and policymakers globally, providing practical solutions for enhancing collaboration between local and government stakeholders in managing natural resources. Articles in this journal often adopt an analytical approach, examining the effects of different policies on climate change and drought outcomes. Other noteworthy journals such as *Climate Risk Management*, *Regional Environmental Change*, and *Global Environmental Change-Human and Policy Dimensions* have also contributed significantly to advancing research in participatory management for climate change and drought. *Climate Risk Management* (6 articles) focuses on risk analysis and management strategies for reducing vulnerabilities and enhancing community resilience against climate-related risks. *Regional Environmental Change* (6 articles) takes a regional perspective on environmental changes, playing a critical role in understanding the localized impacts of climate change and droughts across various geographic areas. *Global Environmental Change-Human and Policy Dimensions* (5 articles) addresses the intersection of human dimensions and global policy responses to climate change and drought, examining how interdisciplinary approaches can inform climate action.

Although other journals have published fewer articles, they still contribute valuable analyses on policymaking, strategies, and management frameworks at different levels, especially in the context of crisis management and environmental governance.

Journal Impact and Citation Influence

The local impact of journals, as indicated by their H-index, reflects their varied scholarly influence (Loan et al., 2022). The H-index measures both the quantity of publications and the frequency of citations received for each article, highlighting the journal's overall academic impact. *Global Environmental Change* leads with an impressive 407 citations, underscoring its significant influence on climate change and environmental policy studies. *Ecology and Society* follows with 323 citations, recognized for its role in exploring the interplay between social and environmental dynamics in natural resource management. *Environmental Science & Policy* also holds substantial influence with 260 citations, reflecting its focus on environmental policy and participatory management in crisis situations.

Additional highly cited journals include *Climatic Change* (149 citations) and *Sustainability* (149 citations), both of which emphasize the importance of sustainable development and climate change within global policy frameworks. The *Journal of Environmental Management* (131

citations) and *International Journal of Disaster Risk Reduction* (114 citations) are also considered vital sources in the field of natural disaster management and climate change mitigation strategies.

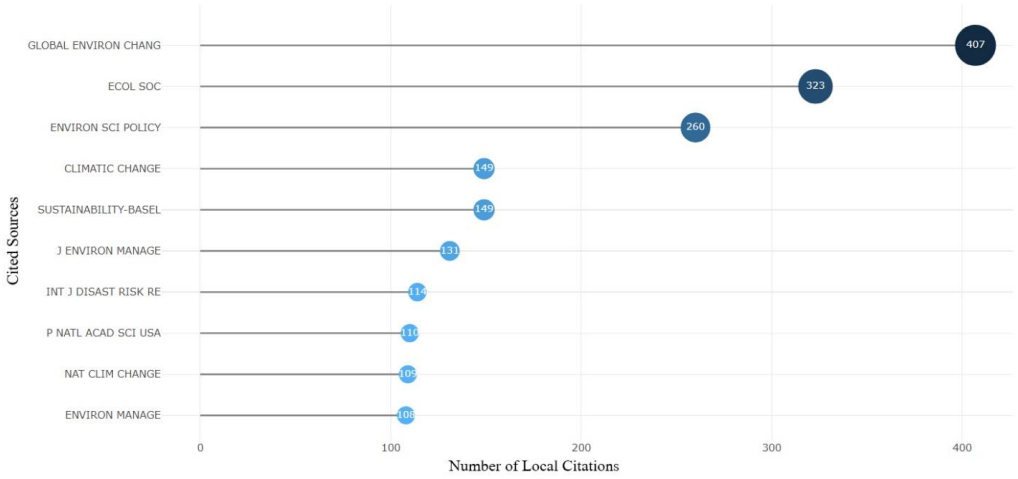

Fig 3. Journals' impact based on H-index

Figure 3 presents a visual representation of journal impact, where the size and color of the nodes correspond to their H-index, with larger and darker nodes indicating higher impact. This type of analysis offers a comprehensive view of the relative influence of each journal, accounting not only for publication volume but also citation frequency. An increased H-index is indicative of greater scholarly influence within the scientific community.

Temporal Trends in Publication Growth

As shown in Figure 4, the growth in journal publications over time reflects the increasing academic attention to participatory management in addressing climate change and drought challenges. *Sustainability* has consistently published the highest number of articles, with a marked increase in publications since 2019, signaling the growing recognition of participatory approaches in climate adaptation strategies. Similarly, *Environmental Science & Policy* has emerged as a central reference in this field, with a steady increase in published articles in recent years.

Notably, *Climate Risk Management* has also experienced significant growth since 2020, contributing to the broader dialogue on climate risk reduction and resilience. Journals such as *Regional Environmental Change* and *Global Environmental Change-Human and Policy Dimensions*, while having fewer articles, have consistently contributed valuable research to the field. The overall growth in publications from 2017 onward illustrates the heightened global interest in participatory management strategies for

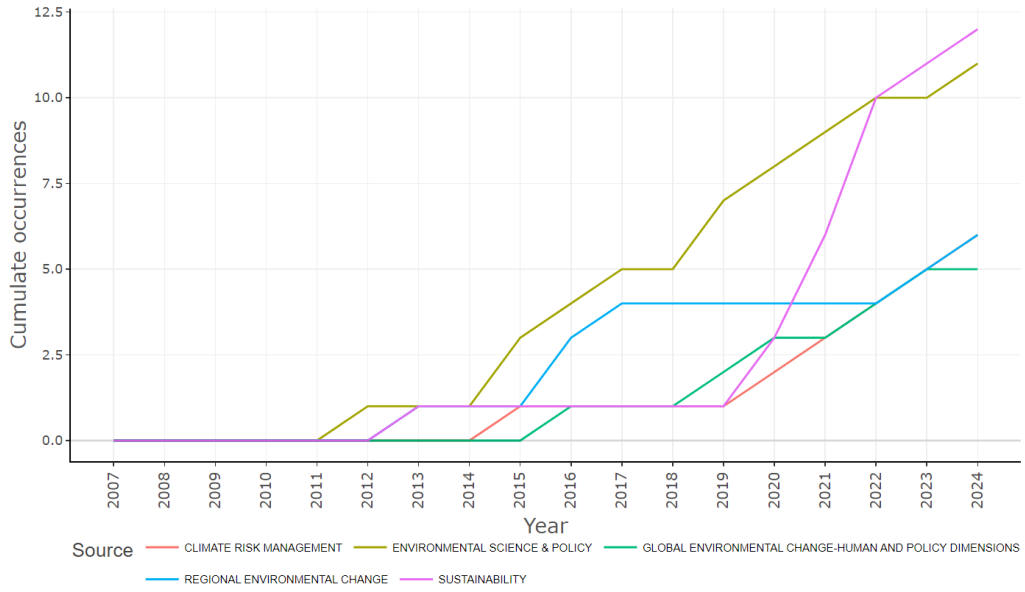

Fig 4. Journals' growth (cumulative) based on the number of papers

climate change and drought resilience. This analysis highlights the increasing scholarly engagement with participatory management as a critical approach for addressing the complex challenges of climate change and drought, both at the global and local levels.

Author Contributions to Participatory Management in Climate Change and Drought Resilience

In the author analysis, we focus on those authors most intricately linked to the subject of participatory management in the context of drought and climate change. The top 10 affiliations, authorship productivity over time, and the leading countries responsible for the highest number of publications are also examined. As depicted in Figure 5, three collaborative clusters emerge. Prominent scholars in the realm of participatory management in the face of climate change and drought challenges include Baird J., Plummer R., Komendantova N., Cilliers L., Williams D.S., and Armitage D. Notably, Armitage D. emerges as the author with the highest degree of collaboration, positioned centrally in the network visualization presented below.

Regarding the timeline of scientific publications, this analysis focuses on the publication trends of the top 10 authors with the highest number of papers. A leading figure in this field is David Armitage, recognized for his substantial contributions in 2017 and 2023, particularly in the areas of collaborative knowledge production and adaptation strategies for climate change in water resources management. His work, especially concerning governance structures and power dynamics in

these processes, has gained significant recognition. For instance, his 2023 article in *Water Resources Management* titled *Collaborative Knowledge Production and Strategies for Supporting Climate-Resilient Water Resources* has been influential, with 17 citations and an annual citation rate of 5.8, underlining the impact and acceptance of his approach (Figure 6).

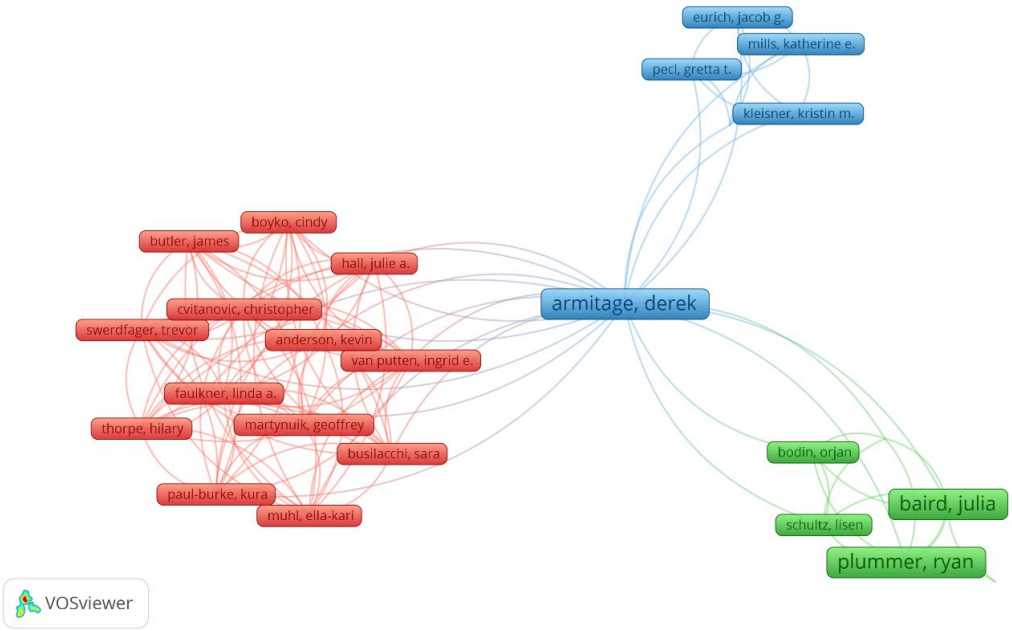

Fig 5. Author Collaboration Network Visualization (Source: Web of Science, 2007-2024)

In addition, the works of Williams and Cilliers, particularly their 2020 articles in *Climate Policy* and *Earth's Future*, have significantly contributed to discussions surrounding local governance capacities required for effective climate change adaptation. These studies emphasize the critical role of strengthening local capacities to confront climate and drought challenges, becoming foundational for subsequent research in governance and social participation.

Similarly, Komendantova and Plummer's papers, published in 2016 and 2017, underscore the growing attention to local participation and its effects on water management under climate change conditions. These works are particularly focused on fostering international cooperation and empowering local communities in the face of climate and drought challenges in Asia and Africa. The works published by Brown and Chapin on societal resilience in the face of climate change and natural hazards, with an emphasis on socio-ecological analyses, highlight their role in shaping decision-making processes and policy development in the context of climate adaptation. Brown's article in *Ecology and*

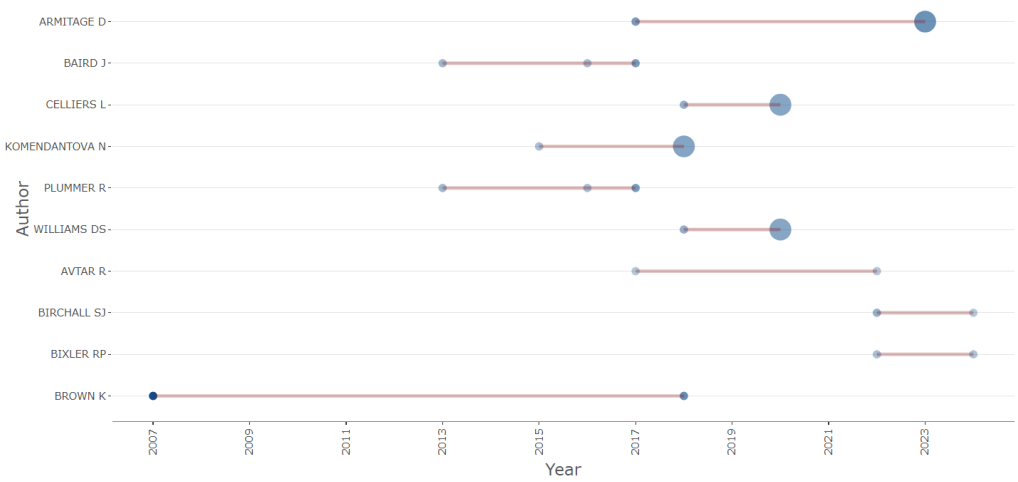

Fig 6. Top 20 Authors' Production over Time

Society, titled *Resilience as an Emerging Characteristic of Socio-Ecological Systems*, emphasizes the importance of community resilience in adapting to climatic crises, such as droughts and storms. Despite these advancements, challenges remain in participatory management, particularly regarding imbalances in power distribution, the lack of accurate information, and governance instability. These structural and institutional challenges continue to slow the decision-making and policy implementation processes.

Figure 7 presents the countries with the highest number of corresponding authors engaged in this research. These authors primarily focus on the application of artificial intelligence in local and regional studies. To identify the countries with the most significant number of corresponding authors, two criteria were considered: Single-Country Publication (SCP) and Multi-Country Publication (MCP). These metrics provided essential insights into the nature and frequency of collaboration between articles. The United States leads this field with 50 articles related to water resources management and addressing drought and climate change challenges, 45 of which are single-country publications (SCP), and 5 are multi-country collaborations (MCP). The high proportion of SCP (90%) indicates a focused, localized approach to addressing drought and climate change issues. The presence of five multi-country publications (MCP) demonstrates the U.S.'s involvement in international projects. This success can be attributed to substantial government and academic support for climate change and drought research, as well as extensive research infrastructure and funding availability in the country.

The United Kingdom follows closely with 26 articles, 14 of which are single-country publications (SCP), while 12 are multi-country collaborations (MCP). The MCP ratio of 0.462 highlights the

UK's significant role in international collaborative research, especially in climate policy and global climate forecasting models. Australia ranks third with 20 articles, with 9 SCP and 11 MCP publications. The higher MCP ratio (0.55) emphasizes Australia's active participation in international collaborations, particularly given the country's frequent droughts and climate variability. The Netherlands, with 19 publications (7 SCP, 12 MCP), has a high MCP ratio (0.632), indicating its active engagement in international water management and drought research, particularly in global water resource modeling. Canada, with 15 articles (8 SCP, 7 MCP), also shows a high level of international collaboration, with an MCP ratio of 0.467, positioning it as a leader in research related to water resources management in cold climates.

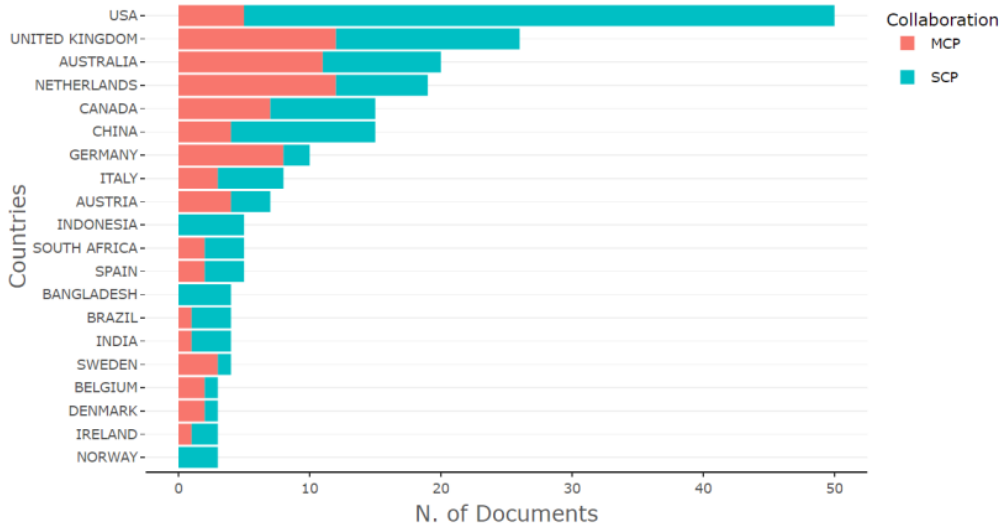

Fig 7. Top 20 Most Relevant Corresponding Authors' Countries

The map in Figure 8 illustrates scientific production based on the country of origin. The gray color represents countries with no scientific output, while varying shades of blue indicate the volume of scientific output from each country. A darker blue shade signifies higher volumes of published articles, whereas lighter shades correspond to fewer articles. The map clearly indicates that some countries lead the global research landscape, while others have a more limited contribution.

The United States, with 156 articles on water resources management and climate change, is undeniably a global leader in this field. This extensive publication output reflects the country's significant emphasis on addressing global climate challenges, particularly in climate modeling and drought management. U.S. research is notably centered on the application of advanced technologies in water resource modeling, such as complex climate models and satellite data integration (Rode et al.,

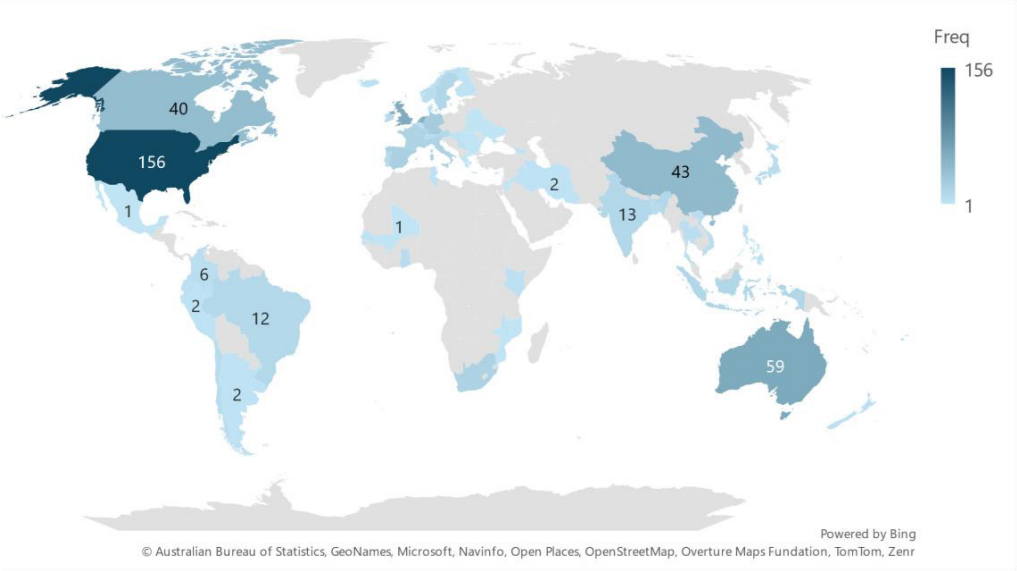

Fig 8. Scientific Production Based on Country

2021). Moreover, the U.S. plays a pivotal role in developing predictive models for climate change impacts and scenario analysis in water resources management, thereby influencing global policy-making on climate change (Barari & Simko, 2023). The United Kingdom, with 57 publications, has made a notable contribution to international climate change research, owing to its geographical location and proactive climate policies. UK research mainly focuses on water resources management under crisis conditions and the prediction of climate change impacts on aquatic ecosystems (Kay et al., 2020). As a leading player in global climate change studies, the UK's research extends to analyzing challenges faced by different climatic regions and participating in international climate policy frameworks such as the IPCC (Bevan, 2020).

Australia, with 59 articles, is particularly prominent in water resources management and climate change research, driven by its unique climatic conditions, which include persistent droughts and significant temperature variations (Walker et al., 2021). Australian research often centers on techniques to bolster water resilience against climate changes and model the impacts of climate change on water resources in arid and semi-arid regions (Marshall & Lobry de Bruyn, 2021). Additionally, Australia actively participates in international projects designed to develop resilience models and perform comparative analyses to address water challenges in similar regions across Asia and the Pacific.

China, with 43 articles, has a particular focus on water resource modeling and predicting water crises. The country has emerged as a leader in utilizing cutting-edge technologies for sustainable water

management and addressing climate change-induced water challenges. China's research priorities include climate change adaptation, integrated water resource management, and the use of satellite data for real-time monitoring of water resources, making it a key player in global climate change research (Qin et al., 2020; Shi et al., 2022).

India (13 papers) has made significant advances in climate change and drought-related research, focusing on agricultural water resource management and the economic and social analysis of drought impacts. India, with its vast and diverse climatic conditions, faces specific challenges in water resource management and the effects of climate change on agriculture (Mahato et al., 2022). Consequently, much of its research has concentrated on improving water resource management predictions in drought-prone areas and assessing the vulnerability of local communities.

In South Africa (18 papers), research is focused on water resource management during drought crises and innovative techniques to address water challenges in arid and semi-arid regions. The country has made notable contributions, particularly in using predictive models to assess the impacts of climate change and drought on aquatic ecosystems and agriculture (Rankoana, 2020). Similarly, Kenya (4 papers) has concentrated its research on agricultural water resource management and strategies for combating water crises in dry areas.

Semantic Trend Analysis of Keywords in Water Resource Management Research

To provide an effective method for reviewing the existing literature or content within scientific documents, an analysis of keywords was conducted. This analysis not only offers valuable insights into the research areas but also uncovers trends or features prevalent in specific domains (Patil et al., 2023). The study of keywords serves as a critical step in understanding the core concepts and terminology within a research field, and it proves highly useful in clarifying certain terms or when there is a need for further elaboration (North & Lombardi, 2020). Moreover, by examining groups of words that frequently appear together within documents, clusters or groupings of related terms can be identified, where each term is connected to others. Furthermore, topics that hold strong relationships within the research domain can be revealed, particularly through the number of citations these specific keywords attract. Consequently, this analysis not only provides a summary of key themes or subfields but also uncovers influential topics within the field of study, as seen in the Word Cloud in Figure 9. A comprehensive analysis of frequently used keywords in the field of study is presented below.

Fig 9. 50 Most Common Words Based on Keywords Plus

1. Core Concepts of Water Resource Management in the Context of Climate Change and Drought

This section examines keywords related to the foundational and general aspects of water resource management in the face of climate change and drought. Terms such as "Management" (46 occurrences) highlight the critical importance of water management in addressing the crises induced by climate change and drought. This term refers to management processes and the need for sustainable strategies in managing water resources. Keywords like "Governance" (24) and "Policy" (25) reflect the governmental and policy-related aspects of water resource management, emphasizing their role in improving resilience and reducing vulnerability to climate change impacts. Additionally, the term "Framework" (24) indicates the significance of establishing scientific management frameworks in this context.

2. Resilience and Vulnerability to Climate Change and Drought

This section focuses on concepts related to assessing and enhancing resilience against the challenges posed by climate change and drought. The term "Vulnerability" (30 occurrences) predominantly addresses the susceptibility of communities and ecosystems to these crises, aiming to identify and evaluate the threats posed by these challenges. The concept of "Resilience" (18) refers to the ability to recover to normal conditions after crises, which is a central concept in climate change studies and water resource management.

Alongside these, terms like "Adaptation" (26) and "Climate-change adaptation" (27) highlight efforts to cope with climate changes and adaptive strategies within the sector.

3. Public Participation and Collaborative Management in Water Resource Decision-Making

Public participation in water resource decision-making and planning is a cornerstone of effective water management. Keywords such as "Participation" (20) and "Public-participation" (9) underline the importance of engaging local communities and the public in water-related decisions and climate crisis management. The term "Co-management" (11) refers to collaborative approaches where responsibility for resource management is shared between governments and local communities, stressing the significance of joint management in ensuring sustainability.

4. Risk Assessment and Challenges in the Face of Climate Change and Drought

This section discusses keywords related to the evaluation and management of risks and challenges arising from climate change and drought. Terms like "Risk" (16) and "Challenges" (15) focus on analyzing the threats and crises related to water resources due to climate change. The term "Impact" (11) highlights the effects of these crises on natural resources and human communities, indicating the importance of understanding the consequences of these changes within water resource studies.

5. The Role of Knowledge and Science in Water Resource Management and Crisis Response

This section emphasizes the importance of scientific knowledge and evidence-based decision-making in addressing water crises. The term "Knowledge" (22) highlights the crucial role of scientific and documented information in water resource management, suggesting that effective decisions require the use of reliable and up-to-date data. Similarly, the term "Science" (29) underscores the foundational role of scientific research in informed decision-making processes concerning climate change and drought management.

6. Modeling and Analytical Tools in Water Resource Management

This section focuses on models and analytical tools that are applied to data analysis and simulation of various scenarios in water resource management and climate change studies. The keyword "Model" (10) specifically refers to the use of simulations and modeling to assess crises and changing conditions. Additionally, the term "Uncertainty" (9) points to the uncertainties inherent in predictions and modeling efforts regarding water resources and climate change, highlighting the ongoing efforts by researchers to mitigate these uncertainties.

By examining these keyword clusters, it is evident that water resource management in the face of climate change and drought is a multifaceted field, involving governance, resilience, vulnerability, public participation, risk assessment, scientific knowledge, and advanced modeling. Each of these aspects plays a vital role in developing effective strategies for addressing current and future water challenges.

Analysis of Past Research Topics and Future Trends in Collaborative Water Resource Management

The analysis of past research trends and the identification of emerging future research directions regarding the role of participatory management in reducing vulnerability and enhancing resilience to climate change and drought was conducted using the R-Studio software, as depicted in Figure 10. This keyword trend analysis from the Web of Science database highlights a shift in the focus of research themes over time. While some concepts have gained prominence, others have gradually diminished in research priority.

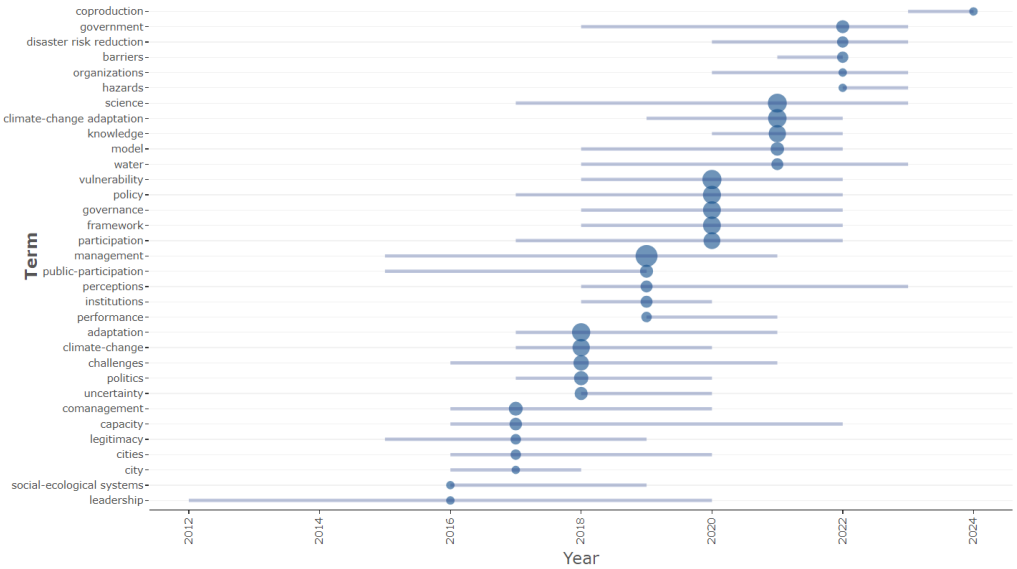

Fig 10. Topic Trends Based on Keywords (Utilizing the Biblioshiny R Package)

Retrospective Trend Analysis

1. Management: The keyword "Management" has seen the highest frequency of use compared to other keywords, exhibiting a notable increase from 2015 to 2021. This trend suggests that the role of management frameworks, including natural, social, and economic resource management in the context of climate change and drought, has garnered significant attention. Moving forward, participatory and co-management approaches are expected to remain central in the field.

Public Participation: The concept of "Public Participation" has steadily appeared in articles from 2015 to 2019, reflecting the growing importance of participatory approaches in addressing climate and drought crises. Given its foundational role in fostering collaborative responses to environmental challenges, this concept is likely to maintain its prominence in future research.

2. **Social-Ecological Systems**: The "Social-Ecological Systems" keyword has emerged in research from 2016 to 2019, focusing on the interactions between human and environmental systems under critical conditions, particularly the impacts of climate change and drought. This approach is expected to continue gaining importance, especially concerning adaptation strategies to mitigate climate impacts.

3. **Policy**: The frequency of the term "Policy" has steadily increased from 2017 to 2022, indicating the growing emphasis on governance, regulatory frameworks, and climate strategies. As participatory management and climate-resilience strategies continue to evolve, policy-related discussions will likely remain critical in future studies.

Prospective Trend Analysis

1. **Co-management**: The keyword "Co-management" gained prominence in research between 2016 and 2020, with an accelerating trend in recent years. Given the pivotal role of local communities in responding climate and drought-related challenges, co-management models—emphasizing shared responsibilities and decision-making between governments and local populations—are expected to become more prominent in future literature.

2. **Resilience**: Keywords related to resilience, such as "Resilience," "Social Resilience," and "Drought Resilience," have increasingly appeared in articles since 2017. Future research will likely focus on strengthening community resilience to the impacts of climate change and water crises, with a particular emphasis on adaptive strategies for vulnerable regions.

3. **Hydrological Systems and Water Scarcity**: This area has gained significant attention, especially from 2018 to 2023, and is expected to remain a key focus in future research. Studies will likely center around modeling hydrological systems and simulating the effects of climate change on water resources and water scarcity. The growing severity of droughts and climate-related water issues suggests this will remain a critical research area, particularly in arid and semi-arid regions.

4. **Decision-making Participation**: The importance of public involvement in decision-making is increasingly recognized, with keywords such as "Participatory Decision-making," "Governance Participation," and "Collective Decision-making" likely to

feature more prominently in the future. This is especially pertinent in the context of natural resource management and water governance, where collaborative decision-making is essential for effective climate adaptation.

5. Co-production and Collaboration: Keywords like "Co-production" and "Collaborative Business" have recently emerged and are expected to gain traction in future research, particularly in the development and implementation of climate policies. These models of collaboration, which emphasize partnerships between stakeholders, could play a critical role in enhancing community resilience to climate and drought impacts.

6. Modeling Approaches: The use of models to predict, evaluate, and manage climate-related crises will continue to be a vital research tool. Keywords associated with modeling have seen an increase since 2018, and are expected to be increasingly utilized in climate data analysis, impact forecasting, and predictive climate modeling. As the complexity of climate scenarios grows, the need for advanced modeling techniques will likely intensify, offering insights into sustainable resource management and climate resilience strategies.

Conclusion

In recent decades, participatory management has emerged as a pivotal research domain in the context of climate change and drought resilience within water resource management sciences. The analysis of scholarly documents extracted from the Web of Science database reflects a notable growth in this field from 2007 to 2024, highlighting the increased attention to this approach in response to global climate crises. The analysis reveals that key terms such as resilience, vulnerability, local governance, social participation, and water resource management have established a scientific framework for assessing and evaluating the role of participatory management in addressing environmental challenges.

From a trend analysis of publication output, there is a marked increase in scientific production in this domain post-2015, directly correlating with the intensification of global climate and drought crises. Research has transitioned from theoretical and conceptual approaches to more practical and data-driven investigations. Notably, the integration of advanced technologies, such as remote sensing, Geographic Information Systems (GIS), and machine learning models, has expanded significantly in participatory management analyses. These tools are critical in facilitating data sharing, modeling the effects of climate change, and enhancing community involvement in decision-making processes.

Geographically, international research,

particularly in North America and Europe, emphasizes the use of predictive models and cutting-edge technologies to manage crises and water resources. In contrast, Asian and African countries, influenced by their unique climatic and hydrological conditions, focus more on predicting water crises and ensuring sustainable water resource management. These geographical and climatic disparities introduce diversity and complexity into the research trajectories and management solutions.

In terms of reputable journals, *Sustainability* and *Environmental Science & Policy* stand out as key references in this field. These journals, through publishing influential and innovative research, significantly contribute to managerial and analytical advancements. They provide a platform for developing scientific and practical solutions to global crises such as climate change and drought, with notable contributions to governance, social-ecological resilience, and local participatory models in water resource management.

Future research is expected to concentrate on critical themes such as co-management, resilience, decision-making participation, and collaborative efforts. The adoption of advanced models, particularly involving real-time data and artificial intelligence, will play a central role in more accurate crisis predictions and water resource management facilitation. These advancements are expected to substantially reduce community vulnerability to climate change and enhance their resilience.

Ultimately, to advance scientific objectives in water resource management and address climate and drought crises, it is essential to more effectively integrate international collaboration and local capacity-building in decision-making and crisis management processes. Key areas for future research include predictive resilience modeling, strengthening local participation, analyzing the effects of international and national policies, and leveraging real-time data. Additionally, interdisciplinary research will be crucial in expanding comprehensive and innovative solutions to address climate change and drought challenges, paving the way for more robust and sustainable water management frameworks.

References

Akbarpour, A., Dastourani, M., Tosan, M., & Gharib, M. (2024). Performance analysis of finite element method in groundwater studies based on web of science using R biblioshiny. *Journal of Auifer and Qanat*, *4*(2), 131-148 [In Persian]. https://doi.org/10.22077/jaaq.2024.7481.1071

Aria, M., & Cuccurullo, C. (2017). Bibliometrix: an r-tool for comprehensive science mapping analysis. *Journal of informetrics*, *11*(4), 959-975. https://doi.org/0.5195/jmla.2022.1434

Arruda, H., Silva, E. R., Lessa, M., Proença Jr, D., & Bartholo, R. (2022). VOSviewer and bibliometrix. *Journal of the Medical Library*

Association: JMLA, *110*(3), 392. https://doi.org/10.5195/jmla.2022.1434

Barari, S., & Simko, T. (2023). LocalView, a database of public meetings for the study of local politics and policy-making in the United States. *Scientific Data*, 10(1), 135. https://doi.org/10.1038/s41597-023-02044-y.

Bevan, L. D. (2020). Climate change strategic narratives in the united kingdom: emergency, extinction, effectiveness. *Energy research & social science*, *69*, 101580. https://doi.org/10.1016/j.erss.2020.101580.

Derviş, H. (2019). Bibliometric analysis using bibliometrix an R package. *Journal of scientometric research*, *8*(3), 156-160. https://doi.org/10.5530/jscires.8.3.32

Ewane, E. B., Mohan, M., Bajaj, S., Galgamuwa, G. P., Watt, M. S., Arachchige, P. P., Hudak, A. T., Richardson, G., Ajithkumar, N., & Srinivasan, S. (2023). Climate-change-driven droughts and tree mortality: assessing the potential of UAV-derived early warning metrics. *Remote Sensing*, *15*(10), 2627. https://doi.org/10.3390/rs15102627.

Feizi, H., & Tosan, M. (2016). Saffron yield variability by climatic factors in the northeast of Iran. V International Symposium on Saffron Biology and Technology: Advances in Biology, Technologies, Uses and Market 1184 [In Persian]. https://doi.org/10.17660/ActaHortic.2017.1184.15.

Hedayat, H., & Kaboli, H. S. (2024). Drought risk assessment: the importance of vulnerability factors interdependencies in regional drought risk management. *International Journal of Disaster Risk Reduction*, 100, 104152. https://doi.org/10.1016/j.ijdrr.2023.104152.

Johnson, R., Stenvinkel, P., Andrews, P., Sánchez-Lozada, L., Nakagawa, T., Gaucher, E., Andres-Hernando, A., Rodriguez-Iturbe, B., Jimenez, C. R., & Garcia, G. (2020). Fructose metabolism as a common evolutionary pathway of survival associated with climate change, food shortage and droughts. *Journal of Internal Medicine*, 287(3), 252-262. https://doi.org/10.1111/joim.12993.

Kapica, J., Jurasz, J., Canales, F. A., Bloomfield, H., Guezgouz, M., De Felice, M., & Kobus, Z. (2024). The potential impact of climate change on European renewable energy droughts. *Renewable and Sustainable Energy Reviews*, 189, 114011. https://doi.org/10.1016/j.rser.2023.114011

Kay, A. L., Watts, G., Wells, S. C., & Allen, S. (2020). The impact of climate change on UK river flows: A preliminary comparison of two generations of probabilistic climate projections. *Hydrological Processes*, 34(4), 1081-1088. https://doi.org/10.1002/hyp.13644.

Loan, F. A., Nasreen, N., & Bashir, B. (2022). Do authors play fair or manipulate Google Scholar h-index? *Library Hi Tech*, 40(3), 676-684. https://doi.org/10.1108/LHT-04-2021-0141.

Mahato, A., Upadhyay, S., & Sharma, D. (2022). Global water scarcity due to climate change and its conservation strategies with special reference to India: a review. *Plant Archives (09725210)*, 22(1). https://doi.org/10.51470/PLANTARCHIVES.2022.v22.no1.009.

Markowska, J., Szalińska, W., Dąbrowska, J., & Brząkała, M. (2020). The concept of a participatory approach to water management on a reservoir in response to wicked problems. *Journal of Environmental Management*, 259, 109626. https://doi.org/10.1016/j.jenvman.2019.109626.

Marshall, G. R., & Lobry de Bruyn, L. A.

(2021). Water policy reform for sustainable development in the murray-darling Basin, australia: insights from resilience thinking. *Water Resilience: Management and Governance in Times of Change*, 65-89. https://doi.org/10.1007/978-3-030-48110-0_4

North, M., & Lombardi, T. (2020). An empirical study of keywords in issues in information system (2000-2019). *Issues in Information Systems*, *21*(1), 249-259. https://doi.org/10.48009/1_iis_2020_249-259.

Patil, R. R., Kumar, S., Rani, R., Agrawal, P., & Pippal, S. K. (2023). A bibliometric and word cloud analysis on the role of the internet of things in agricultural plant disease detection. *Applied System Innovation*, *6*(1), 27. https://doi.org/10.3390/asi6010027.

Pranckutė, R. (2021). Web of Science (WoS) and Scopus: The titans of bibliographic information in today's academic world. *Publications*, *9*(1), 12. https://doi.org/10.3390/publications9010012.

Pulido-Velazquez, D., Collados-Lara, A.-J., & Fernandez-Chacon, F. (2022). The impact of climate change scenarios on droughts and their propagation in an arid mediterranean basin. A useful approach for planning adaptation strategies. *Science of the Total Environment*, *820*, 153128. https://doi.org/10.1016/j.scitotenv.2022.153128.

Qin, J., Ding, Y.-J., Zhao, Q.-D., Wang, S.-P., & Chang, Y.-P. (2020). Assessments on surface water resources and their vulnerability and adaptability in china. *Advances in Climate Change Research*, *11*(4), 381-391. https://doi.org/10.1016/j.accre.2020.11.002.

Rankoana, S. A. (2020). Climate change impacts on water resources in a rural community in limpopo province, South africa: a community-based adaptation to water insecurity. *International Journal of Climate Change Strategies and Management*, 12(5), 587-598. https://doi.org/10.1108/IJCCSM-04-2020-0033.

Rezvani Moghaddam, P., Karbasi, A., Tosan, M., Gharari, F., Feizi, H., & Mohtashami, T. (2016). Saffron agronomy and technology (book of abstracts: 2013-2016). *Saffron agronomy and technology*, *4*(SUPPLEMENT), 1-78. https://doi.org/10.22048/jsat.2016.39250.

Rode, J. B., Dent, A. L., Benedict, C. N., Brosnahan, D. B., Martinez, R. L., & Ditto, P. H. (2021). Influencing climate change attitudes in the united states: a systematic review and meta-analysis. *Journal of Environmental Psychology*, *76*, 101623. https://doi.org/10.1016/j.jenvp.2021.101623.

Rógora Kawano, D. (2024). Bibliometric mapping in skin conductance and advertising using the rpackage-bibliometrix. *GeSec: Revista de Gestao e Secretariado*, *15*(6). https://doi.org/10.7769/gesec.v15i6.3938.

Salvador, C., Nieto, R., Linares, C., Díaz, J., & Gimeno, L. (2020). Effects of droughts on health: Diagnosis, repercussion, and adaptation in vulnerable regions under climate change. Challenges for future research. *Science of the Total Environment*, *703*, 134912. https://doi.org/10.1016/j.scitotenv.2019.134912.

Savari, M., Damaneh, H. E., & Damaneh, H. E. (2022). Drought vulnerability assessment: solution for risk alleviation and drought management among Iranian farmers. *International Journal of Disaster Risk Reduction*, *67*, 102654. https://doi.org/10.1016/j.ijdrr.2021.102654.

Shi, J., Lü, D., Wang, Y., Du, Y., Pang, Y., Yang, D., Wang, X., Dong, X., & Yang, X. (2022).

Recent progress of Earth science satellite missions in China. *Chin. J. Space Sci*, *42*(4), 712-723. https://doi.org/10.11728/cjss2022.04.yg21

Tosan, M., Alizadeh, A., Ansari, H., & Rezvani Moghaddam, P. (2015). Evaluation of yield and identifying potential regions for Saffron (Crocus sativus L.) cultivation in Khorasan Razavi province according to temperature parameters. *Saffron agronomy and technology*, *3*(1), 1-12. [In Persian]. https://doi.org/10.22048/jsat.2014.9605.

Tosan, M., & Beyranvand, Z. (2023). The role of flood analysis in different return periods using empirical relationships for small watersheds in the stability of aquifers. *Journal of Auifer and Qanat*, *4*(1), 169-180. [In Persian] https://doi.org/10.22077/jaaq.2023.6998.1054

Tosan, M., Dastourani, M., Akbarpour, A., & Gharib, M. R. (2024). Global trend analysis of numerical simulation application in groundwater based on WoS database using VOSviewer and Biblioshiny between 1997 and 2023 [Applicable]. *Journal of Rainwater Catchment Systems*, *12*(2), 79-104. DOR:20.1001.1.24235970.1403.12.2.6.1.

Tosan, M., Khashei-Siuki, A., Maroosi, A., & Gharib, M. R. (2024). A Review of smart water management for sustainable agriculture based on the internet of t hings. *Water Management in Agriculture*, *11*(1), 145-166. [In Persian].

Tosan, M., Khashei Siuki, A., Sangari, M., & Rezvani Moghaddam, P. (2024). Analysis of the global research trend of saffron (Crocus sativus L.) between 2000-2023. *Saffron agronomy and technology*, *12*(2), 115-138. [In Persian]. https://doi.org/10.22048/jsat.2024.443037.1524.

Van Eck, N., & Waltman, L. (2010). Software survey: VOSviewer, a computer program for bibliometric mapping. *scientometrics*, *84*(2), 523-538. https://doi.org/10.1007/s11192-009-0146-3.

Van Eck, N. J., & Waltman, L. (2011). VOSviewer manual. *Manual for VOSviewer version*, *1*(0).

Walker, G. R., Crosbie, R. S., Chiew, F. H., Peeters, L., & Evans, R. (2021). Groundwater impacts and management under a drying climate in southern Australia. *Water*, *13*(24), 3588. https://doi.org/10.3390/w13243588.

Yassebi Naeini, S., Mirvahabi Mianroudi, S., & Tosan, M. (2016). A survey on saffron status of Khorasan Razavi and South Khorasan convinces in Iran. V International Symposium on Saffron Biology and Technology: Advances in Biology, Technologies, Uses and Market 1184, https://doi.org/10.17660/ActaHortic.2017.1184.4

Yuan, X., Wang, Y., Ji, P., Wu, P., Sheffield, J., & Otkin, J. A. (2023). A global transition to flash droughts under climate change. *Science*, *380*(6641), 187-191. https://doi.org/10.1126/science.abn6301

Journal of
Drought and Climate change Rrsearch
JDCR
March, 2025, Vol. 2, No.8